Universidade de Aveiro Secção Autónoma de Ciências da Saúde
2012

Sara Catarina Timóteo dos Santos Domingues

Identificação de Complexos Proteicos na Doença de Alzheimer

Identification of Protein Complexes in Alzheimer's Disease

Universidade de Aveiro Secção Autónoma de Ciências da Saúde
2012

Sara Catarina Timóteo dos Santos Domingues

Identificação de Complexos Proteicos na Doença de Alzheimer

Identification of Protein Complexes in Alzheimer's Disease

Tese apresentada à Universidade de Aveiro para cumprimento dos requisitos necessários à obtenção do grau de Doutor em Ciências Biomédicas, realizada sob a orientação científica da Prof. Doutora Odete Abreu Beirão da Cruz e Silva, Professora Auxiliar com Agregação da Secção Autónoma de Ciências da Saúde da Universidade de Aveiro.

Apoio financeiro da FCT e do FSE no âmbito do III Quadro Comunitário de Apoio (Bolsa de Doutoramento SFRH/ BD/ 21559/ 2005).

o júri

presidente

Doutor Artur da Rosa Pires
Professor Catedrático da Universidade de Aveiro

Doutor Uwe Konietzko
Investigador Sénior da Universidade de Zurique

Doutor José António Henriques de Conde Belo
Professor Associado com Agregação da Universidade do Algarve

Doutora Patrícia Espinheira de Sá Maciel
Professora Associada da Escola de Ciências da Saúde da Universidade do Minho

Doutora Odete Abreu Beirão da Cruz e Silva
Professora Auxiliar com Agregação da Universidade de Aveiro

Doutora Margarida Sâncio da Cruz Fardilha
Professora Auxiliar Convidada da Universidade de Aveiro

agradecimentos

I would like to express my gratitude to FCT, for the financial support.
To the Centre for Cell Biology and to the Biology and Health Sciences Departments from the University of Aveiro, for providing the necessary conditions.
To my supervisor Prof. Odete da Cruz e Silva for giving me the opportunity to participate in the APP interactome project, for encouraging me and supporting my projects and ideas.
To Prof. Edgar da Cruz e Silva (1958-2010) for the scientific thinking that challenged mainstream beliefs and also for the wonderful stories that always taught us something. I am grateful for the beneficial scientific discussions, constant positive input and for instilling me self-confidence. Prof. Edgar was a dedicated mentor that will always be remembered. The healthy synergy between the Neurosciences and Signal Transduction Groups was so beneficial for my doctoral education that I will always be very grateful to both, Prof. Odete and Prof. Edgar.
To our collaborator Dr. Uwe Konietzko who welcomed me in his lab with open arms and helped me with the microscopy analyses. I thank Dr. Uwe for collaborating in the RanBP9 project, providing unique tools that made possible the analysis of nuclear structures, and for all the transfections and microscopy work.
To all my colleagues, present and former members of the Neurosciences and Signal Transduction laboratories.
To the graduation and master students that worked with me, contributing also to this project.
Ao meu marido Nuno, pelo incansável apoio e paciência, por toda ajuda e disponibilidade que tornaram possível a realização desta tese. Ao meu querido Francisco, pela compreensão e carinho, apesar da tenra idade… Aos meus pais e toda a família pelo apoio e bons momentos de descontração.

palavras-chave

Doença de Alzheimer, APP, AICD, interactoma, fosforilação, Fe65, splicing alternativo, RanBP9, sinalização nuclear.

resumo

A Doença de Alzheimer (AD) é a maior doença neurodegenerativa a nível mundial, e a principal causa de demência na população idosa. O processamento da proteína precursora de amilóide (APP) pelas β- e γ-secretases origina o peptídeo Aβ, que agrega em oligómeros neurotóxicos e em placas senis. Estes são eventos-chave na patogénese da DA que levam à rutura da neurotransmissão sináptica, morte neuronal e inflamação neuronal do hipocampo e córtex cerebral, causando perda de memória disfunção cognitiva geral. Apesar dos grandes avanços no conhecimento do papel do processamento da APP na DA, a sua função fisiológica ainda não foi totalmente elucidada.

Os mapas de interações proteína-proteína (PPI) humanos têm desempenhado um papel importante na investigação biomédica, em particular no estudo de vias de sinalização e de doenças humanas. O método dois-híbrido em levedura (YTH) consiste numa plataforma para a produção rápida de redes de PPI em larga-escala. Neste trabalho foram realizados vários rastreios YTH com o objetivo de identificar proteínas específicas de cérebro humano que interagissem com a APP, ou com o seu domínio intracelular (AICD), tanto o tipo selvagem como com os mutantes Y687F, que mimetizam o estado desfosforilado do resíduo Tyr-687. De facto, a endocitose da APP e a produção de Aβ estão dependentes do estado de fosforilação da Tyr-687. Os rastreios YTH permitiram assim obter de redes proteínas que interagem com a APP, utilizando como "isco" a APP, APP^{Y687F} e $AICD^{Y687F}$. Os clones positivos foram isolados e identificados através de sequenciação do cDNA. A maior parte dos clones identificados, 118, correspondia a sequências que codificam para proteínas conhecidas, resultando em 31 proteínas distintas. A análise de proteómica funcional das proteínas identificadas neste estudo e em dois projetos anteriores ($AICD^{Y687E}$, que mimetiza a fosforilação, e AICD tipo selvagem), permitiram avaliar a relevância da fosforilação da Tyr-687. Três clones provenientes do rastreio YTH com a APP^{Y687F} foram identificados como um novo transcrito da proteína Fe65, resultante de *splicing* alternativo, a Fe65E3a (*GenBank Accession*: EF103274), que codifica para a isoforma p60Fe65. A p60Fe65 está enriquecida no cérebro e os seus níveis aumentam durante a diferenciação neuronal de células PC12, evidenciando o potencial papel que poderá desempenhar na patologia da DA.

A RanBP9 é uma proteína nuclear e citoplasmática envolvida em diversas vias de sinalização celulares. Neste trabalho caracterizou-se a nova interação entre a RanBP9 e o AICD, que pode ser regulada pela fosforilação da Tyr-687. Adicionalmente, foi identificada uma nova interação entre a RanBP9 e a acetiltransferase de histonas Tip60. Demonstrou-se ainda que a RanBP9 tem um efeito de regulação inibitório na transcrição mediada por AICD, através da interação com a Tip60, afastando o AICD dos locais de transcrição ativos.

O estudo do interactoma da APP/AICD, modelado pela fosforilação da Tyr-687, revela que a APP poderá estar envolvida em novas vias celulares, contribuindo não só para o conhecimento do papel fisiológico da APP, como também auxilia a revelar as vias que levam à agregação de Aβ e neurodegeneração. A potencial relevância deste trabalho relaciona-se com a descoberta de algumas interações proteicas/vias de sinalização que podem que podem ser relevantes para o desenvolvimento de novas estratégias terapêuticas na DA.

keywords

Alzheimer's disease, APP, AICD, interactome, phosphorylation, Fe65, alternative splicing, RanBP9, nuclear signaling.

abstract

Alzheimer's disease (AD) is the most prevalent neurodegenerative disorder worldwide and the leading cause of dementia in the elderly. Processing of amyloid-β precursor protein (APP) by β- and γ-secretases produces Aβ, which aggregates into neurotoxic oligomers and senile plaques. These are key events in the pathogenesis of AD that lead to the disruption of synaptic neurotransmission, neuronal cell death, and inflammation in the hippocampus and cerebral cortex, thus causing memory loss and global cognitive dysfunction. Despite advances in understanding the role of APP processing in AD, the normal physiological function of this protein has proven more difficult to elucidate.

Human protein-protein interaction (PPI) maps play an increasingly important role in biomedical research and have been shown to be highly valuable in the study of a variety of human diseases and signaling pathways. The yeast two-hybrid (YTH) system provides a platform for the rapid generation of large scale PPI networks. Several YTH screens were performed to identify human brain-specific proteins interacting with APP, or with its intracellular domain (AICD), either the wild-type or the Y687F mutant, which mimics the dephosphorylated residue. In fact, APP endocytosis and Aβ generation are dependent upon Tyr-687 phosphorylation. A human APP network comprised of the protein interactions was assembled through YTH screening, using as baits APP, APP^{Y687F} and $AICD^{Y687F}$. Positive clones were isolated and identified by DNA sequencing and database searching. The majority of these clones, 118, matched to a protein coding sequence, yielding 31 different proteins. Functional proteomics analysis of the proteins identified in this study, and two additional screens from previous projects (phospho-mutant $AICD^{Y687E}$ and wild-type AICD), allowed to infer the relevance of Tyr-687 phosphorylation. Three clones from YTH with APP^{Y687F} were identified as a new splice variant of the APP binding protein Fe65, Fe65E3a (GenBank Accession EF103274), encoding the p60Fe65 isoform. Fe65E3a is expressed preferentially in the brain and the p60Fe65 protein levels increased during PC12 cell differentiation. This novel Fe65 isoform and the regulation of the splicing events leading to its production, may contribute to elucidating neuronal specific roles of Fe65 and its contribution to AD pathology.

RanBP9 is an evolutionarily conserved nucleocytoplasmic protein implicated as a scaffolding protein in several signaling pathways. In this work a novel interaction between RanBP9 and AICD, which can be regulated by Tyr-687 phosphorylation, was characterized. Moreover, a novel interaction between RanBP9 and the histone acetyltransferase Tip60 was identified. RanBP9 was demonstrated to have an inhibitory regulatory effect on AICD-mediated transcription, through physical interaction with Tip60, relocating AICD away from transcription factories.

Overall, the APP/AICD interactome shaped by the phosphorylation state of Tyr-687 provided clues to elucidate APP pathways leading to amyloid deposition and neurodegeneration. As such the work here described brings us nearer to unravelling the physiological functions of APP. This in turn is of potential significant relevance in the pathology of AD, and for the design of effective novel therapeutic strategies.

CONTENTS

ABBREVIATIONS

aa	amino acid (s)
Aβ	amyloid-β protein
ActD	transcription activation domain
AD	Alzheimer's disease
AICD	APP intracellular domain
Amp	ampicillin
APP	amyloid-β precursor protein
APS	ammonium persulfate
BD	DNA-binding domain
BLAST	basic local alignment search tool
bp	base pair (s)
cDNA	complementary deoxyribonucleic acid
CDS	DNA coding sequence
Chr	chromosome
CNS	central nervous system
CTF	C-terminal fragment
CTFα (or C83)	APP product of cleavage by α-secratase
CTFβ (or C99)	APP product of cleavage by β-secretase at β site
CTFβ' (or C89)	APP product of cleavage by β-secretase at β' site
DMSO	dimethylsulfoxide
DNA	deoxyribonucleic acid
dNTP	deoxynucleotide triphosphate
dsDNA	double strand deoxynucleic acid
EDTA	ethylenodiaminotetraacetic acid
EOFAD	early-onset familial AD
EST	expressed sequence tag
GAL4	Gal4 transcription factor
GAL4-AD	activation domain of Gal4 transcription factor

GAL4-BD	binding domain of Gal4 transcription factor
GFP	green fluorescent protein
GO	Gene Ontology
GST	glutathione S-transferase
h	hour(s)
HSP	Heat shock protein
IPTG	isopropyl-β-D-thiogalactopyranoside
LB medium	Luria-Bertani Medium (Miller)
LiAc	lithium acetate
LOAD	late-onset AD
min	minute(s)
NCBI	National Center for Biotechnology Information
NFTs	Neurofibrillary tangles
nt	nucleotide
OD	optical density
ORF	open reading frame
PCR	polymerase chain reaction
PEG	polyethylene glycol
PMSF	phenyl methylsulfoxide
PPI	protein-protein interaction
QDO	quadruple dropout medium (lacking Trp, Leu, His and Ade)
RNA	ribonucleic acid
RT	room temperature
RT-PCR	Reverse transcriptase - polymerase chain reaction
SAP	shrimp alkaline phosphatase
sAPP	soluble amyloid precursor protein
sAPPα	proteolyte of APP cleavage by α-secretase
sAPPβ	proteolyte of APP cleavage by β-secretase
SD	synthetic dropout medium
SDS	sodium dodecyl sulfate
SDS-PAGE	sodium dodecyl sulfate – polyacrylamide gel electrophoresis
sec	second(s)
SPs	Senile plaques

TBS	Tris-buffered saline solution
TDO	triple dropout medium (lacking Trp, Leu and His)
TEMED	N,N,N',N'-tetramethyletylendiamine
Tg	Transgenic
TGN	Trans-Golgi Network
Tris	Tris (hydroxymethyl)-aminoethane chloride
UAS	upstream activating sequence
UTR	mRNA untranslated region
UV	ultraviolet
wt	wild-type
X-α-gal	5-bromo-4-chloro-3-indolyl-alpha-D-galactopyranoside
YPD	yeast extract, peptone and dextrose medium for *S. cerevisiae*
YPDA	YPD supplemented with Ade
yr	year(s)
YTH	yeast two-hybrid

TABLES

FIGURES

PUBLICATIONS

The results described in Chapters II and III of this thesis are being prepared for submission:

- **Domingues SC**, Fardilha M, da Cruz e Silva EF and da Cruz e Silva OAB. The interactome of amyloid-β precursor protein is modulated by the phosphorylation state of Tyr-687.

The results from Chapter IV led to a significant publication in an international peer-reviewed journal:

- **Domingues SC**, Henriques AG, Fardilha M, da Cruz e Silva EF and da Cruz e Silva OAB (2011). Identification and characterization of a neuronal enriched novel transcript encoding the previously described p60Fe65 isoform. Journal of Neurochemistry. 2011 Aug 9. [Epub ahead of print].

Additionally a new sequence was submitted to the GenBank database:

- **Domingues SC** and da Cruz e Silva OAB (2006). Homo sapiens amyloid beta A4 precursor protein-binding family B member 1 transcript variant 3 (APBB1) mRNA, partial cds, alternatively spliced. ACCESSION: EF103274; GI: 118582221. Last update: 17-04-2008.

The results from Chapter V were submitted for publication:

- **Domingues SC**, Konietzko U., Henriques AG, Rebelo S, Fardilha M, Nishitani H, Nitsch R, da Cruz e Silva EF and da Cruz e Silva OAB. RanBP9 Prevents Nuclear Signaling by the APP Intracellular Domain through Physical Interaction with Tip60.

During the development of the PhD thesis, I participated in other group projects that led to significant publications in international peer-reviewed journals:

- Esteves S, Fardilha M, **Domingues SC**, Da Cruz e Silva OAB and Da Cruz e Silva EF and (2011). Protein Phosphatase 1alpha Interacting Proteins in Human Brain. OMICS: A Journal of Integrative Biology (in press)

- Fardilha M, Esteves SLC, **Domingues SC**, Rebelo S, Gregório, LK and da Cruz e Silva E (2011). CHARACTERIZATION OF THE PROTEIN PHOSPHATASE 1 INTERACTOME FROM HUMAN TESTIS. Biochemical Pharmacology 2011 Mar 5. [Epub ahead of print]

- da Cruz e Silva OA, Henriques AG, **Domingues SC**, da Cruz e Silva EF. (2010). Wnt signaling is a relevant pathway contributing to amyloid beta- peptide-mediated neuropathology in Alzheimer's disease. CNS & Neurological Disordorders – Drug Targets. 2010 Dec;9(6):720-6.

- Vieira SI, Rebelo S, **Domingues SC**, da Cruz E Silva EF, da Cruz E Silva OA (2009). S655 PHOSPHORYLATION ENHANCES APP SECRETORY TRAFFIC. Molecular and Cellular Biochemistry. 2009 Aug;328(1-2):145-54. Epub 2009 Apr 21.

Previous publications:

- **Domingues SC**, Henriques AG, Wu W, Da Cruz e Silva EF, Da Cruz e Silva OAB (2007). ALTERED SUBCELLULAR DISTRIBUTION OF THE ALZHEIMER'S AMYLOID PRECURSOR PROTEIN UNDER STRESS CONDITIONS. Ann N Y Acad Sci. Jan;1096:184-95.

- Henriques AG, Vieira SI, Rebelo S, **Domingues SC**, da Cruz e Silva EF, da Cruz e Silva OAB (2007). ISOFORM SPECIFIC AMYLOID-BETA PROTEIN PRECURSOR METABOLISM. J Alzheimers Dis. Mar;11(1):85-95.

- Henriques AG, **Domingues SC**, Fardilha M, da Cruz e Silva EF, da Cruz e Silva OAB (2005). SODIUM AZIDE AND 2-DEOXY-D-GLUCOSE-INDUCED CELLULAR STRESS AFFECTS PHOSPHORYLATION-DEPENDENT ABETAPP PROCESSING. J Alzheimers Dis. Jun; 7(3):201-12.

THESIS OUTLINE

The present thesis is organized into six Chapters. In Chapter I, a general introduction to Alzheimer's disease (AD) is presented. It includes a review of the literature in the field of the cellular and molecular aspects that contribute to the pathogenesis of AD. The thesis Introduction is mainly focused on the biology of the amyloid-β precursor protein (APP), including a description of APP trackiffing and processing. The putative functions of APP holo protein and its fragments are also addressed. Phosphorylation of APP intracellular domain (AICD) and the interactome of APP are described in an AICD signaling perspective.

Chapters II to V correspond to different scientific studies. Chapter II presents all the material and methods used to perform three yeast two-hybrid (YTH) screens, using as baits diverse constructs of the amyloid precursor protein (APP), as well as the results obtained in the screens.

Chapter III corresponds to the identification of the positive clones obtained, characterization of the novel putative APP binding proteins by bioinformatics methods and analysis of the protein networks around APP.

Chapter IV presents a novel splice variant of the APP binding protein Fe65, termed Fe65E3a. Fe65 is a well-known APP interacting protein, and the novel Fe65 splice variant generates a neuronal-specific shorter protein, relevant for APP physiological roles and potentially for AD.

In Chapter V, the new interaction between APP intracellular domain and the scaffolding protein RanBP9 is characterized. The new complex AICD-RanBP9-Tip60 is also described, in the perspective of AICD nuclear signaling.

In Chapter VI, a general discussion and conclusions resulting from the data obtained are presented.

OBJECTIVES

Phosphorylation/dephosphorylation of consensus sites in the cytoplasmic domain of amyloid-β precursor protein (APP) affects its subcellular localization, proteolytic processing and, consequently, Aβ production. In fact, the intracellular domain of APP (AICD) contains eigth phosphorylatable residues, and seven of these are hyperphosphorylated in AD brains. For example, Tyr-687 that is contained in the ^{682}YENPTY^{687} motif, is a docking site for interaction with cytosolic proteins that regulate APP metabolism and signaling. In fact, APP endocytosis and Aβ generation are dependent upon Tyr-687 phosphorylation, which was shown *in vivo* using phosphorylation-/dephosphorylation-mimicking mutants. The molecular function of APP is unknown, but Tyr-687 phosphorylation is probably regulating the interactions with other proteins. Therefore, the aim of this work was to identify brain proteins capable of interacting with the APP or AICD harbouring mutations that mimic the phosphorylation state of Tyr-687. The characterization of APP protein complexes shaped by Tyr-687 phosphorylation/ dephosphorylation will contribute to elucidate APP physiological function, and APP pathways leading to AD. Furthermore, APP binding proteins represent potential targets for novel therapeutic approaches. Hence, specific aims were to:

1. Perform preliminary steps for YTH screening, in particular to construct the bait plasmids and verify the expression of the GAL4-BD fusion proteins by immunoblotting.

2. Perform three YTH screens using large-scale yeast mating with pretransformed human brain library and isolate the putative positive clones.

3. Identify the novel APP, APP^{Y687F} and AICD^{Y687F} binding proteins by sequencing of the preys' cDNA plasmids. Perform *in silico* analysis of APP protein networks.

4. Select potentially relevant clone(s) for further functional analysis. To accomplish this specific aim a novel interaction between AICD and RanBP9 was selected for further functional characterization. Addionally, an alternatively spliced Fe65 positive clone was also selected for further studies.

CHAPTER I. INTRODUCTION

I.1 ALZHEIMER'S DISEASE (AD): THE MOST COMMON FORM OF AGE-RELATED DEMENTIA

In 1907, the German psychiatrist and neuropathologist Alois Alzheimer published a report concerning "an unusual illness of the cerebral cortex" (Alzheimer, 1907; Alzheimer *et al.*, 1995), which Emil Kraepelin subsequently named after him (Kraepelin, 1910). Alzheimer described the case of a 51-year-old woman, Auguste D., who initially developed a delusional disorder followed by a rapid loss of short-term memory. Post-mortem brain examination, using a silver staining method, revealed cortical atrophy and the presence of two histopathological modifications: senile plaques (SPs), and neurofibrillary tangles (NFTs) in the cerebral cortex and limbic system, which are known today as the hallmarks of the disease.

Alzheimer's disease (AD) is a slowly progressive disorder, with insidious onset and progressive decline in cognitive and functional abilities as well as behavioral and psychiatric symptoms leading to a vegetative state and ultimately death. AD is the most common cause of dementia, accounting for 50-60% of all cases. The prevalence of dementia increases exponentially with age, from below 1% in individuals aged 60-64 years, up to 24-33% in people over age 85, in the western world. One century after the first description, AD has become the most common age related neurodegenerative disorder. In 2001, around 24 million people worldwide had dementia and the number is expected to double every 20 years, because of the anticipated increase in life expectancy (Ferri *et al.*, 2005; Qiu *et al.*, 2009).

I.1.1 Clinical symptoms of AD

AD, as the prototype of cortical dementias, is characterized by the development of major cognitive defects. The clinical symptomatology begins by episodic memory deficits with preserved alertness and motor function. The syndrome of mild cognitive impairment (MCI), characterized by a subtle decrease in short-term declarative memory although with normal cognition, is often a precursor of AD (Petersen and Negash, 2008; Werner and Korczyn, 2008). Over time, progressive cognitive impairment appears, including impaired judgement, decision-making and orientation, often accompanied, in later stages, by psychobehavioural disturbances as well as language impairment (McKhann *et al.*, 1984). Besides the cognitive decay, patients display dramatic

neuropsychiatric symptoms, namely mood disturbances, delusions and hallucinations, personality changes and behavior disorders, such as aggressiveness, depression and circadian disturbances (Knopman *et al.*, 2001). In contrast with cognitive symptoms, the non-cognitive defects do not show a progressive course (Chung and Cummings, 2000). Patients usually survive 7 to 10 years (range 2-20 years) after the onset of symptoms and typically die from medical complications, such as bronchitis or pneumonia (Beal *et al.*, 2005).

I.1.2 Diagnosis of AD

The patient history, together with clinical, neurological and psychiatric examination, provide the basis for establishing the clinical diagnosis of AD. According to previous criteria, AD could only be definitively diagnosed by postmortem brain biopsy (MRC-CFAS, 2001), but laboratory tests and neuroimaging are today valuable tools to exclude other causes of dementia. Therefore, full confirmation of AD diagnosis requires both presence of progressive dementia (episodic memory impairment and involvement of at least one additional cognitive domain, with impairment in daily living activities) and demonstration of the presence in the brain of SPs and NFTs. Given that the neuropathological hallmarks of the disease, SPs and NFTs, are only observed postmortem, AD diagnosis is primarly probabilistic (probable AD). According to National Institute of Neurological and Communicative Diseases and Stroke/ Alzheimer's Disease and Related Disorders Association (NINCDS/ADRDA) criteria AD could be definite (at autopsy), probable or possible (McKhann et al., 1984).

Meanwhile, Braak and Braak (1991) presented another model of AD stageing, based on the frequency and location of the deposition of neurofibrillary tangles. This has led to the simplified hypothesis testable with *in vivo* imaging that the entorhinal cortex is the first involved area, followed by the hippocampus, and then the neocortical temporal cortex.

Increasing scientific knowledge, regarding the pathobiology of AD, led to research focused on the search for biomarkers. The most reliable biomarkers validated in the last few years include: an abnormal cerebrospinal fluid amyloid-β protein (Aβ) and Tau profile (Blennow *et al.*, 2010; Spitzer *et al.*, 2010); the presence of hippocampal atrophy on magnetic resonance imaging (MRI), glucose hypometabolism on positron emission tomography (PET) scan, or the presence of a known pathogenic mutation in *APP*, *PSEN1* and *PSEN2* genes. Hence, in 2007 new research criteria were proposed (Dubois *et al.*, 2007). According to the new criteria, the diagnosis of AD is

confirmed in the presence of episodic memory impairment and a positive biomarker. It has a high level of accuracy even at the stage of earliest clinical manifestations, i.e. the MCI stage.

I.1.3 Neuropathological phenotype

The histopathological features of AD, described for the first time by Alzheimer and still considered as the two main pathological hallmarks of the disease, are abundant amounts of extracellular plaques composed of the amyloid-β and intracellular neurofibrillary lesions formed of hyperphosphorylated tau protein. Neuronal and synaptic loss and numerous other structural and functional alterations, such as energy dysfunction, oxidative stress (Pappolla *et al.*, 1992; Eckert *et al.*, 2003) and inflammatory responses (Wyss-Coray, 2006) are associated with AD.

Neuronal and synaptic loss

The combined consequences of all the pathological changes lead to massive neuronal and synapse loss at specific brain regions involved in learning, memory and emotional behavioral such as the hippocampus, association cortices and subcortical structures including the amygdala and nucleus basalis of Meynert (Selkoe, 2002; Duyckaerts *et al.*, 2009). Cortical atrophy and concomitant enlargement of ventricles and sulci, particularly in the frontal, temporal and parietal lobes, are characteristic changes in AD (Fig. I.1). The occipital lobe and the sensory and motor regions of cortex are relatively spared. The first neurodegenerative changes are observed in hippocampus and entorhinal cortex and measurement of hippocampal atrophy can discriminate between AD and non-affected elderly people (Robakis, 2011). Atrophy of these regions is, however, also present in other dementias and is not specific for AD. The atrophy in AD is due to decreased number of synapses, degenerated neurites and neuronal loss (Terry *et al.*, 1991). Neurons that use glutamate or acetylcholine as neurotransmitters appear to be particularly affected, but cells that produce serotonin and norepinephrine are also damaged (Whitehouse *et al.*, 1981). At the time of death, the brain of a patient with AD may weigh one-third less than the brain of an age-matched, non-demented individual (Petrovitch *et al.*, 2000).

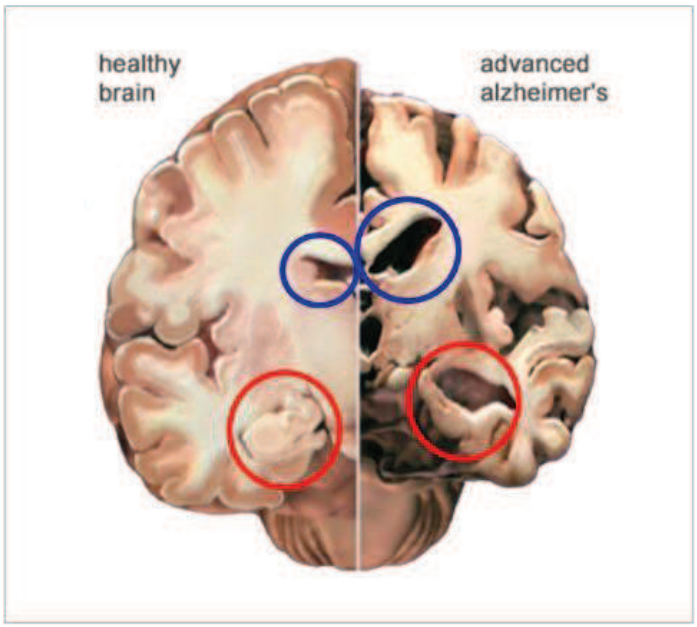

Figure I.1: Image representating a normal brain half, on the left, and an Alzheimer's brain half, on the right (cross-section of brain coronal sections). The Alzheimer's brain is smaller, particularly in the hippocampus (red circle) and there is some widening of the ventricles (blue circles) (Adapted from http://www.alz.org/brain/09.asp).

Senile plaques (SPs)

SPs are extracellular deposits of amyloid-β protein (Aβ), a peptide derived from proteolytic cleavage of amyloid precursor protein (APP) by the sequential action of β- and γ-secretases (detailed in Section I.2.2). Relatively heterogeneous cleavage by γ-secretase produces diverse Aβ species, variable in length (Esch *et al.*, 1990; Zhao *et al.*, 2007). The plaques are composed primarily of the Aβ species from 39 to 43 residues in lengh. Most of the Aβ produced by γ-secretase is the 40-residue form (Aβ40) whereas the 42-residue variant (Aβ42) represents only 5-10% of all Aβ produced. However, the major Aβ species deposited in the plaques is Aβ42 (Iwatsubo *et al.*, 1994; Wolfe, 2008b). SPs can be observed as neuritic plaques or diffuse plaques. Neuritic plaques are microscopic foci of extracellular amyloid deposition and associated axonal and dendritic injury (Fig. I.2). The cores of the neuritic plaques are mostly composed of Aβ42 (Iwatsubo *et al.*, 1994) that occur mainly in a filamentous form, i.e., as star-shaped masses of

amyloid fibrils. Dystrophic neurites occur both within this amyloid deposit and immediately surrounding it (Dickson, 1997). Neuritic plaques are also closely associated with microglia and reactive astrocytes. In contrast, diffuse plaques show a finely granular pattern, without a clearly fibrillar, compacted center and lack the associated dystrophic neurites and glia (Masliah *et al.*, 1993; Selkoe, 2001). The diffuse plaques are not only found in limbic and association cortices, where often large numbers of the neuritic plaques are found, but also in regions which do not generally display the typical AD pathology, such as cerebellum, striatum and thalamus. It has been suggested that diffuse plaques might represent precursor lesions of neuritic plaques (Selkoe, 2001).

Aside from plaques, Aβ deposits can also be found in the walls of blood vessels within the cerebral cortex (mainly Aβ40), leading to the development of cerebral amyloid angiopathy, another pathological condition observed in AD (Miller *et al.*, 1993). In fact, Aβ was first isolated and sequenced from meningeal vessels in AD and Down's syndrome (DS) cases, prior to its isolation from plaques (Glenner and Wong, 1984b).

Neurofibrillary tangles (NFTs)

NFTs are intracellular neurofibrillary lesions composed of the microtubule-associated protein tau (encoded by the *MAPT* gene), which is present in a hyperphosphorylated form (Brion *et al.*, 1985; Hernandez *et al.*, 2010). NFTs are large, non-membrane bound bundles of abnormal fibers that accumulate in the perinuclear region of the cytoplasm (Fig. I.2). Electron microscopy showed that most of these fibers consist of pairs of filaments wound into helices, termed paired helical filaments (PHFs). Tau hyperphosphorylation favours its dissociation from microtubules and stimulates the self-assembly of tau, in paired helical filaments that in turn assemble into neurofibrillary tangles (Selkoe, 2001).

The two classical lesions of AD, SPs and NFTs, can occur independently of each other. Tau aggregates that are biochemically similar to those in AD have been described in other less common neurodegenerative diseases, in almost all of which no Aβ deposits and neuritic plaques are present. Conversely, Aβ deposits can be seen in the brains of cognitively normal-aged humans in the virtual absence of tangles (Terry *et al.*, 1987).

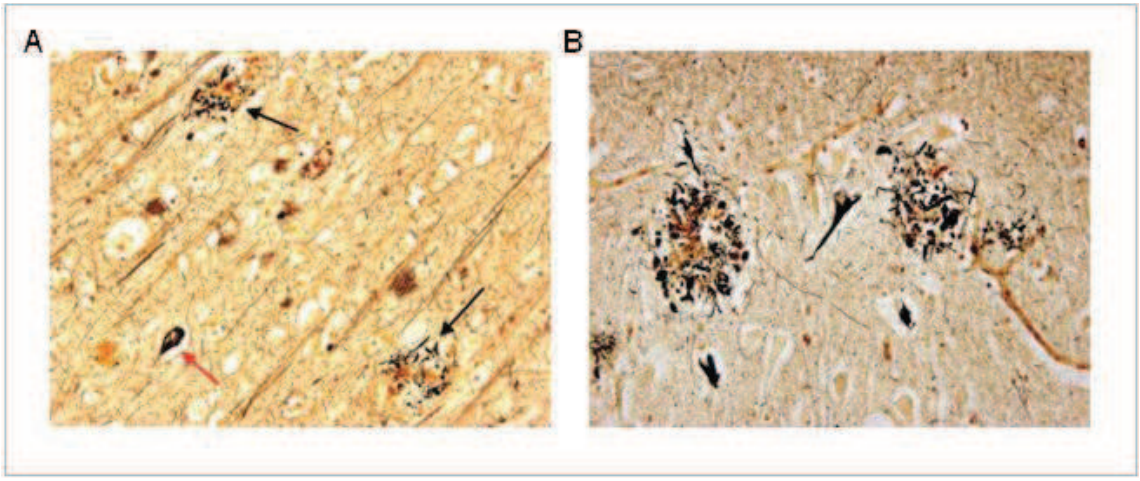

Figure I.2: Photomicrographs of temporal cortices of Alzheimer's disease patients (modified Bielschowski stain). (A) Numerous senile (neuritic) plaques (black arrows) and neurofibrillary tangles (red arrow) are shown (original magnification, 100×). (B) Two senile (neuritic) plaques with a neurofibrillary tangle between them are shown (original magnification, 400×) (Adapted from Perl, 2010).

Other AD microscopic lesions

Besides SPs and NFTs, other microscopic features were identified in AD brains such as Hirano bodies, also named eosinophilic rod-like inclusions (Hirano, 1994). Hirano bodies are eosinophilic perineuronal lesions encountered within the CA1 region of the hippocampus, currently considered to be a non-specific lesion of unknown significance. Immunohistochemical studies indicate the presence of actin, tropomyosin, and vinculin within these bodies (Galloway *et al.*, 1987; Perl, 2010).

Granulovacuolar degeneration is a poorly understood lesion that consists of an intraneuronal cluster of small vacuoles each containing a small, dense basophilic granule. The central granules stain intensely with silver impregnation stains and with antibodies directed against phosphorylated neurofilaments, tubulin, tau, and ubiquitin (Dickson *et al.*, 1987). Little is known about the nature of these lesions or their significance. They are seen in brain specimens derived from elderly individuals with normal cognitive function, but studies have shown that large numbers of such lesions in the boundary zone between the CA1 and CA2 regions of the caudal aspect of the hippocampus correlate well with a diagnosis of Alzheimer's disease (Ball and Lo, 1977; Perl, 2010).

I.1.4 Genetics and risk factors of AD

The etiology of AD is complex and not yet fully understood, however it is widely accepted that inheritance of specific genes plays a critical role in predisposing to onset and/or in modifying disease progression. In particular, the identification of specific, disease-segregating mutations in previously unknown genes has directed attention to specific proteins and pathways that are now considered critical in the pathogenesis of the disease, e.g. mutant amyloid-β precursor proteins that cause AD (Bertram and Tanzi, 2004).

In common with various neurodegenerative diseases, AD shows familial (rare) and apparently non-familial (common) forms. The latter are also frequently described as "sporadic" or "idiopathic", although increasing evidence suggests that a large proportion of these cases are also significantly influenced by genetic factors. These *risk* genes are likely to be numerous, displaying intricate patterns of interaction with each other as well as with non-genetic factors. Therefore, AD is a genetically complex disease , not exhibiting a simple or single mode of inheritance (Bertram, 2011).

Early-onset familial AD (EOFAD)

EOFAD, often transmitted as an autosomal dominant trait with onset ages usually below 65 years of age, is caused by rare, but highly penetrant mutations in at least three genes: *APP* (amyloid precursor protein; located on chromosome 21q21.3), *PSEN1* (presenilin 1; on 14q24.3), and *PSEN2* (presenilin 2; on 1q31-q42) (Tanzi *et al.*, 1987; Goate *et al.*, 1991; Rogaeva, 2002). However, these cases probably represent not more than 5% of all AD cases. An up-to-date overview of AD mutations is found in the "AD and FTD Mutation Database" (http://www.molgen.ua.ac.be/ADMutations/) (Cruts and Van Broeckhoven, 1998; Rovelet-Lecrux *et al.*, 2006).

The mutations in APP occur near or within its cleavage sites (Fig. I.3), thereby altering APP processing such that more Aβ42 is produced (Hardy and Selkoe, 2002). The presenilins are a central component of γ-secretase, the enzyme responsible for liberating from the C-terminal fragment of APP, and mutations in the presenilins also alter APP processing, producing more Aβ42 (Wilquet and De Strooper, 2004). These genetic data are the basis for the amyloid hypothesis of AD (see the Section I.1.5), and suggest that Aβ42 is the initiating molecule in Alzheimer's disease.

Additional data have reinforced this view, with APP gene duplications also causing the disease (Rovelet-Lecrux *et al.*, 2006). Indeed high levels of APP expression were already known to be highly significant, as Down's syndrome patients have an extra copy of chromosome 21 (trisomy 21) and develop AD by the age of 50. Post-mortem analyzes of those who died young showed diffuse intraneuronal deposits of Aβ in the absence of any tau pathology, suggesting that Aβ deposition is an early event in AD (Esler and Wolfe, 2001).

In AD, no mutations have been identified in the gene encoding tau, *MAPT* (located on chromosome 17q21.1). However, more than 30 exonic and intronic mutations in *MAPT* have been found in a familial dementia related to AD, the frontotemporal dementia with Parkinsonism linked to chromosome 17 (FTDP-17). Tau mutations are mainly located in the microtubule binding repeat region or close to it and reduce tau ability to promote microtubule assembly and lead to NFT formation (Hasegawa *et al.*, 1998).

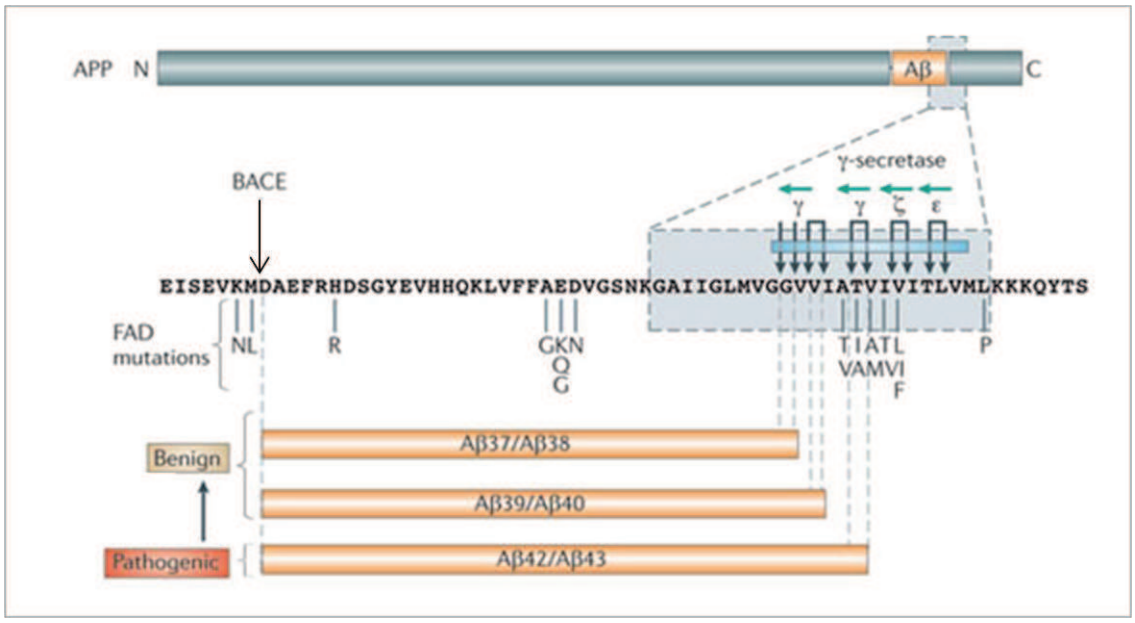

Figure I.3: *APP* mutations associated with early-onset familial Alzheimer's disease (FAD). Most APP mutations are clustered in the close vicinity of β- and γ-secretase-cleavage sites, thereby influencing APP processing (Adapted from Karran *et al.*, 2011).

Late-onset AD (LOAD)

The vast majority of AD cases occurs after the age of 65 years (late-onset; LOAD), and does not show any evident pattern of familial segregation. However, strong evidence exists

suggesting the presence of additional AD genes for both forms of the disease. For example, a large population based twin study showed that the extent of heritability for the sporadic disease is almost 80% (Gatz *et al.*, 1997; Gatz *et al.*, 2006).

The identification of complex disease genes is affected by several factors: locus and/or allelic heterogeneity; small effect sizes of the underlying variants; unknown and difficult to model interaction patterns; population differences; insufficient sample sizes/sampling strategies; and, linkage disequilibrium among polymorphisms other than those initially associated with the disease. The emergence of powerful and efficient genotyping technologies, e.g. genome-wide association studies (GWAS), has suggested the existence of over three dozen potential new AD susceptibility genes. To date, the results of 15 GWAS have been published for AD, reporting more than 40 different loci as potential AD susceptibility modifiers. Interestingly, all published AD GWAS to date share the highly significant association between increased AD risk and the presence of the apolipoprotein E (APOE) ε4 allele (Bertram, 2011).

There are three allelic variants of the *APOE* gene: ε3, ε2 and ε4, encoding the corresponding isoforms. Meta-analysis showed that the *APOE* ε4 allele increases the risk of the disease by three times in heterozygotes and by 15 times in homozygotes (Poirier *et al.*, 1993; Saunders *et al.*, 1993; Dickson *et al.*, 1997). In contrast, ε2, the least common allele, is suggested to be protective (Corder et al., 1994). The apoE isoforms are suggested to influence the risk of developing AD by differentially affecting the aggregation and clearance of Aβ (Kim et al., 2009), presumably through a direct interaction between apoE and Aβ (Strittmatter et al., 1993).

Table I.1: Established susceptibility genes for non-Mendelian forms of Alzheimer's disease.

Gene	Protein	Location	Physiological/Pathogenic relevance
APOE	Apolipoprotein E	19q13	Aggregation and clearance of Aβ; cholesterol metabolism
BIN1	Bridging integrator 1	2q14	Production and clearance of Aβ
CLU	Clusterin	8p21.1	Aggregation and clearance of Aβ; inflammation
CR1	Complement component (3b/4b) receptor 1	1q32	Clearance of Aβ; inflammation
PICALM	Phosphatidylinositol-binding clathrin assembly protein	11q14	Production and clearance of Aβ; synaptic transmission

"AlzGene" is a publicly available internet database (http://www.alzgene.org) that uncovers the information of every peer-reviewed genetic association study in AD (Bertram et al., 2007). Of the more than 40 loci implicated in AD etiology in addition to *APOE* by GWAS, only five currently show sufficient evidence of representing genuine associations with AD risk (Table I.1), being all associated with Aβ generation, aggregation or clearance: *APOE*; *BIN1*; *CLU*; *CR1*; and *PICALM*. A few others show at least some evidence for replication in independent follow-up studies, though no association at genome-wide significance in meta-analyzes (Bertram, 2011): *CD33* (siglec-3), *GAB2* (GRB2-associated binding protein 2), or *GWA_14q32* (not assigned to a specific gene).

Epidemiological studies also suggested that other factors such as aging, traumatic brain injury (Jellinger, 2004), female gender, low physical and social activity, hypertension and high serum cholesterol levels at midlife are associated with AD (Pasinetti et al., 2011; Sakurai et al., 2011). Nevertheless, further work is needed to elucidate the impact of some of these factors and their possible role in pathogenesis.

I.1.5 The amyloid cascade hypothesis

Genetic data provided the intellectual basis for the amyloid hypothesis of AD, suggesting that Aβ is the initiating molecule in the disease process (Hardy and Allsop, 1991; Selkoe, 1991). Indeed, familial AD is caused by highly penetrant mutations in genes that affect the release of Aβ from APP (*APP*, *PSEN1* and *PSEN2*), leading to increased production of its amyloidogenic forms, namely Aβ42. The dementia associated with Trisomy 21 and *APP* locus duplications causing the disease had reinforced this view. The genetic polymorphism in the *APOE* gene (allele ε4) is also believed to induce higher Aβ aggregation by interaction of apoE with Aβ in the process of its clearance (Biere *et al.*, 1995). Therefore, an increase in production of either total Aβ or the amyloidogenic $A\beta_{1-42}$ isoform is well established in familial AD, but only limited evidence exists for a specific disturbance in Aβ clearance in sporadic AD.

The amyloid hypothesis states that overproduction of Aβ, i.e. the imbalance between the production and clearance of Aβ in the brain, causing an increase in the Aβ levels, and its aggregation into senile plaques is a primary event in AD pathogenesis (Hardy and Selkoe, 2002). The original amyloid cascade hypothesis had proposed that the key event in AD development is

the extracellular accumulation of insoluble fibrillar Aβ, nevertheless the "extracellular insoluble Aβ toxicity" hypothesis was later modified to acknowledge the role of soluble Aβ oligomers as pathogenic agents (Klein *et al.*, 2004; Lesne *et al.*, 2006). In both familial and sporadic AD, soluble Aβ is believed to undergo a conformational change that causes its aggregation into soluble oligomers and the larger insoluble fibrils found in plaques. At the molecular level, the mechanisms underlying this conformational change are largely unknown but diffuse neurocentric amyloid deposits would evolve over time and eventually would become neuritic SP. The deposition of Aβ42 may form a "precipitation core" to which soluble Aβ40 could aggregate, in an AD-specific process. The *in vivo* aggregation of Aβ may originate a chronic and destructive inflammatory process in the brain, occurring in the immediate vicinity of SPs in AD patients' brains (Selkoe, 2001).

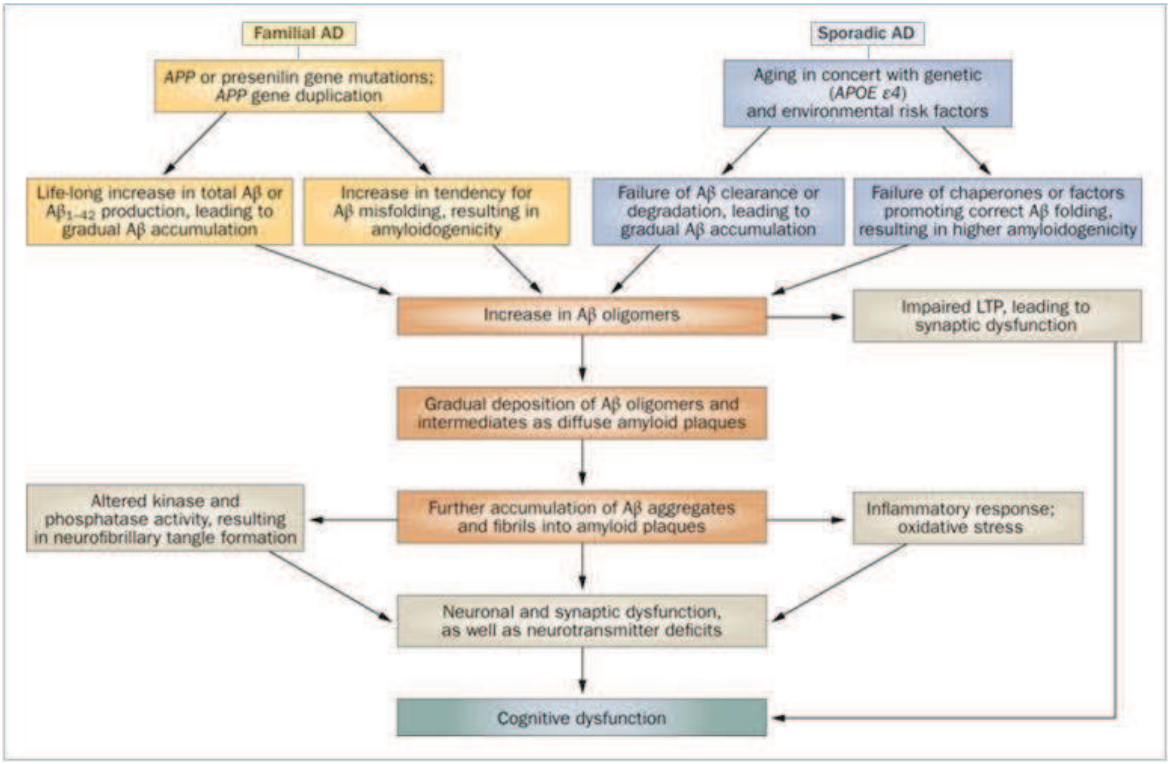

Figure I.4: The amyloid cascade hypothesis of AD. An imbalance between the production and clearance of Aβ in the brain, causing an increase in the level of the peptide, is the initiating event in AD, and ultimately leads to neuronal degeneration and dementia (Adapted from Blennow *et al.*, 2010).

Fibrillar Aβ deposited in plaques might be neurotoxic; however, synaptic loss and clinical progression of the disease mainly correlate with soluble Aβ levels. Subsequently, the gradual accumulation of aggregated Aβ initiates a complex, multistep cascade (Fig. I.4) that includes

gliosis, inflammatory changes, neuritic/synaptic change, NFTs and neurotransmitter loss (Selkoe, 2001). Data suggest that soluble Aβ oligomers might inhibit LTP in the hippocampus and, hence, disrupt synaptic plasticity. Tau phosphorylation and subsequent neurofibrillary tangle formation, as well as inflammation and oxidative stress, are regarded as downstream events.

The amyloid hypothesis generated testable predictions that have been the basis for most work on the pathogenesis of AD. Some predictions have been fulfilled and others have not been shown to be true. Therefore, undertstanding the normal physiological function of amyloid-β precursor protein is a major scientific need to unravel the disease process.

I.1.6 Current therapeutic approaches for AD

In addition to the impact on the lives of AD patients, their families and caregivers, AD is of major public health concern. Even though of symptomatic benefit, neither of the treatments available today stops the progression of the disease and efficient pharmacological treatment is needed. Two classes of medications are approved by North American and European Union regulatory criteria and marketed for AD: cholinesterase inhibitors (for example, donepezil [Aricept], galantamine [Razadyne], and rivastigmine [Exelon]) and the N-methyl-D-aspartate (NMDA)-receptor antagonist memantine (Namenda, Axura, Ebixa, etc.) (Hooli and Tanzi, 2009; Aisen *et al.*, 2012). These drug classes work on different but complementary neurochemical pathways; both are important in cortical information processing, and cognitive functions, especially memory, learning, attention, and stimulation. Hence, these drugs treat mainly the symptoms, with no known effects on disease progress (Aisen *et al.*, 2012).

Currently there are 75 drugs in clinical trials and other 200 or more in development. The drugs being developed are targeting different intra- and extra-cellular targets as well as different mechanisms of action. They include both symptomatic and disease modifying approaches. For example, dimebolin, which is currently in clinical trials, is a retired antihistamine that is thought to be neuroprotective based on mitochondria stabilization properties (Hooli and Tanzi, 2009). All four of the established AD genes lead to enhanced accumulation of Aβ42 in the brain (*APP*, *PSEN1* and *PSEN2* mutations increase Aβ production and *APOE* decreases Aβ clearance), most of the current AD therapies in development aim at either reducing Aβ42 production/aggregation or potentiating its degradation/clearance. Pharmaceutical approaches have focused primarily on inhibitors and modulators of the β- and γ-secretases, compounds that attenuate Aβ aggregation (for example, by preventing interaction of the peptide with copper and zinc), and anti-Aβ

immunotherapy aimed at stimulating the degradation of the Aβ peptide (Selkoe, 2007; Nitsch and Hock, 2008; Aisen *et al.*, 2012). Approaches aimed at modulating the abnormal aggregation of tau protein into neurofibrillary tangles, and those targeting metabolic dysfunction, are also being pursued (Citron, 2010).

I.2 THE AMYLOID PRECURSOR PROTEIN (APP)

I.2.1 APP isoforms and gene family

In 1984, Glenner and Wong isolated Aβ from deposits in blood vessels from AD brains and DS brains and provided a partial sequence (Glenner and Wong, 1984a, b). A year later, Aβ was identified as the main component of neuritic plaques in AD brain (Masters *et al.*, 1985). Shortly thereafter, the APP gene was cloned and shown to localize to chromosome 21 (Kang *et al.*, 1987).

APP is one of three members of a larger gene family. These include *APLP1* and *APLP2* in humans, *Appl* (fly), and *apl-1* (worm) (Coulson *et al.*, 2000). All genes encode type I membrane proteins with a large extracellular domain and a short cytoplasmic region that undergo similar processing (see below). Importantly, only *APP*, but not any of the other *APP* related genes, contains a sequence encoding the Aβ domain. Therefore, *APLP1* and *APLP2* are not the precursors of Aβ and if these two genes contribute to AD pathogenesis, then their roles must be indirect. *APP* and *APLP2* are ubiquitously expressed although alternative splicing generates isoforms that may be cell type specific. In contrast, *APLP1* is expressed selectively in the nervous system (Thinakaran and Koo, 2007).

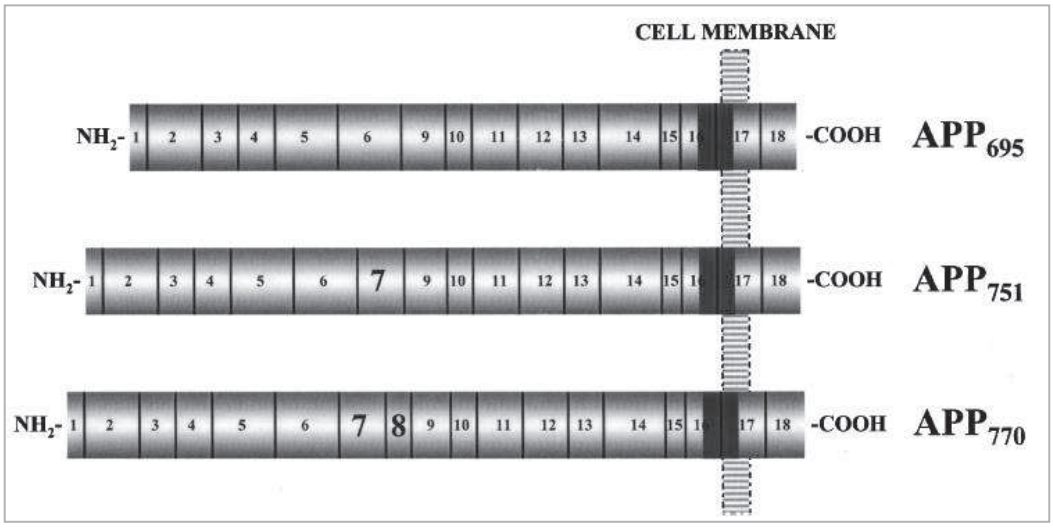

Figure I.5: Schematic representation of the predominant APP isoforms in mammalian tissues. Numbers indicate the corresponding exons. The most abundant neuronal isoform, comprising 695 amino acids, is APP_{695}. APP_{751} and APP_{770} are alternatively spliced isoforms that differ from APP_{695} in the expression of exons 7 and 8, as shown. The solid gray region represents the Aβ peptide (Adapted from da Cruz e Silva and da Cruz e Silva, 2003).

The human *APP* gene consists of 18 exons (Fig. I.5), spanning approximately 300 kb of genomic DNA with parts of exons 16 and 17 encoding the Aβ sequence (Yoshikai *et al.*, 1990; Rooke *et al.*, 1993). Alternative splicing of exons 7, 8 and 15 of the APP mRNA produces eight isoforms, ranging in size from 677-770 aminoacids (L-677, 695, L-696, 714, L-733, 751, L-752, 770) (Tanzi et al., 1993). The three major isoforms are APP_{695}, APP_{751} and APP_{770} (Palmert *et al.*, 1988; Sandbrink *et al.*, 1994). APP_{695} lacks exons 7 and 8, which encode the Kunitz protease inhibitor (KPI) domain (56-amino acid motif homologous to the Kunitz-type of serine protease inhibitors) and the MRC antigen OX-2 homologous domain (Kitaguchi *et al.*, 1988; Tanzi *et al.*, 1988). Exon 15 can also be spliced out generating an isoform that forms the core protein of the secreted chondroitin sulfate proteoglycans, appicans, named L-APP isoforms after their initial discovery in leucocytes (Konig *et al.*, 1992; Pangalos *et al.*, 1995).

APP is ubiquitously expressed in mammalian cells with a broad tissue distribution. The APP splice variant containing 695 amino acids is expressed at higher levels in neurons, whereas the 751- and the 770-residues isoforms are widely expressed in non-neuronal cells but also occur in neurons (Haass *et al.*, 1991; Sandbrink *et al.*, 1997). The ratio of APP 770:751:695 mRNA is 1:10:20 in cortex. However, in cultured astrocytes, the KPI-containing APP predominates, APP 770:751:695 mRNA ratio is 2:4:1 (Tanaka *et al.*, 1989; Turner *et al.*, 2003).

APP is a type I transmembrane glycoprotein originally predicted to be a type of cell surface receptor (Kang *et al.*, 1987). APP has a large extracellular amino-terminal domain and a small intracellular cytoplasmic domain (Fig. I.6). Within the extracellular domain the protein has a cysteine-rich subdomain close to the extreme amino terminus, followed by an acidic subdomain, and two other subdomains, one of which has been deduced to have a neuroprotective function (De Strooper and Annaert, 2000). Numerous other subdomains have also been identified on APP extracellular tail related with its attributed functions (Turner *et al.*, 2003).

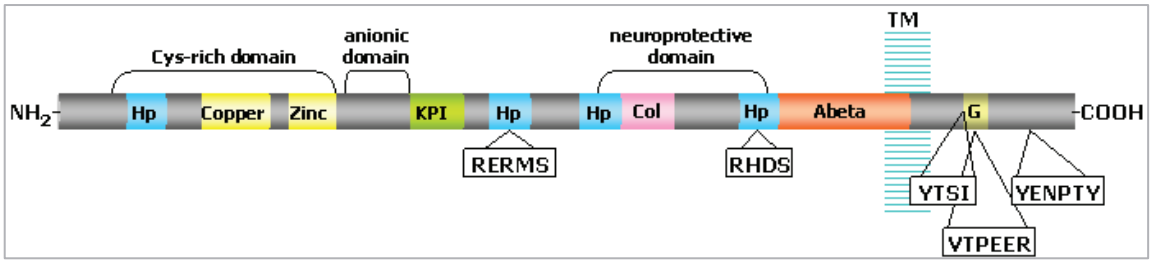

Figure I.6:. Structure of APP showing several functional domains and motifs. TM: membrane; Binding domains: Heparin (Hp), Copper, Zinc, Collagen (Col), G_o proteins (G).

I.2.2 Proteolytic processing of APP

Full-length APP undergoes sequential proteolytic processing, being first cleaved by α-secretase (non-amyloidogenic pathway; Fig. I.7.A) or by β-secretase (amyloidogenic pathway; Fig. I.7.B), resulting in the shedding of the ectodomain and generation of membrane tethered α- or β-C-terminal fragments (termed CTFα or C83; CTFβ or C99). γ-Secretase cleavage of C83 and C99 results in the generation of p3 and Aβ, respectively, as well as the APP intracellular domain (AICD) (reviewed in Turner *et al.*, 2003).

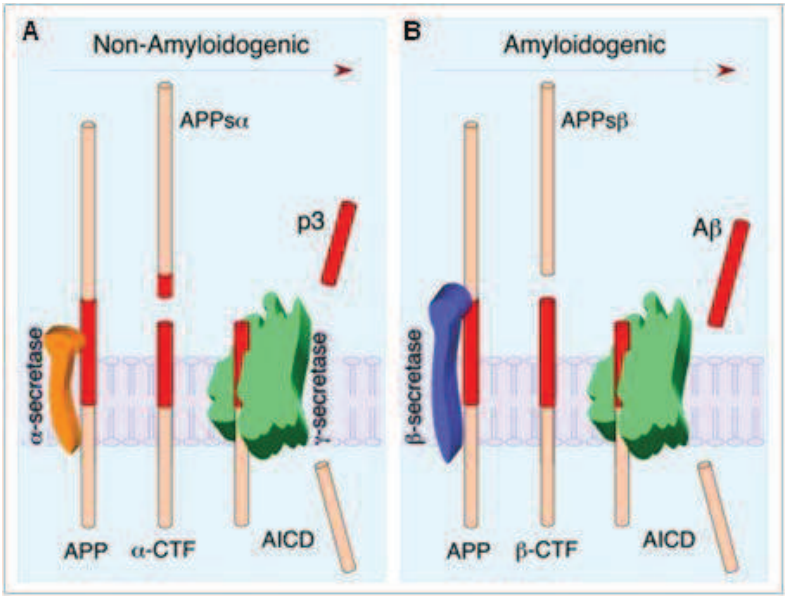

Figure I.7:. Proteolytic processing of APP. (A) Non-amyloidogenic processing of APP refers to sequential processing of APP by membrane-bound α- and γ-secretases. α-Secretase cleaves within the Aβ domain, thus precluding generation of intact Aβ peptide. (B) Amyloidogenic processing of APP is carried out by sequential action of membrane-bound β- and γ-secretases. CTF, C-terminal fragment (Adapted from Thinakaran and Koo, 2008).

A novel pathway for APP processing had been recently described, where α- and β-secretase pathways may converge to produce short carboxy-terminal truncated Aβ peptides, independent from γ-secretase, including Aβ1-14, Aβ1-15 and Aβ1-16 (Cook *et al.*, 2010; Portelius *et al.*, 2011).

β-Secretase

The major neuronal β-secretase is BACE1 (β-site APP cleaving enzyme), also known as Asp-2 or memapsin-2. BACE1 is a membrane tethered aspartyl protease that cleaves APP within the ectodomain, generating the N-terminus of Aβ (Vassar *et al.*, 1999). However, the principal BACE (β') cleavage site in native APP is between Glu +11 and Val +12 of the Aβ peptide (Fig. I.8). Amyloidogenic processing is the favoured pathway of APP metabolism in neurons largely due to the greater abundance of BACE1, and non-amyloidogenic pathway is predominant in all other cell types.

The relatively low affinity of BACE1 toward APP led to the suggestion that APP is not its sole physiological substrate. Indeed, several transmembrane proteins were reported as BACE1 substrates, such as Golgi-localized membrane-bound α2,6-sialyltransferase, P-selectin glycoprotein ligand-1 (PSLG-1), the APP homolog proteins APLP1 and APLP2, low-density lipoprotein receptor-related protein (LRP), the voltage-gated sodium channel (Na_v1) β2 subunit ($Na_v\beta_2$), neuregulin-1 (NRG1), and neuregulin-3 (NRG3) (Vassar *et al.*, 2009).

BACE1 activity increases with age (Nistor et al., 2007) and in AD-affected brains (Li et al., 2011).

α-Secretase

The activity of α-secretase is mediated by one or more enzymes from the family of disintegrin and metalloproteinase domain proteins (Lammich *et al.*, 1999), such as TACE/ADAM17, ADAM9, ADAM10 and MDC-9, also by and an aspartyl protease, BACE2. APP cleavage at, or near, the α-secretase site, located within the Aβ domain (between residues Lys16 and Leu17 of the Aβ peptide; Fig. I.8), precludes the generation of intact Aβ (Allinson *et al.*, 2003).

Besides APP, α-secretase also cuts several others transmembrane proteins such as pro-TNFα and pro-TGFα (Buxbaum *et al.*, 1998).

γ-Secretase

The second proteolytic event in APP processing involves intramembranous cleavage of α- and β-CTFs by γ-secretase, that liberates p3 (3 kDa) and Aβ (4 kDa) peptides, respectively, into the extracellular milieu. γ-Secretase is a membrane embedded multiprotein complex with presenilin-1 or -2 (PSEN1 or PSEN2), as the catalytic component. Besides presenilin, which is an unusual intramembranous aspartyl protease (Wolfe *et al.*, 1999), the other members of the γ-secretase complex are the membrane proteins nicastrin, APH1, and PEN2 (Haass, 2004). Protein subunits of the γ-secretase complex assemble early during biogenesis and cooperatively mature as they leave the endoplasmic reticulum. APH-1 and PEN2 are thought to stabilize the γ-secretase complex and nicastrin to mediate the recruitment of APP CTF to the catalytic site of the γ-secretase (Wolfe, 2008a).

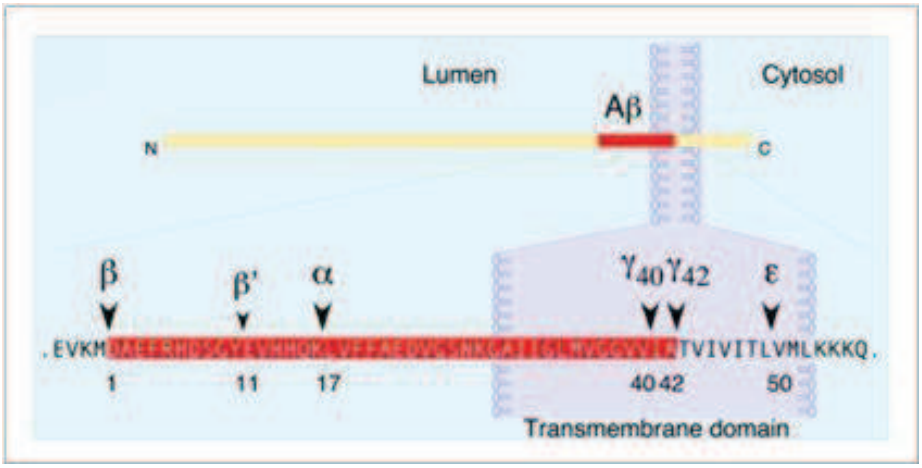

Figure I.8:. The major sites of APP cleavage by α-, β-, and γ-secretases are indicated, along with Aβ numbering from the N terminus of Aβ (Asp-1) (Adapted from Thinakaran and Koo, 2008).

γ-Secretase cuts within the transmembrane domain of APP CTF and determines the length of Aβ peptides. The major sites of γ-secretase cleavage correspond to positions 40 and 42 of Aβ (Fig. I.8). Nevertheless, the 40-residue peptide is the predominant and Aβ42 accounts for less than 10% of total Aβ. Moreover, minor amounts of shorter Aβ peptides such as Aβ38 and Aβ37

have also been detected. γ-secretase cleavage at a distal ε-site (Fig. I.8) generates a cytoplasmic polypeptide, termed APP intracellular domain (AICD) (Thinakaran and Koo, 2008).

Additional secretase activities had been described in intermediate positions, between the γ- and ε-sites, such as the δ- and ζ-sites (Zhao *et al.*, 2004). ζ-cleavage is another PS-dependent cleavage within the transmembrane domain of APP that leads to Aβ46 generation, which recently has been suggested as a previous step to Aβ40 and Aβ42 generation (Zhao *et al.*, 2007).

The different Aβ species are proposed to be produced by γ-secretase cleavage of APP CTFs in a stepwise manner starting at the ε-site and then cleaving approximately every third residue via the ζ-site to the γ-site (Qi-Takahara *et al.*, 2005). Importantly, Aβ40 and Aβ42 are suggested to be generated through independent production lines. The ε-cleavage might occur before proteolysis at the γ-site. Indeed, analysis of intracellular Aβ reveals a small but significant amount of longer forms of this peptide, up to Aβ49, which is the proteolytic counterpart to the 50-residue AICD. This model of processive proteolysis of APP transmembrane domain by γ-secretase, beginning at the ε-cleavage site and cleaving every three residues explains how reduction of proteolytic function due to presenilin mutations might lower Aβ peptide production but increase the ratio of Aβ42 to Aβ40. Longer forms of Aβ, including most of the hydrophobic transmembrane domain, might be more likely to be retained in the active site of the protease, whereas the shorter forms are more likely to be released. Less catalytically efficient γ-secretase complexes would allow more time for the release of longer Aβ peptides. In addition, AD-causing presenilin mutations shift the initial ε-cleavage site to produce more Aβ48, which would lead to Aβ42 (Xu, 2009).

Presenilin catalytic function is required for intramembraneous γ-secretase cleavage of several type I membrane proteins other than APP, such as the Notch1 receptor and its ligands, Delta and Jagged2, cell-surface adhesion protein CD44, the receptor tyrosine kinase ErbB4, netrin receptor DCC, LRP, lipoprotein receptor ApoER2, cell adhesion molecules N- and E-cadherins, synaptic adhesion protein nectin-1α, cell surface heparin sulfate proteoglycan syndecan-3, p75 neurotrophin receptor, etc (Koo and Kopan, 2004). Uniformly these substrates all undergo an ectodomain shedding by α-secretases, which in many cases is triggered by the binding of extracellular ligands. On the other hand, several noncatalytic γ-secretase-independent functions have been assigned to presenilins, such as regulation of intracellular calcium homeostasis, neuronal signaling, protein trafficking, protein degradation, fine-tuning of the immune system, neurite outgrowth, apoptosis, memory and synaptic plasticity (Sisodia *et al.*, 1999; Koo and Kopan, 2004; Wakabayashi *et al.*, 2007).

Additional reports have revealed that APP can also be proteolytic processed at it C-terminus by caspases like caspase-3, caspase-6, caspase-7 or caspase-8 (Gervais et al., 1999; Pellegrini et al., 1999; Soriano et al., 2001). *In vitro* assays identified a major caspase cleavage site at Asp-664 (VEVD; APP_{695} numbering) (Weidemann et al., 1999). The resultant C-terminus peptide, termed C31 is a potent inducer of apoptosis, and this cleavage was shown to reduce APP internalization and to have varying effects on the Abeta secreted levels (Lu *et al.*, 2000; Soriano *et al.*, 2001).

I.2.3 Intracellular trafficking

The APP proteins mature in the endoplasmic reticulum (ER) and Golgi (G) apparatus and undergo post-translational modifications, such as phosphorylation, glycosylation and sulfation (Weidemann et al., 1989; Godfroid and Octave, 1990). In fact, APP is a sialoglycoprotein that is post-translationally modified through the constitutive secretory pathway (Georgopoulou et al., 2001). Following protein synthesis on membrane-bound polysomes APP is transported to the ER where it undergoes N-glycosylation and is then transported to the Golgi, where it goes through N- and O-glycosylation, phosphorylation, and tyrosine sulfation (Oltersdorf et al., 1990; Caporaso et al., 1992; Hung and Selkoe, 1994). APP can be packaged into secretory vesicles in the *trans*-Golgi network (TGN) and delivered to the plasma membrane (PM). In cultured cells, it is estimated that only about 10% of nascent APP molecules are successfully delivered to the PM. Cell surface APP may be cleaved to sAPP or reinternalized into the endocytic pathway (Koo et al., 1996; Yamazaki et al., 1996).

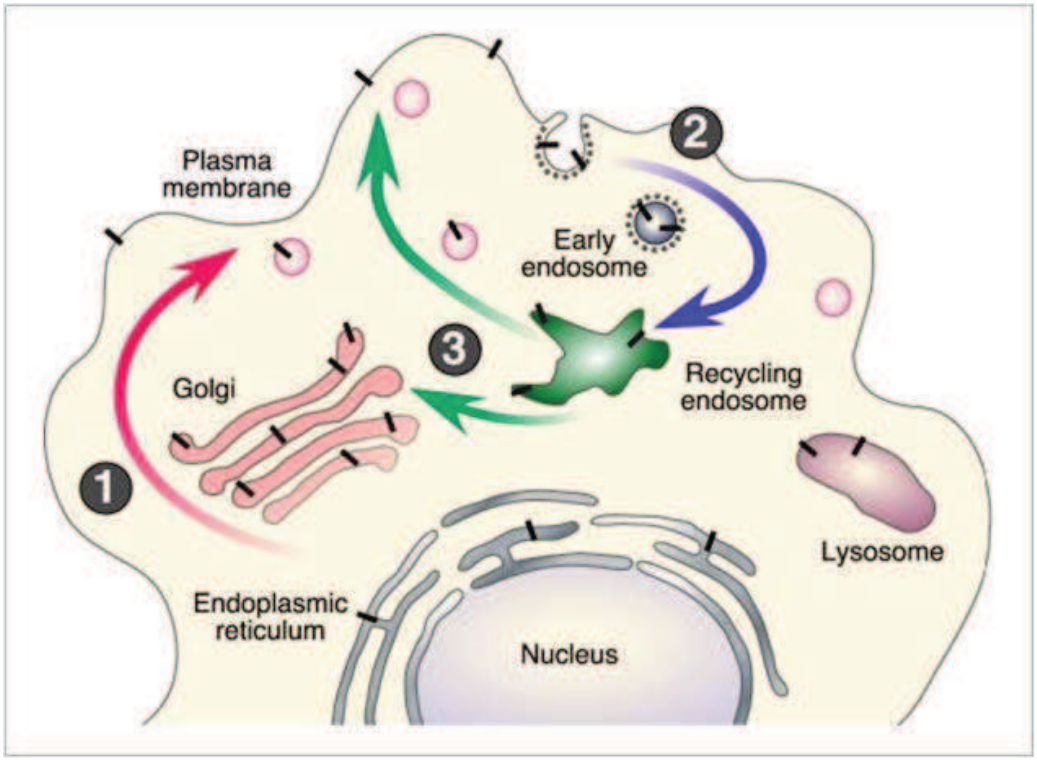

Figure I.9: Intracellular trafficking of APP. Nascent APP molecules (*black bars*) mature through the constitutive secretory pathway (*step 1*). Once APP reaches the cell surface, it is rapidly internalized (*step 2*) and subsequently trafficked through endocytic and recycling compartments back to the cell surface (*step 3*) or degraded in the lysosome. Non-amyloidogenic processing occurs mainly at the cell surface, where α-secretases are present. Amyloidogenic processing involves transit through the endocytic organelles, where APP encounters β- and γ-secretases (Adapted from Thinakaran and Koo, 2008).

APP trafficking is tightly regulated and the protein can be proteolytically processed at the cell surface mainly by α-secretases, resulting in the shedding of sAPPα ectodomain (Sisodia, 1992). Activation of protein kinase C increases sAPPα secretion by mechanisms involving the formation and release of secretory vesicles from the trans-Golgi network, thus enhancing APP trafficking to the cell surface (Caporaso et al., 1992; da Cruz e Silva et al., 1993). Approximately 70% of surfacebound APP is internalized within minutes of arriving at the plasma membrane. The ^{682}YENPTY^{687} internalization motif at APP C-terminus (APP_{695} isoform numbering) is responsible for this efficient internalization. Following endocytosis, APP is delivered to late endosomes and a fraction of endocytosed molecules is recycled to the cell surface (Fig. I.9) or APP can also undergo degradation in the lysosome (Small and Gandy, 2006). APP retrieval to the TGN is mediated by the retromer protein complex. This recycling pathway is enhanced by direct APP phosphorylation

at its cytoplasmic Ser-655 residue, which lies in the ^{653}YTSI^{656} (human APP_{695} isoform numbering) basolateral sorting motif, at APP C-terminus (Vieira *et al.*, 2010).

BACE1 predominantly localizes to the late Golgi/TGN and endosomes, consistent with amyloidogenic cleavage of wild-type APP during endocytic/recycling steps (Koo and Squazzo, 1994). Active γ-secretase was detected in multiple compartments, including the ER, ER-Golgi intermediate compartment (ERGIC), Golgi, TGN, endosomes, and plasma membrane. Studies conducted in non-neuronal and neuroblastoma cell lines show that Aβ is generated mainly in the TGN and endosomes as APP is trafficked through the secretory and recycling pathways. Evidence converging from a number of studies also indicates that amyloidogenic processing occurs in cholesterol- and sphingolipid-enriched membrane raft microdomains of intracellular organelles (Riddell *et al.*, 2001; Ehehalt *et al.*, 2003; Vetrivel *et al.*, 2005).

In the brain, where BACE1 is highly expressed, APP is preferentially processed trough the amyloidogenic pathway. Moreover, in neurons, APP is transported anterogradely along peripheral and central axons and proteolytically processed during trafficking (Koo *et al.*, 1990). Axonal transport of APP is thought to be mediated by direct or indirect binding of APP to the kinesin light chain subunit of kinesin-1. It has also been proposed that APP may represent a kinesin cargo receptor, linking kinesin-1 to a unique subset of transport vesicles (Kamal *et al.*, 2001). However, this notion remains highly controversial (Lazarov *et al.*, 2005). Nevertheless, the intracellular organelles/transport vesicles where Aβ is generated in neurons are not fully characterized.

I.2.4 APP function

Despite advances in our understanding of the role of APP processing in AD, the *in vivo* function(s) of the molecule remain unclear. *APP* knockout (KO), knockdown and transgenic phenotypes in different organisms have provided clues to physiological functions of the APP protein family. Moreover, information from APP functional domains and motifs, the discovery of APP interacting proteins and gene expression profiling have led to the identification of putative pathways for APP associated with cellular and developmental changes.

I.2.4.1 APP knockouts and transgenics

In *Caenorhabditis elegans*, deletion of one copy of the *APP* orthologue *apl-1* caused pharyngeal pumping defects, while loss of both copies led to larval lethality (Zambrano *et al.*, 2002; Hornsten *et al.*, 2007). This lethality could be rescued by neuronal expression of the APL-1 ectodomain, which indicates that APP plays a role in development through its extracellular domain (Hornsten *et al.*, 2007). In *Drosophila*, deletion of the single APP-like gene (*appl*) resulted in only subtle behavioral defects that could be rescued by wild-type but not mutant APPL or APP (Luo *et al.*, 1992), and a later study suggested that deletion and mutation affects kinesin-mediated axonal transport and neuronal viability (Gunawardena and Goldstein, 2001).

In mice, single KOs of APP gene family members were viable, but exhibited impaired spatial learning and long-term potentiation (LTP). These deficits could be rescued by a knock-in allele of sAPPα, indicating that the ectodomain of APP is sufficient for APP function in the adult mouse brain (Ring *et al.*, 2007). Conversely, the APP-APLP2 and APLP1-APLP2 double KO or APP-APLP1-APLP2 triple KO resulted in loss of viability. APP-APLP2 double KO mice displayed neuromuscular junction defects (Wang *et al.*, 2005), whereas the triple KO has neuronal ectopias resembling type II lissencephaly (Herms *et al.*, 2004). These findings demonstrated the importance of the APP family in development, and suggest functional redundancy consistent with a role in neuronal cell adhesion and migration. Interestingly, APP KO phenotypes are similar to those seen knocking out Fe65 (an AICD interacting protein), in worms (Zambrano *et al.*, 2002), or the double Fe65-Fe65L1 KO in mice (Guenette *et al.*, 2006). This suggests that APP and Fe65 are involved in a common developmental pathway.

Transgenics have also elucidated APP potential physiological roles. In *Drosophila*, overexpression of APP family members affected the development of the peripheral nervous system and displayed Notch gain-of-function phenotypes, possibly due to the interaction of APP with Numb, a negative regulator of Notch signaling (Merdes *et al.*, 2004). Additionally, APP and Notch can interact directly through their transmembrane domains (Fassa *et al.*, 2005; Oh *et al.*, 2005). Transgenic APP flies also showed increased axonal arborization, which depends on the cytosolic domain of APP and its interaction with c-Abl (Leyssen *et al.*, 2005).

APP transgenic mice mostly recapitulated AD genetic data. Mice with APP mutant transgenes developed amyloid plaque pathology, and this pathology was enhanced by crossing them with mice with mutant presenilin transgenes. However, APP transgenic mice neither developed extensive neuronal loss nor exhibit tangle pathology (LaFerla and Oddo, 2005). Crossing the APP mice with plaque pathology with the mutant tau mice potentiated the tangle pathology but had no effect on the plaque pathology, which suggested that, in the pathological cascade, the Aβ/amyloid pathology is upstream to the tau/tangle pathology (Hardy *et al.*, 1998).

A later study showed that pathological, physiological and behavioral deficits in APP-transgenic mice were not observed in those with a mutation at the caspase-cleavage site of APP, but still produce Aβ and amyloid deposits (Galvan *et al.*, 2006). This suggests a role for the APP intracellular domain and possibly for the caspase-released cytosolic tail in the pathogenesis of AD.

I.2.4.2 APP physiological roles

A number of functional domains have been mapped to the extra- and intracellular regions of APP (Fig. I.6), which include: metal binding (copper and zinc); extracellular matrix binding (heparin, collagen, and laminin); neurotrophic and adhesion domains; and protease inhibition (the Kunitz protease inhibitor domain present in APP_{751} and APP_{770} isoforms). Zn(II)-binding is assumed to play a structural role, whereas APP was shown to catalyse the reduction of Cu(II) to Cu(I) (Multhaup *et al.*, 1994; Maynard *et al.*, 2005).

Initial reports speculated that APP was a cell-surface receptor that transduces signals within the cell in response to an extracellular ligand (Kang *et al.*, 1987; Kimberly *et al.*, 2001), but until recently, extracellular ligands have not been identified. Several physiological roles have been attributed to APP, such as regulation of neuronal survival, neurite outgrowth, synaptic plasticity and cell adhesion (Mattson, 1997; Turner *et al.*, 2003).

Cell adhesion

It has also been suggested that APP may have CAM (Cell Adhesion Molecule) and SAM (Substrate Adhesion Molecule) like activities. Several domains in APP extracellular tail promote binding to extracellular matrix proteins, such as heparin and collagen (Fig. I.6), which implicate cell-surface APP in cell-substrate adhesion (Breen, 1992; Multhaup, 1994; Beher *et al.*, 1996). The

most C-terminus heparin-binding contains the ^{676}RHDS^{679} (APP_{770} numbering) sequence, which is an integrin-binding motif (Ghiso *et al.*, 1992). In fact, APP colocalizes with integrins on the surface of axons and at sites of adhesion (Storey *et al.*, 1996; Yamazaki *et al.*, 1997). Evidence of interaction with laminin and collagen provides further evidence of adhesion-promoting properties (Ho and Sudhof, 2004). Homo- and heterodimerization between the APP family members in adjacent cells has also been suggested to promote intercellular adhesion (Soba *et al.*, 2005), analogous to that of known cell adhesion molecules such as cadherins and nectins.

Furthermore, binding of the APP heparin binding domain to heparan sulfate proteoglycan glypican-1 stimulates neurite outgrowth and the latter has been proprosed as an APP ligand (Qiu *et al.*, 1995; Williamson *et al.*, 1996). It is difficult to separate the cell adhesion from the neurite outgrowth roles of APP, since neuronal migration, neurite outgrowth, and even synaptogenesis involve substrate adhesion. Consistently, APP is required for migration of neuronal precursors to the cortical plate; furthermore, this activity is mediated by Dab1 acting downstream of APP (Young-Pearse *et al.*, 2007). The phenotypes of APP/APLP KOs are in agreement with these proposed physiological activities of APP.

Trophic properties

A trophic role for APP has been the best established function for the molecule. Initial evidences of APP function came from knocking down APP levels in fibroblasts (Saitoh *et al.*, 1989). These cells showed growth retardation that could be restored by treatment with sAPP. The active domain was subsequently mapped to the pentapeptide domain ^{403}RERMS^{407} (APP_{770} numbering) in the APP ectodomain (Ninomiya *et al.*, 1994). Infusion of this pentapeptide as well as sAPP into brain resulted in increased synaptic density and improved memory retention in animals (Yamamoto *et al.*, 1994; Meziane *et al.*, 1998). In fact, the APP ectodomain released through α-secretase has neurotrophic and neuroprotective properties (Furukawa *et al.*, 1996; Meziane *et al.*, 1998), but the underlying molecular mechanisms and a potential receptor for APP remain to be identified. Conversely, the APP ectodomain released through β-secretase cleavage appears to have a proapoptotic function, at least during early development, by binding and activating the death receptor 6 (DR6) on neurons (Nikolaev *et al.*, 2009). Since sAPP is constitutively released from cells following α-secretase cleavage, these findings indicated that APP has autocrine and paracrine functions in growth regulation.

APP has been shown to stimulate neurite outgrowth in a variety of experimental models. This phenotype is compatible with the up-regulation of APP expression during neuronal maturation (Hung *et al.*, 1992). Brain injury also increases APP expression, which suggests that APP plays a repair role in this context (Graham *et al.*, 1996). The correlation of AD with head trauma may reflect an increase in APP expression (causing adversely an increase in Aβ generation).

The N-terminal heparin-binding domain of APP also stimulates neurite outgrowth and promotes synaptogenesis (Fig. I.6). Interestingly, the crystal structure of this domain shows similarities to known cysteine-rich growth factors (Rossjohn *et al.*, 1999). Moreover, in adult rodent brains, sAPPα acts as a cofactor with EGF to stimulate the proliferation of EGF-responsive neural stems cells in the subventricular zone (Caille *et al.*, 2004).

Several studies have also demonstrated a role for sAPP in regulating stem cells. Indeed, sAPPα induces the differentiation of neural stem cells into astrocytic lineage (Kwak *et al.*, 2006).

APP and its intracellular binding partner, Fe65, have also been reported to influence cell motility, and several regulators of actin dynamics (transgelin, α2-actin) were recently found to be regulated by AICD (Sabo *et al.*, 2001, 2003; Guenette *et al.*, 2006; Muller *et al.*, 2007).

APP as a putative receptor

Given the APP structure as a type I integral membrane protein, which resembles a membrane-anchored receptor molecule, several studies demonstrated that full-length APP could function as a cell surface G-protein-coupled receptor (Okamoto et al., 1995). Despite being controversial, these results demonstrated that APP binds to heterotrimeric G proteins (Go), involved in signal transduction.

The idea that APP functions as a receptor arose from analogy with the Notch receptor signaling, which was found to undergo a proteolytic processing pathway that is remarkably similar to that of APP (Annaert and De Strooper, 1999; Selkoe and Kopan, 2003). Notch is a type I transmembrane receptor involved in differentiation events during development and adulthood. Activation of the Notch heterodimer by binding of its ligands Delta1 or Jagged1, presented by neighboring cells, induces Notch processing. Notch is initially cleaved by ADAM metalloproteases, ADAM10 or ADAM17, similarly to APP in the α-secretase pathway, followed by γ-secretase intramembrane cleavage (De Strooper *et al.*, 1999). An additional γ-secretase cleavage occurs at Notch S3-site corresponding to the ε-site of APP, releasing an intracellular domain (De Strooper

et al., 1999; Sastre *et al.*, 2001). Both the Notch Intracellular Domain (NICD), and the APP intracellular domain (AICD) can translocate to the nucleus (Cupers *et al.*, 2001) and interact with transcription factors to control gene expression. The AICD fragment is extremely small when compared with the NICD and lacks motifs commonly found in transcriptional regulators, suggesting that it may function in signaling in a different way, specifically by interaction with other proteins, forming multimeric active complexes or by activating transcription in an indirect manner.

The role of AICD in transcription has been controversial and APP proteolysis was even suggested as a degradative mechanism for turning off normal APP functions. γ-Secretase, which cleaves many type I integral membrane proteins, was even compared to a proteasome of the membrane (Kopan and Ilagan, 2004). Nevertheless, in addition to APP and Notch, γ-secretase cleaves more than 60 other substrates (McCarthy *et al.*, 2009) within their transmembrane domains, by a highly conserved process, called regulated intramembrane proteolysis (RIP) (Brown *et al.*, 2000; Lichtenthaler and Steiner, 2007). RIP controls the activity of membrane proteins and is required for signal transduction and diverse cellular processes, such as cell differentiation, transcriptional regulation, axon guidance, neurite outgrowth, cell adhesion, lipid metabolism, cellular stress responses and the degradation of transmembrane protein fragments. In animals, RIP is essential for a variety of physiological processes, such as embryonic development, the normal functioning of the immune system and the nervous system. The RIP process appears to be tightly regulated, and a deregulation of RIP is associated with diseases, such as AD and cancer (Lichtenthaler *et al.*, 2011).

Recent reports have demonstrated the role of the cytosolic fragment of APP in the regulation of gene expression, and several AICD-target genes were identifiued (detailed in Section I.3.3). Nuclear signaling of AICD was also shown to occur predominantly through the amyloidogenic pathway of APP, and through the neuronal 695 isoform, providing evidences for a role of AICD nuclear signaling in AD pathology (Konietzko, 2011).

Until recently, the search for APP ligands had not been successful, although several molecules were proposed, e.g. fibrillar forms of Aβ were reported to bind to cell-surface APP, exerting neurotoxicity (Lorenzo *et al.*, 2000). Proteins interacting with the extracellular domain of APP and were suggested to have a role in signaling events. However, unlike the cytoplasmic C-terminus of APP, the N-terminus is surprisingly devoid of known specific neuronal interacting proteins. Candidate interacting proteins thus far known include ApoE (Barger and Harmon, 1997)

and the most recently identified F-spondin. F-spondin, a secreted neuronal protein involved in cell-cell interactions, was identified as an extracellular ligand for APP. F-spondin expression prevents shedding of the APP ectodomain by β-secretase and reduces Aβ production (Ho and Sudhof, 2004).

Another APP ectodomain binding protein is reelin, an extracellular matrix protein essential for cortical development that shares homology with F-spondin. Reelin was shown to increase APP binding to Dab1, a reelin signaling mediator (Hoe *et al.*, 2006). Moreover, reelin is depleted in the entorhinal cortex of *APP*-transgenic mice and AD brains (Chin *et al.*, 2007). The Nogo-66 receptor, implicated in axonal sprouting in the adult CNS, has also been reported to interact with the APP ectodomain and inhibit Aβ production (Park *et al.*, 2006). LRP and SORL1 (SorLA, LR11) also bind to the APP ectodomain and influence Aβ production (Andersen *et al.*, 2005; Bu *et al.*, 2006).

The cell adhesion molecule TAG1 (transient axonal glycoprotein I) was discovered to act as a binding partner for full-length APP (Ma *et al.*, 2008). TAG1 binding to APP induced APP processing (preferentially through α- and γ-secretase). Both TAG1- and APP-deficient animals showed more neuroprogenitor cells than did wild-type animals. In this proposed pathway, it is the release of AICD that suppresses neurogenesis in a pathway that may be dependent on the binding to Fe65 because the NPTY motif of AICD is required. These findings demonstrate a critical role of TAG1–APP signaling in brain development and suggest the potential involvement of TAG1 in adult neuroplasticity and pathogenesis of Alzheimer's disease.

APP plays essential roles in the development of the nervous system, however APP signaling pathways and their activation/regulation are not fully elucidated.

I.3 APP INTRACELLULAR DOMAIN (AICD)

I.3.1 AICD production and degradation

As already described (Section I.2.2), γ-secretase-mediated cleavage of APP CTF releases AICD (Passer et al., 2000), specifically the ε-cleavage of APP in the cytosol, close to the inside membrane leaflet (Gu et al., 2001; Sastre et al., 2001; Weidemann et al., 2002). The 50-residue AICD was detected by mass spectroscopy in neuroblastoma cells, corresponding to aa 50-99 of C99 (or CTFβ) (Yu et al., 2001). It appears that ε-cleavage occurs before γ-cleavage, since C59 and C57 have not been detected and in turn, Aβ48 and Aβ49 are processed into Aβ40 and Aβ42 in cells (Funamoto et al., 2004).

Initially it was thought that γ- and ε-cleavages could result from the same proteolytic activity, because presenilin mutations, presenilin KO or presenilin inhibitors affected the production of both Aβ42 and AICD (Qi-Takahara et al., 2005; Kakuda et al., 2006). However, evidences arose of independent γ- and ε-cleavages, such as presenilin or APP mutations that could trigger opposite effects on Aβ and AICD productions (Chen et al., 2002). Moreover, it appears that Aβ and AICD are differently regulated by intracellular proteins, such as the APP-binding protein Fe65 that increases AICD production and concomitantly reduces Aβ42 formation (Wiley et al., 2007), suggests that ε-cleavage is a limiting step and controls γ-clevage (Pardossi-Piquard and Checler, 2012).

Both C83 and C99 undergo subsequent cleavage by γ-secretase and therefore, can be potential precursors of AICD. However, AICD is mainly produced via the amyloidogenic pathway. Acidic proteases as is the γ-secretase complex, are more active in a lower pH environment, (Checler, 2001), and ε-cleavage is also modulated by pH changes, suggesting that AICD production is more likely associated with endosomal/lysosomal pathway (Fukumori et al., 2006; Vingtdeux et al., 2007b). Moreover, Goodger et al. (2009) recently showed that AICD nuclear signaling occurs predominantly through the amyloidogenic pathway of APP cleavage, and another report confirmed that β- and γ-secretase inhibitors but not α-secretase blockers abolished AICD-mediated function (Belyaev et al., 2010).

AICD is usually poorly detectable in cells and human tissues due to its extreme lability, having a very rapid turnover (around 5 minutes) (Cupers et al., 2001), which presents a difficulty in establishing a physiological role for AICD. However, AICD was initially detected by MALDI mass spectroscopy in sporadic AD brains (Passer et al., 2000). Once produced, AICD undergoes rapid inactivation by the insulin-degrading enzyme insulysin, which is mainly cytosolic and endosomal (Edbauer et al., 2002; Venugopal et al., 2007). Interestingly, insulysin levels decrease with aging in the hippocampus of human brains as well as in transgenic mice models of AD (Caccamo et al., 2005). Therefore, in the aging brain there is increased β-secretase processing of APP (section I.2.2), leading to increased C99 formation, and concomitantly lowered insulysin-mediated degradation of AICD, which would lead to increased AICD (and Aβ) production, contributing to AD pathology.

Finally, degradation of AICD can also occur via caspase cleavage, however it is not clear if the caspase substrate is AICD, FL APP or a membrane-bound CTF. Processed of APP C-terminal tail by caspase-3 releases a cytotoxic fragment referred to as C31 (Lu et al., 2000).

I.3.2 AICD functional motifs

The functions attributed to AICD are related either to its phosphorylation state or to interactions with other proteins. The carboxy-terminus of APP contains three functional motifs corresponding to phosphorylation sites, critical for interaction with binding proteins that are thought to regulate the rate of APP secretion, endocytosis, and Abeta production (da Cruz e Silva *et al.*, 2004a). The ^{653}YTSI^{656} (APP_{695} isoform numbering) sequence matches YXXI tyrosine-based internalization and/or basolateral sorting signal. The motif ^{667}VTPEER^{672}, containing the Thr-668, which is important for controlling interactions with APP binding proteins. The ^{682}YENPTY^{687} motif, which is absolutely conserved across APP homologues and across species (Fig. I.10), contains a NPXY internalization signal, which is found in several cell surface proteins, including growth factor receptors, transporters and adhesion molecule receptors.

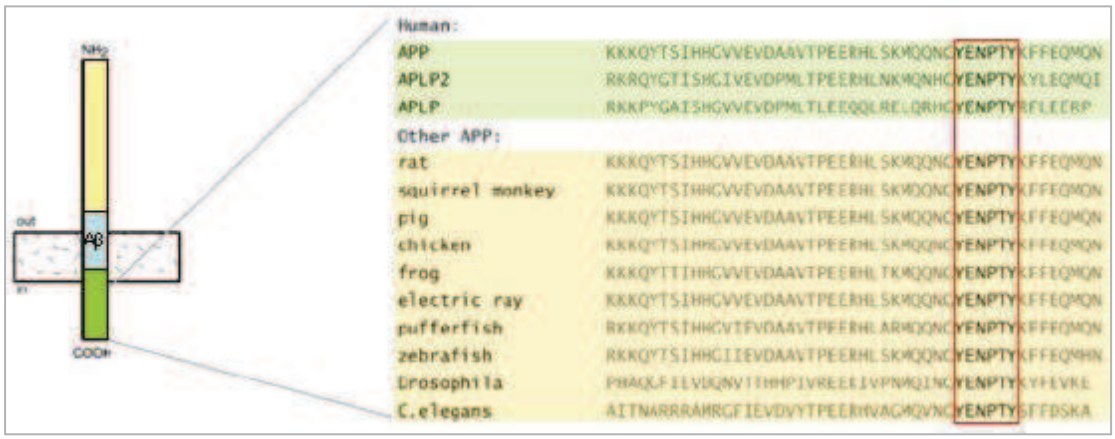

Figure I.10: The short cytoplasmic tail of APP and its homologues contains the YENPTY sequence, which is phylogenetically conserved (Adapted from Sabo and Ikin 2002).

The NPXY sequence was first identified as the sequence required for internalization of LDL receptors. In some cases, NPXY motifs are required for anchoring of receptors in clathrin-coated pits (Chen et al., 1990). NPXY motifs are also important for the function of some molecules, e.g. in insulin-like growth factor receptors. The NPXY motif is required for efficient ligand-mediated internalization and biological signaling (Hsu et al., 1994). In the cytoplasmic tail of integrin β3 the NPXY sequence is essential for post-ligand-binding events involved in cell migration (Filardo et al., 1995). Furthermore, the NPXY motifs found in many integrin β subunits regulate the affinity for their ligands. Interestingly, an NPXY sequence in the integrin β1 cytoplasmic domain is required for localization to focal adhesions (Reszka et al., 1992), which in turn is necessary for integrins accurate functioning. In the EGF receptor, tyrosine phosphorylation of NPXY is required for recognition by Shc and subsequent signaling (Russo et al., 2002).

The YENPTY sequence was also demonstrated to be important in the regulation of APP processing and trafficking (Lai *et al.*, 1995; Rebelo *et al.*, 2007a). APP deletions within the YENPTY sequence results in increased secretion of sAPP and decreased secretion of Aβ (Koo and Squazzo, 1994). The effects of these deletions are thought to be the result of altered internalization of APP from the cell surface. Mutation of the second tyrosine in the YENPTY sequence to alanine also increases sAPP secretion but has no effect on Aβ secretion (Jacobsen et al., 1994), suggesting that secretion of Aβ and sAPP may be regulated independently by signals in the cytoplasmic tail of

APP. These observations bring together the AICD YENPTY-dependent regulation and the AICD role in AD.

I.3.3 Phosphorylation of AICD

Protein phosphorylation is a major control mechanism of eukaryotic organisms, allowing for rapid and reversible regulation of multiple protein activities in response to diverse environmental and developmental changes. Protein phosphorylation is a reversible process in which a protein kinase transfers a phosphate group from ATP to a substract, thus altering the substrate's conformation and function. A protein phosphatase removes the phosphate and the protein reverts to its dephosphorylated state. The phosphorylation state of a single protein depends on the balance between the highly regulated cellular activities of multiple protein kinases and protein phosphatases.

As knowledge on the molecular basis of AD expands, interest on protein phosphorylation continues to increase, as misregulation of normal phosphorylation/dephosphorylation control mechanisms is found to underlie an increasing number of pathologies. Since so many diseases have at their core a deficiency in cellular signaling involving protein phosphorylation, kinases have for some time been considered viable targets for the design of novel therapeutics, contrary to phosphatases, that only recently have started to be considered targets for the development of therapeutic strategies (da Cruz e Silva *et al.*, 2004a).

Brain aging is characterized by a progressive decline in cognitive functions and memory loss. Protein phosphorylation may be one of the fundamental processes associated with memory and brain function, playing a role in the processing of neuronal signals and in the short-term or long-term modulation of synaptic transmission. In neurodegenerative disorders such as AD there is evidence for abnormal regulation of protein phosphorylation, which appears to contribute to the disease condition (Wagey and Krieger, 1998).

The high levels of protein kinases and phosphatases in the brain suggest that phosphorylation is critically important in brain function. Misregulation of the cellular phosphorylation system has been reported to occur in AD. These include abnormalities in both expression and activity levels of kinases, and/or phosphatases, thus leading to alterations in the processing of APP and Abeta production (Gandy *et al.*, 1993; da Cruz e Silva *et al.*, 1995). For instance, altered activities of protein kinase C (PKC), decreased activity of phosphatases PP1 and PP2A, overexpression of calcineurin mRNA levels, protein tau and β-tubulin hyperphosphorylated

state have all been associated with AD (Gong *et al.*, 1993; Matsushima *et al.*, 1996; Bennecib *et al.*, 2000; Vijayan *et al.*, 2001; da Cruz e Silva and da Cruz e Silva, 2003). Concomitantly, many proteins that are relevant to AD, including APP, tau, presenilin-1 and presenilin-2, or BACE, are phosphoproteins. It is also worth noting that alterations on the phosphorylation state of AICD were recently reported in the brains of AD patients (Lee et al., 2003).

AICD has eight phosphorylatable residues, which belong to three APP functional motifs previously mentioned in section I.3: ^{653}YTSI^{656}, ^{667}VTPEER^{672}, and ^{682}YENPTY^{687} (Fig. I.11).

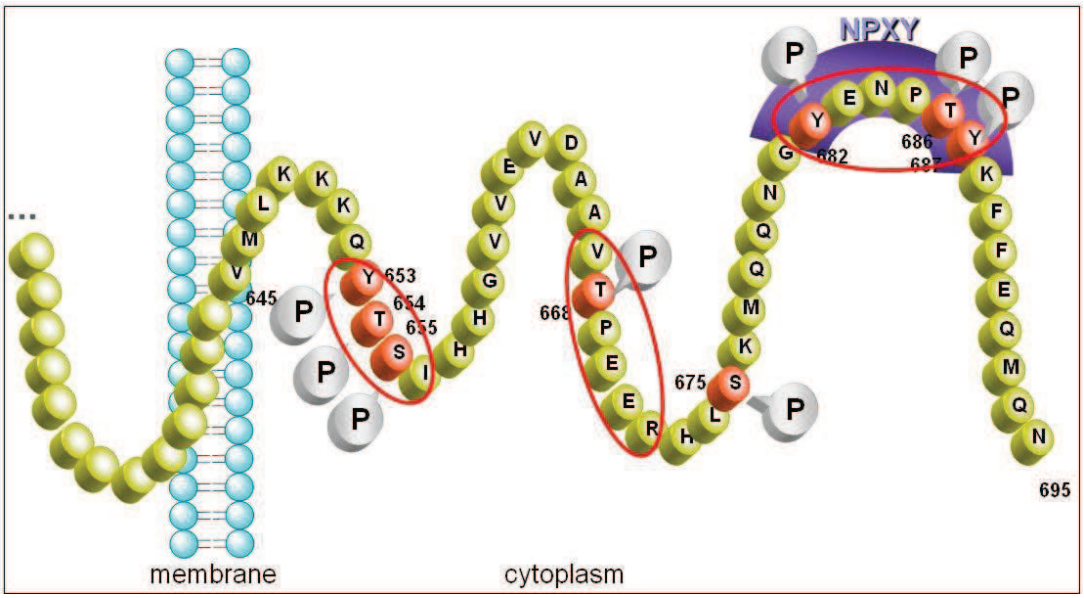

Figure I.11: The cytoplasmic domain APP contains three functional motifs (red lines) that encompass almost all phosphorylatable residues (highlighted in red; numbering is according to the APP_{695} neuronal isoform). AICD phosphorylation sites were shown *in vivo* in cultured cells and adult rat brain for Thr-654, Ser-655 and Thr-668 (Oishi *et al.*, 1997). Abnormal enhanced phosphorylation of 7 AICD residues (Tyr-653; Ser-655; Thr-668; Ser-675; Tyr-682; Thr-686; Tyr-687) was detected in AD brains (Lee *et al.*, 2003).

In the internalization signal domain ^{682}YENPTY^{687}, Tyr-682 phosphorylation is a consensual site, in contrast with Tyr-687 phosphorylation. APP phosphorylation on Tyr-682 was detected *in vivo* (Suzuki *et al.*, 1994; Zambrano *et al.*, 2001) and in AD brains, suggesting a pathogenic role (Oishi *et al.*, 1997; Lee *et al.*, 2003). Tyr-682 can be phosphorylated by the nerve growth factor receptor TrkA, c-Abl or Fyn (Zambrano *et al.*, 2001; Tarr *et al.*, 2002a; Hoe *et al.*, 2008), but for Tyr-687, kinases were not described yet. Nevertheless Tyr-687, which is within the internalization signal NPXY, was reported to be phosphorylated *in vivo* (Lee *et al.*, 2003). Concomitantly, previous work from our laboratory has addressed the role of Tyr-687 phosphorylation by mimicking its

constitutive phosphorylation (Y687E) and dephosphorylation (Y687F) (da Cruz e Silva *et al.*, 2004c). APP^{Y687E}-GFP was shown to be targeted to the plasma membrane and could not be detected in endocytic vesicles, the major site of β-secretase activity, exhibiting a concomitant dramatic decrease in Aβ production. In contrast, APP^{Y687F}-GFP was endocytosed similarly to wild type APP, but was relatively favoured for beta-secretase cleavage (Rebelo *et al.*, 2007a).

I.3.4 AICD binding proteins

Given the characteristics of the APP cytoplasmic tail, the complex network of protein-protein interactions that centred around it became an exciting new target for therapeutic intervention (Russo *et al.*, 1998; Annaert and De Strooper, 2002). Many proteins, indeed, interact with this C-terminal domain of APP, most of them possessing multiple protein-protein interacting domains, which in turn form complexes with other proteins. This suggests that these proteins function as adaptor proteins bridging APP to specific molecular pathways (Fig. I.12).

Several laboratories have used the AICD as ‘‘bait’’ in the yeast hybrid systems, identifying two major families of APP binding proteins, the FE65 proteins and the X11/Mint proteins (Fiore *et al.*, 1995; Bressler *et al.*, 1996; Guenette *et al.*, 1996; McLoughlin and Miller, 1996; Borg *et al.*, 1998b; Lau *et al.*, 2000a; Lau *et al.*, 2000b; Mueller *et al.*, 2000; Minopoli *et al.*, 2001; Zambrano *et al.*, 2001).

The endocytosis mediating motif ^{653}YTSI^{656} binds to the microtubule interacting protein PAT1 (Zheng *et al.*, 1998) and the motif ^{667}VTPEER^{672} is responsible for interaction with 14-3-3γ (Sumioka *et al.*, 2005). The conserved ^{682}YENPTY^{687} internalization motif is, recognized by phosphotyrosine binding domains of several proteins such as the Fe65 protein family (Fe65, Fe65L1 and Fe65L2) (Fiore *et al.*, 1995; Bressler *et al.*, 1996; Guenette *et al.*, 1996; Duilio *et al.*, 1998); the X11/Mint proteins (X11, X11L, X11L2) (Borg *et al.*, 1996; McLoughlin and Miller, 1996; Zhang *et al.*, 1997; Tanahashi and Tabira, 1999b); Shc A and Shc C (Tarr *et al.*, 2002b); JIP-1 and JIP-2 (Scheinfeld *et al.*, 2002); Dab1 (Trommsdorff *et al.*, 1998) ; Numb and Numb-like (Roncarati *et al.*, 2002); GULP1 (Beyer *et al.*, 2010). Other AICD binding proteins have been identified, such as Go (Nishimoto *et al.*, 1993); cAbl (Zambrano *et al.*, 2001); APP-BP1 (Chow *et al.*, 1996); UV-damaged DNA-binding protein (Watanabe *et al.*, 1999); ARH (Noviello *et al.*, 2003); Grb2 (Zhou *et al.*, 2004); Pin1 (Pastorino *et al.*, 2006); FKBP12 (Liu *et al.*, 2006); AIDA-1 (Ghersi *et al.*, 2004); SET (Madeira *et al.*, 2005); CPEB (Cao *et al.*, 2005); Flotillin-1 (Chen *et al.*, 2006); and SNX17 (Lee *et al.*, 2008).

APP binding proteins involved in APP subcellular localization include PAT1, kinesin and JIP-1 (c-Jun-amino-terminal kinase-interacting protein 1) and the X11/MINT family proteins, the latter with a role in microtubule association, and putative functions as an APP vesicle coat-protein (Okamoto and Sudhof, 1997). The already mentioned binding to G_0, which links APP to G-protein signaling, is likely to play a role in APP targeting, since G_0 and other related heterotrimeric G-proteins were found to be located at subcellular membranes domains that are specialized in the sorting of trafficking proteins (Turner *et al.*, 2003). The function of all the APP binding proteins has yet to be completely elucidated, but considerable contributions have already been made.

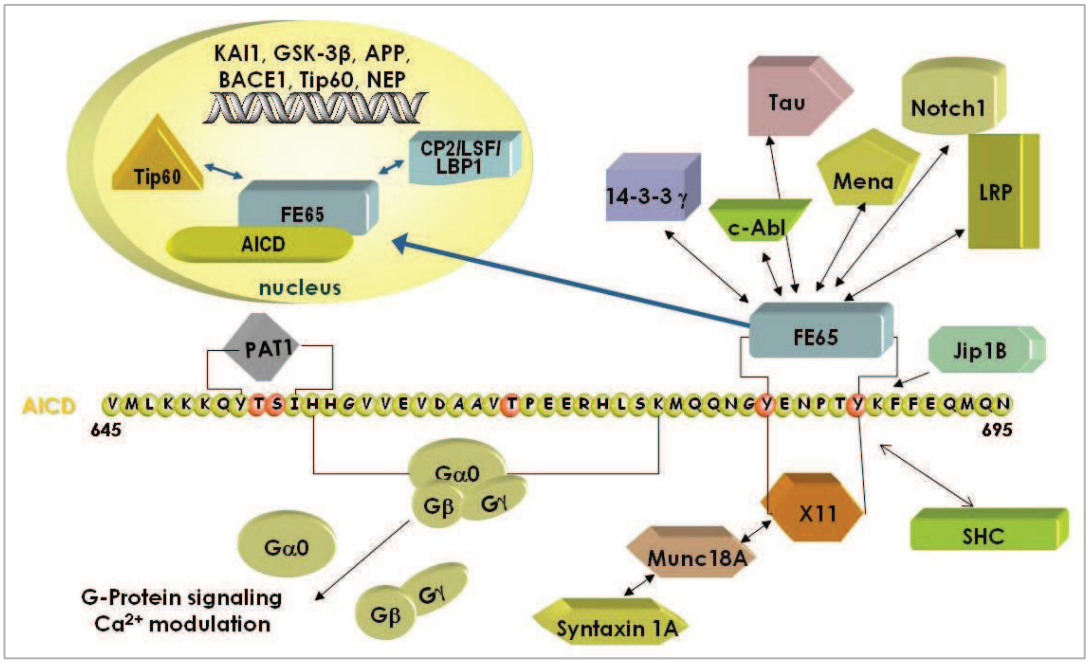

Figure I.12: Protein network around the cytoplasmic domain of APP (Adapted from Turner et al., 2003).

The X11/mint protein family comprises three members: X11α, β, and γ or mint-1, -2, and -3 or X11, X11-L and X11-L2 (McLoughlin and Miller, 1996; Tanahashi and Tabira, 1999a, b). X11 family members contain divergent N-terminal sequences but highly conserved C-termini consisting of a PTB domain and two PDZ domains. The "Mint" designation arose from interaction of X11 and X11-L, but not X11-L2, with munc 18-1, a protein essential for synaptic vesicle docking and exocytosis (Biederer *et al.*, 2002). While X11-L2 expression is ubiquitous, X11 and X11-L are expressed only in the brain (McLoughlin *et al.*, 1999; Hase *et al.*, 2002).

Besides binding to the YENPTY of APP, through its PTB domain, several other proteins have been reported to interact with X11 (Fig. I.8), for instance it interacts with CASK–Veli to form a heterotrimeric complex that may target transmembrane receptor proteins in polarized cells (Borg *et al.*, 1998a).

A yeast two-hybrid screen of a brain cDNA library using the X11 PTB domain as bait reveals a specific interaction with APP, APLP-1, and APLP-2 (Borg *et al.*, 1996; McLoughlin and Miller, 1996; Tomita *et al.*, 1999). In contrast, the PDZ domains of X11 may interact with several proteins (Fig. I.8) including presenilin-1 (Lau *et al.*, 2000a), spinophilin–neurabin II, the copper chaperone of SOD1, the dendritic kinesin KIF-17 and, via X11-CASK-Veli, to the N-methyl-D-aspartate receptor NR2B subunit (King and Scott Turner, 2004). X11 was also reported to potentially interacting with itself by PDZ domain dimerization (Walhout et al., 2000). The X11/MINT protein family was implicated in APP vesicle coat-protein (Okamoto and Sudhof, 1997; Hill *et al.*, 2003). Several X11 binding proteins mediate synaptic functions, implying an adaptor role for X11 in the pre- and postsynaptic complex.

I.3.4.1 The Fe65 protein family

FE65 is a multimodular adaptor protein, possessing three protein-protein interacting domains: a WW domain (a protein module with two conserved triptophans) and two tandem phosphotyrosine binding domains – PTB1 and PTB2 (or phosphotyrosine interaction domains – PID1 and PID2) (Bressler *et al.*, 1996; McLoughlin and Miller, 1996). The Fe65 family comprises three members: FE65, FE65L1 and FE65L2, being all reported to interact with APP (Fiore *et al.*, 1995). Whereas, the FE65L1 and FE65L2 are ubiquitously expressed the FE65 is neuronally enriched and a splice variant of FE65 (E9) is neuronal specific (Fiore *et al.*, 1995; Duilio *et al.*, 1998).

The most extreme C-terminal phosphotyrosine binding domain (PTB2) of FE65 is responsible for the interaction with the Alzheimer's Amyloid Precursor Protein (APP) intracellular domain, through the latter's YENPTY motif. The pathways for APP processing are particularly important with respect to the generation of the Abeta peptide, which is deposited in the Alzheimer's disease (AD) brain. The amyloidogenic processing, with the subsequent Abeta production is affected by the interaction of APP with FE65 (Sabo *et al.*, 1999). Likewise FE65 also appears to bind to APP like proteins (APLP1 and APLP2) (Duilio *et al.*, 1998).

Interaction of the FE65 PTB2 domain with APP requires the YENPTY motif as well as Thr-668, 14 residues N-terminal to the internalization sequence. Phosphorylation of APP Thr-668 impairs FE65 interaction suggesting that adaptor protein interactions with APP are differentially regulated by phosphorylation states. APP has been demonstrated to act as a cytosolic anchor for FE65, able to regulate its nuclear translocation (Ando *et al.*, 2001).

Besides APP-binding, FE65 in turn forms complexes with other proteins, suggesting that it bridges APP to specific molecular pathways (Fig. I.12). For instance, FE65 has been found to be associated with Neurofibrillary Tangles (NFTs) in AD. The main constituent of NFTs is Tau, a protein involved in neurite morphogenesis, axonal growth and axonal transport (Shahani and Brandt, 2002; Stamer *et al.*, 2002). In AD Tau is hyperphosphorylated, which favours expansion of NFTs. Barbato et al. demonstrated the interaction of FE65 PTB1 domain with N-terminal domain of Tau *in vivo* and *in vitro*. The physical interaction between the adaptor protein FE65 and Tau is dependent on microtubule network integrity and is regulated by Tau phosphorylation, apparently via the proline-directed kinases GSK3β and Cdk5, since they are reported to be complexed with phosphorylated Tau (Hamdane *et al.*, 2003; Barbato *et al.*, 2005). This interaction suggests that FE65 bridges Tau to APP, representing a functional link between the two hallmarks of AD, namely NFTs and amyloid plaques.

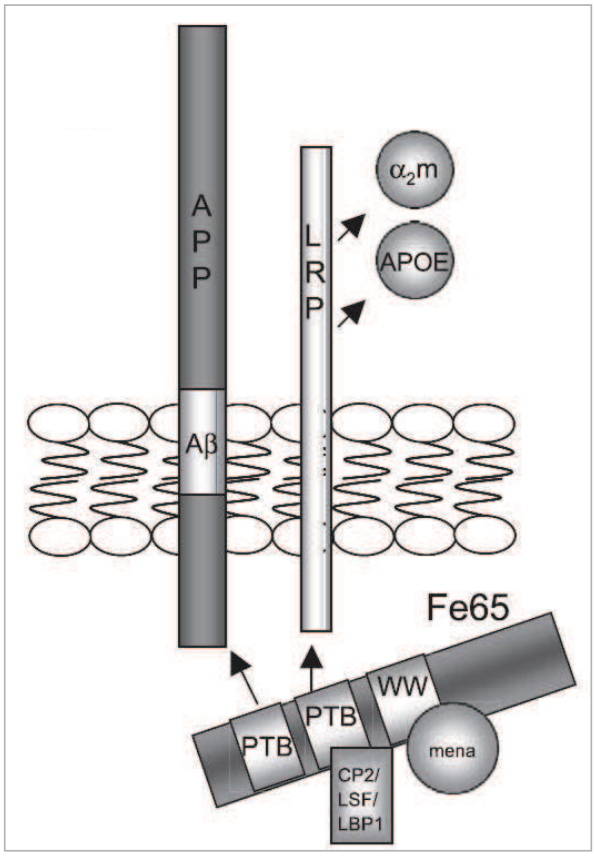

Figure I.13: FE65 contains multiple protein interaction domains: the PTB1 domain interacts with the transcription factor complex CP2/LSF/LBP1 and with LRP, linking FE65 to α2M and ApoE; the PTB2 domain interacts with APP; the WW interacts with Mena, thus linking FE65 and APP to actin (adapted from (King and Scott Turner, 2004).

The PTB1 domain of FE65 binds the low density lipoprotein receptor-related protein (LRP), a transmembrane glycoprotein which mediates the internalization and degradation of extracellular ligands, including α-2-macroglobulin, apolipoprotein E and KPI-containing isoforms of APP (Trommsdorff *et al.*, 1998; Herz and Strickland, 2001). LRP interacts with APP also by an extracellular ligand-receptor interaction. FE65 in turn interacts with the cytoplasmic tails of APP and LRP, acting as a bridging protein. Pietrzik et al. demonstrated that FE65 can also be a functional linker between APP and LRP and the APP-FE65-LRP complex formation is critical for APP processing (Pietrzik *et al.*, 2004).

The WW domain of FE65 binds proline-containing motifs (PPXY or PPLP) of Mena (mammalian homologue of enabled), a protein involved in the regulation of actin dynamics (Ermekova *et al.*, 1997). Mena belongs to the Ena/VASP family of proteins, which concentrate in focal adhesions and stress fibers and are found in dynamic actin remodeling areas, e.g.

lamellipodia and axonal growth cones (Ermekova *et al.*, 1997). FE65 and APP colocalize with Mena in lamellipodia, which associates the FE65-APP complex to cytoskeletal dynamics and cellular motility and morphology (Sabo *et al.*, 2001). Integrins are concentrated in lamellipodial adhesion sites, where they co-localize with FE65 and APP. FE65 PTB1 binds the β1-integrin cytoplasmic domain, at one of the two NPXY motifs of the latter. Integrins are a family of cell adhesion receptors that mediate cell–matrix interactions, playing a role in cell proliferation, differentiation, and migration (Sabo *et al.*, 2001). Another ligand for FE65 WW domain is the c-Abl tyrosine kinase, which phosphorylates FE65 on Tyr-547, in the PTB2 domain. Tyrosine kinase c-Abl is localized within the nucleus and phosphorylates APP, on Tyr-682 (Zambrano *et al.*, 2001; Perkinton *et al.*, 2004).

The FE65 N-terminal PTB1 domain binds the transcription factor CP2/LSF/LBP1, involved in the regulation of several genes. The FE65-CP2/LSF/LBP1 complex was found both in nuclear and non-nuclear fractions (Zambrano *et al.*, 1998); however the ternary complex AICD–FE65–CP2/LSF/LBP1 can assemble in the nucleus, inducing GSK-3β expression which can potentially increase Tau phosphorylation, contributing to AD (Kim *et al.*, 2003). Other transcriptional factors may also be formed, for example the PTB1 FE65 domain functionally interacts with the histone acetyltransferase Tip60, forming the complex AICD–FE65–Tip60 which may regulate gene transcription (Cao and Sudhof, 2001). Alternatively, APP may anchor FE65 in the cytoplasm impairing its nuclear translocation (Minopoli *et al.*, 2001).

I.3.5 AICD in nuclear signaling

The interaction between AICD and Fe65 has been extensively studied with respect to the transactivation properties of the AICD/Fe65/Tip60 complex (Cao and Sudhof, 2001). After intramembranous γ-secretase cleavage of APP, AICD is released and may translocate to the nucleus where it participates in transcriptional regulation, in a manner analogous to Notch signaling. In the canonical Notch signaling pathway, sequential cleavage by α-/γ-secretases releases the intracelular domain of Notch (NICD) that translocates to the nucleus to modulate gene expression, through binding to transcription factors (De Strooper *et al.*, 1999). In the nucleus, AICD was reported to associate in multiple spherical nuclear spots with Fe65 and the histone acetyltransferase Tip60, known as the AFT-complexes, which were demonstrated to correspond to transcription factories (von Rotz *et al.*, 2004; Konietzko *et al.*, 2010). Indeed,

several AICD target genes have been identified, such as the genes coding for KAI1 (Baek *et al.*, 2002), thymidilate synthase (Bruni *et al.*, 2002), GSK-3β (Kim *et al.*, 2003; Ryan and Pimplikar, 2005), APP, BACE, Tip60 (von Rotz *et al.*, 2004), neprilysin (Pardossi-Piquard *et al.*, 2005), p53 (Alves da Costa *et al.*, 2006), α2-actin, transgelin (Muller *et al.*, 2007), EGF receptor (Zhang *et al.*, 2007), LRP1 (Liu *et al.*, 2007), the mouse Nme1 and Nme2 (Napolitano *et al.*, 2008), and, in *Caenorhabditis elegans*, acetylcholinesterase (Bimonte *et al.*, 2004).

APP and Notch are analogous to many other membrane proteins that are subject to regulated intramembrane proteolysis (RIP) (Kang *et al.*, 1987; Kopan and Goate, 2000). Nevertheless, the cytoplasmic tail of APP is relatively short and is rapidly degraded after release from the membrane by the insulin degrading enzyme or by the endosomal/lysosomal system (Cupers et al., 2001; Edbauer et al., 2002; Vingtdeux et al., 2007a). However, the half-life of AICD can be considerably increased by interaction with Fe65, facilitating the translocation of AICD to the nucleus (Kimberly *et al.*, 2001). Moreover, only the AICD generated through the amyloidogenic pathway exhibited nuclear signaling, due to the localization of β-secretase processing of APP at the endosomes, allowing a faster microtubule-based transport to the nuclear vicinity before γ-cleavage releases AICD (Goodger *et al.*, 2009).

CHAPTER II. ISOLATION OF APP/AICD BINDING PROTEINS BY YEAST-TWO HYBRID SCREENING

II.1 INTRODUCTION – THE YEAST TWO-HYBRID SYSTEM

II.1.1 Principles of the yeast two-hybrid system

Protein-protein interactions (PPIs) are fundamental to all cellular processes. It is often possible to infer the function of an unknown protein by identifying the proteins with which it interacts. The YTH system has become one of the most popular and powerful tools to study PPIs, providing a sensitive *in vivo* assay for interaction analysis. The YTH system, was initially developed as a simple method to probe PPIs (Fields and Song, 1989; Fields and Sternglanz, 1994). It takes advantage of the modular architecture of eukaryotic transcription activators, which comprise two functionally independent domains: a DNA-binding domain (BD) that recognizes a specific DNA sequence in the promoter region and a transcription activation domain (ActD) that brings the transcriptional machinery to the promoter's proximity, leading to activation of gene transcription. The original two-hybrid system was based on the yeast GAL4 transcription factor, involved in galactose metabolism, and is known as the GAL4 system (Fields and Song, 1989). This system relied on a single reporter gene for the detection of an interaction. The LexA or interaction trap system is a similar approach that utilized the BD of the bacterial repressor protein LexA in combination with the *Escherichia coli* B42 ActD (Gyuris *et al.*, 1993).

The two functional domains of a transcriptional activator, the BD and the ActD, can be split apart and each fused to one of a pair of partner proteins in order to reconstitute the activator's ability to turn on a reporter gene. These two elements can be cointroduced into yeast strains modified with one or more reporter genes (the use of multiple reporter genes decreases the number of false positives obtained). These reporter genes have a binding site specific to the BD on their promoter region, causing the transcription of those genes to be dependent on the interaction between prey and bait proteins. Interaction of the BD-bait fusion with the ActD-prey fusion, positions the ActD in the proximity of the reporter gene, thus activating its transcription (Fig. II.1) (Causier and Davies, 2002).

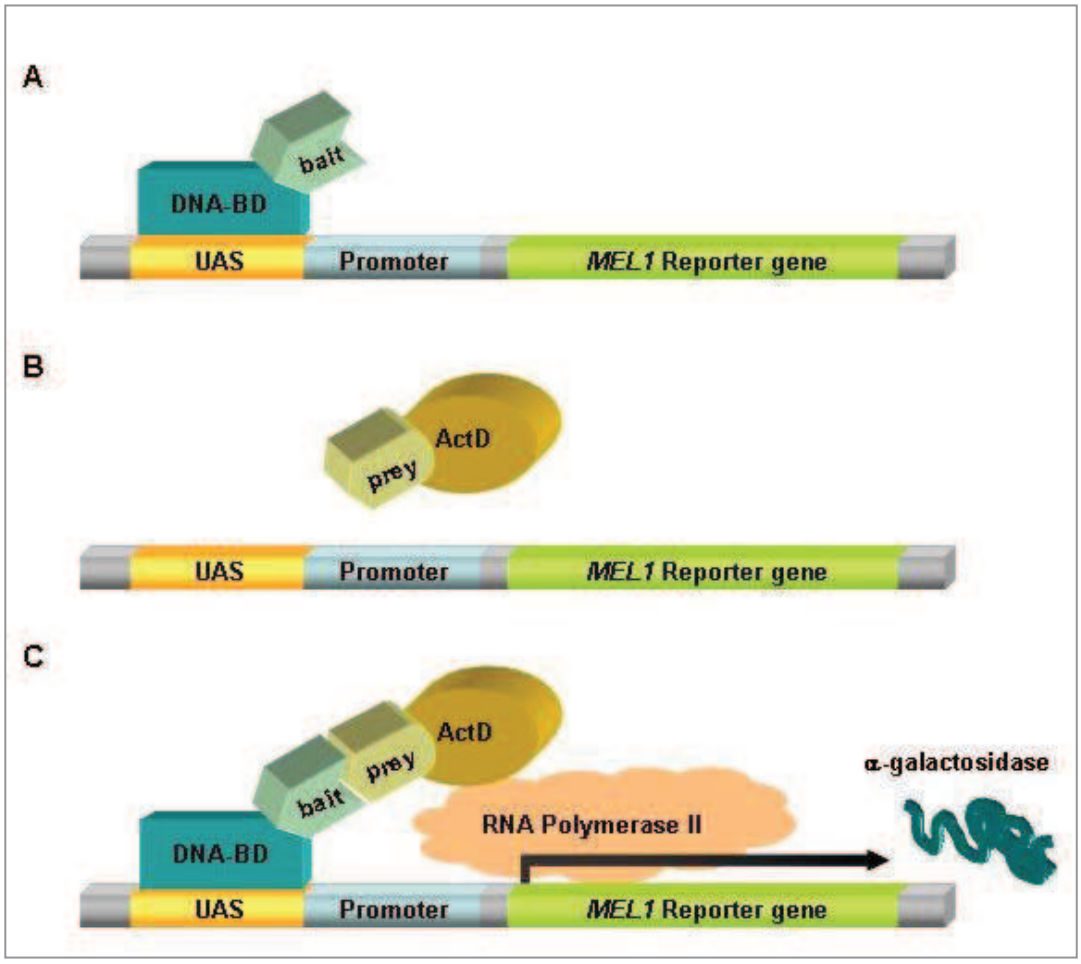

Figure II.1: The yeast two-hybrid system principle. Two hybrid proteins are expressed in yeast: GAL4 DNA-binding domain (BD) fused to a bait protein and GAL4 activation domain (ActD) fused to a prey protein. **A.** The BD-bait hybrid protein can bind to upstream activation sequences (UAS) but cannot activate transcription). **B.** The ActD-prey protein cannot recognize the UAS, thus, alone it is not capable of initiating transcription. **C.** When the bait and the prey interact, the BD and ActD are brought together and can activate reporter gene's transcription.

The YTH technique was automated for high-throughput studies of protein interactions, allowing the identification of a large number of proteins capable of interacting with a protein of interest. A large number of clones can be simultaneously tested using a cDNA expression library from a particular tissue. Larger scale two-hybrid approaches typically rely on interaction mating (Serebriiskii *et al.*, 2001). In this method, a yeast strain expressing the bait protein is mated with another yeast strain of opposite mating type pretransformed with the cDNA library. Interaction between two proteins can then be determined by the activation of one or more reporter genes in the diploid strain. One advantage of this approach is the possibility of using frozen aliquots of pretransformed yeast cells saving time and resources. Additional benefits of using yeast mating

are that diploid cells are more tolerant to expression of toxic proteins and, because the reporter genes are less sensitive to transcription activation in diploids than they are in haploids, yeast mating reduces the background from proteins that activate transcription, which results in fewer false positives (Kolonin *et al.*, 2000).

Since its introduction, the YTH system has been modified, greatly expanding its biological and technological applications. First developed as an agent of biological discovery, the YTH has been a tool in proteomics and, additionally, as a means towards engineering novel pharmaceutical agents. Some YTH alternative systems have been developed and in many cases resulted in remarkably elegant hybrid systems, e.g. one-hybrid, tri-hybrid, reverse two-hybrid, membrane yeast two-hybrid (MYTH) and mammalian two-hybrid (Serebriiskii *et al.*, 2001; Tyree and Klausing, 2003; Causier, 2004).

Although the YTH system has been widely used both to demonstrate and to identify novel protein interactions with proteins from multiple sources, from prokaryotes to plants and mammals, this system has some intrinsic limitations that should be considered. It relies on yeast expression of two hybrid proteins and on their action as transcription factors in the yeast nucleus, which is dependent on their interaction. Limitations exist if one of the proteins cannot be expressed, folded or post-translationally modified in yeast cells, or if the GAL4 fusion impairs correct folding. In addition, if any of the fusion proteins are capable of activating reporters' gene transcription by itself, false positives will arise. One also has to bear in mind that a legitimate PPI may have no functional significance if it involves two proteins that never co-localize in physiological systems (e.g. proteins that are expressed in different tissues or cellular organelles). Additionally, the inability of fusion proteins to migrate to the nucleus may also lead to false results. The limitations of the YTH system do not exclude it from protein networks research, but reinforce the need to validate all the interactions. These should be tested in different systems, preferably, by confirming the physical association of the native proteins in the cell where the functional interactions are predicted to occur. Nevertheless, it is important to remember the usefulness of the YTH in the construction of large interaction networks, and in identifying unsuspected interactions that may later be confirmed by a variety of independent methods.

II.1.2 YTH Screening workflow

The MATCHMAKER Two-hybrid System 2 (Clontech) was used to perform YTH screening, according to the manufacturers' instructions. A flow chart of the general procedures is shown in Fig. II.2. Briefly, the cDNA library, which expresses fusions with the Gal4-AD, was provided in the yeast strain Y187 (MATCHMAKER human brain cDNA library, Contech). The bait protein was expressed as a fusion with the Gal4-BD in yeast strain AH109. A bait culture was combined with one aliquot of pretransformed cDNA library overnight, allowing mating to occur. The diploid cells are plated in selective media with X-α-Gal. Four reporter genes: *HIS3*, *ADE2*, *MEL1* and *lacZ*, which are activated in response to two-hybrid interaction (expression from the *lacZ* reporter can only be detected if the cells are lysed in a colony lift assay), allow for the identification of the positive clones.

The key components and features of MATCHMAKER Two-hybrid System 2 (Clontech) are (i) the reporter genes used, (ii) the yeast host strains, (iii) the optimized plasmids and (iv) the cDNA libraries, as detailed below:

---

i) Reporter genes

The reporter genes used in this system are the ***MEL1*** gene (coding for α-galactosidase, that is secreted into the culture medium) and the ***lacZ*** (coding for β-galactosidase, which can only be detected if the cells are lysed in a colony lift assay). Additionally, the auxotrophic reporter genes ***HIS3*** and ***ADE2*** allow yeast cells carrying interacting proteins to grow in medium lacking histidine and adenine. The nutritional selection reporter genes allow for easy recovery of interacting clones in large screening procedures, using a cDNA library, designed to identify new interacting proteins with a selected bait. Additionally, the YTH bait plasmid pAS2-1 and the library plasmid pACT2, which contain the *TRP1* and *LEU2* genes, respectively, allow for selection in medium lacking tryptophan and leucine. Hence, the high-stringency selection consists of medium lacking tryptophan, leucine, histidine and adenine, and also in the presence of X-α-Gal. The selection of positive clones with the "five" reporter genes *TRP1*, *LEU2*, *HIS3*, *ADE2* and *MEL1* (Matchmaker Yeast Two-Hybrid System 2, Clontech) was designed to reduce the number of false positives, thus allowing faster identification of true interactions with the bait protein.

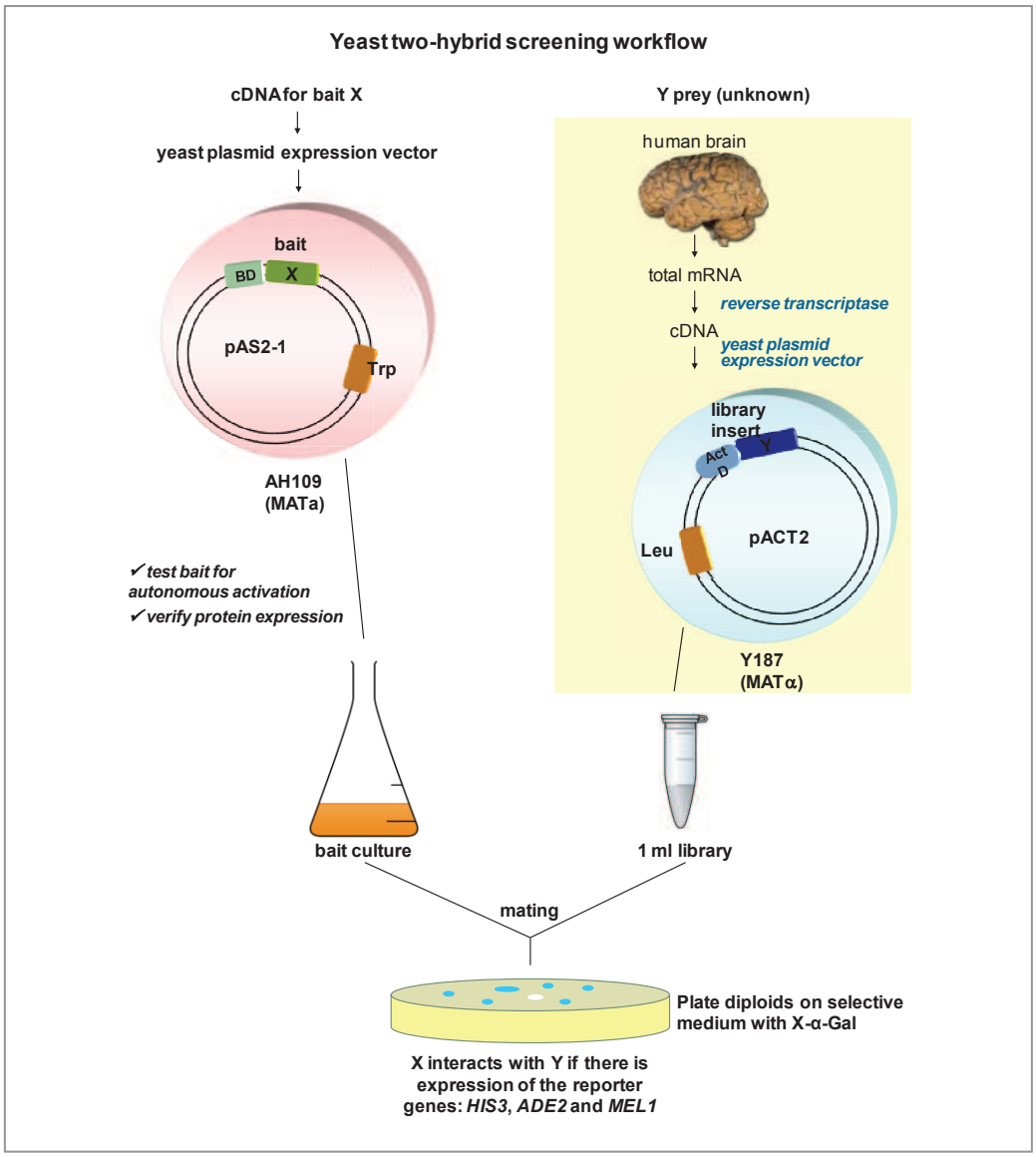

Figure II.2: Flow chart of the yeast two-hybrid screening methodology. The bait protein was expressed as a fusion with the Gal4-BD in yeast strain AH109. The high-complexity pretransformed cDNA library, which expresses fusions with the Gal4-AD, was provided in the yeast strain Y187 (Matchmaker human brain cDNA library, Contech; yellow box). When cultures of the two transformed strains are mixed together overnight, they mate to create diploids. Four reporter genes, *HIS3*, *ADE2*, *MEL1* and *lacZ*, are activated in response to fusion protein interaction.

ii) Yeast host strains

Saccharomyces cerevisiae strains of two opposite mating types were used: **AH109** (MATa) and **Y187** (MATα). The complete genotypes are provided in Appendix III. The AH109 yeast strain virtually eliminates false positives by using three reporters – *ADE2*, *HIS3* and *MEL1* (or *lacZ*) – under the control of distinct GAL4 upstream activating sequences (UAS) and TATA boxes (Fig. II.3). The *lacZ, HIS3, ADE2 and LEU2* reporter genes are under control of artificial promoter constructs comprised of a TATA and UAS (or operator) sequence derived from another gene.

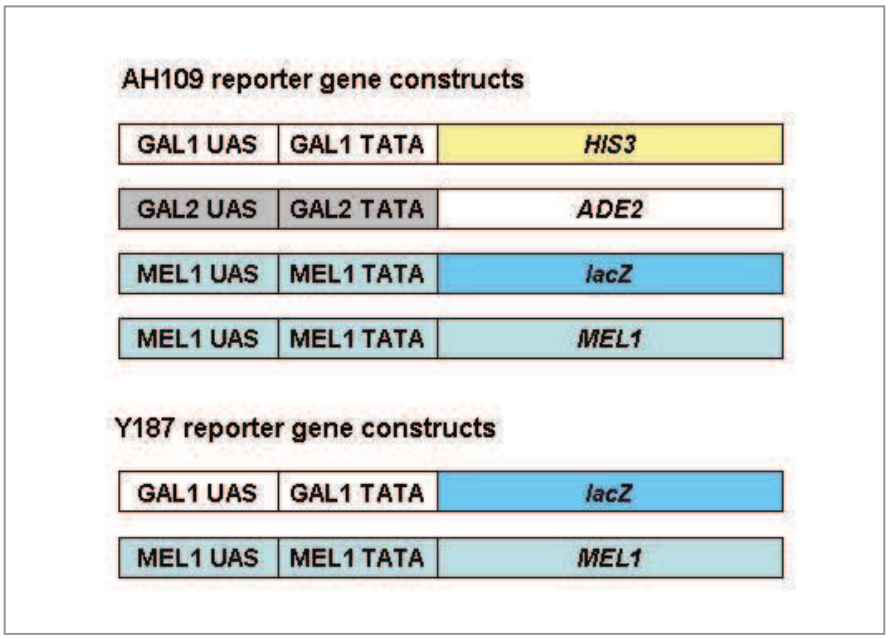

Figure II.3: Reporter gene constructs in yeast strains AH109 and Y187. In AH109, the *HIS3*, *ADE2*, and *MEL1/lacZ* reporter genes are under the control of three completely heterologous Gal4-responsive UAS and promoter elements - *GAL1*, *GAL2*, and *MEL1*, respectively. The protein-binding sites within the UAS are different, although each is related to the 17-mer consensus sequence recognized by Gal4 (*Adapted from Pretranformed MATCHMAKER Libraries User Manual, Clontech*).

iii) Plasmids

The Gal4 DNA-BD fusion vector **pAS2-1** and the Gal4-AD fusion vector **pACT2** have multiple cloning sites that allows for the insertion of bait or library cDNA, respectively (Appendix IV). They also carry a bacterial replication origin and an ampicilin resistance gene, for selection in bacteria.

pAS2-1 contains the *TRP1* gene for selection in Trp^- auxotrophic yeast strains (AH109, Y187 or diploids) and pACT2 contains the *LEU2* gene for selection in Leu^- auxotrophic yeast strains (AH109, Y187 or diploids).

Additionally, the YTH system includes yeast plasmids carrying Gal4-BD and Gal4-AD fusion cDNAs that provide controls for negative and positive interactions, pVA3-1, pTD1-1 and pLam5'-1, which were used to validate interactions (Chapters III and V).

iv) cDNA libraries

Three YTH screens were performed in the context of this thesis (YTH-s1, YTH-s2 and YTH-s3). Two aliquots of a Pretransformed Human Brain MATCHMAKER cDNA Library (CAT. HY4004AH; Clontech) were used for YTH-s1 and YTH-s2. This library was constructed using whole brain mRNA from a 37 years old Caucasian male (cause of death: trauma). Pretransformed MATCHMAKER libraries are high-complexity cDNA libraries cloned into the yeast Gal4-AD vector pACT-2 and pretransformed into *S. cerevisiae* Y187 host strain.

For YTH-s3 a human brain MATCHMAKER cDNA library was obtained in *E. coli* BNN132 (CAT:HL4004AH, Clontech). The mRNA source was the whole brain from a 60 years old Caucasian male (cause of death: sudden death). To make this cDNA library available for YTH screening, several steps were previously carried out in our laboratory: library amplification in *E. coli*; library DNA isolation; library-scale transformation in yeast strain AH109; plating the transformation mixture; and harvesting the transformants at high viability and density in freezing medium. The frozen aliquots were thus ready for YTH screening.

II.1.3 The baits for YTH screening

The full-length cDNA encoding human APP (isoform 695) was used as bait in screen YTH-s1. The YTH-s2 was performed with APP^{Y687F}, which mimics the dephosphorylated state of Tyr-687. For YTH-s3 only the cytoplasmic domain of the mutant APP, $AICD^{Y687F}$ was used as bait (Table II.1).

Table II.1: Description of the cDNA baits used in each YTH screen.

YTH screen	Bait	Description
YTH-s1	APP (bait-1)	human wild-type APP cDNA, coding for the neuronal isoform with 695 amino acids (APP_{695}) (GenBank Accession NM_201414)
YTH-s2	APP^{Y687F} (bait-2)	human APP cDNA, coding for the neuronal 695 amino acids isoform with the Y687F mutation, which mimics the dephosphorylated state of Tyr-687
YTH-s3	$AICD^{Y687F}$ (bait-3)	cDNA coding for the intracellular domain of human APP_{695} with 50 amino acids(C50)

Several steps were required to prepare each YTH screen, namely to:

(i) Construct the Gal4-BD-bait fusion genes: each bait cDNA was subcloned into the yeast expression vector pAS2-1, in frame with Gal4-BD;

(ii) Transform the bait plasmids in the appropriate yeast strain;

(iii) Verify that Gal4-BD fusion constructs do not activate reporter genes: the transformants from the previous step were assayed for autonomous activation of the reporter genes *HIS3*, *ADE2* and *MEL1*;

(iv) Verify protein expression: yeast protein extracts were prepared from the transformants mentioned above and the expression of each bait cDNA fused to the Gal4-BD was verified by immunoblotting.

After all the prerequisites were verifiyed, the YTH screens were performed by large-scale yeast mating, as described in the following sections.

II.2 CONSTRUCTION OF THE BAIT PLASMIDS

The same strategy was followed to prepare all bait fusion constructs (Table II.2).

Table II.2: Cloning strategy followed to obtain the Gal4-BD-Bait fusion constructs.

Vector	**Inserts**
pAS2-1	**APP/APP^{Y687F}/AICD^{Y687F}**
DNA amplification in *E. coli* XL1-blue	Insert amplification by PCR
DNA isolation by Megaprep	PCR fragments purification (silica-membrane-based column)
Sequential digestion with NcoI and SmaI	Sequential digestion with NcoI and SmaI
Ethanol precipitation	Ethanol precipitation
Incubation with alkaline phosphatase	
Ligation of vector and insert	
Transformation of ligation mixtures into *E.coli*	
Identification of insert-containing plasmids by restriction analysis	
Verification of orientation, sequence and reading frame by DNA sequencing	

II.2.1 Materials and Methods

For the complete composition of all reagents, media and solutions used, see Appendix I. All the reagents were cell culture grade or ultrapure.

II.2.1.1 Isolation of pAS2-1 plasmid from bacteria - PROMEGA "Megaprep"

A 1 L cell culture was pelleted by centrifugation at 1,500*g* for 20 min at RT. The cell pellet was resuspended in 30 ml of Cell Resuspension Solution by manually disrupting the pellet with a pipette. 30 ml of Cell Lysis Solution were added to the cells and the solution mixed gently by inverting, until it became clear and viscous. Then, 30 ml of Neutralization Solution were added and immediately mixed by inverting the tube. After centrifugation at 14,000*g* for 15 min at RT the

clear supernatant was transferred by filtering through gauze swabs to a new tube and the volume of supernatant was measured. At this stage 0.5 volumes of room-temperature (RT) isopropanol were added and the solution mixed by inversion. This solution was centrifuged at 14,000*g* for 15 min at RT, the supernatant was discarded and the pellet resuspended in 4 ml of TE buffer. 20 ml of Wizard™ Megapreps DNA purification resin (Promega) were added to the DNA and mixed by swirling. A Wizard™ Megacolumn (Promega) was inserted into the vacuum manifold port and the DNA/resin mix was transferred into the Megacolumn. Vacuum was applied to pull the mix through the Megacolumn. Two washes with 25 ml of Column Wash Solution were performed and the resin was rinsed with 10 ml of 80% ethanol. The Megacolumn was inserted into a 50 ml screw cap tube and centrifuged at 4000*g* for 5 min using a swinging bucket rotor centrifuge. The Megacolumn was placed in a clean tube and 3 ml of pre-heated nuclease-free water (70°C) were added to the column. After waiting 1 min the DNA was eluted by centrifugation at 4000*g* for 5 min. The DNA was stored at -20°C.

This procedure was used to prepare a large amount of plasmid DNA for storage and subsequent cloning, yeast transformation and other purposes.

II.2.1.2 Plasmid DNA digestion with restriction enzymes

Plasmid DNA was sequentially digested with SmaI and NcoI with the DNA being precipitated between the digests.

For a typical DNA digestion the manufacturer's instructions were followed. In a microtube the following components were added:

- 100 µg/ml DNA
- 1x reaction buffer (specific for each restriction enzyme)
- 1 U/µg DNA of restriction enzyme

The mixture was incubated at the appropriate temperature (30°C for SmaI; 37°C for NcoI) for a few hours (or overnight if convenient).

II.2.1.3 Plasmid DNA purification with ethanol

This method was used to concentrate nucleic acids as well as to purify them. Approximately 1/10 volume of 3 M sodium acetate (pH 5.2) was added to the DNA solution to adjust the salt concentration, followed by 2 volumes of ice-cold ethanol. The solution was well mixed and stored

at -20°C for 30 min to allow the DNA precipitate to form. DNA was recovered by centrifugation at 4°C for 15 min at 12,000*g*. The supernatant was carefully removed without disturbing the pellet. The microtube was half filled with ice-cold 70% ethanol and recentrifuged at 12,000*g* for 5 min. The supernatant was again removed and the pellet allowed to dry before being resuspended in sterile water.

II.2.1.4 Baits cDNA amplification by PCR

The baits cDNA fragments were generated by PCR with the NcoI and SmaI restriction sites incorporated into the forward and reverse primers, respectively (Table II.3).

Table II.3: Primers used to amplify each bait cDNA (for primers' sequences see Appendix II).

Bait	Forward primer (NcoI RE site)	Reverse primer (SmaI RE site)
bait-1: APP	NAPPII	APPCTERMIII
bait-2: APP^{Y687F}	NAPPII	APPCTERMIII
bait-3: $AICD^{Y687F}$	NAPPC	APPCTERMIII

The reaction was carried out in a 0.5 ml tube where the following components were added:

- 10 ng template DNA
- 10 pmol forward primer
- 10 pmol reverse primer
- 2 µl dNTP's 10 mM
- 5 µl reaction Pfu buffer 10x
- 2 Units of Pfu
- H_2O to a final volume of 50 µl

The PCR reactions were then carried out in a thermo cycler using different conditions. Inserts for bait-1 (APP_{695} cDNA) and bait-2 (APP_{695}^{Y687F} cDNA) are approximately 2100 bp and were

amplified using the same PCR settings. Bait-3 ($AICD^{Y687F}$) is shorter, with only 150 bp, and was amplifyied using specific PCR conditions (Table II.4).

Table II.4: Specific conditions for bait cDNA amplification by PCR.

Bait 1 - APP		Bait 2 - APP^{Y687F}		Bait 3 - $AICD^{Y687F}$	
95°C 4 min		95°C 4 min		95°C 4 min	
95°C 1 min		95°C 1 min		95°C 30 sec	
60°C 1 min	5 cycles	60°C 1 min	5 cycles	55°C 30 sec	5 cycles
72°C 6 min		72°C 6 min		72°C 1 min	
95°C 1 min		95°C 1 min		95°C 30 sec	
68°C 1 min	25 cycles	68°C 1 min	25 cycles	60°C 30 sec	25 cycles
72°C 6 min		72°C 6 min		72°C 1 min	
72°C 7 min		72°C 7 min		72°C 4 min	

II.2.1.5 Insert DNA purification – *QIAGEN DNA Purification kit*

The QIAGEN DNA Purification kit was used to purify DNA fragments from PCR and other enzymatic reactions. It permitted purification from primers, nucleotides, polymerases and salts by using QIAquick spin columns (silica-membrane-based columns). Briefly, 5 volumes of buffer PB (QIAGEN) were added to 1 volume of the solution to be purified and mixed. The spin column was placed in a collection microtube and the sample was applied to the column and centrifuged for 1 min at 12,000*g* to bind the DNA. The flow-through was discarded and the column was washed with 0.75 ml of buffer PE (QIAGEN), centrifuged for 1 min at 12,000*g* and the flow-through discarded. The column was placed back in the same microtube and centrifuged again to remove traces of washing buffer. Then, the column was placed in a clean microtube, 50 µl of H_2O were added and allowed to stand for 1 min. To elute the DNA, the column was centrifuged for 1 min at 12,000*g*.

II.2.1.6 Insert digestion with restriction enzymes

The PCR products were sequentially digested with SmaI and NcoI, with a purification step between the two reactions, as described in sections II.2.1.2 and II.2.1.3.

II.2.1.7 DNA ligation

Alkaline phosphatase treatment

In order to prevent self ligation of vector molecules, the digested plasmid DNA was incubated with shrimp alkaline phosphatase (SAP) (ROCHE) before ligation. According to the manufacturer's instructions, the reaction mixture was adjusted with 1/10 volume 10X concentrated dephosphorylation buffer, and incubated with 1 µl of SAP at 37°C for 1 h. Finally, SAP was inactivated by heating the reaction mixture at 65°C for 15 min.

DNA Ligation

To carry out the ligation reaction, 50 ng of vector DNA from the previous step were transferred to a microtube with three times the equimolar amount of insert DNA. 2µl of 10x T4 DNA ligase buffer and 1 µl of T4 DNA ligase (NEB) were added to the reaction mix and H_2O was added to a final volume of 20 µl. The reaction was carried out for 16 h at 16°C. One additional control reaction was set up that contained the plasmid vector alone.

II.2.1.8 Bacteria transformation with plasmid DNA

Preparation of *E. coli* competent cells

A single colony of *E. coli* XL1-Blue was incubated in 10 ml of SOB medium at 37°C overnight. Then, 1 ml of this culture was used to inoculate 50 ml of SOB and the culture was incubated at 37°C with shaking at 220 rpm for 1-2 h, until OD_{550nm}=0.3. The culture was cooled on ice for 15 min and centrifuged at 4,000*g* at 4°C for 5 min. The supernatant was discarded and then resuspended in 15 ml of Solution I. After standing on ice for 15 min, the cells were centrifuged at 4,000*g* for 5 min at 4°C and 3 ml of Solution II were added to resuspend the cell pellet. The cells were immediately divided in 100 µl aliquots and stored at -80°C.

Bacteria transformation with plasmid DNA

Competent cells were thawed on ice and the appropriate amount of DNA (plasmid DNA: 0.1-50 ng; ligation mixture: 5 µl) were added each cell aliquot (100 µl) and gently swirled. The microtube was incubated on ice for 20 min and heat shocked at 42°C for 90 sec. The microtubes

were then incubated on ice for 30 min before adding 0.9 ml of SOC medium. The tubes were subsequently incubated at 37°C for 30 min with shaking at 220 rpm. The culture was centrifuged at 12,000*g* and the supernatant discarded. The cells were then resuspended in 100 µl of the selective medium and spread on the appropriate agar medium. The plates were incubated at 37°C for 16 h until colonies appeared. Control transformations were also performed in parallel. These always included a negative control transformation without DNA and a positive control transformation with 0.1 ng of non digested plasmid, such as pAS2-1.

II.2.1.9 Isolation of plasmids from transformants "Miniprep"

In order to screen for the recombinant plasmid in the transformants, the plasmid DNA was extracted from several isolated bacterial colonies for subsequent restriction fragment analysis and sequencing.

Method 1 – Alkaline lysis "miniprep"

A single bacterial colony was transferred into 3 ml of LB medium containing ampicillin (100 µg/ml) and incubated overnight at 37°C with vigorous shaking (220-250 rpm). 1.5 ml of this culture were transferred into a microtube and centrifuged at 12,000*g* for 1 min at 4°C and the supernatant was discarded. The cell pellet was resuspended in 100 µl of ice-cold Solution I by vigorous vortexing. Then, 200 µl of freshly prepared Solution II were added to the microtube that was mixed by inverting several times. Keeping the microtube on ice, 150 µl of ice-cold Solution III were added and again the microtube inverted several times. After the microtube was allowed to stand on ice for 5 min, it was centrifuged at 12,000*g* for 10 min at 4°C and the supernatant transferred to a clean microtube. The DNA was precipitated by adding 2 volumes of ice-cold ethanol. The mixture was vortexed and placed at -20°C for 30 min. After centrifugation at 12,000*g* for 10 min at 4°C, the supernatant was completely removed and the pellet washed with 70% ethanol. Following centrifugation, the pellet was allowed to dry. The DNA was dissolved in H_2O containing DNAase-free RNAase (20 µg/ml) and stored at -20°C.

Method 2 – QIAGEN "miniprep"

The bacterial pellet was obtained as described above. The pellet was then resuspended in 250 µl of buffer P1 (QIAGEN), 250 µl of buffer P2 (QIAGEN) were added and the microtube was mixed by gently inverting until the solution became viscous and slightly clear. Afterwards, 350 µl

of buffer N3 were added and the microtube was repeatedly inverted until the solution became cloudy. The microtube was centrifuged for 10 min and the resulting supernatant was applied to a QIAprep spin column placed in a microtube. After a 1 min centrifugation (12,000*g*) the flow-through was discarded. The column was washed by adding 0.75 ml of buffer PE (QIAGEN) and centrifuged for 1 min to discard the flow-through, and then a subsequent 1 min centrifugation to remove residual wash buffer. Finally, the column was placed in a clean microtube and 50 µl of H_2O were added to elute the DNA by centrifuging for 1 min having let it stand for 1 min. This method gives a cleaner DNA preparation than Method 1 with better yields. This method was used when the DNA was subsequently processed for DNA sequencing. For enzymatic restriction the first method was commonly employed.

II.2.1.10 Restriction fragment analysis of DNA

Plasmid DNA was analyzed throughout the digestion with a convenient restriction endonuclease, namelly HindIII. For the plasmid DNA digestion the manufacturer's instructions were followed, as described previously (section II.2.1.2).

II.2.1.11 Electrophoretic analysis of DNA

The electrophoresis apparatus was prepared and the electrophoresis tank was filled with enough 1x TAE buffer to cover the agarose gel. The appropriate amount of agarose was transferred to an Erlenmeyer with 50 ml 1x TAE. The slurry was heated until the agarose was dissolved and allowed to cool to 60°C before adding ethidium bromide to a final concentration of 0.5 µg/ml. The agarose solution was poured into the gel cast and the comb was positioned. After the gel became solid the comb was carefully removed and the gel immersed in the tank. The DNA samples were mixed with the 6x loading buffer (LB) (0.25% bromophenol blue/ 30% glycerol in water) and the mixture was loaded into the slots of the submerged gel using a micropipette. Marker DNA was also loaded into the gel (1kb ladder or 1 Kb plus, Invitrogen). The lid of the gel tank was closed and the electrical leads were attached so that the DNA migrated towards the anode. The gel was run until the bromophenol blue had migrated the appropriate distance through the gel. At the end, the gel was examined by UV light and photographed or analyzed on a Molecular Imager (Biorad).

II.2.1.12 DNA sequencing

All the DNA samples to be sequenced were subjected to the same protocol. If the DNA was obtained by the "alkaline lysis miniprep" method and had not been purified by QIAGEN miniprep spin column (section II.2.1.9), it was purified in a QIAquick spin column (QIAGEN DNA Purification Kit) as described bellow.

QIAGEN DNA Purification kit

Briefly, 5 volumes of buffer PB (QIAGEN) were added to 1 volume of the solution to be purified and mixed. The QIAquick spin column was placed in a collection microtube and the sample was applied to the column and centrifuged for 1 min at 12,000*g* to bind the DNA. The flow-through was discarded and the column was washed with 0.75 ml of buffer PE (QIAGEN), centrifuged for 1 min at 12,000*g* and the flow-through discarded. The column was placed back in the same microtube and centrifuged again to remove traces of washing buffer. Then, the column was placed in a clean microtube, 50 µl of DNAse-free water were added and allowed to stand for 1 min. To elute the DNA the column was centrifuged for 1 min at 12,000*g*. The DNA was stored at -20°C.

Sequencing reaction

In a 0.5 ml microtube the following components were added:

- 500 ng of dsDNA
- 4 µl of Ready Reaction Mix*
- 3.2 pmol primer
- H_2O to a final volume of 20 µl

* Ready Reaction Mix is composed of: dye terminators, deoxynucleoside triphosphates, AmpliTaq DNA polymerase, FS, rTth pyrophosphatase, magnesium chloride and buffer (Applied Biosystems).

This reaction mixture was mixed and spun down for a few seconds. The cycle sequencing reaction was then performed using the following conditions:

96°C 1 min

96°C 30 sec
42°C 15 sec
60°C 4 min
} 25 cycles

Afterwards, the samples were purified by ethanol precipitation. Briefly, 2.0 µl of 3 M sodium acetate (pH 4.6) and 50 µl of 100% ethanol were added to the reaction mixture in a microtube, mixed and incubated at RT for 15 min to precipitate the extension products. The microtube was then centrifuged at 12,000*g* for 20 min at RT. After discarding the supernatant, 250 µl of 70% ethanol were added, the microtube was briefly vortexed and recentrifuged for 5 min at 12,000*g* at RT. The supernatant was discarded and the pellet dried. After this procedure, the DNA was ready to be applied in an Automated DNA Sequencer (ABIPRISM 310, Applied Biosystems).

II.2.2 Results

The resulting bait plasmids were sequenced using the GAL4-BD sequencing primer (Clontech), which anneals with the pAS2-1 vector, to check the orientation of the insert and the reading frame. For bait-3, pAS2-1-AICD^{Y687F}, whose insert is only 150 bp this sequencing reaction was enough to span the entire insert and both insert-vector junctions (Fig. II.4). Baits 1 and 2 were also sequenced with several insert-specific primers and MATCHMAKER DNA-BD 3' Insert Screening Amplimer (pAS2-1, reverse; Clontech).

The three bait plasmids, pAS2-1-APP, pAS2-1-APP^{Y687F} and pAS2-1-AICD^{Y687F} showed correct insert sequence, correct orientation and correct reading frame with Gal4-BD.

```
atgaagctactgtcttctatcgaacaagcatgcgatatttgccgacttaaaaagctcaag 60
M  K  L  L  S  S  I  E  Q  A  C  D  I  C  R  L  K  K  L  K   20

tgctccaaagaaaaaccgaagtgcgccaagtgtctgaagaacaactgggagtgtcgctac 120
C  S  K  E  K  P  K  C  A  K  C  L  K  N  N  W  E  C  R  Y   40

tctcccaaaaccaaaaggtctccgctgactagggcacatctgacagaagtggaatcaagg 180
S  P  K  T  K  R  S  P  L  T  R  A  H  L  T  E  V  E  S  R   60

ctagaaagactggaacagctatttctactgatttttcctcgagaagaccttgacatgatt 240
L  E  R  L  E  Q  L  F  L  L  I  F  P  R  E  D  L  D  M  I   80

ttgaaaatggattctttacaggatataaaagcattgttaacaggattatttgtacaagat 300
L  K  M  D  S  L  Q  D  I  K  A  L  L  T  G  L  F  V  Q  D   100

aatgtgaataaagatgccgtcacagatagattggcttcagtggagactgatatgcctcta 360
N  V  N  K  D  A  V  T  D  R  L  A  S  V  E  T  D  M  P  L   120

acattgagacagcatagaataagtgcgacatcatcatcggaagagagtagtaacaaaggt 420
T  L  R  Q  H  R  I  S  A  T  S  S  S  E  E  S  S  N  K  G   140

caaagacagttgactgtatcgccggtattgcaatacccagctttgactcatatggccatg 480
Q  R  Q  L  T  V  S  P  V  L  Q  Y  P  A  L  T  H  M  A  M   160

gtgatgctgaagaagaaacagtacacatccattcatcatggtgtggtggaggttgacgcc 540
V  M  L  K  K  K  Q  Y  T  S  I  H  H  G  V  V  E  V  D  A   180

gctgtcaccccagaggagcgccacctgtccaagatgcagcagaacggctacgaaaatcca 600
A  V  T  P  E  E  R  H  L  S  K  M  Q  Q  N  G  Y  E  N  P   200

accttcaagttctttgagcagatgcagaactgacccggggatccgtcgacctgcagccaa 633
T  F  K  F  F  E  Q  M  Q  N  ^^^                            210
```

Figure II.4: Partial sequence of the pAS2-1-AICD^{Y687F} fusion construct (Bait-3). Human AICD^{Y687E} sequence is in blue; Gal4-BD sequence that is fused to AICD is in black; mutation site in Tyr-687 is in red; NcoI restriction site is in green and Sma I is in brown; Stop codon is in pink.

II.3 BAIT AUTO-ACTIVATION TEST

After obtaining the Gal4-BD fusion constructs, it was necessary to demonstrate that the bait proteins do not autonomously activate the reporter genes *HIS3*, *ADE2* and *MEL1*, for example, due to intrinsic DNA-binding and/or transcriptional activation sequences.

In order to analyze the ability of the recombinant constructs to activate the reporter genes, they were independently transformed into the AH109 yeast strain. The transformed cells were selected on medium without tryptophan, because the pAS2-1 carries the *TRP1* gene for selection in Trp^- auxotrophic yeast strains. In order to verify that Gal4-BD fusion constructs do not activate reporter genes: the transformants from the previous step were assayed for growth in medium lacking histidine and adenine and for blue appearance of the colonies in the presence of X-α-Gal.

II.3.1 Materials and Methods

II.3.1.1 Yeast transformation with plasmid DNA

Preparation of competent yeast cells

One yeast colony was inoculated into 1 ml of YPD medium in a 1.5 ml microtube and vortexed vigorously to disperse cell clumps. The culture was transferred into a 250 ml flask containing 50 ml of YPD and incubated at 30°C with shaking at 230 rpm overnight, until it reached the stationary phase with OD_{600nm}>1. An amount of this culture (20-40ml), sufficient to produce an OD_{600nm}=0.2-0.3, was transferred into 300 ml YPD in a 2 L flask. The culture was incubated for 3 h at 30°C with shaking at 230 rpm, and then centrifuged at 4000*g* for 5 min at room temperature. The supernatant was discarded and the cells resuspended in 25 ml of sterile H_2O. The cells were recentrifuged and the pellet was resuspended in 1.5 ml of freshly prepared, sterile 1x TE/LiAc.

Yeast transformation- Lithium acetate (LiAc)-mediated method

In a microtube 200 ng of plasmid DNA were added to 100 µg of herring testes carrier DNA. Then, 100 µl of freshly prepared competent cells were added to the microtube, followed by 600 µl of sterile PEG/LiAc (40% PEG 4000/ 1x TE/LiAc). The mixture was incubated at 30°C for 30 min with shaking (200 rpm). After adding 70 µl of DMSO the solution was mixed gently and then heat-

shocked for 15 min in a 42°C water bath. The cells were pelleted after being chilled on ice, centrifuged for 5 sec at 12,000*g* and resuspended in 0.5 ml of sterile 1x TE buffer. The cells were then plated in the appropriate SD selection medium (SD/-Trp selects transformants with pAS2-1 plasmid constructs), and incubated at 30°C for 2-4 days, until colonies appeared.

II.3.1.2 Bait autoactivation tests

The AH109 yeast cells independently transformed with the three bait plasmids (pAS2-1-APP, pAS2-1-APP^{Y687F} and pAS2-1-AICD^{Y687F}) and with the pAS2-1 empty vector, were replica plated on SD/-Trp/X-α-Gal, SD/-Trp/-His/X-α-Gal and SD/-Trp/-Ade/X-α-Gal. The plates were incubated at 30°C for 2-4 days.

II.3.2 Results

The three bait plasmids (pAS2-1-APP, pAS2-1-APP^{Y687F} and pAS2-1-AICD^{Y687F}) were independently tested for growth in selective media lacking His and Ade. None of the bait plasmids were able to drive the expression of the nutritional reporter genes *HIS3* and *ADE2*, since no growth was detected. Likewise, the colorimetric reporter gene *MEL1* was not activated by any of the fusion constructs, since no blue color was detected in the SD/-Trp/X-α-Gal. All the Gal4-BD fusion genes behaved similarly to the pAS2-1 empty vector, which was expressed as a negative control (Table II.5).

Table II.5: Results of the baits autoactivation tests.

Bait	*Growth and Blue color*		
	SD/-Trp/X-α-Gal	**SD/-Trp/-His/X-α-Gal**	**SD/-Trp/-Ade/X-α-Gal**
Bait 1 – APP	white colonies	no growth	no growth
Bait 2 - APP^{Y687F}	white colonies	no growth	no growth
Bait 3 - AICD^{Y687F}	white colonies	no growth	no growth
Negative control (empty pAS2-1)	white colonies	no growth	no growth

II.4 EXPRESSION OF THE BAIT PROTEINS IN YEAST

In order to verify the ability of the recombinant constructs to drive the Gal4-BD-bait fusion protein expression, the bait constructs were independently transformed into the yeast strain AH109. The transformed cells were grown on the appropriate selective medium (SD/-Trp) and each Gal4-BD-bait expression was confirmed by immunobloting of the corresponding protein extracts.

II.4.1 Materials and Methods

II.4.1.1 Expression of proteins in yeast

Preparation of yeast cultures for protein extraction

A colony of each previously transformed yeast was inoculated in 5 ml of the appropriate SD selection medium (SD/-Trp) and incubated at 30°C with shaking at 230 rpm overnight. As a negative control an untransformed yeast colony was inoculated in YPD. The overnight cultures were vortexed and separately added to 50 ml aliquots of YPD. These cultures were incubated at 30°C with shaking (220 rpm) until OD_{600nm}=0.4-0.6. At this point the cultures were quickly chilled by pouring them into a prechilled 50 ml centrifuge microtube halfway filled with ice. The tubes were immediately centrifuged at 1,000 g for 5 min at 4°C. The supernatant was discarded and the cell pellet was washed in 50 ml of ice-cold water. The pellet was recovered by centrifugation at 1,000 g for 5 min at 4°C and immediately frozen by placing tubes in liquid nitrogen.

Preparation of protein extracts

The cell pellets were quickly thawed by resuspending each one in 100 µl of prewarmed cracking buffer (60°C) per 7.5 OD_{600} units of cells (OD_{600} of a 1 ml sample multiplied by the culture volume). The samples were briefly thawed in a 60°C water bath. After 15 min an additional aliquot (1 µl of 100x PMSF per 100 µl of cracking buffer) of the 100x PMSF stock solution was added to the samples and every 7 min thereafter during the procedure. Each cell suspension was transferred into a 1.5 ml microtube containing 80 µl of glass beads per 7.5 OD_{600} units of cells. The samples were heated at 70°C for 10 min to release the membrane-associated proteins. Then, the

microtubes were vortexed vigorously for 1 min and centrifuged at 12,000*g* for 5 min at 4°C. The supernatants were transferred to fresh microtubes and placed on ice. The pellets were boiled for 5 min, vortexed for 1 min and centrifuged again, the resulting supernatants were combined with the first ones. The samples were boiled and loaded immediately on a gel.

II.4.1.2 SDS-PAGE

The Gal4 DNA-binding domain encoded by the yeast vector pAS2-1 migrates around 21 kDa in SDS-PAGE. Full-length APP_{695} (bait-1 and bait-2) is predicted to migrate around 100 kDa, and the predicted molecular weight of APP C-terminus of 50 amino acids (bait-3) is around 5 kDa (Table II.6).

Table II.6: Approximate sizes of Gal4-BD and control fusion proteins.

Bait	Fusion construct	Fusion protein	Predicted MW of fusion protein (kDa)
Bait-1	pAS2-1-APP	Gal4-BD-APP	120
Bait-2	pAS2-1-APP^{Y687F}	Gal4-BD-APP^{Y687F}	120
Bait-3	pAS2-1-AICD^{Y687F}	Gal4-BD-AICD^{Y687F}	26
control	pAS2-1 empty vector	Gal4-BD	21

In order to visualize the expression of the fusion proteins Gal4-BD-APP and Gal4-BD-APP^{Y687F}, a 6.5% gel was used. The shorter Gal4-BD-AICD^{Y687F} fusion peptide was visualized in a 12% gel (Table II.7).

Each running gel was prepared by sequentially adding the components indicated on Table II.7 (APS and TEMED were added last, as they initiate the polymerizing process). The solution was then carefully pipetted down the spacer into the gel sandwich, leaving some space (4 cm) for the stacking gel. Then, water was carefully added to cover the top of the gel and the gel was allowed to polymerize for 1 h. The stacking gel was prepared according to Table II.7. The water was poured out and the stacking gel was added to the sandwich; a comb was inserted and the gel was

allowed to polymerize for 30 min. Then, the samples were prepared by the addition of ¼ volume of loading gel buffer. The microtube was boiled and centrifuged, the combs removed and the wells filled with running buffer. The samples were carefully applied into the wells that were filled with running buffer, and the samples were run at 45 mA (1 gel in the system) or 90 mA (2 gels in the system) until the bromophenol blue from the LB reached the bottom of the gel.

Table II.7: Composition of the running and stacking gels for SDS-PAGE (*Buffers composition is in Appendix I). Recipes for one gel (30 ml; 1.5 mm thick Hoefer SE 600/400).

Components	Running gel final concentrations				Stacking gel
	12%	10%	7.5%	6.5%	(3.5%)
Water	10.4 ml	12.6 ml	14.6 ml	15.8 ml	6.6 ml
30%Acryl./8%Bisacryl.	12.0 ml	9.9 ml	7.5 ml	6.5 ml	1.2 ml
4X LGB*	7.5 ml	7.5 ml	7.5 ml	7.5 ml	-------
5X UGB*	-------	-------	-------	-------	2.0 ml
SDS 10%	-------	-------	-------	-------	100.0 µl
10% APS	150.0 µl	150.0 µl	150.0 µl	150.0 µl	100.0 µl
TEMED	15.0 µl	15.0 µl	15.0 µl	15.0 µl	10.0 µl

II.4.1.3 Western blot transfer

For immunoblotting the tank transfer system (Hoefer) was used as follows: 3MM blotter paper was cut to fit the transfer cassette and a nitrocellulose membrane of the gel size was also cut. The gel was removed from the electrophoresis device and the stacking gel removed and discarded. The transfer sandwich was assembled under transfer buffer to avoid trapping air bubbles. The cassette was placed in the transfer device filled with transfer buffer. Transfer was allowed to proceed overnight at 200 mA. Afterwards, the transfer cassettes were disassembled; the membrane carefully removed and allowed to air dry prior to further manipulations.

II.4.1.4 Immunodetection by enhanced chemiluminescence (ECL)

ECL™ (GE Healthcare) is a light emitting non-radioactive method for the detection of immobilized antigens, conjugated directly or indirectly with horseradish peroxidase-labelled antibodies.

Fusion proteis corresponding to bait-1 and bait-2 were detected with the mouse monoclonal antibody 22C11 (Boehringer), targeted to APP N-terminus. To visualize the fusion protein GAL4-BD-AICD^{Y687F} two distinct blots were probed with different antibodies: GAL4 DNA-BD monoclonal antibody (Clontech) and 369 polyclonal antibody, that recognizes the carboxy-terminus of human APP (a kind gift from Professor Samuel E. Gandy - Mount Sinai Medical Center, NY, USA).

Protocol for the 22C11 monoclonal antibody

The membrane was soaked in 1x TBS for 10 min. Non-specific binding sites were blocked by immersing the membrane in 5% low fat milk in TBST for 2 h. After washing with 1x TBST, the membrane was incubated with a solution of the primary antibody diluted (1:150) in 5% low fat milk in TBST for 4 h with shaking. The membrane was allowed to stand in the primary antibody/milk solution overnight at 4°C. After three washes of 10 min with 1x TBST the membrane was incubated with a solution of the anti-mouse secondary antibody diluted (1:5000) in 5% low fat milk in TBST for 1 h with shaking. The membrane was then washed 3 times for 10 min.

Protocol for the GAL4 DNA-BD monoclonal antibody

The membrane was soaked in 1x TBS for 10 min. Non-specific binding sites were blocked by immersing the membrane in 5% low fat milk in TBST for 2 h. After washing with 1x TBST, the membrane was incubated with a solution of the primary antibody diluted (0.5 µg/µl) in 5% low fat milk in TBST for 2 h with shaking. After three washes of 10 min with 1x TBST the membrane was incubated with a solution of the anti-mouse secondary antibody diluted (1:5000) in 5% low fat milk in TBST for 1 h with shaking. The membrane was then washed 3 times for 10 min.

Protocol for the 369 polyclonal antibody

The procedure was similar to that described above, but the membrane was blocked by immersing it in 5% low fat milk in TBST for 3 h, with shaking, plus an overnight incubation at 4°C. After washing with 1x TBST, the membrane was incubated with a solution of the primary antibody diluted in 5% low fat milk in TBST for 2 h with shaking. After washing 6 times for 15 min in 1x TBST the membrane was incubated with the anti-rabbit secondary antibody diluted (1:5000) in 5% low fat milk in TBST for 1h30min with shaking. The membrane was then washed 6 times for 15 min.

Subsequently the membrane was incubated for 1 min at RT with the ECL detection solution (a mixture of equal volumes of solution 1 and solution 2 from the ECL kit, approximately 0.125ml/cm2 membrane). Inside the dark room, the membrane was gently wrapped with cling-film, eliminating all air bubbles and placed in a film cassette and an autoradiography film (XAR-5 film, KODAK) was placed on the top. The cassette was closed and the blot exposed for short periods of time. The film was then removed and developed in a developing solution, washed in water and fixed in fixing solution. If needed, a second film was exposed for a longer or shorter period depending on the outcome the first exposure.

II.4.2 Results

To carry out a YTH screen it is necessary to demonstrate that the Gal4-BD-bait fusion protein is expressed in yeast cells. In order to analyze the ability of the three bait recombinant constructs to be expressed in yeast, they were independently transformed into the AH109 yeast strain. The protein extracts produced in section II.4.1.1 were analyzed by western blotting using antibodies targeted to the Gal4-BD or the fusion APP peptide.

Expression of bait-1 and bait-2 were analyzed in the same blot, since the sizes of the corresponding fusion proteins, Gal4-BD-APP and Gal4-BD-APP^{Y687F}; are practically the same. The anti-APP 22C11 antibody detects the expected band around 120 kDa for both bait fusion proteins. As expected, no signal is dected in the control yeast protein extract, which expresses the Gal4-BD alone (Fig. II.5, A).

The expression of Gal4-BD-AICD^{Y687F} (bait-3) was probed with GAL4 DNA-BD monoclonal antibody, which recognized the GAL4-BD peptide (Fig. II.5, B). A band of the expected molecular mass (26 KDa) was detected in the protein extract from yeast cells containing the bait-3 plasmid

(Fig. II.5, B, lane 2), demonstrating that the yeast cells are expressing the fusion protein. As expected for the control yeast, the peptide is smaller (21 kDa), because it is encoded by pAS2-1 vector without the fusion construct. When probed with 369 antibody, in the first lane the GAL4-BD is not detected (Fig. II.5, C).

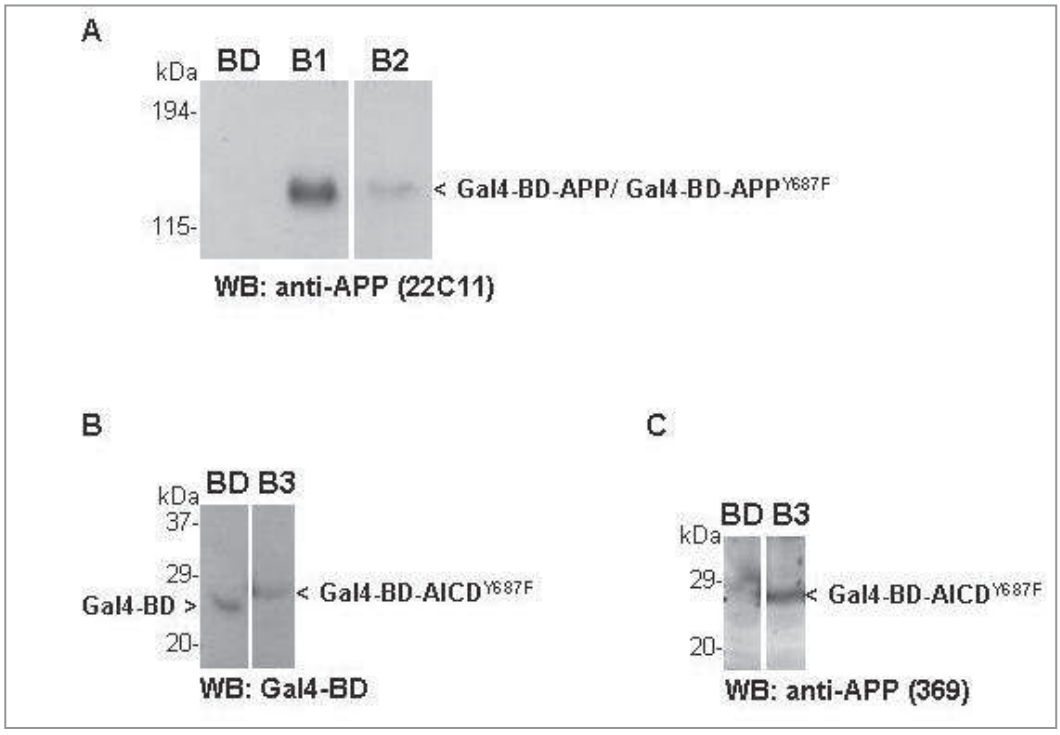

Figure II.5: Immunoblot analysis of yeast protein extracts. (A) The 22C11 antibody was used to detect bait-1 (B1) and bait-2 (B2), which corresponds to the fusion proteins Gal4-BD-APP and Gal4-BD-APP^{Y687F}, respectively. BD, control yeast transformed with empty pAS2-1 vector. (B) Expression of bait-3 (B3; Gal4-BD-AICD^{Y687F}) probed with GAL4-BD antibody and (C) with the anti-APP antibody 369. *In A, B and C two parallel sections from the same gel are represented.*

In summary, the three bait fusion constructs were successfully obtained. Having demonstrated that they do not autonomously activate reporter gene expression and that the fusion proteins are expressed in yeast, all the prerequisites were verifyed, the YTH screens were thus carried out.

II.5 TWO-HYBRID LIBRARY SCREENING USING YEAST MATING

To unravel the interactome of wild-type APP, APP^{Y687F} and AICD^{Y687F}, three YTH screens were performed (Table II.8). Two aliquots of a Pretransformed Human Brain MATCHMAKER cDNA Library (CAT. HY4004AH; Clontech) were used for YTH-s1 and YTH-s2. This library was constructed using whole brain mRNA from a 37 years old Caucasian male (cause of death: trauma). Pretransformed MATCHMAKER libraries are high-complexity cDNA libraries cloned into the yeast Gal4-AD vector pACT-2 and pretransformed into *S. cerevisiae* Y187 host strain.

Table II.8: Description of the bait and corresponding cDNA library for each YTH screen.

YTH screen	**Bait**		**cDNA Library**	
	Gal4-BD fusion	*host strain*	*Gal4-AD fusion*	*host strain*
YTH-s1	APP (Bait 1)	AH109	Pretransformed Human Brain MATCHMAKER cDNA library (Clontech) *mRNA source: whole brain from a 37-yr-old Caucasian male (cause of death: trauma)*	Y187
YTH-s2	APP^{Y687F} (Bait 2)	AH109		Y187
YTH-s3	AICD^{Y687F} (Bait 3)	Y187	Human brain MATCHMAKER cDNA library (Clontech) *mRNA source: whole brain from a 60-yr-old Caucasian male (cause of death: sudden death)*	AH109

For YTH-s3 a Human brain MATCHMAKER cDNA library in *E. coli* BNN132 was obtained (CAT:HL4004AH, Clontech). The mRNA source was the whole brain from a 60 years old Caucasian male (cause of death: sudden death). To make this cDNA library available for YTH screening, several steps were previously carried out in our laboratory: library amplification in *E. coli*; library DNA isolation; library-scale transformation in yeast strain AH109; plating the transformation

mixture; and harvesting the transformants at high viabilityand density in freezing medium. The frozen aliquots were thus ready to use for YTH screening.

II.5.1 Methods

The procedure adopted to perfom three distinct YTH screens, using as baits APP (YTH-s1), APP^{Y687F} (YTH-s2) and $AICD^{Y687F}$ (YTH-s3), was the same.

II.5.1.1 cDNA library screening by yeast mating

A concentrated overnight culture of the bait strain was prepared by inoculating a colony of the bait strain into 50 ml of SD/-Trp and incubating it at 30°C overnight with shaking at 250 rpm. The next day, when OD_{600}>0.8, the culture was centrifuged at 1,000 g for 5 min, the supernatant was decanted and the pellet was resuspended in the residual liquid (5 ml) by vortexing. The cells' concentration (> $1x10^9$ cells/ml) was verified in an haemocytometer. Just prior to use, a frozen aliquot (1 ml) of the library culture was thawed in a water bath at room temperature. The library was gently mixed and 10 µl were set aside for titering. The entire bait strain culture was combined with the 1 ml library aliquot in a 2 L sterile flask, 45 ml of 2x YPDA were added and gently swirled. This culture was incubated at 30°C for 20-24 h, with shaking at 40 rpm. After 20 h of mating a drop of the mating culture was checked under a phase-contrast microscope, to check for the presence of zygotes, thereafter allowing the mating to proceed for another 4 h. The mating mixture was transferred to a sterile 50 ml tube and the cells spun down at 1,000 g for 10 min. The mating flask was rinsed twice with 2x YPDA (50 ml) and the rinses were combined and used to resuspend the first pellet. The cells were centrifuged again at 1,000 g for 10 min, the pellet resuspended in 10 ml of 0.5x YPDA and the total volume (cells + medium) was measured. Half of the library mating mixture was plated on SD/QDO (SD without Leu, Trp, Ade and His), and the other half on SD/TDO (SD without Leu, Trp and His), at 200 µl per 150 mm plate. For mating efficiency controls, 100 µl of 1:10,000, 1:1,000; 1:100 and 1:10 dilutions of the mating mixture were plated on 100 mm SD/-Leu, SD/-Trp and SD/-Leu/-Trp plates. All plates were incubated at 30°C until colonies appeared, generally 3-8 days on TDO and 8-21 days on QDO medium. Then, growth of the control plates was scored and the mating efficiency and number of clones screened was calculated. All positive clones were replated twice in SD/QDO medium containing X-α-Gal and incubated at 30°C for 3-8 days. True positives formed blue colonies. The master plates were

sealed with parafilm and stored at 4°C. Stocks in 25% glycerol were prepared for all the positive clones and stored at -80°C.

II.5.1.2 Library titering

A library aliquot (10 µl) was transferred to 1ml of YPDA in a 1.5 ml microtube – dilution A (dilution factor 10^{-2}). 10 µl from dilution A were added to 1 ml of YPDA in another microtube and mixed gently – dilution B (dilution factor 10^{-4}). From dilution B, 100 µl were spread onto three SD/-Leu plates. All the plates were incubated at 30°C for 3 days after which the number of colonies was counted. The titer of the library was calculated using the following formula: [#colonies]/[plating volume (ml)x dil factor] = cfu/ml.

II.5.2 Results

II.5.2.1 Mating efficiency and number of clones screened

The three YTH screens were performed by yeast mating, whereby more unique positive clones are usually obtained, due primarily to the "jump-start" that the new diploids receive before being plated on selective medium (Serebriiskii *et al.*, 2001). Additionally, diploid yeast cells are more vigorous than haploid cells and can better tolerate the expression of toxic proteins. Also, in diploids, the reporters are less sensitive to transcription activation than they are in haploids, reducing the incidence of false positives from transactivating baits (Kolonin *et al.*, 2000).

Three human brain cDNA library aliquots were screened to identify new interacting partners for bait-1, bait-2 and bait-3. The mating cultures was observed under a phase-contrast microscope to check for the occurrence of zygotes (Fig. II.6), indicative that mating was occurring as expected.

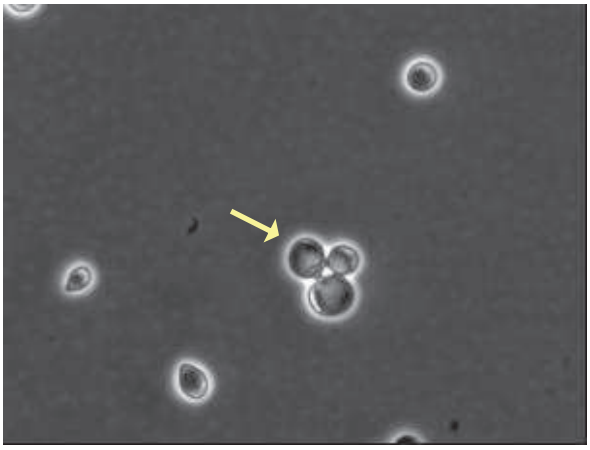

Figure II.6: Zygote formation in the mating mixture with its typical three-lobed shape. The arrow is pointing the budding diploid cell. The other two lobes are the two haploid (parental) cells. This picture was taken using an inverted microscope in phase contrast mode, during the mating event (40x magnification).

After plating the mating mixture in the appropriate selective media and waiting several days for colonies to appear, the growth on the control plates was scored and the mating efficiency and number of clones screened were calculated (Table II.9).

Table II.9: Estimation of mating efficiency and number of clones screened. To calculate the mating efficiency the following equation was used [# cfu (in SD –Leu/-Trp) X 1000µl/ml/ volume plated (µl) x dilution factor] / [# cfu (in SD -Trp) X 1000µl/ml/ volume plated (µl) X dilution factor] X 100. To estimate the number of clones screened the following equation was used [# cfu/ml of diploids X resuspension volume].

YTH screen	Bait (Gal4-BD fusion)	Mating efficiency (% diploids)	Clones screened
YTH-s1	APP (bait-1)	4.6 %	5.6×10^5
YTH-s2	APP^{Y687F} (bait-2)	7.9 %	4.2×10^6
YTH-s3	$AICD^{Y687F}$ (bait-3)	19.8 %	6.0×10^5

II.5.2.2 Positive clones isolation and re-testing

In each YTH screen performed, the mating mixture was plated on 40 150 mm plates (20 SD/TDO + 20 SD/QDO). Some colonies started to appear after 2-3 days, but the plates were incubated for 8 days (TDO) or 16 days (QDO) to allow slower growing colonies to appear. According to the Clontech's MATCHMAKER YTH System User Manual, true His^+, Ade^+ colonies are robust and can grow to more than 2 mm in diameter. The small, pale colonies that may appear after 2 days but never grow more than 1 mm should not be considered as positives clones. Nevertheless, all the colonies isolated from the SD/TDO and SD/QDO selective media plates were restreaked twice in SD/QDO plates in order to retest for the expression of the nutritional reporter genes *HIS3* and *ADE2* (Fig. II.7, A). His^+, Ade^+ colonies were further tested for *MEL1* expression, another reporter gene, by growing these putative primary positive clones in SD/QDO media with X-α-Gal. True positive clones grew and developped blue color (Fig. II.7, B).

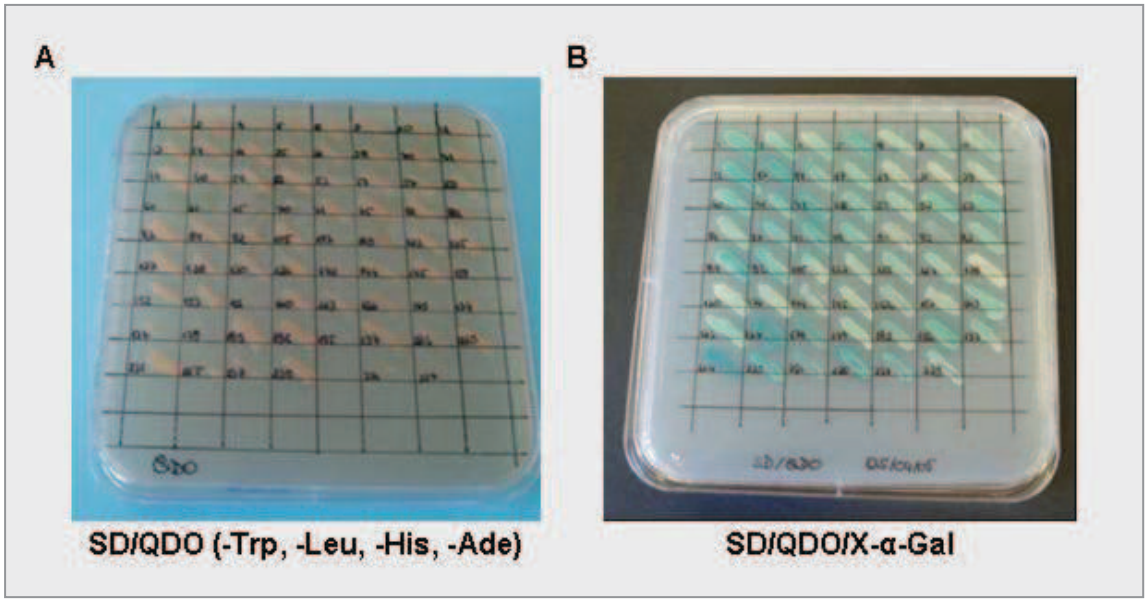

Figure II.7: Positive clones isolation and retesting. (A) Primary positive clones isolated from the original SD/TDO or SD/QDO plates and were all retested for growth in SD/QDO selective medium (lacking Trp, Leu, His and Ade). (B) *MEL-1* expression test of the positive clones obtained in the YTH screen. Light blue colonies also represent positive interactions, but took longer to turn blue in the presence of X-α-GAL.

The colonies isolated did not always grow or turned blue in SD/QDO/X-α-Gal, in particular the pale smaller colonies, which were isolated despite doubting that they were true positives. In Table II.10 the number of clones isolated and the number or true positive clones is summarized.

Table II.10: Number of colonies isolated and true positive clones in each YTH screen. All the colonies isolated from the SD/TDO and SD/QDO selective media plates were restreaked twice in SD/QDO plates. His^+, Ade^+ colonies were further tested for *MEL1* expression in SD/QDO/X-α-Gal. True positive clones grew and turned blue.

YTH screen	Bait (Gal4-BD fusion)	Colonies isolated	True positive clones
YTH-s1	APP (bait-1)	161	**60**
YTH-s2	APP^{Y687F} (bait-2)	579	**131**
YTH-s3	$AICD^{Y687F}$ (bait-3)	134	**88**

II.6 DISCUSSION

As with all detection methods, the YTH system is known to result in the detection of some false positives. This was a relatively serious problem in the early days of the YTH method but the elimination of such false positive results has been greatly improved by the recent YTH systems. False positive signals result from cells in which the reporter genes are active even though the bait and prey do not interact. There are several classes of false positives. For example, false positives may arise from preys that interact with DNA upstream of the reporter genes or with proteins that interact with promoter sequences. These two classes of false positives can be eliminated by the use of more than one reporter gene under the control of different promoters, as was the case with the present work. Another inherent problem with the system is that not all proteins will be efficiently folded and/or post-translationaly modified in the yeast nucleus, which may result in the protein not interacting with the true partner. In the same way, the protein may adopt a different tertiary structure when expressed as fusions with the transcription factor domains. Also, some proteins may be toxic when expressed as fusions in yeast, inhibiting growth when expressed at high levels. This can be avoided to some extent by the use of inducible expression plasmids. Other false positive results include interactions that occur in the YTH screen but not in a physiological context, because the partners are not expressed in the same cellular or subcellular environment at the same time.

By screening 5.1 x 10^4 clones from a human brain cDNA library with APP_{695} as bait 60 positive clones were obtained as accessed by their ability to grow on SD/QDO selective media and to turn blue in the presence of X-α-Gal. In YTH-s2, using as bait APP^{Y687F}, with a mutation that mimics the dephosphorylated state of Tyr-687, 4.2 x 10^6 clones were screened, resulting in 131 positive clones. These should include the APP interactome when it is dephosphorylated on Tyr-687. The YTH-s3 was carried out with the 50 aa C-terminus of mutant APP, $AICD^{Y687F}$ and 6 x 10^5 clones were screened resulting in isolation of 88 true positive clones.

Subsequently the positive clones were identified (Chapter III). Validation of protein protein interactions and subsequent analysis can be later applied to some positive clones, since numerous molecular and cellular biology methods can be employed to explore new protein interactions.

CHAPTER III. IDENTIFICATION OF THE POSITIVE CLONES AND *IN SILICO* ANALYSIS OF APP/AICD NETWORKS

III.1 INTRODUCTION

Human protein interaction maps play an increasingly important role in biomedical research and have been shown to be highly valuable in the study of a variety of human diseases and signaling pathways. The yeast two-hybrid (YTH) system provides a platform for the rapid generation of large scale protein-protein interaction (PPI) networks. The majority of the APP binding proteins that have been identified to date were discovered using the two-hybrid methodology, which allows for the identification of binary interactions. Other methods, such as the affinity purification/mass spectrometry approach, can identify larger protein complexes, containing reciprocal interactions among complex components (Goudreault *et al.*, 2009). Since the YTH system is based on the interaction of hybrid proteins in a living yeast cell, it offers numerous advantages in comparison to biochemical methods, such as detection of PPIs *in vivo*, high sensitivity to detect rare interactions and avoidance of expensive production of antibodies or protein purifications. Nevertheless, the novel PPIs identified by YTH screening should be validated, at first in the YTH system, and then confirmed by other *in vivo* and *in vitro* methods. These confirmatory studies can virtually exclude all classes of false positives. The main objectives are to prove that a new interaction between two proteins is specific and direct, prove that the two proteins can "meet" in the same subcellular environment, and investigate the physiological relevance of the interaction. Often, when performing an YTH screen, only a few clones are selected for validation and for further functional investigation in a relevant biological system.

Several protocols are suggested for the initial identification of the positive clones by the YTH system manufacturer (Clontech). One can make a decision according to the number of clones to analyze, expertise/affinity with a given method, time and resources available, etc. In the work here described the strategy adopted for each positive clone isolated was the following:

i. Extraction of plasmid DNA from yeast cells;
ii. Rescue of library plasmids via transformation in *E.coli*;
iii. Analysis of library inserts by restriction digestion and DNA sequencing;
iv. Identification of interacting proteins by database searching;
v. Validation of selected positive clones.

Classes of presumed false positives:

Arbitrary criteria have been used to define false positives in the YTH system. For instance, a false positive can be any clone that fails to reproduce the interaction with the bait upon retransformation; a clone that is subsequently shown to interact with multiple unrelated baits; a protein that appears implausible as a partner based on the known physiology of bait and prey (e.g., the proteins are not known to be expressed in the same subcellular compartment at the same time); or a clone for which interaction cannot be confirmed by other methods (e.g. co-immunoprecipitations, GST pull-downs, etc.), although the interaction can be real but below the sensitivity threshold of non two-hybrid methods (Serebriiskii and Golemis, 2001). Hence, classification of a positive clone as a presumed false positive can arise from: (1) the initial analysis of the library insert sequence; (2) failure to validate the bait-prey interaction using the YTH system; or (3) failure to validate the bait-prey interaction by other non two-hybrid methods. The majority of the criteria summarized below are not exclusion rules, some are purely judgment calls. Nevertheless, wasting time and resources to exclude a presumed false positive should be avoided, when the main interest is the bait biology.

1) False positive clones arising from the analysis of library cDNA sequence and ORF identification:

- *alignment out of coding sequence* – The library insert sequence aligns with the 3'-untranlated region (3'-UTR) of a given cDNA. However, it might be a real positive if another open reading frame (ORF) is present downstream of the stop codon, since nontranslated gaps upstream of ORF inserts are commonly found in genomic libraries. Due to occasional translational read-through, two different ORFs may be expressed as a fusion with the Gal4-AD, eventhough a nontranslated gap comes between them.

- *early stop in the sequence* – A very small peptide (less than 10 aa) is fused to the Gal4-AD or no fusion peptide is present at all. Though it might be a real positive if another ORF is present downstream this stop codon, as described above.

- *inverted library insert* – The library insert is in the reverse orientation relative to the Gal4-AD fusion. Nevertheless, it might be a real positive given that the insert can be transcribed in

the reverse orientation from a cryptic promoter within the *ADH1* terminator. Such proteins function as transcriptional activators as well as interacting with the bait protein (Chien *et al.*, 1991).

▪ *wrong reading frame* – When the library insert is in a different reading frame from the Gal4-AD. If it is a large ORF, it can be a genuine positive clone because yeasts tolerate translational frameshifts and can express the correct fusion protein, which will promote survival in the selective medium (Gesteland and Atkins, 1996).

▪ *mitochondrial clones* – Library inserts aligning with mitochondrial genome encoded proteins are unlikely to interact with the bait if the latter is not known to be expressed in mitochondria.

▪ *"sticky proteins"* – Broadly interactive proteins may have intrinsic secondary structure properties (e.g. exposed hydrophobic or charged patches) that lead to non-specific frequent interactions or the biological function of a protein may involve binding a large number of different proteins (e.g. HSPs, proteasomal subunits, proteins involved in transport functions, etc.) (Serebriiskii and Golemis, 2001). A survey of published data and web resources might lead to lists of proteins frequently isolated in YTH screens, less likely to be of biological significance. However, these preys are not always false positives, since the natural function of the bait may involve binding to HSPs, proteins involved in transport, etc.

▪ *proteins inducing biological effects in yeast cells* – Expression of a prey that induces indirect effects on yeast metabolism (altered growth rate, viability, cell permeability, etc.) might bias transcriptional activation of reporter genes (Serebriiskii and Golemis, 2001).

2) False positive clones failing the validation using the YTH system:

▪ *prey auto-activates reporter genes* – The library-encoded protein can activate the reporter genes due to non-specific interaction with the DNA-BD of the bait fusion. This class of false positives also includes proteins that interact directly with promoter sequences or with DNA upstream of reporter genes (e.g. chromatin or transcription operating proteins) (Fig. III.1). The

occurrence of these false positive clones is reduced in YTH systems that use several independent reporter genes, nevertheless any α-galactosidase positive colonies that contain the library plasmid alone should be discarded.

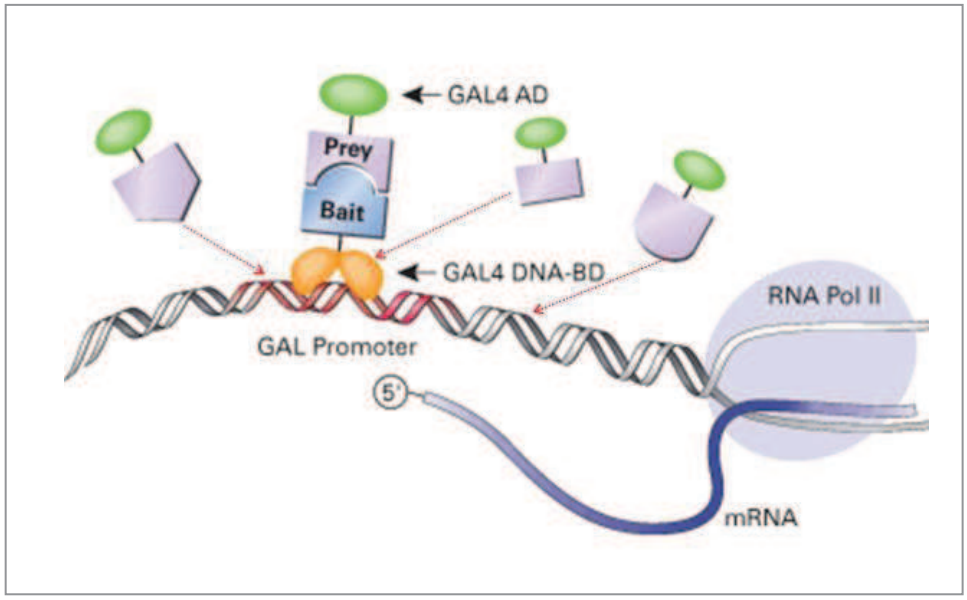

Figure III.1: False positive clones that auto-activate reporter genes. Library-derived prey fusion proteins auto-activate reporter genes if they interact non-specifically with the DNA-binding domain, or if they interact directly with promoter sequences or with DNA upstream of reporter genes (*Adapted from http://www.clontech.com/images/brochures/BR943071_MMGold_IN.pdf*).

▪ *fails to reproduce the interaction in the YTH* – Yeast cells can incorporate more than one library plasmid, therefore an isolated prey plasmid should be co-introduced in yeast with the bait plasmid, by co-transformation or yeast mating, to confirm the positive interaction. A prey that fails to reproduce the interaction with the bait upon retransformation should be discarded.

3) False positives failing the validation by other non two-hybrid methods:

▪ *fails to interact with bait by other methods* – The new protein-protein interactions (PPIs) confirmed in the YTH system should be further validated by other methods. *In vitro* methods such as GST pull-downs or blot overlay can be employed to prove that the interaction between two proteins is specific and direct. Cell-based co-immunoprecipitations and co-localization studies are also important to confirm a new PPI in a biological context, assaying

proteins in their native state. If a new YTH interaction cannot be readily confirmed by other means it is unlikely to occur naturally, although the interaction can be real but below the sensitivity threshold of the non two-hybrid method.

▪ *interaction appears implausible based on know physiology* – Eventhough a new interaction has been reproducibly validated, the known physiology of bait and prey may suggest that the interaction is implausible, i.e. the two proteins have to be expressed in the same cellular/subcellular compartment at the same time for the interaction to occur naturally. This is not an exclusion criterion, since the PPI may still occur and contribute to regulatory pathways yet to be discovered.

III.2 MATERIALS AND METHODS

For the complete composition of all reagents, media and solutions used, see Appendix I. All reagents were cell culture grade or ultrapure.

III.2.1 Plasmid isolation from yeast

The extraction of plasmid DNA from yeast cells was carried out with one of the three methods described below. The "Boiling" method or the "Breaking Buffer" method were employed for the analysis of the majority of the positive clones. The "High Efficiency Yeast Plasmid Rescue" method was performed in selected clones in an attempt to improve the transformation efficiency in *E. coli*.

"Boiling" Method

A frozen aliquot of the yeast culture was thawed, transferred into 3 ml of SD/TDO medium and incubated overnight at 30°C with vigorous shaking (220-250 rpm). 1.5 ml of this culture were transferred into a microtube, centrifuged at 12,000*g* for 3 min and the supernatant was discarded. The cell pellet was resuspended in 100 µl of STET buffer by vortexing. Then, 0.3 g of 0.5 mm acid-washed glass beads (Sigma) were added and the mixture was vigorously vortexed for 5-8 min. After adding 100 µl of STET the mixture was boiled for 5 min (96-100°C). The tubes were cooled down briefly on ice and cetrifuged at 12,000*g* for 10 min, at 4°C. The supernatant was transferred to a new microtube, 0.5 ml of 7.5 M amonium acetate were added. The tube was incubated at -20°C overnight and centrifuged at 12,000*g* for 10 min. The supernatant (approximately 400 µl) was transferred to 1000 µl ice-cold 100% ethanol. The solution was well mixed and stored at -20°C for 30 min to allow the DNA precipitate to form. DNA was recovered by centrifugation at 4°C for 15 min at 12,000*g*. The supernatant was carefully removed without disturbing the pellet. The microtube was half filled with ice-cold 70% ethanol and recentrifuged at 12,000*g* for 5 min. The supernatant was again removed and the pellet allowed to dry before being resuspended in 30 µl of H_2O containing DNAse-free RNAse (20 µg/ml).

"Breaking Buffer" Method

Yeast plasmid DNA was extracted by resuspending the cell pellet in 0.2 ml of breaking buffer, adding 0.3 g of 0.5 mm acid-washed glass beads (Sigma) plus 0.2 ml 25:24:1(v/v/v)

phenol/chloroform/isoamyl alcohol and vortexing for 4 min before centrifuging for 5 min at 12,000*g*. The upper layer was transferred to a new microtube and once more, 0.2 ml 25:24:1 (v/v/v) phenol/chloroform/isoamyl alcohol were added, followed by vortexing for 2 min and centrifugation for 5 min. The upper layer was transferred to a new microtube and 0.2 ml chloroform were added, vortexed for 1 min and centrifuged for 5 min. The DNA in the upper layer was ethanol precipitated.

"High Efficiency Yeast Plasmid Rescue" Method

An alternative method was used for isolating yeast plasmid DNA: 3 ml of yeast cells were pelleted and the DNA extracted using the QIAprep kit (QIAGEN). The pellet was resuspended in 250 µl of buffer P1, added about 250 µl of 0.5 mm acid-washed glass beads and vortexed on high for 5 min. Afterwards, 250 µl of buffer P2 were added and the microtube was mixed by gently inverting until the solution became viscous and slightly clear. Then 350 µl of buffer N3 were added and the microtube was repeatedly inverted until the solution became cloudy. The microtube was centrifuged for 10 min and the resulting supernatant was applied to a QIAprep (QIAGEN) spin column placed in a microtube. After a 1 min centrifugation the flow-through was discarded. The column was washed by adding 0.75 ml of buffer PE and centrifuging 1 min to discard the flow-through. The column was centrifuged for an additional 1 min to remove residual wash buffer. Finally, the column was placed in a clean microtube and 50 µl of H2O were added to elute the DNA by centrifuging for 1 min having let it stand for 1 min.

III.2.2 Rescue of library plasmids via transformation in *E. coli*

Yeast plasmid DNA isolated from the positive clones was tranformed in *E. coli* XL1-blue, as described in section II.2.1.8. The Gal4-BD and Gal4-AD cloning vectors carry the Amp^r marker, to select for bacteria transformants by their resistance to ampicillin.

Several isolated colonies of transformed *E. coli* were independently inoculated in 3 ml of LB with 50 µg/ml ampicillin to extract the plasmid DNA by "Alkaline lysis miniprep", as described in section II.2.1.9.

Plasmid DNA was digested with the restriction endonuclease HindIII, and fragments produced were separated by agarose gel electrophoresis as described in sections II.2.1.10-11.

III.2.3 Identification of the positive clones by DNA sequencing and database searching

The HindIII-digested pACT-2 vector produced a characteristic pattern of fragments that allowed its differentiation from colonies resulting from transformation by the bait vector. Plasmids generating DNA fragments characteristic of the pACT-2+library insert digested with HindIII were further sequenced.

Plasmid DNA samples selected for sequencing were first purified in a QIAquick spin column (QIAGEN DNA Purification Kit). Sequencing reactions were performed using the GAL4-AD primer (Clontech), as described in section II.2.1.12. Additional sequencing reactions with different primers, such as 3' AD Amplimer (Clontech) or insert specific primers, were performed for selected positive clones.

A search for similar sequences in the GenBank database was performed using the latest release of BLASTN, nucleotide BLAST (Basic Local Alignment Search Tool) (Altschul *et al.*, 1990), on the NCBI web site (http://blast.ncbi.nlm.nih.gov/Blast.cgi).

III.2.4 Verifying protein interactions in yeast by co-transformation

The initial positive clones may contain more than one ActD/library plasmid. Therefore, it is important to confirm the interaction of each library plasmid with the bait in yeast. This procedure was adopted only for selected clones.

Protein interactions were verified by co-transformation of the AH109 yeast strain with each BD-bait and ActD-library plasmid pairs. The Gal4-BD and Gal4-AD empty plasmids were co-transformed as an interaction negative control. A positive control is given by co-transformation of pVA3-1 and pTD1-1 vectors, that express the Gal4-BD-p53 and the Gal4-AD-SV40 large T antigen fusions, respectively. The protocol was described in section II.3.1.1, but 200 ng of each plasmid were transformed. The co-transformants were selected in SD/-Trp/-Leu medium. To confirm protein interactions, the fresh colonies of the co-transformants were assayed for growth on SD/QDO plates and for X-α-Gal activity.

In the case of RanBP9 prey clone (A10), the library plasmid was first tested for autonomous activation of a GAL4-dependent HIS3 promoter in the AH109 strain in the presence of different concentrations of 3-aminotriazole (3-AT) establishing 60 mM as the optimal concentration to use in the subsequent tests.

III.2.5 Quantitative α-Gal activity assay

For the quantitative α-Galactosidase activity assay fresh yeast colonies expressing the pairs of interacting proteins being analyzed were grown on 4 ml of SD/TDO (-Trp, -Leu, -His). The negative control AH109 (pAS2-1 + pACT2) was grown on SD/-Trp/-Leu. The cultures were incubated overnight at 30°C with shaking at 200 rpm. The optical density of the culture at 600 nm was recorded. 1ml of the culture was centrifuged for 5 minutes at 12,000*g*, and the supernatant was removed for analysis. The assay was performed by combining 8 µl of culture supernatant with 24 µl of Assay Buffer (100 mM PNP-α-Gal solution, 1X NaOAc [1:2 (v/v) ratio]). After incubation for 60 minutes at 30°C the reaction was terminated with 960 µl of 1X stop solution (0.1 M NaCO3) and the optical density at 410 nm was recorded. The α-galactosidase milliunits were calculated with the following formula, as described by the manufacturer (Yeast Protocols Handbook, Clontech) for the 1ml assay format: [milliunits/(ml x cell)] = OD_{410} x 992 x 1000 / [OD_{600} x time (min) x 16.9 x 8]. Data are expressed as mean ± SEM of three independent experiments. Statistical significance was determined by one way analysis of variance followed by Tukey-Kramer multiple comparisons test.

III.2.6 Bioinformatics analysis of the proteins identified in the YTH screens

The proteins identified in each YTH screen were analyzed with respect to the presence of protein domains and motifs, transmenbrane domains and signal peptides. A bioinformatics approach was followed for each protein sequence, using several web-based tools (Table III.1), such as InterPro, Scansite and ELM, InterPro is an integrated documentation resource of protein families. Searches simultanously in Pfam, PRINTS, ProDom, PROSITE, SMART, SWISS-PROT, TIGRFAMs, PIRSF (PIR Superfamily), and Superfamily for domains, families, repeats and short sequence motifs. Scansite is a database of motifs within proteins that are likely to be phosphorylated by specific protein kinases or bind to specific protein domains. ELM is a resource for predicting functional sites in eukaryotic proteins. Putative functional sites are identified by patterns (regular expressions), which have a slightly different syntax than PROSITE patterns. TMHMM is a program for prediction of transmembrane helices in proteins. HPRD is a database of human protein and was also checked for each protein in the datasets for information concerning domains, motifs and protein families.

Table III.1: Web resources for bioinformatics analysis of protein sequences.

Database	Searched items	Database location	Reference
ELM	Functional sites prediction	http://elm.eu.org/	(Dinkel et al., 2011)
HPRD	Protein family	http://www.hprd.org/	(Prasad et al., 2009)
InterPro	Domains and motifs prediction Transmembrane domains Protein family	http://www.ebi.ac.uk/Tools/pfa/iprscan/	(Hunter et al., 2012)
PROSITE	Domain and motifs	http://prosite.expasy.org/	(Sigrist et al., 2010)
Scansite	Motifs Posttranslational modification	http://scansite.mit.edu/	(Obenauer et al., 2003)
TMHMM	Transmembrane domains	http://www.cbs.dtu.dk/services/TMHMM/	(Krogh et al., 2001)

III.2.7 Curation and Gene Ontology mining of each putative new interactor

Each putative new interactor was expertly curated to gather pertinent information via a comprehensive and targeted literature and database search (last updated in January 2011; Table III.2). To facilitate the analysis of each putative new interactor all proteins were unambiguously matched to a human gene in the HGNC (HUGO Gene Nomenclature Committee) database (Eyre et al., 2006). The Entrez Gene database, available via interactive browsing, was used to collect information for each interactor, such as nomenclature, genomic location, gene products and their attributes, phenotypes and links to citations, sequences, variation details, maps, expression, homologs, protein domains and interactions.

Curation of all the proteins identified in the screens was also achieved through interactive browsing the universal protein resource (UniProt), a comprehensive resource for protein sequence and annotation data. UniProtKB, the UniProt Knowledgebase, is a collection of functional information on proteins which provided information on protein domains,

posttranslational modifications and Gene Ontology (GO) annotations. GO terms were also collected from the Gene Ontology website (http://www.geneontology.org/). Then the collected GO terms were manually and expertly categorized for each YTH screen dataset. The aim of this analysis was to determine whether particular GO terms were disproportionately represented in a particular protein set.

For all proteins in this study, information about participation in signaling pathways was obtained from KEGG Pathway Database and NetPath.

The AlzGene database, that uncovers the information of every peer-reviewed genetic association study in AD (Bertram et al., 2007), was checked for the genes in the YTH dataset that were positively associated with AD. Association with genetic disorders was checked in the OMIM database at NCBI. Information concerning predisposition or risk for a particular disease/condition was collected from literature curation.

Table III.2: Web resources for curation and Gene Ontology mining.

Database	Searched items	Database location	Reference
Alzgene	AD risk genes	http://www.alzgene.org	(Bertram et al., 2007)
Entrez Gene	Chromosome mapping phenotypes, links to citations, variation details, expression, protein domains, interactions	http://www.ncbi.nlm.nih.gov/gene/	(Maglott et al., 2010)
Gene Ontology	Molecular function (MF), Biological process (BP), Cellular component (CC)	http://www.geneontology.org/	(Ashburner et al., 2000)
HGNC	Gene symbol - HUGO Gene Nomenclature Committee	http://www.genenames.org/	(Eyre et al., 2006)
KEGG Pathway Database	Signaling pathways	http://www.genome.jp/kegg/pathway.html	(Kanehisa et al., 2010)
NetPath	Signaling pathways	http://www.netpath.org/index.html	(Kandasamy et al., 2010)
OMIM	Mendelian disorders	http://www.ncbi.nlm.nih.gov/sites/entrez?db=omim	(McKusick, 2007)
UniProt	Molecular function (MF), Biological process (BP), Cellular component (CC), Posttranslational modifications citations	http://www.uniprot.org/	(Consortium, 2012)

III.2.8 PPI datasets and networks representation

The PPI networks around each YTH bait, were generated with Cytoscape version 2.8.2 (Shannon et al., 2003; Smoot et al., 2011). The curated APP interactome was obtained from Perreau et al. (2010) and several APP interactions published after that were added (last updated March 2011; APPENDIX VII). The APBB1 (Fe65; APPENDIX VIII) and RANBP9 (RanBP9/RanBPM; APPENDIX IX) interactomes were manual curated via a broad and targeted literature and database search. PPI databases were collected from Entrez Gene, which is a meta-database that includes information from BIND (Alfarano et al., 2005), HPRD (Keshava Prasad et al., 2009) and BioGRID (Stark et al., 2010).

The curated PPI networks were crossed with the YTH networks using Cytoscape. MiMI, a Cytoscape plugin, was used to search online PPI databases (Gao et al., 2009).

III.3 RESULTS

III.3.1 Preliminary analysis of the positive clones

In order to identify the library insert present in a given positive clone, the plasmid DNA was first isolated from yeast. Each yeast cell can incorporate more than one library plasmid. Therefore, a mixture of different plasmid DNAs can be isolated from a single yeast clone, namely the bait plasmid (Figure III.2, lane 6) and one or more library plasmids. In order to isolate library plasmids and obtain pure DNA for sequence analysis, the plasmid DNA isolated from yeast cells was used to transform *E. coli* XL1-Blue. The plasmid DNA obtained from the resulting transformants was further analyzed by restriction digestion with the endonuclease HindIII and the restriction fragments were separated by agarose gel electrophoresis. Figure III.2 exemplifies a typical result obtained after this procedure.

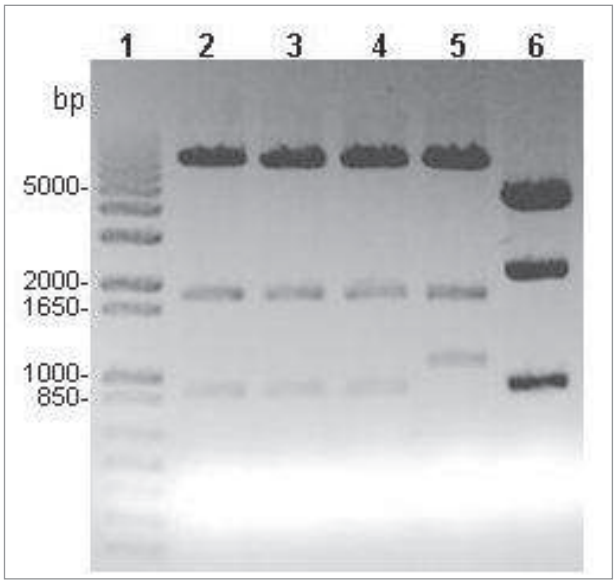

Figure III.2: HindIII restriction analysis of plasmid DNA isolated from *E. coli* colonies. *Lanes: 1,* 1 Kb Plus DNA Ladder (Invitrogen); *2-4,* pACT-2+library insert CF2 (7.4+1.7+0.9 Kb); *5,* pACT-2+library insert CF1 (7.4+1.7+1.1 Kb); *6,* pAS2-1-AICD^{Y687F} plasmid (bait-3) (4.6+2.2+0.9 Kb).

The plasmid DNA extracted from the positive clone CF2 (from YTH screen 3) was transformed in *E. coli*. Plasmid DNA from three isolated *E. coli* colonies was digested with HindIII

and the resulting fragments were resolved on an agarose gel, showing a similar pattern of bands (Fig. III.2, lanes 2-4). One of these plasmids (CF2.1) was further analized by DNA sequencing.

The same strategy was adopted for each positive clone. After identifying transformants carrying the cDNA library plasmids, their respective inserts were sequenced with the GAL4-AD primer (Appendix II). Figure III.3 is a representative example obtained with one of the positive clones, CF2:

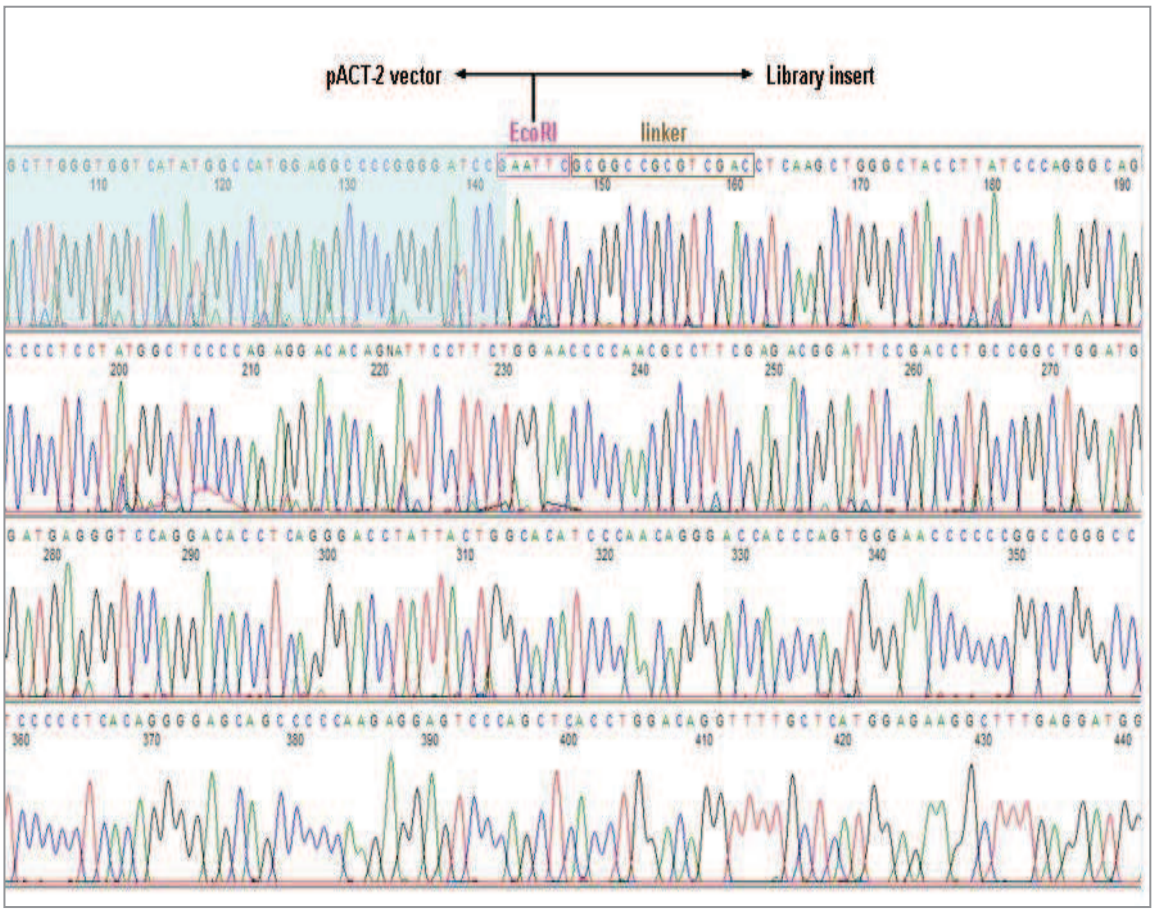

Figure III.3: Partial nucleotide sequence of the positive clone CF2. The shadow area limits the vector sequence. The EcoRI restrition site is highlighted in pink and the library linker sequence is shown by a brown box "GCGGCCGCGTCGAC".

The nucleotide sequence of each clone (flat file) was then converted to FASTA format (Fig. III.4). In this format, in the first line the signal ">" precedes the name or additional information on the sequence and the sequence itself starts on the second line.

```
>VCF2_sequence_FASTA
CTCAAGCTGGGCTACCTTATCCCAGGGCAGCCCCTCCTATGGCTCCCCAGAGGACACAGA
TTCCTTCTGGAACCCCAACGCCTTCGAGACGGATTCCGACCTGCCGGCTGGATGGATGAG
GGTCCAGGACACCTCAGGGACCTATTACTGGCACATCCCAACAGGGACCACCCAGTGGGA
ACCCCCCGGCCGGGCCTCCCCCTCACAGGGGAGCAGCCCCCAAGAGGAGTCCCAGCTCAC
CTGGACAGGTTTTGCTCATGGAGAAGGCTTTGAGGATGGAGAATTTTGGAAGGATGAACC
CAGTGATGAGGCCCCAATGGAGCTGGGACTGAAGGAACCTGAGGAGGGGACGTTGACCTT
CCCAGCTCAGAGCCTCAGCCCAGAGCCGTTGCCCCAAGAGGAGGAGAAGCTTCCCCCACG
```

Figure III.4: Partial sequence of clone CF2 in FASTA format.

A search for similar sequences in the GenBank database was performed using the BLAST (Basic Local Alignment Search Tool) algorithm on the NCBI (National Center for Biotechnology Information) web site (http://www.ncbi.nlm.nih.gov). The query sequence in FASTA format was copied to the nucleotide BLAST (BLASTN) window to be compared with the GenBank Database of nucleotide sequences (Fig. III.5).

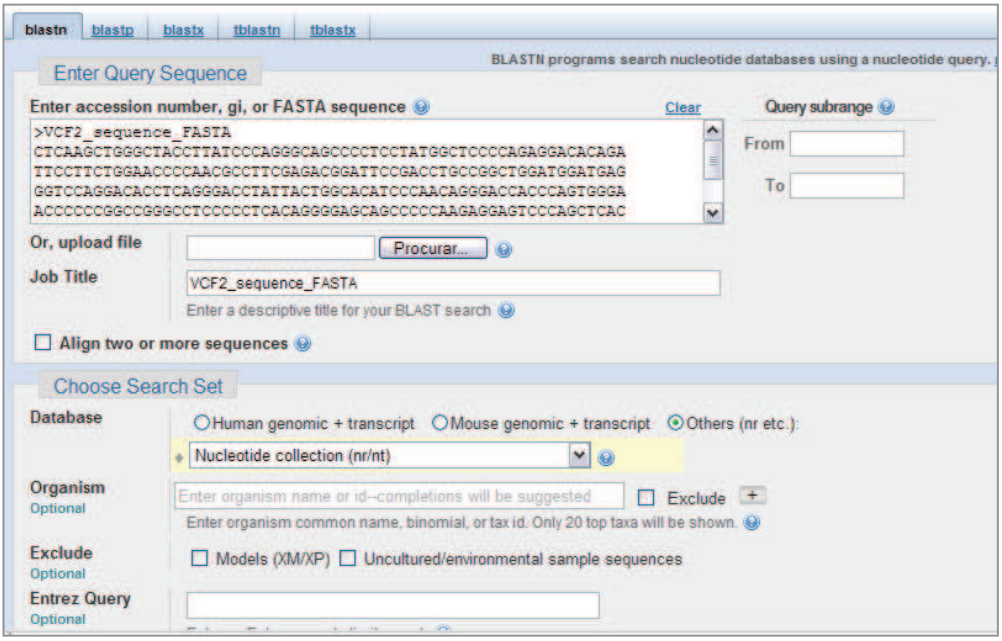

Figure III.5: Blast window to introduce the query sequence.

The BLASTN algorithm was selected to search the non-redundant (NR) database, which is wide and indeed integrates several databases, GenBank, EMBL (European Molecular Biology Laboratory) and DDBJ (DNA Database of Japan), and actually is not non-redundant.

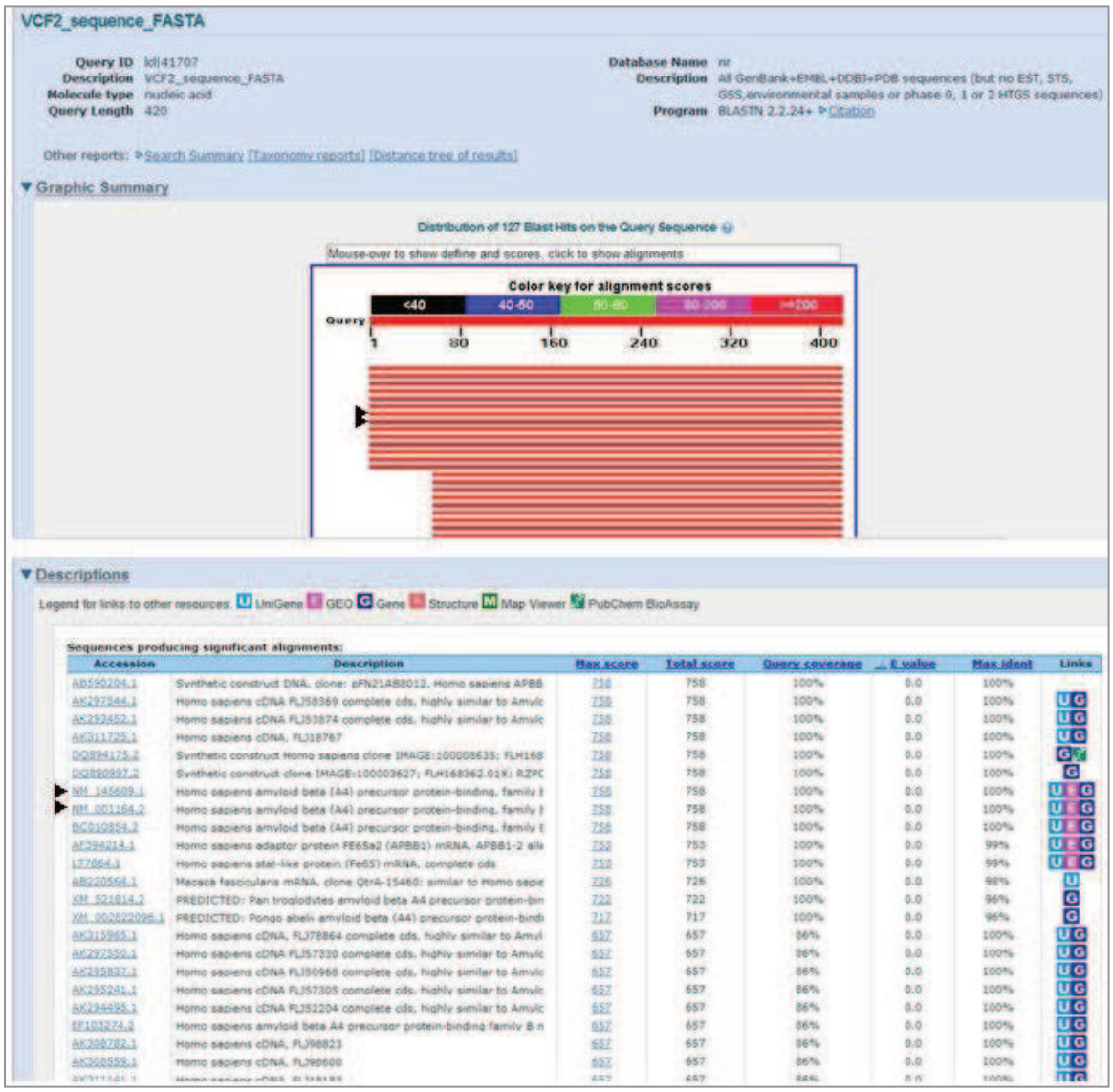

Figure III.6: Blast results for clone CF2. Clone CF2 aligned both with NM_001164 and NM_145689 mRNA Refseqs, with 100% of sequence coverage and E-value=0.0 (*arrowheads*).

As an example of the bioinformatic analysis performed for the initial identification of all positive clones, analysis of the clone CF2 is described. In the BLASTN results window there are two mRNA refseqs (NM_145689 and NM_001164) on the top hits (Fig. III.6). “mRNA Refseqs” are curated mRNA sequences from NCBI Reference Sequence Project. These GenBank records show the cDNA sequence, protein translation, chromosome mapping, coding sequence, relevant references and links to Entrez Gene, HGNC (HUGO Gene Nomenclature Committee), HPRD (Human Protein Reference Database) and OMIM (Online Mendelian Inheritance in Man), which provide additional information.

Clone CF2 aligned both with NM_001164 and NM_145689 mRNA Refseqs, with 100% of sequence coverage and E-value=0.0. The E-value is the expected threshold and specifies the statistical significance threshold for reporting matches against database sequences. The lower the E-value, the more significant the score. The GenBank records NM_001164 and NM_145689 correspond to transcript variants 1 and 2, respectively, of *Homo sapiens* Fe65, also known as Amyloid beta precursor protein-binding, family B member 1. The human Fe65 oficial gene symbol is *APBB1*. Hence, the library insert on clone CF2 codes for Fe65, a protein already described to interact with AICD. The library insert is a partial cDNA: the alignment with NM_001164 starts in nt 763 and alignment with NM_145689 starts at nt 746. The coding sequence (CDS) starts at nt 101 (NM_001164) or nt 84 (NM_145689). The sequence of clone CF2 obtained with GAL4-AD primer does not cover the entire library insert. Therefore, it is not possible to distinguish between transcript variants 1 and 2, which only differ in the presence or absence of 6 nucleotides.

All positive clones sequenced were subjected to sequence similarity searching and the information gathered was organized in a table for each YTH screen. However, different BLAST algorithms and changes in searching parameters were tried for clones that did not immediately match mRNA Refseqs or when no ORFs where found. Comparison of DNA:DNA (BLASTN) to translated DNA:protein (BLASTX) searches were also performed to look for the presence of conserved protein domains and motifs that could help to characterize the putative interaction with the bait.

III.3.2 YTH screen with full-length APP

For YTH screen-1 the human APP cDNA, coding for the neuronal isoform with 695 amino acids (APP_{695}) (GenBank Accession NM_201414), was used as bait to search for interacting proteins in a pretransformed Human Brain MATCHMAKER cDNA library (mRNA source: whole brain from a 37-yr-old Caucasian male; Clontech). The mating efficiency was 4.6% and 5.6 x 10^5 clones were screened. YTH-s1 resulted in the isolation of 60 positive clones, for their ability to activate the three reporter genes *HIS3*, *ADE2* and *MEL1*.

Of the original 60 positive clones isolated, 47 were recovered from yeast and transformed in *E. coli*. From these, 44 were successfully analyzed by DNA sequencing. The results obtained are summarized in Table III.3. Analysis of the 44 positive clones resulted in the identification of nucleotide sequences that could be divided into the following categories:

- 22 positive clones matched a protein coding sequence (CDS);
- 6 library inserts aligned with Open Reading Frames (ORFs);
- 6 clones matched genomic clones;
- 6 library inserts aligned with mitochondrial genes;
- 2 library inserts aligned with 3’ untranslated regions of mRNA (UTRs);
- 2 clones contained an inverted cDNA.

Table III.3: Complete list of the positive clones from YTH screen-1 (APP_{695}) identified by partial sequencing of the library insert using a primer targeting the GAL4-AD.

GenBank Accession	Definition	Gene symbol	Chr	No. of clones	Clones	Insert size (kb)	Full-length cDNA	Frame with Gal4-AD
library inserts encoding known proteins identified as putative APP interactors								
NM_022735.3	Acyl-Coenzyme A binding domain containing 3	ACBD3	1q42.12	2	A52	3.5		
					A132	3.6		✓
NM_015367.2	BCL2-like13	BCL2L13	22q11.1	1	A44	0.5		
NM_001704.2	Brain specific angiogenesis inhibitor 3	BAI3	6q12	2	A9	2.8		✓
					A20	2.2		✓
NM_016279.3	Cadherin 9 type 2 (T1-cadherin)	CDH9	5p14	1	A11	3.0		
NM_001122898.1	CD99 transcript variant 2	CD99	Xp22.32/ Yp11.3	1	A12	1.3	✓	✓
NM_025134.4	Chromodomain helicase DNA binding protein 9	CHD9	16q12.2	1	A98	2.3		✓
NM_022742.3	Coiled-coil domain containing 136	CCDC136	7q33	1	A43	1.1	✓	
NM_001945.2	Heparin-binding EGF-like growth factor	HBEGF	5q23	1	A18	2.3	✓	
NM_020738.2	Kinase D-interacting substance 220 kDa	KIDINS220	2p24	1	A16	0.7		✓
NM_005573.2	Lamin B1	LMNB1	5q23.3-q31.1	1	A51	3.2		
NM_005732.3	RAD50 homolog	RAD50	5q31	1	A101	1.3		✓
NM_005493.2	Ran binding protein 9	RANBP9	6p23	1	A10	2.8		✓
NM_021136.2/ NM_206857.1	Reticulon 1 transcript variant 1/2 [(a)]	RTN1	14q23.1	1	A92	1.4		
NM_206852.1	Reticulon 1 transcript variant 3	RTN1	14q23.1	1	A71	1.4	✓	
NM_006054.2	Reticulon 3 transcript variant 1	RTN3	11q13	2	A26, A129	2.6		
NM_201429.1	Reticulon 3 transcript variant 3	RTN3	11q13	1	A3	2.7	✓	✓
NM_020532.4/ NM_207521.1	Reticulon 4 transcript variant 1/5 [(b)]	RTN4	2p14-p13	1	A75	2.4		
NM_015602.2	Torsin A interacting protein 1	TOR1AIP1	1q24.2	1	A5	3.3		✓
NM_001002261.3	Zinc finger FYVE domain containing 27 transcript variant 1/2/3/4/6 [(c)]	ZFYVE27	10q24.2	1	A13	2.2		✓
library inserts encoding ORFs								
NM_173821.2	Chromosome 2 open reading frame 45	C2orf85	2q37.3	1	A21	1.4		✓
NM_024104.3	Chromosome 19 open reading frame 42	C19orf42	19p13.11	1	A105	1.4		✓
NM_024293.4	Family with sequence similarity 134 member A	FAM134A	2q35	4	A14, A17, A34, A145	2.8		✓
library inserts matching genomic clones								
AC008440.9	clone CTC-331H23		19	2	A30, A122	0.6		
AC109912.10	clone RP11-640G21		3	1	A150	1.5		
AL358175.18	clone RP11-343N15		1	1	A151	1.3		
AC009477.4	clone RP11-209H16		2	1	A99	1.7		
AC007255.4	clone RP11-550A18		7	1	A126	1.3		
library inserts encoding mitochondrial proteins								
NC_012920.1	Cytochrome c oxidase II	MT-CO2	mtDNA	1	A82	0.8		✓
				2	A37, A60	0.8		✓
				1	A49	0.8		✓
				1	A53	0.7		✓

NC_012920.1	NADH dehydrogenase subunit 4 (complex I)	MT-ND4	mtDNA	1	A142	1.1		✓
library inserts aligning with 3' UTRs								
NM_002545.3/ NM_001012393.1	Opioid binding protein/ cell adhesion molecule-like transcript 1/2 [(d)]	OPCML	11q25	2	A35, A149	1.3		✓
inverted cDNAs								
NM_005277.3/ NM_201591.1/ NM_201592.1	Glycoprotein M6A transcript variant 1/2/3 [(e)]	GPM6A	4q34	2	A65, A67	2.3		

[(a)] Similar alignment score with transcript variants 1 and 2.
[(b)] Similar alignment score with transcript variants 1 and 5.
[(c)] Similar alignment score with transcript variants 1, 2, 3, 4 and 6.
[(d)] Similar alignment score with transcript variants 1 and 2.
[(e)] Similar alignment score with transcript variants 1, 2 and 3.

III.3.3 YTH screen with APP^{Y687F} dephospho-mutant

The YTH screen-2 was carried out using as bait the human APP_{695} cDNA, with the Y687F mutation, which mimics the dephosphorylated state of Tyr-687, APP^{Y687F}. A pretransformed Human Brain MATCHMAKER cDNA library (mRNA source: whole brain from a 37-yr-old Caucasian male; Clontech) was screened to search for APP^{Y687F} interacting proteins. The mating efficiency was 7.9% and 4.2 x 10^6 clones were screened. YTH-s2 resulted in the isolation of 131 positive clones, for their ability to activate the three reporter genes *HIS3*, *ADE2* and *MEL1*.

Of the original 131 positive clones isolated, 34 were successfully recovered from yeast and transformed in *E. coli*. These were all analyzed by DNA sequencing. The results obtained are summarized in Table III.4. Analysis of the 34 positive clones resulted in the identification of nucleotide sequences that could be divided into the following categories:

- 30 clones matched a protein coding sequence (CDS);
- 1 library insert aligned with a mitochondrial gene;
- 1 library insert aligned with a 3' UTR;
- 1 library insert aligned with an intronic sequence;
- 1 clone contained an inverted cDNA.

Table III.4: Complete list of the positive clones from YTH screen-2 (APP^{Y687F}) identified by partial sequencing of the library insert using a primer targeting the GAL4-AD.

GenBank Accession	Definition	Gene symbol	Chr	No. of clones	Clones	Insert size (kb)	Full-length cDNA	Frame with Gal4-AD
library inserts encoding known proteins identified as putative APP^{Y687F} interactors								
NM_001164.2/ NM_145689.1	Amyloid beta precursor protein-binding family B member 1 transcript variant 1/2 [(a)] (Fe65; p97Fe65)	APBB1	11p15	12	AF69	2.6	✓	✓
					AF38	2.4		
					AF19, AF55	2.3		
					AF82	2.3		
					AF27, AF39, AF47	2.3		
					AF51	2.3		
					AF52	1.8		
					AF42	1.8		
					AF67	1.8		
EF103274.2	Amyloid beta precursor protein-binding family B member 1 transcript variant 3 (p60Fe65) - new splice variant [(b)]	APBB1	11p15	3	AF18, AF41	1.9		
					AF29	1.8		
NM_006368.4	cAMP responsive element binding protein 3	CREB3	9p13.3	7	AF58	1.4	✓	
					AF26, AF40, AF46, AF54	1.4		
					AF13, AF53	1.4		
NM_017801.2	CKLF-like MARVEL transmembrane domain containing 6	CMTM6	3p22.3	1	AF81	1.6		✓
NM_152609.2	Consortin, connexin sorting protein, transcript variant 1	CNST	1q44	1	AF22	5.4		
NM_016129.2	COP9 constitutive photomorphogenic homolog subunit 4	COPS4	4q21.22	1	AF20	2.4	✓	✓
NM_001945.2	Heparin-binding EGF-like growth factor	HBEGF	5q23	2	AF70, AF71	2.2	✓	✓
NM_018928.2	Protocadherin gamma subfamily C 4 transcript variant 1	PCDHGC 4	5q31	1	AF43	2.6		✓
NM_006054.2	Reticulon 3 transcript variant 1	RTN3	11q13	1	AF65	1.2		
NM_003006.3	Selectin P ligand	SELPLG	12q24	1	AF78	2.2		✓
library inserts encoding mitochondrial proteins								
NC_012920.1	NADH dehydrogenase subunit 4L (complex I)	MT-ND4L	mtDNA	1	AF49	2.5		
library inserts aligning with 3' UTRs								
NM_001968.3/ NM_001130679.1/ NM_001130678.1	Eukaryotic translation initiation factor 4E transcript variant 1/2/3 [(c)]	EIF4E	4q21-q25	1	AF60	1.6		✓
library inserts aligning with intronic sequences								
AF111168.2	Serine palmitoyl transferase subunit II	SPTLC2	14q24.3	1	AF68	2.1		
inverted cDNAs								
M31423.1	Cerebellar degeneration-related protein 1	CDR1	Xq27.1-q27.2	1	AF32	0.8		

[(a)] *Similar alignment score with transcript variants 1 and 2.*
[(b)] *Distinct 5' sequence - new transcript variant.*
[(c)] *Similar alignment score with transcript variants 1, 2 and 3.*

III.3.4 YTH screen with AICD^{Y687F}

The YTH screen-3 was performed with the cDNA coding for intracellular domain of APP with 50 amino acids (C50), with the Y687F mutation, which mimics the dephosphorylated state of Tyr-687, AICD^{Y687F}. A Human Brain MATCHMAKER cDNA library (mRNA source: whole brain from a 60-yr-old Caucasian male; Clontech) was used as bait to search for proteins interacting with AICD^{Y687F}. The mating efficiency was 19.8% and 6.0 x 10^5 clones were screened. The YTH-s3 resulted in the isolation of 88 positive clones, for their ability to activate the three reporter genes *HIS3*, *ADE2* and *MEL1*.

Of the original 88 positive clones isolated, 85 were successfully recovered from yeast and transformed in *E. coli*. From these, 50 were analyzed by restriction enzyme digestion and DNA sequencing and 35 were only analyzed by restriction digestion. The results obtained are summarized in Table III.5. Analysis of the 85 positive clones resulted in the identification of nucleotide sequences that could be divided into the following categories:

- 61 clones matched a protein already known to interact with APP;
- 5 clones matched other proteins;
- 4 library inserts aligned with genomic clones;
- 3 library inserts aligned with mitochondrial genes;
- 8 library inserts aligned with 3' UTRs;
- 1 clone contained an inverted cDNA;
- 2 clones were chimeric, containing sequences from two distinct chromosomes;
- 1 clone did not have library insert.

The majority of positive clones interacting with AICD^{Y687F} were hits on the Fe65 protein (amyloid beta precursor protein-binding family B member 1), already described to interact with the intracellular domain of APP.

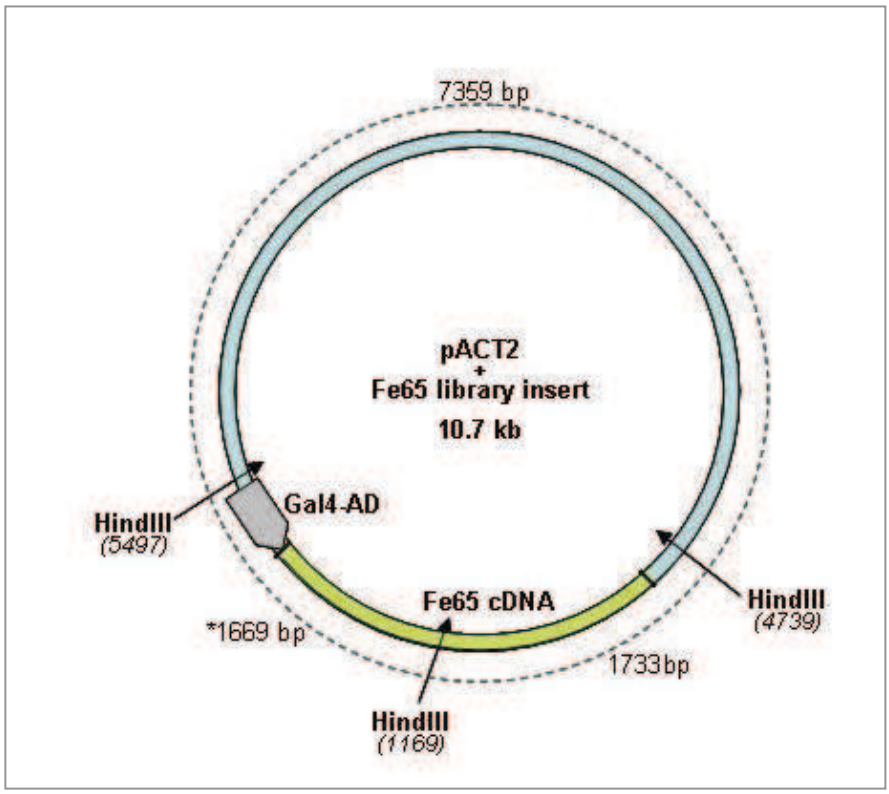

Figure III.7: Restriction map of a pACT2 plasmid that carries a Fe65 full-length cDNA insert. The 1669 bp fragment can be smaller if the library insert does not contain the full-length cDNA (*).

The HindIII restriction enzyme digestion analysis of these clones, performed prior to DNA sequencing, showed a pattern of bands on agarose gels characteristic of a pACT2 plasmid carrying a Fe65 library insert: 7359 bp, 1733 bp and 1669 bp. The 7359 bp and 1733 bp bands were common to all the HindIII-digested Fe65 clones, but the "1669 bp" band can be smaller if the library insert does not contain the full-length cDNA (Fig. III.7). For that reason, analysis of the HindIII fragment sizes by agarose gel electrophoresis revealed 5 different patterns of bands for the Fe65 clones, which were classified in group A, B, C, D, E or F (Table III.5). Several Fe65 clones from each group were selected for sequencing analysis.

Table III.5: Analysis of the 56 positive clones from YTH screen-3 (AICD^{Y687F}) identified as Fe65 (Amyloid beta precursor protein-binding family B member 1), by HindIII fragment sizes pattern and sequencing of selected clones using the GAL4-AD primer.

Group	HindIII Restiction analysis (kb)	Insert size (kb)	Library insert sequenced	Clones	No. of clones	GenBank Accession	Transcript variant	mRNA (bp)	Coding sequence on mRNA	Library insert start	Full-length cDNA
A	7.4 + 1.7 + 1.7	2.7	✓	CF11	17	NM_001164.2	transcript variant 1	2653	101-2233	6	✓
				CF8, CF9.2, CF12, CF14, CF15						18	✓
				CF3, CF4, CF13						25	✓
				CF16, CF17, CF21, CF34, CF39, CF45, CF126, CF130.2							
B	7.4 + 1.7 + 1.6	2.6	✓	CF10	8	NM_145689.1	transcript variant 2	2634	84-2210	49	✓
			✓	CF7.1		NM_001164.2	transcript variant 1	2653	101-2233	91	✓
				CF25, CF26, CF27, CF33, CF42, CF54							
C	7.4 + 1.7 + 1.3	2.3	✓	CF18, CF23, CF24	3	NM_001164.2/ NM_145689.1	transcript variant 1/2 (a)				
D	7.4 + 1.7 + 1.1	2.1	✓	CF1, CF128.2	13	NM_001164.2/ NM_145689.1	transcript variant 1/2 (a)	2653	101-2233	571	
				CF28, CF35, CF46, CF48, CF63, CF64, CF65, CF67, CF86, CF131.1, CF133							
E	7.4 + 1.7 +0.9	1.9	✓	CF2	10	NM_001164.2/ NM_145689.1	transcript variant 1/2 (a)			763	
			✓	CF5, CF6, CF7.2, CF9.1		NM_001164.2	transcript variant 1	2653	101-2233	813	
				CF22, CF31, CF49, CF53, CF66							
F	7.3 + 1.7 + 0.7	1.7		CF32, CF41, CF43, CF47, CF61	5						

(a) *Similar alignment score with transcript variants 1 and 2.*

The HindIII fragment sizes analysis revealed that a high percentage (around 70%) of the positive clones from YTH-s3 appeared to contain library inserts coding for the same protein, Fe65. Restriction analysis allowed to eliminate the Fe65 duplicates and all the library inserts that presented a different pattern of bands were sequenced. The results obtained are summarized in Table III.6.

Table III.6: Complete list of the positive clones from YTH screen-3 ($AICD^{Y687F}$).

GenBank Accession	Definition	Gene	Chr	No. of clones	Clones	Insert size (Kb)	full-length cDNA	frame with Gal4-AD
library inserts encoding known proteins identified as putative $AICD^{Y687F}$ interactors								
NM_001164.2/ NM_145689.1	Amyloid beta precursor protein-binding family B member 1 transcript variant 1/2 [(a)] (Fe65)	APBB1	11p15	56	*group A:* CF11, CF8, CF9.2, CF12, CF14, CF15, CF3, CF4, CF13, CF16, CF17, CF21, CF34, CF39, CF45, CF126, CF130.2	2.7	✓	
					group B: CF10, CF7.1, CF25, CF26, CF27, CF33, CF42, CF54	2.6	✓	
					group C: CF18, CF23, CF24	2.3		
					group D: CF1, CF128.2, CF28, CF35, CF46, CF48, CF63, CF64, CF65, CF67, CF86, CF131.1, CF133	2.1		
					group E: CF2, CF5, CF6, CF7.2, CF9.1, CF22, CF31, CF49, CF53, CF66	1.9		
					group F: CF32, CF41, CF43, CF47, CF61	1.7		
NM_005503.3	Amyloid beta precursor protein-binding family A member 2 transcript variant 1 (X11L; MINT2)	APBA2	15q11-q12	2	CF51	3.4		
					CF69	3.4		
NM_005456.2	Mitogen-activated protein kinase 8 interacting protein 1 (JIP1)	MAPK8IP1	11p12-p11.2	3	CF91	2.8		✓
					CF131.3	2.8		
					CF112	2.0		
NM_033271.2	BTB (POZ) domain containing 6	BTBD6	14q32	1	CF105	0.7		✓
NM_001005920.2	Jumonji domain containing 8	JMJD8	16p13.3	1	CF90	2.3		✓
NM_015026.2	MON2 homolog	MON2	12q14.1	1	CF108	2.6		
NM_001033549.1/	Chromosome 19 open reading frame	BABAM1	19p13.11	1	CF106	0.9		

NM_014173.2	62 transcript variant 1/2 [b]							
NM_000305.2/ NM_001018161.1	Paraoxonase 2 transcript variant 1/2 [c]	PON2	7q21.3	1	CF110	1.0		✓
library inserts matching genomic clones								
AC018628.13	clone RP11-342K2		17	1	CF93	5.0		
AK090888.1	cDNA FLJ33569 clone BRAMY2010317	SNRPN	15q11.2	1	CF94	4.0		
AL512599.33	clone RP11-115D7	CAP1	1p34.3	1	CF115	3.4		
AC007027.3	clone RP5-832O14	CNTNAP2	7q35	1	CF117	1.0		
library inserts encoding mitochondrial proteins								
NC_012920.1	Cytochrome c oxidase II	MT-CO2	mtDNA	1	CF114.1	0.7		✓
NC_012920.1	Cytochrome c oxidase III	MT-CO3	mtDNA	2	CF100	0.9	✓	
					CF114.3	0.8		
library inserts aligning with 3' UTRs								
NM_020844.2/ NM_001099677.1	Chromosome 8 open reading frame 79 transcript variant 1/2 [d]	C8orf79	8p22	1	CF116.1	1.1		
NM_001001132.1	Intersectin 1 transcript variant 2	ITSN1	21q22.1-q22.2	1	CF131.2	1.4		
NM_002338.3	Limbic system-associated membrane protein	LSAMP	3q13.2-q21	1	CF119.3	2.2		
NM_005907.2	Mannosidase alpha class 1A member 1	MAN1A1	6q22	1	CF97	1.4		
NM_002654.3/ NM_182471.1	Pyruvate kinase, muscle, transcript variant 1/3 [e]	PKM2	15q22	1	CF72	0.7		
NM_001039355.1	Solute carrier family 25 member 29	SLC25A29	14q32.2	1	CF98	0.8		
NM_015894.2	Stathmin-like 3	STMN3	20q13.3	1	CF120	2.1		
NM_003165.3/ NM_001032221.3	Syntaxin binding protein 1 transcript variant 1/2 [f]	STXBP1	9q34.1	1	CF114.2	1.8		
inverted cDNAs								
NM_021959.2	Protein phosphatase 1 regulatory (inhibitor) subunit 11	PPP1R11	6p21.3	1	CF116.3	2.8		
other alignments								
NM_004426.2 + NM_012347.4/ NM_033480.2/ NM_033481.3	*chimeric clone:* Polyhomeotic homolog 1 (3'UTR) + F-box protein 9 transcript 1/2/3 [g]	PHC1 + FBXO9	12p13 6p12.3-p11.2	1	CF128.3	2.1		
BX324178.9	*chimeric clone:*		22	1	CF134	2.8		

+ NM_001455.3/ NM_201559.2	genomic clone WI2-81516E3 + Forkhead box O3 transcript variant 1/2 [(h)] (3'UTR)	FOXO3	6q21					

(a) Similar alignment score with transcript variants 1 and 2.
(b) Similar alignment score with transcript variants 1 and 2.
(c) Similar alignment score with transcript variants 1 and 2.
(d) Similar alignment score with transcript variants 1 and 2.
(e) Similar alignment score with transcript variants 1 and 3.
(f) Similar alignment score with transcript variants 1 and 2.
(g) Similar alignment score with transcript variants 1, 2 and 3.
(h) Similar alignment score with transcript variants 1 and 2.

III.3.5 Clones matching a protein coding sequence

The majority of the clones identified in the three YTH screens were assigned to known proteins: 50% (YTH screen-1), 88% (YTH screen-2) and 78% (YTH screen-3), as summarized in Table III.7. The number of clones for each identified binding protein varied considerably, from 1 clone (e.g. clone A44, corresponding to BCL2L13) to 56 clones (in YTH-s3, corresponding to APBB1) as discussed below. This group of clones include positive clones isolated from high and medium stringency selection.

Among the positive clones identified as 'known proteins' are some well established APP interactors, such as Fe65 (official gene symbol: *APBB1*). Fe65 was isolated in YTH-s2 (12 clones) and in YTH-s3 (56 clones). Other known APP binding proteins were detected in YTH-s3: X11L (gene symbol *APBA2*; 2 clones) and JIP-1 (gene symbol *MAPK8IP1*; 3 clones). It is worthwhile noting that Fe65, X11L and JIP-1 are known to interact with the intracellular domain of APP, but the interactions with the phospho-mimicking mutants APP^{Y687F} (bait 2) and $AICD^{Y687F}$ (bait 3) had not been previuosly described. In YTH-s1 there were no hits in any previously described APP binding proteins.

Overall, in the YTH screens here described, numerous proteins never before related to APP were identified as potencial novel APP binding proteins (31 proteins, encoded by 45 positive clones). These were all analyzed by bioinformatics tools. Two positive clones were selected for further characterization and functional studies, presented in Chapters IV and V. These are p60Fe65 (clones AF18, AF41 and AF29; from YTH-s2) and RanBP9/RanBPM (clone A10; from YTH-

s1). p60Fe65 is a shorter isoform of Fe65 (encoded by *APBB1*), that arises from alternative splicing of Fe65 pre-mRNA. The novel transcript, Fe65E3a, was identified in YTH-s2 (encoded by 3 clones) and was further characterized in Chapter IV.

The other protein that was further investigated was RanBPM/RanBP9 (encoded by *RANBP9*), a protein involved in signal transduction, axon guidance and neurite outgrowth that had not been associated with APP at the time the work was started. Another report in 2009 described that APP and RanBP9 co-immunoprecipitated together (Lakshmana *et al.*, 2009).

Table III.7: Comparison of the results obtained in the three YTH screens.

	YTH-s1	YTH-s2	YTH-s3	total
No. of positive clones isolated	60	131	88	279
No. of positive clones identified (RE or sequencing)	44	34	85	163
No. of clones encoding known proteins	22	30	66	118
Known proteins identified	*17*	*9*	*8*	*31**
No. of clones encoding APP binding proteins	0	12	61	73
Known APP binding proteins identified	*0*	*1*	*3*	*3**
No. of clones encoding other known proteins	22	18	5	45
Other proteins identified	*17*	*8*	*5*	*28**
No. of clones encoding mtDNA encoded proteins	6	1	3	10
mtDNA encoded proteins identified	*2*	*1*	*2*	*4**
No. of clones encoding ORFs	6	0	0	6
ORFs/ uncharacterized genes and proteins	*3*	*0*	*0*	*3*
Genomic clones	6	1	4	11
Clones aligning with 3'UTRs	2	1	8	11
Clones with inverted cDNAs	2	1	1	4
Other	0	0	3	3

** The total number of clones does not correspond to the sum of the three YTH screens because some proteins were common to different screens.*

Although several positive clones identified as known proteins were not in frame with the activation domain of Gal4, they were not assigned as false positives. These clones are potentially genuine positive clone because yeasts tolerate translational frameshifts and can express the correct fusion protein, which will promote survival in the selective medium (Gesteland and Atkins, 1996). Moreover several clones encoding well established APP binding proteins, such as Fe65,

were in the wrong reading frame providing further evidence that thay are likely to be true positives.

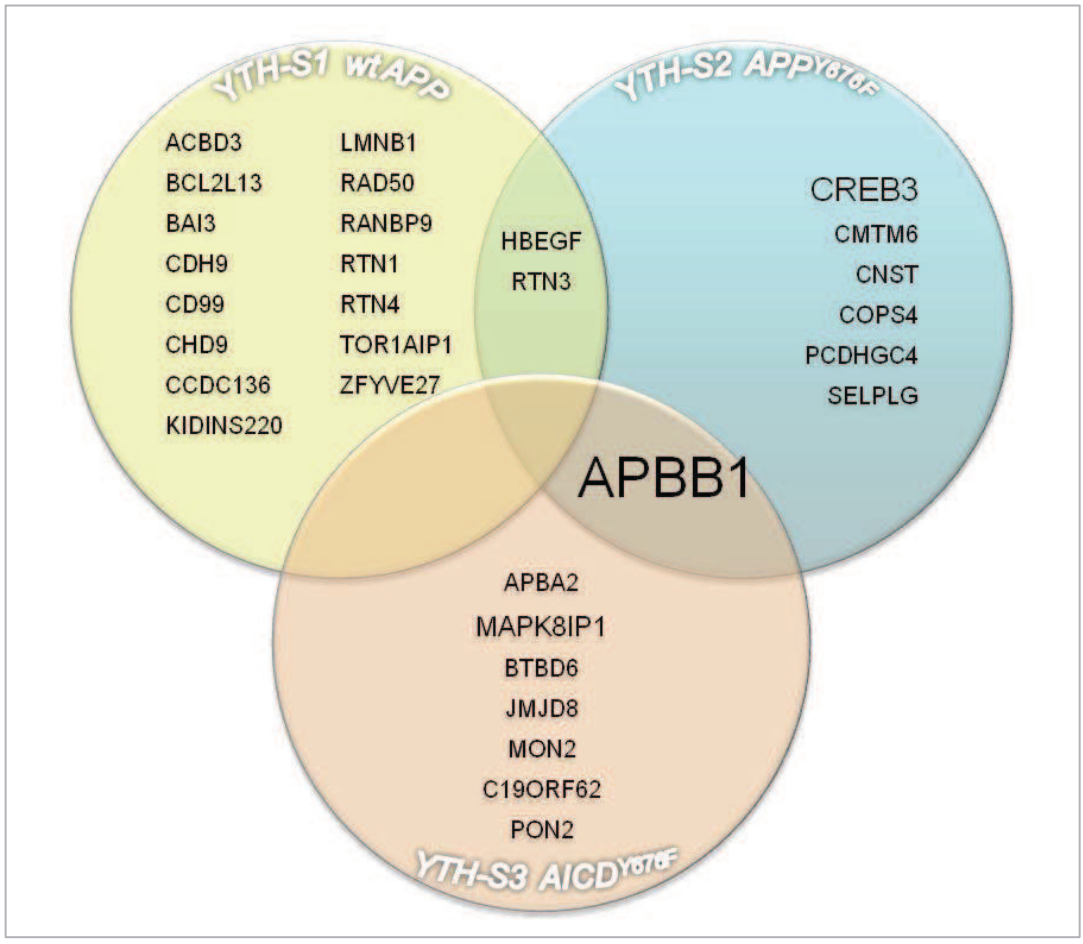

Figure III.8: Venn diagram of the proteins obtained within and between each YTH screen. Gene symbols were used instead of the proteins' common names. Frequent clones are highlighted by bigger font size.

III.3.6 Mitochondrial clones

Mitochondria have a specific genetic code, different from the standard one used by the nuclear translation machinery, and as a result some mitochondrial amino acid codons are read as stop codons in cytoplasmatic translation (Anderson *et al.*, 1981). Hence, in order to be detected in a two-hybrid assay, the plasmid encoded inserts must be expressed in the cytoplasm as GAL4-AD fusion proteins and imported to the nucleus, where they interact with a GAL4-BD-bait fusion to

activate reporter gene expression, mitochondrial translation is unlikely to be occurring. Mitochondrial clones (including cytochrome c oxidase) have previously been described as common false positives in two-hybrid screens (Serebriiskii *et al.*, 2001).

Table III.8: BLASTX results of the mitochondrial cDNA clones translated using the standard genetic code against the Refseq protein database (http://blast.ncbi.nlm.nih.gov/Blast.cgi#). Premature stop codons (*) resulting from translation using the standard genetic code are highlighted in yellow.

clone	gene	BLASTX *Query: translated cDNA using standard genetic code* *Subjet: Homo sapiens mitochondrial protein (Refseq protein database)*
A82 (YTH-s1)	MT-CO2	Query 1 AAQVGLQDATSPIIEELITFHDHALIIIFLICFLVLYALFLTLTTKLTNTNISDAQEIET 180 Sbjct 4 .....M.....M.....M.. 63 Query 181 V*TILPAIILVLIALPSLRILYIXDEVNDPSLTIKSIGHQWY*TYEYTDYGGLIFNSYIL 360 Sbjct 64 .W.....MT.....W.....M. 123 Query 361 P 363 Sbjct 124 . 124
A142 (YTH-s1)	MT-ND4	Query 16 GNQPERLNAGTYFLFYTLVGSLPLLIALIYTHNTLGSLNILLLTLTAQELSNS*ANNLI* 195 **Sbjct** 137 .....**W....M-** 195 Query 196 XXLHQLAFIVKIPLYGLHL*LPKAHVEAPIAGSIVLAAVLLKLGGYGIIRLKLILNPLXK 375 **Sbjct** 196 **WLAYTM..M..M.....W.....M.....MM..T.....T.** 255 Query 376 X*PTPSL 396 **Sbjct** 256 **HMAY.F.** 262
AF49 (YTH-s2)	MT-ND4L	Query 17 INIILAFTISLLGILVYRSHLISSLLCLEGIILSLFIIATLITLNTHSLLANIVPIAILV 196 Sbjct 6 M..M.....M.....M.....MM.....M...M.....M.. 65 Query 197 FAACEAAVGLALLVSISNTYGLDYVHNLNLLQC 295 Sbjct 66 .....S.... 98
CF100 (YTH-s3)	MT-CO3	Query 60 MTHQSHAYHIVKPSP*PLTGALSALLMTSGLAM*FHFHSITLLILGLLTNTLTIYQ*WRD 239 **Sbjct** 1 .....**M.....W.....W.....M...M.....M..W...** 60 Query 240 VTRESTYQGHHTPPVQKGLRYGIILFITSEVFFFAGFF*AFYHSSLAPTPQLGGHWPPTG 419 **Sbjct** 61 .....**M.....W.....** 120 Query 420 ITPLNPLXVPLLNTSVLLASGVSIT*AHHSLIENNRNQIIQALLITILLGLYFTLLQA 593 **Sbjct** 121 .....**E.....W.....M.....M.....** 178

Translation of the cDNA of mitochondrial clones using the standard genetic code revealed premature stop codons in all reading frames, corroborating the hypothesis that these clones are likely to be false positives (Table III.8). Partial DNA sequencing of clone CF100 (from YTH-s3) showed a stretch of thymine nucleotides after the linker sequence followed by an in-frame stop codon and by the sequence aligning with the MT-CO3 gene (also with a premature stop codon). This clone is unlikely to be a genuine positive.

Table III.9: Genetic association studies in mitochondrial genes performed in AD.

gene	YTH screen	*References*
MT-CO2	YTH-s1, YTH-s3	(Davis *et al.*, 1997; Coon *et al.*, 2006)
MT-CO3	YTH-s3	(Corral-Debrinski *et al.*, 1994; Hamblet *et al.*, 2006; Lakatos *et al.*, 2010)
MT-ND4	YTH-s1	(Corral-Debrinski *et al.*, 1994; Coon *et al.*, 2006; Lakatos *et al.*, 2010)
MT- ND4L	YTH-s2	(Corral-Debrinski *et al.*, 1994; Chagnon *et al.*, 1999)

Despite the criteria used to classify the mitochondrial clones as false positives, for all the corresponding mitochondrial genes there are polymorphisms associated with Alzheimer's disease (Table III.9 and Figure III.9).

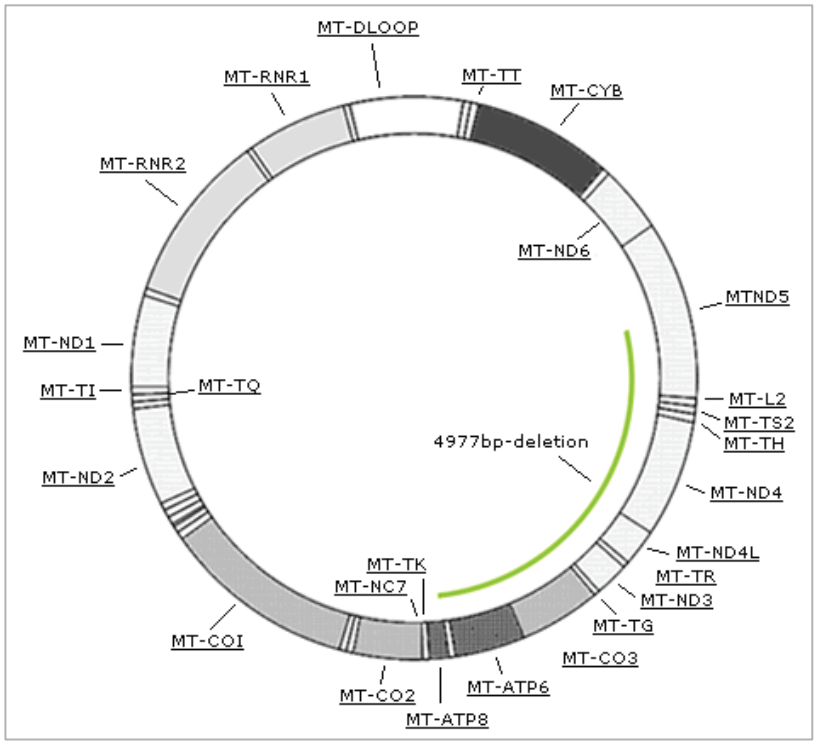

Figure III.9: Location of published AD candidate genes in the mitochondrial DNA. Adapted from the Alzgene website: http://www.alzgene.org (Bertram *et al.*, 2007).

The Gal4-AD fusion protein synthesized from the cDNA translation of clone AF49, using the cytoplasmic machinery of the yeast cells, has misdifferences with the original NADH dehydrogenase subunit 4L protein (encoded by the MT-ND4L gene). However, the interaction of the bait with the 92 amino acids peptide of clone AF49 might be relevant. Translating the cDNA from clone AF49, using the standard genetic code, and performing protein domain search using the InterPro scan tool, publicly available at http://www.ebi.ac.uk/Tools/pfa/iprscan/ (Hunter *et al.*, 2009), revealed the presence of the NADH-ubiquinone oxiredutase chain 4L/K, a signal peptide and three predicted transmembrane domains, similarly to the mitochondrial protein ND4L.

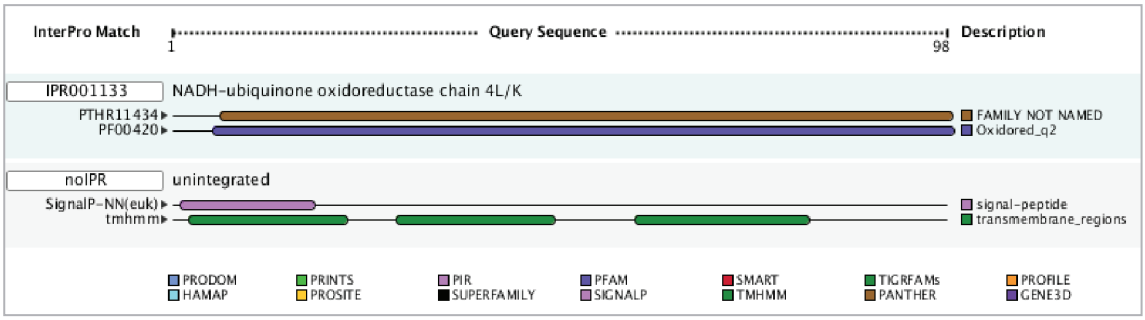

Figure III.10: InterPro domain search of clone AF49, translated using the standart genetic code (http://www.ebi.ac.uk/Tools/pfa/iprscan/). SignalP, Signal peptide; Tmhmm, predicted transmembrane domains.

III.3.7 Clones aligning with non-coding sequences

3' UTRs

In various cases the searches performed did not reveal any homologies within the coding sequences (CDS) of a known protein, or predicted gene product, for the sequenced insert portion. Several of these clones matched mRNA sequences, although aligning with the 3' UTR (untranslated regions). This is the case of the prey clones A35 and A149 (from screen 1), and CF72, CF97, CF98, CF114.2, CF116.1, CF119.3, CF120 and CF131.2 (from screen 3).

The translation of these clones in all three forward reading frames revealed premature stop codons, therefore it may be possible that these small DNA fragments encode peptides with strong affinity to the respective APP bait. However, it cannot be ruled out that these small peptides may instead interact directly with the GAL4-DNA Binding Domain, leading to transcription of the reporter genes. Further testing would be required to clarify this issue, such as co-expressing the prey plasmid with the bait protein in yeast cells.

The particial sequencing of the prey plasmids, in general, does not cover the entire library inserts. Therefore, it is also advisable to obtain the insert's full sequence in this case. It might be a real positive if another open reading frame (ORF) is present downstream of the stop codon, since nontranslated gaps upstream of ORF inserts are commonly found in genomic libraries. Due to occasional translational read-through, two different ORFs may be expressed as a fusion with the Gal4-AD, eventhough a nontranslated gap comes between them (Serebriiskii and Golemis, 2001). Nevertheless, 3' UTR clones were here assigned as false positives. For the same reasons the chimeric clones CF128.3 and CF134 (from screen 3) were here considered false positives.

Intronic sequences

One library insert, AF68 (from screen 2), matched an intronic region of the *SPTLC2* gene, which encodes the Serine palmitoyl transferase subunit II. Despite being classified as a false positive, AF68 should be fully sequenced to roule out the existence of another ORF downstream the intronic region detected, for the above-mentioned reason that nontranslated gaps upstream of ORF inserts are commonly found in genomic libraries. The two different ORFs may be expressed as a fusion with the Gal4-AD due to occasional translational read-through, eventhough a nontranslated gap comes between them.

Intron retention is a mechanism used to expand the diversity of mRNA splice variants and their consequent protein products, e.g. by hippocampal neurons (Bell *et al.*, 2010). The presence of intronic sequences in library's cDNAs might reflect the expression of uncharacterized transcripts, but this has to be further investigated.

Inverted clones

In all YTH screens there were library inserts that were in the reverse orientation relative to the Gal4-AD fusion: A65 and A67 (screen 1); AF32 (screen2); CF116.3 (screen 3). These might be real positives given that the insert can be transcribed in the reverse orientation from a cryptic

promoter within the *ADH1* terminator. As already mentioned, such proteins function as transcriptional activators as well as interacting with the bait protein (Chien *et al.*, 1991). Nevertheless, a plausible interaction between APP and an inverted prey clone demands for thorough validation experiments. Therefore, the inverted clones were here assigned as false positives and were not considerer for further studies.

III.3.8 Library inserts matching genomic clones

Library inserts matching human genomic clones were present in YTH screen 1 (A30, A99, A122, A126, A150, A151) and in YTH screen 3 (CF93, CF94, CF115, CF117). Since the library inserts were derived from mRNAs isolated from human brain, these clones might reveal the expression of brain transcripts yet to be identified. In fact, the human genome is fully sequenced but the human transcriptome and proteome are not yet fully characterized. The expression of such transcripts could be further investigated, however genomic clones were here classified as "uncharacterized proteins" and were not considered for further analysis.

III.3.9 Validation of protein interactions and quantitative α-Gal activity assay

Selected protein interactions were verified by co-transformation of the bait and the prey plasmids in the yeast AH109. This was achieved for Fe65, RanBP9 and other clones that were followed for different projects (RTN3, CDH9, CREB3, BAI3, BCL2L13, SELPLG).

RanBP9

The authenticity of the interaction between the RANBP9 clone, encoding a N-terminal truncated RanBP9, and the bait was confirmed by the ability to grow and turn blue on QDO/X-α-Gal plates due to the expression of all the reporter genes *HIS3*, *ADE2* and *MEL1*. RanBP9 interaction with AICD wt and phospho-mutants was also analyzed. AH109 yeast cells were co-transformed with the following plasmid pairs: AICD-pAS2-1/RanBP9-pACT2; $AICD^{Y687F}$-pAS2-1/RanBP9-pACT2; $AICD^{Y687E}$-pAS2-1/RanBP9-pACT2. The co-transformants were plated on SD/QDO/X-α-Gal/60mM 3-AT. RanBP9 interacts with AICD wt and both mutants, since the appearance of the colonies is similar to the positive control which co-expressed the BD-p53 and

AD-SV40 fusion proteins (Fig. III.11A). The Gal4-BD and Gal4-AD empty vectors (pAS2-1 and pACT2) were co-expressed as a negative control. Another negative control suggested by the YTH manufacturer is the co-expression of the AD-prey with a BD-Lamin C fusion protein, which showed a residual growth. YTH tests were also carried out with yeast cells transformed with a single bait or prey constructs. While all yeast constructs were able to grow on the YPD rich medium (data not shown), only co-expression of BD-bait and AD-prey fusion proteins conferred survival on SD/QDO plates (Fig. III.11A).

Quantitative X-α-Gal assays of liquid cultures showed that the AICD-RanBPM interaction is 8.3 fold ($P < 0.001$) stronger than the negative control GaL4-BD + AD, confirming the plate assays. The interactions AICD^{Y687F}-RanBP9 and AICD^{Y687E}-RanBP9 were also significantly higher than the negative control (Fig. III.11B). Moreover, α-Gal activity revealed that RanBPM had less affinity for AICD^{Y687E} than for the wild-type AICD or AICD^{Y687F}.

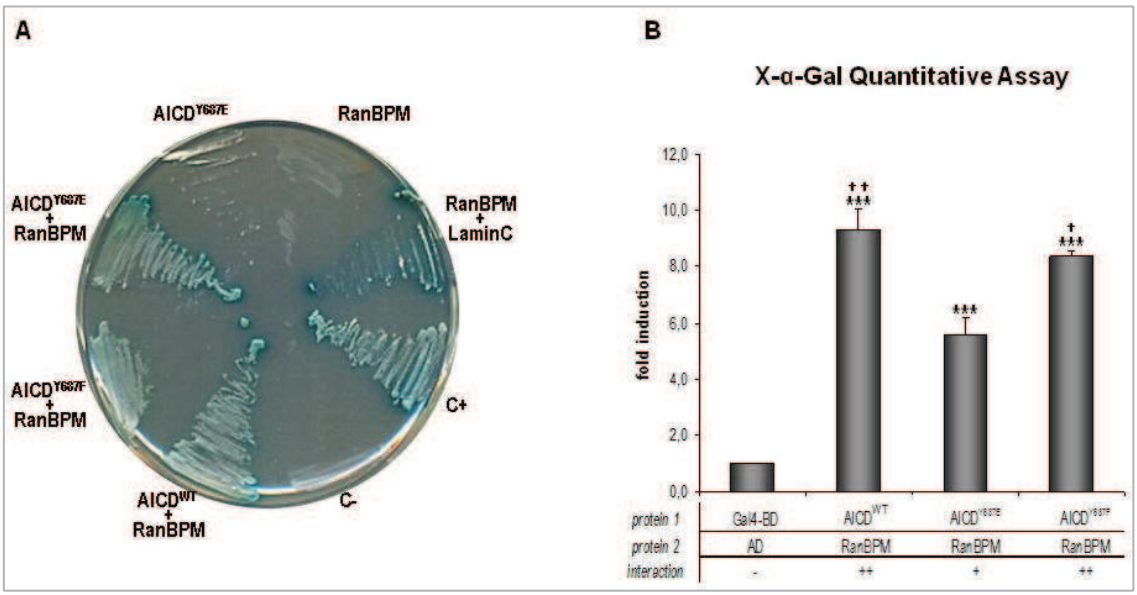

Figure III.11: Qualitative and quantitative confirmation of interaction between RanBP9 and AICD in the YTH system. (A) Growth of yeast cells containing different protein constructs was analyzed by streaking onto quadruple dropout (QDO; -Trp, -Leu, -His, -Ade) plates containing X-α-Gal. (B) Quantitative X-α-Gal assays of liquid cultures confirmed the interactions between RanBPM and all AICD constructs (*** $P < 0.001$ vs. negative control). RanBPM had less affinity for AICD^{Y687E} than for the wild-type AICD or the Y687F mutant (††, $P < 0.01$ vs. E; †, $P < 0.05$ vs. E).

Fe65 (encoded by *APBB1*) is a well known AICD interacting protein and was a very frequent clone in the YTH screens with AICD^{Y687F} and APP^{Y687F}. The YTH qualitative assay was performed in order to confirm that the Y687F mutant of AICD, and also Y687E, interact with Fe65. As shown in Fig. III.12A Fe65 associates with wt AICD, as described before, and also with both AICD mutants. The positive interaction is shown by growth on SD/-Trp/-Leu/-His plates and by the blue color of the colonies, which indicates expression of the *MEL1* reporter gene.

In order to determine the relative strength of the interaction of Fe65 with wt AICD and with the Y687E and Y687F mutants, the activity of α-galactosidase was measured in yeast culture supernatants. The α-galactosidase activity of AICD^{Y687F}-Fe65 was 1.36 fold higher than the interaction with wt. In contrast, the yeast cultures expressing AICD^{Y687E} and Fe65 showed a very low α-galactosidase activity of 0.07 fold (Fig. III.12B).

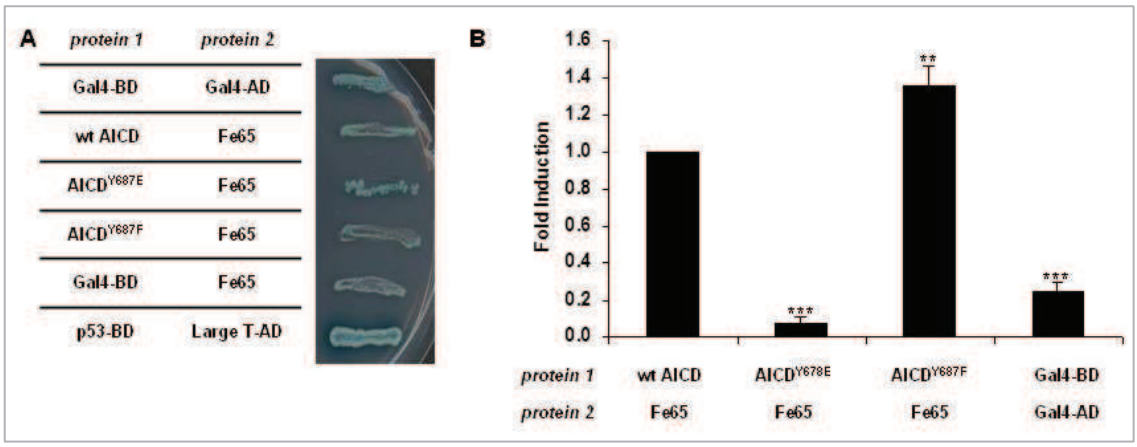

Figure III.12: YTH interaction of Fe65 with wt AICD, AICD^{Y687E} and AICD^{Y687F}. The yeast strain AH109 was co-transformed with the following pairs of plasmids: pACT2 + pAS2-1; Fe65-pACT2 + pAS2-1; Fe65-pACT2 + AICD^{WT}-pAS2-1; Fe65-pACT2 + AICD^{Y687E}-pAS2-1; Fe65-pACT2 + AICD^{Y687F}-pAS2-1; pVA3-1 + pTD1-1. (A) Yeast cells were grown on SD-Trp/-Leu/-His selective medium with X-α-Gal to test for the α-galactosidase expression. (B) Yeast cells containing the various two-hybrid constructs were grown overnight in selective medium, after which cell-free supernatants were assayed for α-galactosidase activity. Results shown are mean ± S.E. of the fold induction of α-galactosidase actity compared to the AICD^{WT}+FE65 interaction. ***P < 0.001 vs. wild-type interaction.

It is worthwhile noting that the negative control usually shows a residual α-galactosidade activity, which in this case, appears to be higher than the AICD^{Y687E}-Fe65 interaction, and was also reported by the YTH system manufacturer. Though, the yeast cells that contain the pAS2-1 and pACT2 empty vectors were grown in SD/-Trp/-Leu, which only select for the plasmids transformation, and thus the residual value does not represent a positive interaction.

The same data from Figs.III.11B and III.12B were re-plotted for comparing the interactions between AICD (wt and mutants) and the prey proteins Fe65 and RanBP9. From the graph, both prey clones, RanBP9 and Fe65, had less affinity for AICD^{Y687E} than for wt or Y687F dephospho-mutant (Fig. III.13). Moreover, wt AICD and AICD^{Y687F} interacted preferentially with Fe65, and AICD^{Y687E} had more affinity for RanBP9.

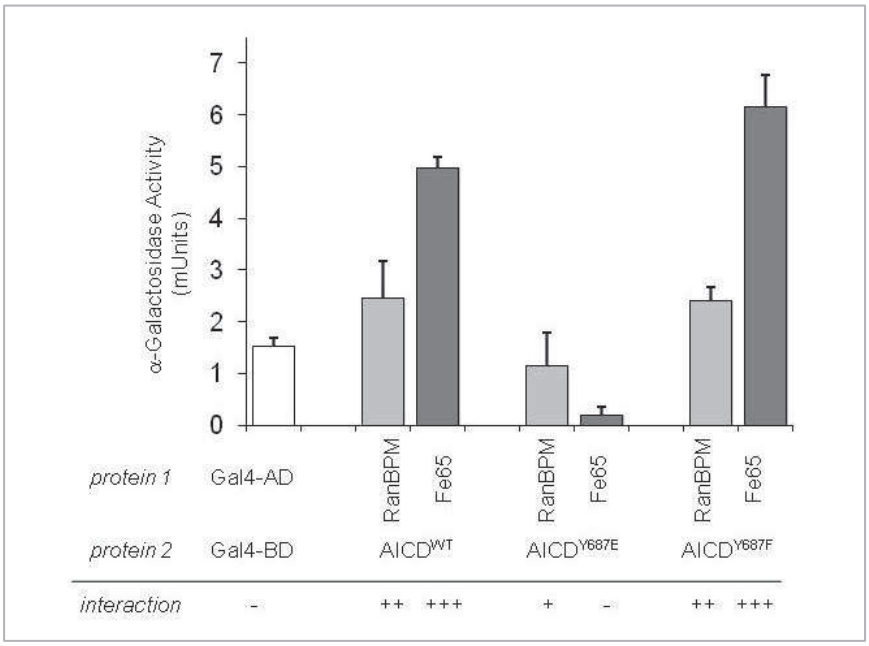

Figure III.13: YTH interaction of RanBP9 with wt AICD, AICD^{Y687E} and AICD^{Y687F} (light gray) and Fe65 interaction with wt AICD, AICD^{Y687E} and AICD^{Y687F} (dark gray).

These results validate the interactions between RanBP9 and Fe65 with wt and mutant AICDs and also show that these interactions can be regulated by Tyr-687 phosphorylation. Furthermore, these results correlate with clone frequencies in the YTH screens (AICD^{Y687E} and wt AICD were also used as baits in similar YTH screenings, in previous group projects; APPENDIX V and APPENDIX VI).

III.3.10 Analysis of the putative new APP/AICD binding proteins by bioinformatics tools

To assign a biological context for APP/AICD phosphorylation at Tyr-687 a series of YTH screens against human adult brain libraries were performed using diverse baits: APP (YTH-s1),

APP^{Y687F} (YTH-s2), and AICD^{Y687F} (YTH-s3) are described in this thesis. Two other YTH screens of adult brain libraries were performed previously using as baits AICD^{Y687E} and wild-type AICD phospho-mutant (APPENDIX V and APPENDIX VI). All the clones identified in these five YTH screens, which encode known proteins or ORFs, were considered for producing protein-protein interaction (PPI) maps, by bioinformatics means. Given that the new PPI identified were not all confirmed neither in the YTH system, nor by other methods, the following data should be carefully interpreted. To facilitate the analysis of the PPIs, all interacting proteins were unambiguous matched to the official gene symbol, using HUGO Gene Nomenclature Committee database (http://www.genenames.org/) (Eyre *et al.*, 2006).

As a first approach, PPI networks were derived around each YTH bait using Cytoscape version 2.8.2 (Shannon *et al.*, 2003; Smoot *et al.*, 2011). The same strategy was followed for each individual screen (Fig. III.14).

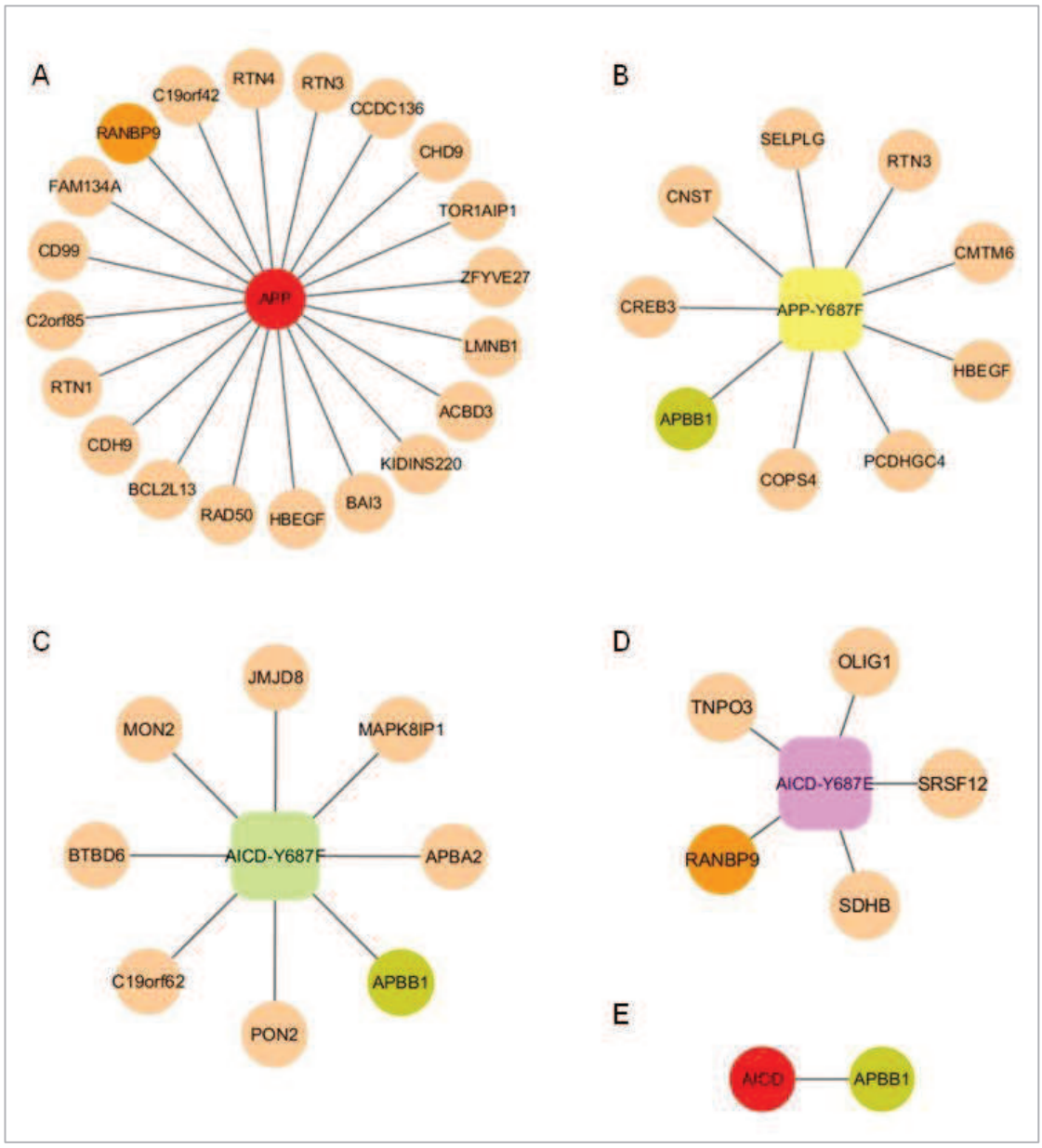

Figure III.14: APP/AICD subnetworks of PPIs obtained in the YTH screens. The nodes represent proteins, described using the official gene symbol (http://www.genenames.org/). The central node in each map corresponds to the bait protein. Wild-type APP and AICD are highlighted in red. APP phospho-mutants are represented by rectangular nodes. Fe65 (encoded by the *APBB1* gene), a well-established APP/AICD interactor, is highlighted in green. The orange node is RanBP9, whose interaction with APP is characterized in Chapter V.

Combination of these five maps produced a more complex network and highlighted the protein links between full length APP and AICD and between wild-type and phospho-/dephospho-mutants (Fig. III.15). *APBB1*, the gene encoding Fe65, interacts with three baits: APP^{Y687F}, $AICD^{Y687F}$

and AICD. Wild-type APP and APP^{Y687F} dephospho-mutant share two nodes: RTN3 and HBEGF. AICD^{Y687E} is linked to wild-type APP only by RanBP9 (Fig. III.12).

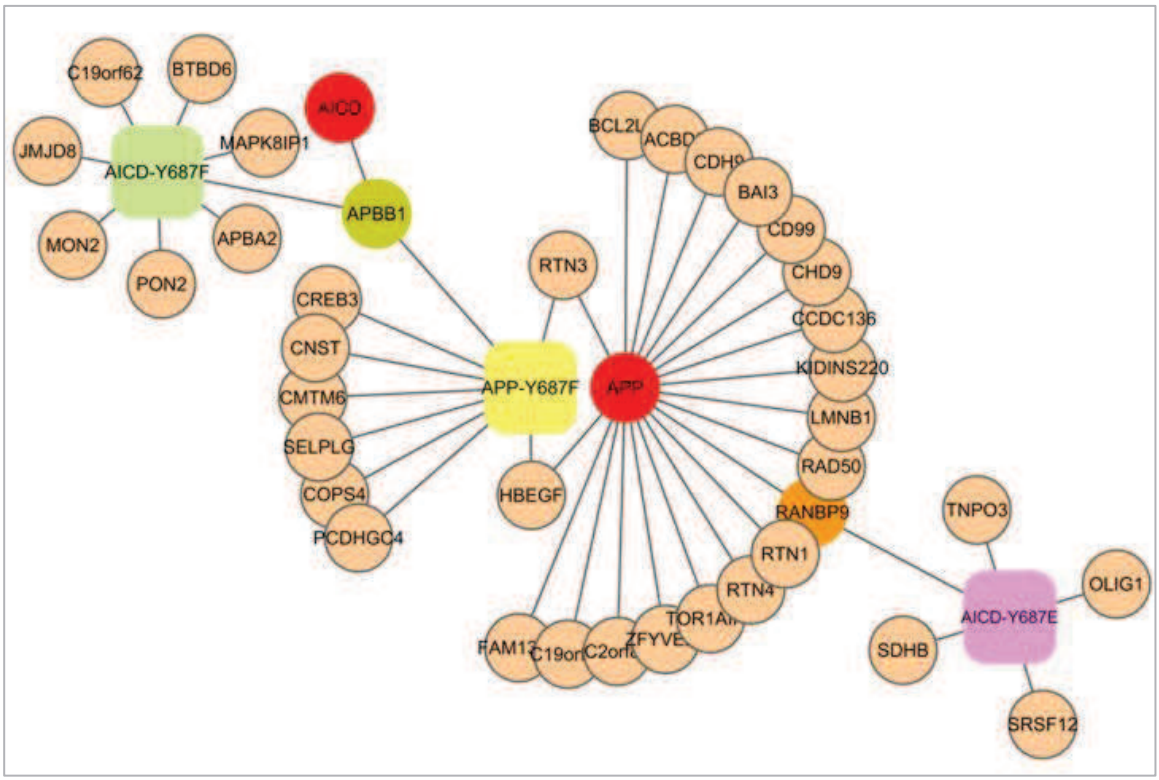

Figure III.15: Cross-complex APP/AICD network of PPIs obtained in five YTH screens against human adult brain libraries using the baits: APP, AICD, APPY687F, AICDY687F and AICDY687E. The nodes represent proteins, described using the official gene symbol (http://www.genenames.org/).

III.3.10.1 Biological interpretation of the interaction networks

To aid interpretation of the PPI data sets, the participant genes/proteins were analyzed with respect to chromosome mapping (Fig. III.16) and protein domains (Fig. III.17). The results are displayed in two-dimensional tables, where colors represent the number of proteins, per group.

Genes from the wild-type APP screen (screen 1) are more evenly distributed throughout the 23 pairs of chromosomes, which is likely be related to a higher number of proteins in this group (Fig. III.16).

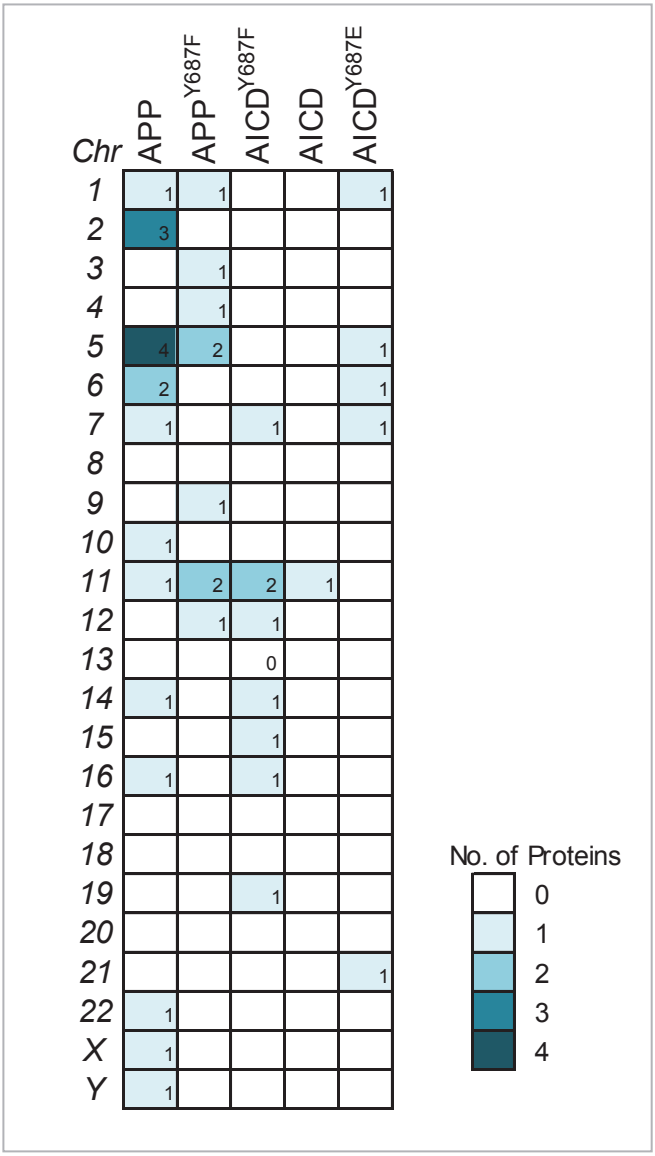

Figure III.16: Chromosome mapping of the prey-proteins from each YTH screen.

A higher number of clones in the APP PPI map, is also responsible for a greater diversity in the protein domains and motifs of the same group (Fig. III.17). Full-length wt APP harbours more interactions with proteins with transmembrane domains (13), signal peptides (5) and coiled-coil regions (6). Moreover, proteins containing G-coupled receptor domains were exclusive for the wt APP interactome (clone BAI3). The EGF-like (clone HBEGF), Cadherin (clones CDH9 and PCDHGC4) and Reticulon domains (clones: RTN1, RTN3, RTN4, FAM134A) are shared by the full-length APP baits, wt and Y687F dephospho-mutant.

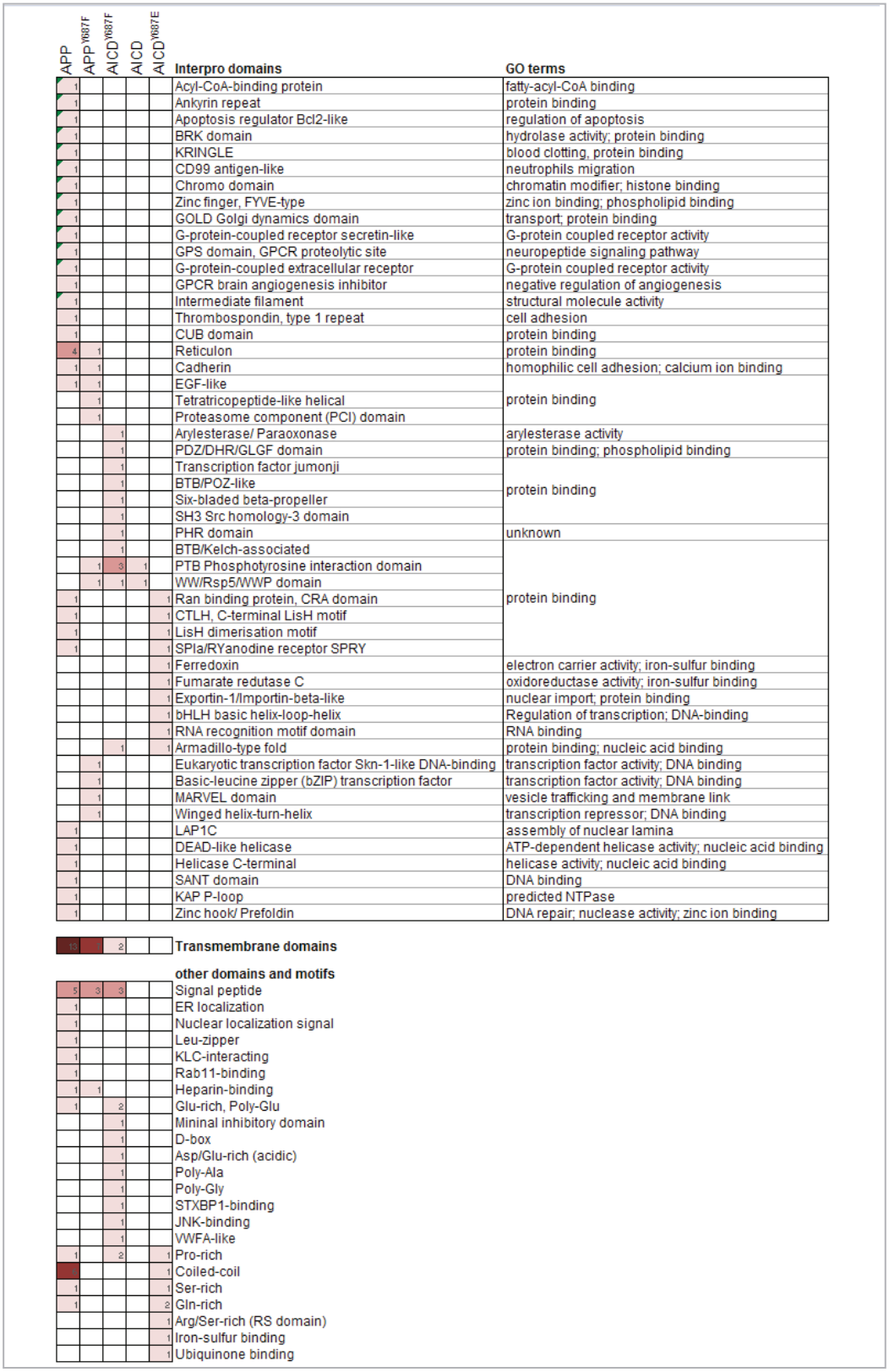

APP	APP^{Y687F}	AICD^{Y687F}	AICD	AICD^{Y687E}	Interpro domains	GO terms
1					Acyl-CoA-binding protein	fatty-acyl-CoA binding
1					Ankyrin repeat	protein binding
1					Apoptosis regulator Bcl2-like	regulation of apoptosis
1					BRK domain	hydrolase activity; protein binding
1					KRINGLE	blood clotting, protein binding
1					CD99 antigen-like	neutrophils migration
1					Chromo domain	chromatin modifier; histone binding
1					Zinc finger, FYVE-type	zinc ion binding; phospholipid binding
1					GOLD Golgi dynamics domain	transport; protein binding
1					G-protein-coupled receptor secretin-like	G-protein coupled receptor activity
1					GPS domain, GPCR proteolytic site	neuropeptide signaling pathway
1					G-protein-coupled extracellular receptor	G-protein coupled receptor activity
1					GPCR brain angiogenesis inhibitor	negative regulation of angiogenesis
1					Intermediate filament	structural molecule activity
1					Thrombospondin, type 1 repeat	cell adhesion
1					CUB domain	protein binding
4	1				Reticulon	protein binding
1	1				Cadherin	homophilic cell adhesion; calcium ion binding
1	1				EGF-like	protein binding
	1				Tetratricopeptide-like helical	
	1				Proteasome component (PCI) domain	
		1			Arylesterase/ Paraoxonase	arylesterase activity
		1			PDZ/DHR/GLGF domain	protein binding; phospholipid binding
		1			Transcription factor jumonji	protein binding
		1			BTB/POZ-like	
		1			Six-bladed beta-propeller	
		1			SH3 Src homology-3 domain	
		1			PHR domain	unknown
		1			BTB/Kelch-associated	protein binding
	1	3	1		PTB Phosphotyrosine interaction domain	
	1	1	1		WW/Rsp5/WWP domain	
1				1	Ran binding protein, CRA domain	
1				1	CTLH, C-terminal LisH motif	
1				1	LisH dimerisation motif	
1				1	SPla/RYanodine receptor SPRY	
				1	Ferredoxin	electron carrier activity; iron-sulfur binding
				1	Fumarate redutase C	oxidoreductase activity; iron-sulfur binding
				1	Exportin-1/Importin-beta-like	nuclear import; protein binding
				1	bHLH basic helix-loop-helix	Regulation of transcription; DNA-binding
				1	RNA recognition motif domain	RNA binding
		1		1	Armadillo-type fold	protein binding; nucleic acid binding
	1				Eukaryotic transcription factor Skn-1-like DNA-binding	transcription factor activity; DNA binding
	1				Basic-leucine zipper (bZIP) transcription factor	transcription factor activity; DNA binding
	1				MARVEL domain	vesicle trafficking and membrane link
	1				Winged helix-turn-helix	transcription repressor; DNA binding
1					LAP1C	assembly of nuclear lamina
1					DEAD-like helicase	ATP-dependent helicase activity; nucleic acid binding
1					Helicase C-terminal	helicase activity; nucleic acid binding
1					SANT domain	DNA binding
1					KAP P-loop	predicted NTPase
1					Zinc hook/ Prefoldin	DNA repair; nuclease activity; zinc ion binding

					Transmembrane domains
13	1	2			

					other domains and motifs
5	3	3			Signal peptide
1					ER localization
1					Nuclear localization signal
1					Leu-zipper
1					KLC-interacting
1					Rab11-binding
1	1				Heparin-binding
1		2			Glu-rich, Poly-Glu
		1			Mininal inhibitory domain
		1			D-box
		1			Asp/Glu-rich (acidic)
		1			Poly-Ala
		1			Poly-Gly
		1			STXBP1-binding
		1			JNK-binding
		1			VWFA-like
1		2		1	Pro-rich
2				1	Coiled-coil
1				1	Ser-rich
1				2	Gln-rich
				1	Arg/Ser-rich (RS domain)
				1	Iron-sulfur binding
				1	Ubiquinone binding

Figure III.17: Domains and motifs of the prey-proteins, as obtained by sequence analysis using Interpro (http://wwwdev.ebi.ac.uk/interpro/), ELM (http://www.elm.eu.org/) and Prosite (http://prosite.expasy.org/).

One protein from the wt APP screen (clone ZFYVE27) is a zinc finger protein and has a zinc finger FYVE domain. FYVE domains bind to PI(3)Ps, membrane phospholipids enriched in the early endosomes (Seet and Hong, 2006). FYVE domain binding of PI(3)P has also been implicated it in a signaling role downstream of PI(3)kinase. Furthermore, FYVE containing proteins have been implicated in the regulation of the vacuolar/lysosomal membrane trafficking pathway and in regulation of signaling by TGFβ-receptors (Kutateladze, 2006).

Very diverse protein binding domains were seen in all groups and, all together, these were the most frequent domains found. DNA binding domains were also present in all the groups, except for AICD, whose YTH screen resulted in hundreds of clones matching only one protein, Fe65 (APPENDIX VI).

The proteins identified in the several YTH screens were further analyzed with respect to Posttranslational modifications and Gene Ontology (GO) categories: Cellular component (CC), Molecular function (MF) and Biological process (BP). This survey was performed by database searching in the web sites: Entrez Gene (http://www.ncbi.nlm.nih.gov/gene); UniProt (http://www.uniprot.org/); and HPRD (http://www.hprd.org/).

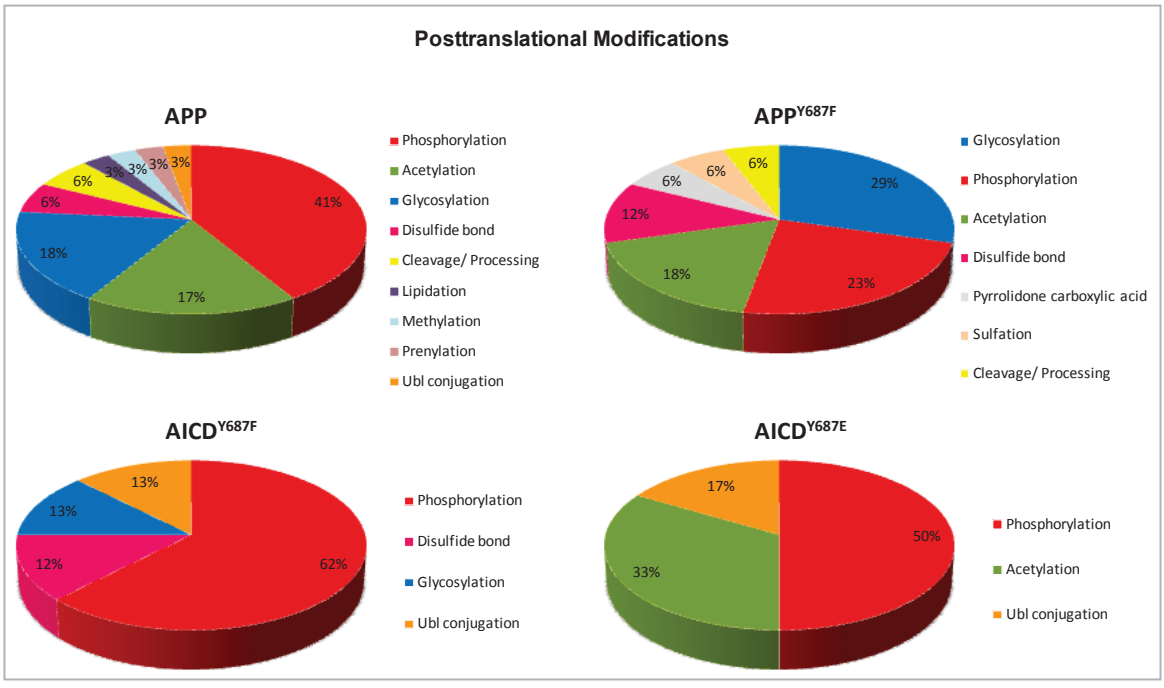

Figure III.18: Posttranslational modifications of the proteins identified in the several YTH screens. The pie charts depict the relative number of proteins from each respective screen.

The proteins identified in YTH screen with full-length APP (wt and Y687F dephospho-mutant) are mostly post-translationally modified by phosphorylation, acetylation and glycosylation. Proteins identified with AICD mutants, Y687F and Y687E, are mostly modified by phosphorylation (Fig. III.18). Fe65, the only protein identified with wt AICD is also a phospho-protein.

Cleavage/Processing were detected only for proteins in FL APP (wt and Y687F-mutant) interactomes (Fig. III.18).

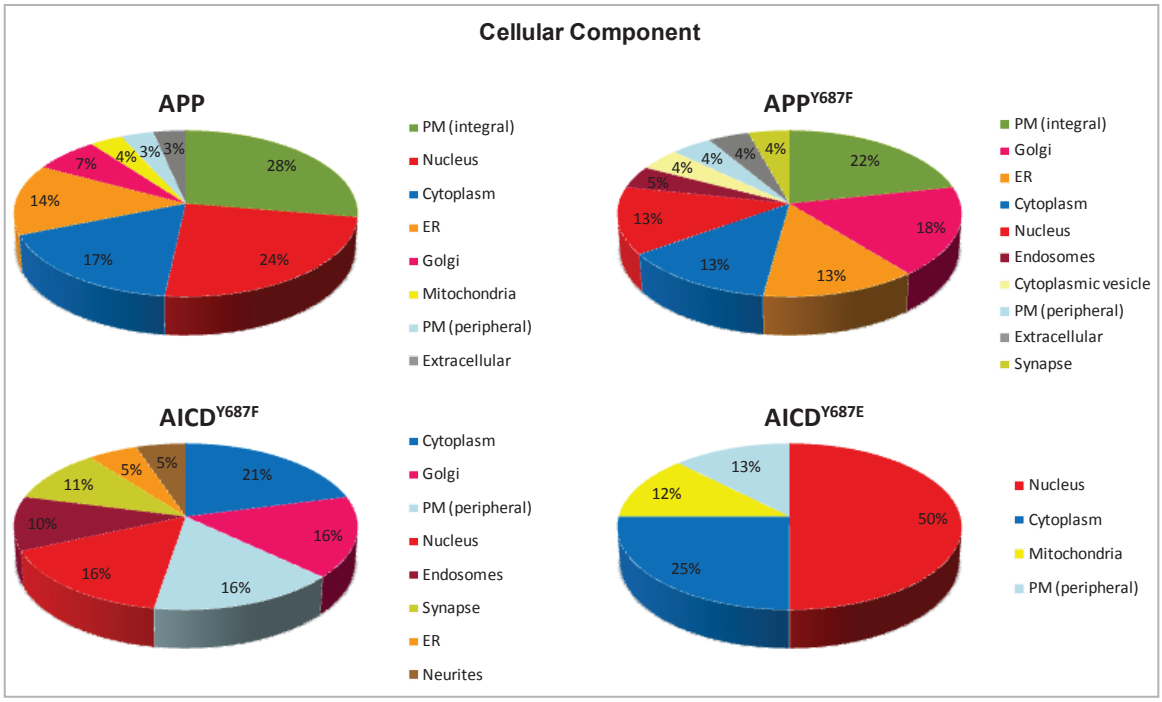

Figure III.19: Analysis of the proteins identified in the several YTH screens in terms of the GO classification 'Cellular component'. The pie charts depict the relative number of proteins from each respective screen. PM, Plasma membrane; ER, Endoplasmic reticulum.

Analysis of the proteins identified in the several YTH screens in terms of the GO classification 'Cellular component' revealed that proteins in FL APP (wt and Y687F-mutant) interactomes are mostly plasma membrane integral proteins (Fig. III.19), which is in accordance with their enrichment in transmembrane domains. Nuclear proteins are among FL APP interactions in the YTH system. *In vivo*, only the liberated AICD translocates to the nucleus, but in the YTH system APP interactors include proteins that interact with the FL molecule and also with its proteolitic fragments. Moreover, most nuclear proteins in these interactomes are also detected in other subcellular locations, except RAD50 and TOR1AIP1 (from the APP screen) which are exclusively nuclear.

Is is worthwhile mentioning that the GO terms analyzed here are as it appears in the databases mentioned. More accurate information from the literature was not taken into consideration for the GO classification.

Interestingly, the cellular components endosomes, synapses and neurites had only been identified with the Y687F dephospho-mutants (FL and AICD). The endocytic vesicles are the major site of β-secretase activity and the APP^{Y687F} mutant was previously shown to be preferentially endocytosed and targeted for β-secretase cleavage, in contrast to the APP^{Y687E} phospho-mimicking mutant (Rebelo et al., 2007a).

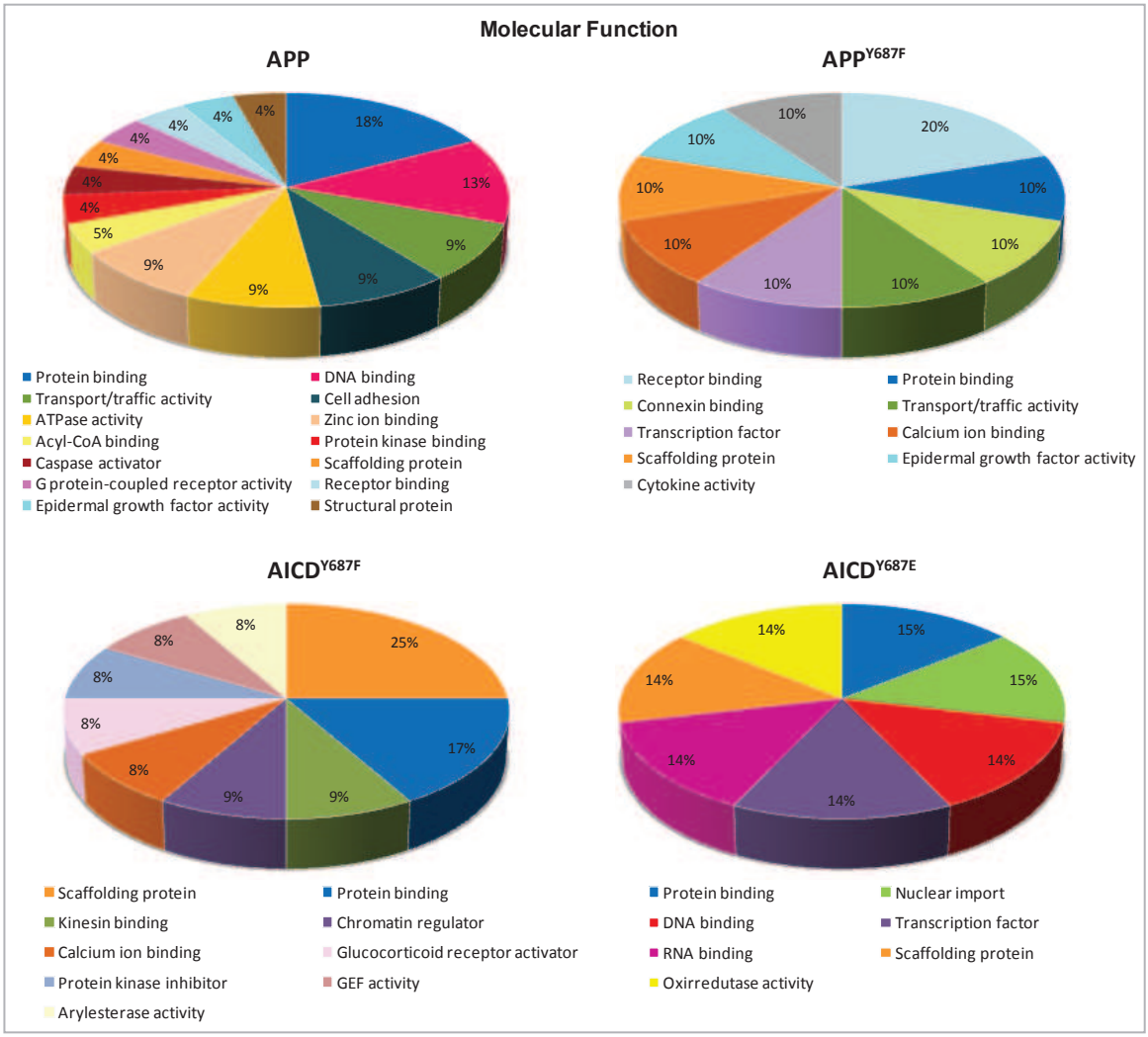

Figure III.20: Analysis of the proteins identified in the several YTH screens in terms of the GO classification 'Molecular function'. The pie charts depict the relative number of proteins from each YTH screen.

The molecular function of the proteins identified in the YTH screens, as given by the above mentioned databases, revealed that most mediate protein interactions (Fig. III.20). This again is in agreement with the domain analysis. Most APP and AICD^{Y687E} interactors are involved in DNA binding, in contrast with the Y687F mutants interactions. Most AICD^{Y687F} are scaffolding proteins, which is the case for APBB1, APBA1 and BTBD6.

Interestingly, interactions with AICD (de)phospho-mutants revealed a kinesin binding protein (MAPK8IP1) and a nuclear import protein (TNPO3). In the 'Biological processes' analysis, these proteins are classified in the 'transport and trafficking' group, important in AICD^{Y687F} and AICD^{Y687E} interactomes (Fig. III.21).

Full-length APP (wt and mutant) interacted preferentially with proteins involved in signaling and regulation. Proteins involved in cell growth and proliferation and cell migration were common to these interactomes. Interestingly in the APP^{Y687F} interactome 'cell migration' contained more proteins and this category also appears in the AICD^{Y687F} group. The AICD^{Y687E} interactome contains proteins involved in cell growth and proliferation, and this is a prominent category in the APP interactome (Fig. III.21).

Although the GO categories contain different proteins that are involved in the same biological processes, they help to interpret the protein interaction maps. Full-length APP (wt and dephospho-mutant) share two protein nodes (HBEGF and RTN3; Fig. III.15) and are also closely associated by the 'Biological process' GO categories.

APP^{Y687F} and AICD^{Y687F} share one protein node (APBB1; Fig. III.15) and are also linked by the 'Cellular component' categories endosomes and synapses, potentially involved in AD pathology.

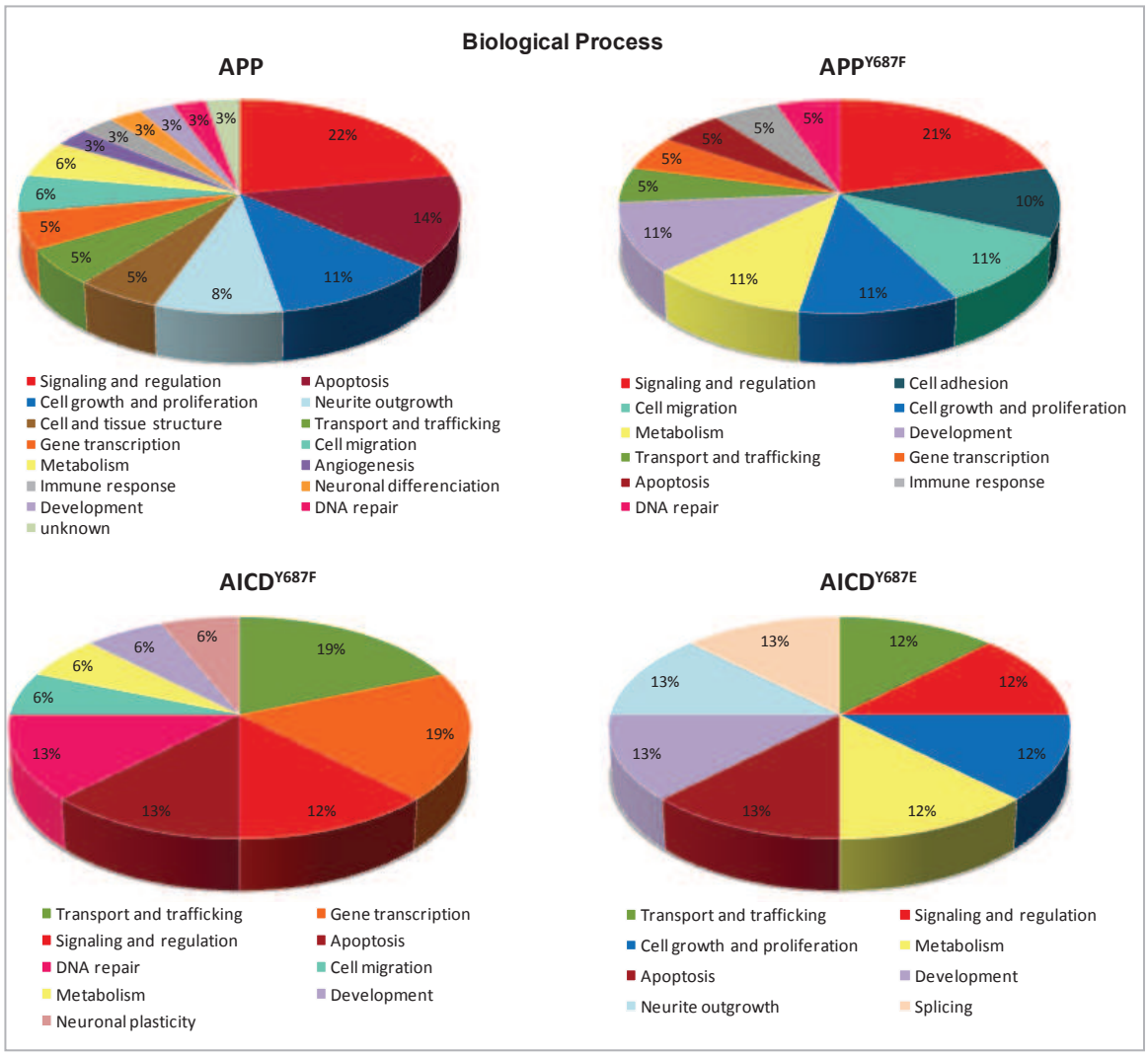

Figure III.21: Analysis of the proteins identified in the several YTH screens in terms of the GO classification 'Biological process'. The pie charts depict the relative number of proteins from each YTH screen.

III.3.10.2 APP/AICD networks focusing on disease association

Searching the AlzGene database, a field synopsis of genetic association studies in AD available at http://www.alzgene.org (Bertram *et al.*, 2007), showed that besides the bait APP, only *APBB1* (Hu *et al.*, 1998; Lambert *et al.*, 2000), *MAPK8IP1* (Helbecque *et al.*, 2000) and *PON2* (Shi *et al.*, 2004; Erlich *et al.*, 2006) show positive association with AD (Fig. III.22, red nodes). From the OMIM (Online Mendelian Inheritance in Man) database and literature curation, a set of genes could be associated with diseases with neuropathological features (Fig. III.22, orange nodes).

Genes associated with other diseases are represented by yellow nodes and genes with unknown disease association are colorless (Fig. III.22). AICD^{Y687F} holds all the AD risk genes found (APBB1, MAPK8IP1 and PON2), while wt APP exhibits more interactions with proteins involved in non-AD pathologies.

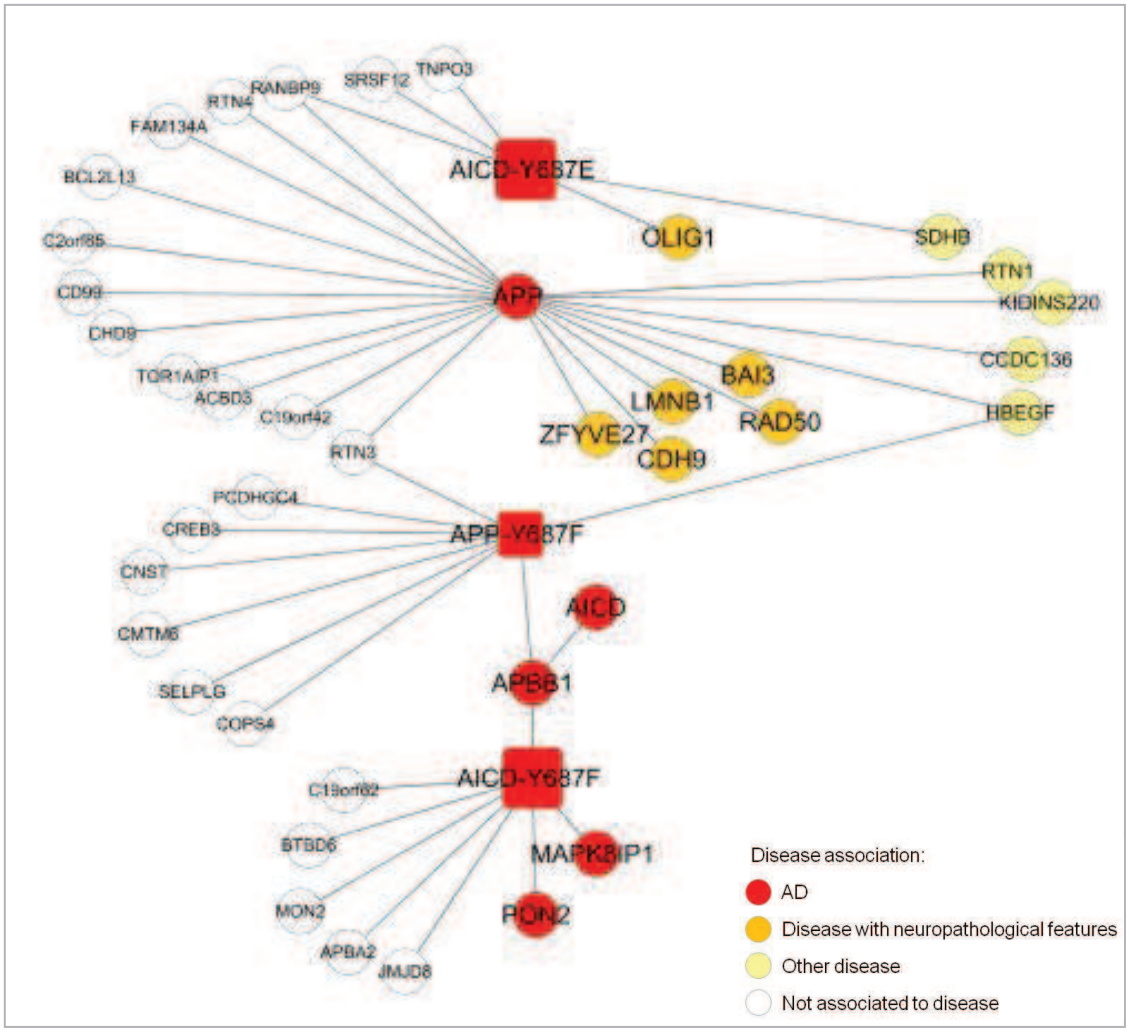

Figure III.22: Representation of the APP PPI network generated from five YTH screens against human adult brain libraries using the baits: APP, AICD, APP^{Y687F}, AICD^{Y687F} and AICD^{Y687E}. The nodes represent proteins, described using the official gene symbol (http://www.genenames.org/). Information concerning disease association data (AD, disease with neuropathological features or other) was attributed to the nodes and the network was re-plotted, using Cytoscape. *Network statistics: diameter= 8; radius=4; centralization=0.449; heterogeneity= 1.625; no. of nodes=43; average no. of neighbors=2.*

The disease association network was merged with the APP curated network (201 nodes), the APBB1 curated network (26 nodes) and RanBP9 curated network (73 nodes). The resulting cross-complex network in represented in Fig. III.23, but here only the AD associated genes are

highlighted (red nodes). All APP/AICD baits are highlighted in red, due to disease association of APP, however APP fragments and (de)phospho-mutants might lead to distinct outcomes in the context of AD.

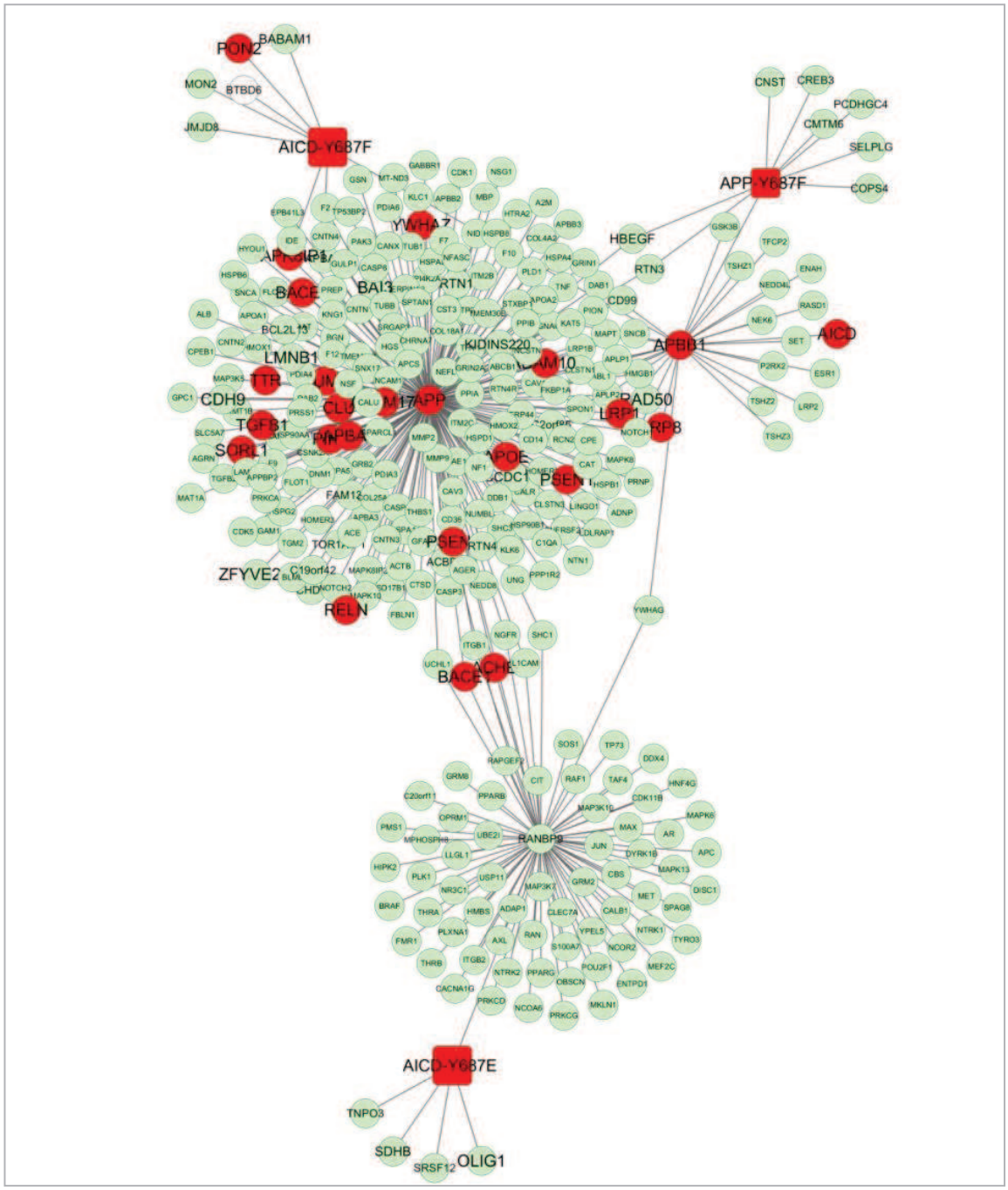

Figure III.23: Cross-complex of the disease association network with networks of literature curated PPIs of APP, APBB1, RanBP9, using Cytoscape. *Network statistics: diameter= 6; radius=3; centralization=0.693; heterogeneity= 6.082; no. of nodes=316; average no. of neighbors=2.133.*

III.4 DISCUSSION

The great diversity of human proteome and protein interactions are spatio-temporally regulated to perform specific tasks. Additionally the proteome seems to have diverged more rapidly in the brain than in other tissues (Enard *et al.*, 2002), making proteomic analysis significantly more challenging than genomic or transcriptomic approaches. A major goal of functional proteomics is to identify the complete protein interaction network, or interactome, of an organism. Within these networks, proteins of similar function and cellular localization tend to cluster together (Bader and Hogue, 2002), making the study of PPIs a powerful approach for inferring information about protein function. Large-scale PPI network studies combine multiple approaches, such as manual curation, automated text mining, computational predictions and PPIs discovered by high-throughput methods, such as YTH and co-affinity purification followed by mass spectrometry (AP/MS).

YTH interactions generated in the early days of this technology were thought to have a high level of false positives; however, recent reports proved that these data sets are mostly reliable and accurate (Yu *et al.*, 2008; Braun *et al.*, 2009). YTH data generally yielded high quality data on direct binary interactions. However, even high quality YTH networks are predicted to encompass only 20% of binary PPIs (Yu *et al.*, 2008) and involve the expression of proteins in a non-physiological environment resulting in a loss of spatial and temporal control. In addition to methodological limitations, many neuronal-specific interactions may be missed in these YTH screens due to posttranslational modifications, proteolytic processing, etc. In this work, using Tyr-687 phosphorylation-mimicking mutants of APP/AICD successfully revealed numerous novel putative interactions, that can potentially help to understand the biology of APP, and, ultimately, APP pathways leading to AD.

At this stage, the new putative protein interactions found by YTH screening should be confirmed. As such, supplementary data from other sources should be used to evaluate the credibility of interactions in an YTH screen. Thereby, the verification of a putative interaction can be achieved in a variety of ways. The first approach would be to retest each new bait-prey interaction in yeast cells, by co-transformation of the respective plasmids. These tests were performed for only a few selected positive clones. As such, the *in silico* analysis of PPI networks is speculative and future work should start by validating the new PPIs. Validation of PPIs by several

in vitro and *in vivo* methods strengthens the accuracy of PPI data and increases the knowledge on functional proteomics.

In depth bioinformatics analysis of the three APP/AICD interactomes generated in this study, and two additional screens from previous projects in the group, revealed some distinctive characteristic within and between the PPI networks. The interpretation of these PPI data sets is particularly relevant since it allows to infer the distinct physiological context of FL APP and its liberated cytoplasmic fragment, AICD, and also, more importantly, among wt and dephospho-/phospho-mimicking mutants. The generated Tyr-687 mutations have already proved effective in elucidating the role of APP/AICD phosphorylation in AD. The APP^{Y687F} mutant, which mimics dephosphorylation at Tyr-687, was preferentially endocytosed and targeted for β-secretase cleavage, in contrast with the APP^{Y687E} phospho-mimicking mutant (Rebelo *et al.*, 2007a). Interestingly, analysis of GO terms also pointed in the same direction, in particular 'Cellular component', where endosomes, the major site of β-secretase activity, occurs only in the Y687F-mutants interactomes. However, these data should be carefully interpreted. Validation of the novel putative interactions should be carried out with wt APP/AICD and also with (de)phospho-mimicking mutants. As seen for Fe65 or RanBP9, clones interacting with dephospho-/phospho-mutants may interact with the wt protein and vice versa. Additionally, comparing the interaction strengths among wt AICD and several dephospho-/phospho-mimicking mutants, by quantitative α-Gal assays, elucidated the role of Tyr-687 phosphorylation in the regulation of AICD protein interactions. The same strategy could be applied to other AICD phosphorylatable residues.

In the YTH screen with FL APP, preys include proteins that interact with the FL molecule and also proteins that interact *in vivo* with APP fragments, such as sAPP, Aβ, C99, C83 or AICD. For this reason, exclusively nuclear proteins were found with FL APP. Further validation experiments with different APP constructs can narrow down the interaction region/domain of APP.

The GO categories presented contain different proteins that were grouped together due to their involvement in the same cellular component, molecular function or biological process, thus helping to interpret the protein interaction maps. Full-length APP (wt and dephospho-mutant) share two protein nodes (HBEGF and RTN3) and are also closely associated by the 'Biological process' GO categories. APP^{Y687F} and $AICD^{Y687F}$ share one protein node (APBB1) and are also linked by the 'Cellular component' categories endosomes and synapses, potentially involved in AD pathology. However, it is worthwhile mentioning that the GO terms analyzed here were taken

from online databases, instead of literature manual curation. Another limiting factor might be a poor characterization of the proteins (or genes) in this analysis.

The APP/AICD PPI maps focusing on disease association elucidate the APP baits that are closer to AD genes and are in agreement to the GO information obtained for the nodes. AICD^{Y687F} harbors all the AD risk genes found, while wt APP exhibits more interactions with proteins involved in non-AD pathologies. The cross-complex network generated by merging the disease association network with curated APP, Fe65 (a major Y687F binding protein in this study) and RanBP9 (the most frequent in the AICD^{Y687E} screen) networks also show that AICD^{Y687E} and its binding partners are more distant from the AD genes, in contrast with the Y687F dephospho-mimicking mutants.

The YTH screens here described, although should be further validatied by YTH and other non-hybrid methods, showed numerous novel putative binding partners that can be selected for further studies. The PPI maps around APP/AICD, in particular, the differences between wt, Y687E and Y687F mutants reflect the known information about the role of AICD Tyr-687 phosphorylation in an AD context. Therefore, integrating genetic and protein networks to infer pathway organization in complex diseases, such as AD, seems an appropriate approach to unravel the disease mechanisms and more effectively find targets for therapeutic intervention.

CHAPTER IV. CHARACTERIZATION OF A NEW SPLICE VARIANT OF THE APP BINDING PROTEIN FE65

The work described in the Chapter IV was included in the following research paper:
Journal of Neurochemistry 2011 Dec;119(5):1086-98. doi: 10.1111/j.1471-4159.2011.07420.x. Epub 2011 Oct 14.

"Identification and characterization of a neuronal enriched novel transcript encoding the previously described p60Fe65 isoform"

Sara C. Domingues[1], Ana G. Henriques[1], Margarida Fardilha[2], Edgar F. da Cruz e Silva[2,†] and Odete A.B. da Cruz e Silva[1]

[1]Neuroscience Laboratory, Centre for Cell Biology, University of Aveiro, Portugal

[2]Signal Transduction Laboratory, Centre for Cell Biology, University of Aveiro, Portugal

[†]Deceased on March 2, 2010

Abstract:

Fe65 is a multimodular adaptor protein that interacts with the cytosolic domain of the β-amyloid precursor protein (APP), the major component of Alzheimer's disease (AD) senile plaques. In the work here presented, we describe the existence of a new Fe65 transcript variant (GenBank Accession EF103274). A unique 5' sequence of 69 nucleotides, spanning a region between exons 2 and 3 of the *FE65* gene, was present in a yeast two-hybrid clone from a human brain cDNA library. *In silico* analysis and RT-PCR revealed the presence of a novel exon of 133 bp, and we redefined the structure of the human *FE65* gene. The novel exon 3a-inclusive transcript generates a shorter isoform, p60Fe65. The migration pattern of the p60Fe65 isoform was observed previously and attributed to an alternative translation initiation site within the p97Fe65 transcript. Here, we provide evidence for the origin of the previously unexplained p60Fe65 isoform. Moreover, Fe65E3a is expressed preferentially in the brain and the p60Fe65 protein levels increased during PC12 cell differentiation. This novel Fe65 isoform and the regulation of the splicing events leading to its production, may contribute to elucidating neuronal specific roles of Fe65 and its contribution to AD pathology.

IV.1 INTRODUCTION

Many proteins which interact with the intracellular domain of APP (AICD) have been reported, most of them possessing multiple protein-protein interaction domains, which in turn form complexes with other proteins. This suggests that these interacting proteins function as adaptor proteins, linking APP to specific molecular pathways. Several laboratories have used the AICD as ''bait'' in two-hybrid systems, identifying two major families of APP binding proteins, the Fe65 proteins and the X11/Mint proteins (Fiore *et al.*, 1995; Borg *et al.*, 1996; Bressler *et al.*, 1996; Guenette *et al.*, 1996; McLoughlin and Miller, 1996; Duilio *et al.*, 1998; Tanahashi and Tabira, 1999b). The Fe65 protein family comprises three members, encoded by distinct genes: Fe65, Fe65L1 and Fe65L2, which have all been reported to interact with APP. Whereas the Fe65L1 and Fe65L2 are ubiquitously expressed, Fe65 expression is enriched in the brain, although it is detected in smaller amounts in other tissues (Fiore *et al.*, 1995; Bressler *et al.*, 1996; Duilio *et al.*, 1998).

Fe65 was described to modulate APP processing and increase the generation of the APP-derived Aβ peptide, the major constituent of Alzheimer's disease (AD) senile plaques (Sabo *et al.*, 1999; Xie *et al.*, 2007). Fe65 was also demonstrated to have a role in the regulation of AICD-mediated gene expression, and KAI1 gene the most consensual target (Baek *et al.*, 2002). Both KAI1 and APP gene promoters are targets for the AICD/Fe65/Tip60 complex but other targets have been reported, such as the genes coding for GSK3β, BACE1, Tip60, Neprilysin, p53, α2-actin, Transgelin and EGF receptor (Kim *et al.*, 2003; von Rotz *et al.*, 2004; Pardossi-Piquard *et al.*, 2005; Ryan and Pimplikar, 2005; Alves da Costa *et al.*, 2006; Muller *et al.*, 2007; Zhang *et al.*, 2007; Konietzko *et al.*, 2008). Other cellular functions attributed to Fe65 include: regulation of cell movement (Sabo *et al.*, 2001, 2003; Ikin *et al.*, 2007); regulation of cell cycle progression (Bruni *et al.*, 2002) and response to DNA damage (Minopoli *et al.*, 2007). Fe65 was reported to interact with the APP protein family (APP, APLP1 and APLP2), Mena, LRP, Notch1, 14-3-3γ, $P2X_2$ receptor, Alcadein, ApoE receptor 2, Estrogen receptor α, microtubule associated protein Tau, Nek6 kinase, cAbl kinase, transcription factor CP2/LSF/LBP1, histone acetyltranferase Tip60 and nucleosome assembly factor SET. The capacity of assembling tripartite complexes between APP or AICD and most of the Fe65 binding proteins, places Fe65 as a key molecule in pathways potentially involved in AD.

Fe65 is a multimodular adaptor protein, possessing three protein-protein interacting domains: a WW domain (a protein module with two conserved tryptophans) and two tandem

phosphotyrosine binding domains – PTB1 and PTB2. The C-terminal phosphotyrosine binding domain of Fe65, PTB2, is responsible for the interaction with the intracellular domain of APP through its YENPTY motif (Fiore *et al.*, 1995; Borg *et al.*, 1996; Bressler *et al.*, 1996; McLoughlin and Miller, 1996; Zambrano *et al.*, 1997). Interaction of the Fe65 PTB2 domain with APP is dependent on the phosphorylation state of the latter at Thr-668, 14 residues N-terminal to the YENPTY sequence. Phosphorylation of APP Thr-668 (695-isoform numbering) impairs Fe65 interaction suggesting that adaptor protein interactions with APP are differentially regulated by phosphorylation states, through altering the conformation of AICD (Ando *et al.*, 2001; Radzimanowski *et al.*, 2008) or modulating APP intracellular trafficking (Chang *et al.*, 2006; Rebelo *et al.*, 2007a, b; Vieira *et al.*, 2009). The intracellular domain of APP has eight potentially phosphorylatable residues (Lee *et al.*, 2003). Seven of which reside in the three AICD functional motifs: ^{653}YTSI^{656}, ^{667}VTPEER^{672}, and ^{682}YENPTY^{687} (da Cruz e Silva *et al.*, 2004a). Previous work from our laboratory has addressed the role of Tyr-687 phosphorylation by mimicking its constitutive phosphorylation (Y687E) and dephosphorylation (Y687F) (da Cruz e Silva *et al.*, 2004c). APP^{Y687E}-GFP was shown to be targeted to the plasma membrane and could not be detected in endocytic vesicles, the major site of β-secretase activity, exhibiting a concomitant dramatic decrease in Aβ production. In contrast, APP^{Y687F}-GFP was endocytosed similarly to wild type APP, but was relatively favoured for beta-secretase cleavage (Rebelo *et al.*, 2007a).

The use of the yeast two-hybrid (YTH) method for the identification of interacting proteins allows for the selection, among a large number of clones, from a human brain cDNA library, of proteins interacting with a bait protein. Therefore, the aim of this work was to identify brain proteins capable of interacting with APP harboring a mutation that mimics the dephosphorylated state of tyrosine-687. A YTH screen was carried out using as bait the APP^{Y687F} cDNA. The positive clones were analyzed and several matched Fe65.

The human *FE65* gene comprises 15 exons and three distinct splice variants have already been reported. Transcript variant 1 (GenBank Accession NM_001164) represents the longest transcript and encodes the longest isoform (Fe65E9). Transcript variant 2 (Accession NM_145689) encodes a protein that maintains the reading frame but is a shorter isoform (Fe65ΔE9). The expression of the Fe65E9 and Fe65ΔE9 isoforms is regulated by alternative splicing of the pre-Fe65 mRNA in a cell type-dependent pattern. Among the 15 exons of the human *FE65* gene, exon 9, which encodes part of PTB1 domain, is the shortest with only 6 bp (AGAGAG). This miniexon is alternatively spliced and the exon 9-inclusive form (Fe65E9) is exclusively expressed, at high

levels, in neurons, while the exon 9-exclusive form (Fe65ΔE9) is widely expressed, at relative low levels, in non-neuronal cells (Hu *et al.*, 1998; Hu *et al.*, 1999). Both alternatively spliced Fe65 mRNAs were present in the neuronal derived cell line PC12, as well as in the total brain mRNA (Duilio *et al.*, 1991). However, the non-neuronal tissues (lung, kidney, testis and liver) and the non-neuronal derived cell lines (C6 glioma cells, BRL liver cells, FAO liver cells and Rat2 fibroblasts) were reported to contain only the Fe65ΔE9 transcript. Another human Fe65 transcript variant results from alternative splicing of the terminal exon 14 by selection of an alternative acceptor site, which was attributed to an intronic polymorphism within intron 13. This allele 2 encoded isoform, Fe65a2, has an altered C-terminal region, lacking part of the PTB2 domain. Since the PTB2 domain is the APP binding site, the Fe65a2 isoform binds APP less efficiently, suggesting a protective contribution to very late onset AD (VLODAT) (Hu *et al.*, 2002).

A putative shorter isoform of 60 KDa has been reported by several independent groups (Sabo *et al.*, 2003; Wang *et al.*, 2004; Cool *et al.*, 2010) referred to as p60. The p60Fe65 expression was attributed to an alternative translation of the Fe65p97 transcript initiated in a methionine present in exon 3 (Wang *et al.*, 2004). Here we describe a new splice variant of Fe65, Fe65E3a (GenBank Accession EF103274), and provide evidence that the novel transcript is the origin of the brain enriched p60Fe65 isoform, which appears to be particularly relevant in neuronal systems, and thus potentially physiologically significant in AD.

IV.2 MATERIALS AND METHODS

IV.2.1 Yeast Two-Hybrid Screening

MATCHMAKER GAL4 Two-hybrid System 2 (Clontech, Enzifarma, Portugal) was used to perform a YTH screen according to the manufacturer's instructions, with minor modifications (Fardilha *et al.*, 2004). The bait plasmid (pAS2-1-APP^{Y687F}, see below) was transformed in the yeast strain AH109 (Clontech, Enzifarma, Portugal) using the lithium acetate transformation method. The transformants were assayed for *HIS3*, *ADE2* and *MEL1* reporter genes' activation and the BD-bait fusion protein expression was verified by Western blotting. A total of 4.2 x 10^6 transformants from a human brain matchmaker cDNA library were screened by large scale yeast mating. Half of the diploid mixture was plated on SD/QDO (SD without Leu, Trp, Ade and His), and the other half on SD/TDO (SD without Leu, Trp and His). All plates were incubated at 30°C until colonies appeared. All positive clones were replated twice in SD/QDO medium containing X-α-Gal and incubated at 30°C for 3-8 days. True positives were identified as His^+, Ade^+ colonies and were positive for the α-galactosidase activity. Yeast plasmid DNA was extracted from the positive clones using the breaking buffer method and the AD-library plasmids were rescued by transformation of *E. coli*. Bacterial plasmid DNA was digested with HindIII and fragments produced were separated by agarose gel electrophoresis. Plasmids generating DNA fragments characteristic of the pACT-2+library insert digested with HindIII were further ABI sequenced using the GAL4 AD primer (Clontech, Enzifarma, Portugal). A search for similar sequences in the Genbank database was performed using the BLAST algorithm on the NCBI web site (http://blast.ncbi.nlm.nih.gov/). The library insert on plasmid F18, identified as a Fe65 new splice variant, was fully sequenced using specific primers.

IV.2.2 Plasmid Construction

To perform the YTH screen, the vector used to insert the bait cDNA, was Clontech's GAL4 binding domain (GAL4 DNA-BD) expression vector pAS2-1 (Clontech, Enzifarma, Portugal). The cDNA for human APP_{695} isoform, with a Y687F mutation was used as bait (da Cruz e Silva *et al.*, 2004c). The bait cDNA was PCR amplified (5'CCGCGCACCATGGCGATGCTGCCCGGTTTGG-3';

5’GTGGCCCCGGGCTAGTTCTGCATCTGCTCAAAG-3’) and inserted in the vector pAS2-1 using NcoI/SmaI restriction enzyme sites, in frame with the GAL4 DNA-BD.

Plasmids were also prepared for other procedures. The p97Fe65-CMV was obtained from the I.M.A.G.E. consortium (MRC Geneservice, UK) and corresponds to the Fe65ΔE9 cDNA (GenBank Accession: BC010854) inserted in the mammalian expression vector pCMV-SPORT6. The p60Fe65-CMV construct was obtained by substitution of the p97Fe65-CMV with the unique sequence of Fe65E3a from the RT-PCR clone G4-pCRblunt. Both p97Fe65-CMV and G4-pCRblunt were digested with KpnI and BglII and the desired fragments were excised from an agarose gel. The fragments were purified using the QIAquick Gel Extraction Kit (QIAGEN, IZASA, Portugal) and T4-ligated to produce the p60Fe65-CMV construct. All the constructs were verified by sequencing with specific primers, using a ABI PRISM 310 Genetic Analyzer (Applied Biosystems, Portugal).

IV.2.3 Bioinformatics analysis

Database searches were performed using BLAST (Altschul *et al.*, 1990) and ALIGN algorithms (http://www.ncbi.nlm.nih.gov) in order to find homology with the YTH clone F18 5’ unique sequence of 69 nucleotides. The splice site prediction was achieved by making use of the programs NNSPLICE (http://www.fruitfly.org/seq_tools/splice.html), SPLIGN (http://www.ncbi.nlm.nih.gov/sutils/splign) and the gene prediction program GENSCAN (http://genes.mit.edu/GENSCAN.html) (Burge and Karlin, 1997; Reese *et al.*, 1997; Burge and Karlin, 1998; Kapustin *et al.*, 2008). Multiple sequence alignment was performed using the CLUSTALW version 2.0 alignment tool (Larkin *et al.*, 2007) on the EMBL-EBI web site (http://www.ebi.ac.uk/Tools/msa/clustalw2/).

IV.2.4 RT-PCR and sequencing of the Fe65 transcript variant 3 in human brain

Adult brain poly A+ RNA (Clontech, Enzifarma, Portugal) was reverse transcribed using the AccuScript High Fidelity RT-PCR System (Stratagene, Soquimica, Portugal) and the reverse primer E14RV (5'-GGAAGGTGGGGGCTTCTTCATGG-3’) targeted to exon 14. The synthesized cDNA was amplified using the forward primer E3AFW (5’-TACTGCCTCTTGGACCAGTCAGG-3’, targeted to exon 3a and the reverse primer E10RV (5'-CGGCCATGATCTTAGAGCAGATC-3’), targeted to the exon 10 and exon 11 boundary. PCR fragments were analyzed on a 1.7% agarose gel stained with ethidium bromide. The RT-PCR products were excised from a 1% agarose gel and purified by using

QIAquick Gel Extraction Kit (QIAGEN, IZASA Portugal). The purified fragment was cloned into the pCR-blunt vector (Zero Blunt PCR Cloning Kit; Invitrogen, Alfagene, Portugal). One clone was selected by restriction analysis, clone G4, and the insert was sequenced using the M13RV primer, the T7 primer and Fe65 specific primers.

IV.2.5 Northern-blot analysis of FE65 gene transcripts

Probe 1 was prepared by EcoRI digestion of the G4 clone, obtained by RT-PCR, and corresponds to exons 3a to 10 of Fe65E3a. The probe cDNA was purified by low melting-point agarose gel electrophoresis, labeled by the random primed method using the High prime DNA labeling kit (Roche Applied Science, Portugal) and [α-32P]dCTP (GE Healthcare, VWR, Portugal). The labeled probe was purified by passage through a NucTrap column (Stratagene, Soquimica, Portugal) to remove unincorporated nucleotides. A human multiple tissue Northern blot (Ambion, Applied Biosystems, Portugal), a human brain Northern blot (Clontech, Enzifarma, Portugal) and a rat multiple tissue Northern blot (Clontech, Enzifarma, Portugal), were incubated at 68°C in the presence of the denatured radiolabeled DNA and hybridizing mRNAs were detected using a PhosphorImager (Bio-Rad Laboratories, Portugal). After probe stripping in 0.5% SDS at 90–100°C for 10 min, the same blot was re-used with a β-actin probe as a control gray.

IV.2.6 Cell culture and transfections

COS-7 cells (monkey kidney cell line) were grown in Dulbecco's modified Eagle's medium (DMEM; Gibco Invitrogen, Alfagene, Portugal) supplemented with 100 U/ml penicillin, 100 mg/ml streptomycin, 3.7 g/l NaHCO3 and 10% (v/v) fetal bovine serum (FBS). For transient transfection experiments, COS-7 cells were grown on 100 mm plastic culture dishes and transfected using LipofectAMINE 2000 (Invitrogen, Alfagene, Portugal), according to the manufacturer's instructions. PC12 cells (rat pheochromocytoma cell line) were grown in RPMI 1640 (Gibco Invitrogen, Alfagene, Portugal) supplemented 100 U/ml penicillin, 100 mg/ml streptomycin, 0.85 g/l NaHCO3 and 10% (v/v) horse serum and 5% (v/v) FBS. For differentiation, PC12 cells were treated for 12 days with 75 ng/ml NGF (Gibco Invitrogen, Alfagene Portugal), with serum reduced to 1%. SH-SY5Y cells (human neuroblastoma cell line) were grown in a 1:1 combination of minimum essential medium (MEM, Gibco Invitrogen, Alfagene Portugal) and Ham's F12 medim

(Gibco Invitrogen, Alfagene, Portugal), with 10% (v/v) FBS, 2 mM L-glutamine, 0.1 mM non-essential amino acids, supplemented 100 U/ml penicillin, 100 mg/ml streptomycin and 1.5 g/l sodium bicarbonate.

Primary rat neuronal cultures were established from embryonic day 18 fetuses, as previously described (Henriques *et al.*, 2007). After dissociation with trypsin and deoxyribonuclease I (0.15 mg/ml) in Hank's balanced salt solution (HBSS) (0.45 mg/ml or 0.75 mg/ml for cortical or hippocampal cultures, respectively, during 5-10 min at 37°C) cells were plated on poly-D-lysine-coated dishes at a density of 1.0x105 cells/cm2 in B27-supplemented Neurobasal medium (Gibco Invitrogen, Alfagene, Portugal), a serum-free medium combination (Brewer *et al.*, 1993). The medium was supplemented with glutamine (0.5 mM), gentamicin (60 µg/ml), and with or without glutamate (25 µM) for hippocampal or cortical cultures, respectively, for 9 days before the experimental procedures. All cultures were maintained at 37°C and 5% CO2.

IV.2.1 Western blotting

Cells in culture were harvested in 1% SDS and boiled. The protein content of all lysates was determined by the BCA method (Pierce, Dagma, Portugal) and the normalized samples were resolved by SDS-PAGE and transferred to nitrocellulose membranes. Immunoblotting analysis for Fe65 protein was carried out by first blocking possible nonspecific binding sites with nonfat dry milk in 10 mM Tris-HCl (pH 8.0)/150 mM NaCl. The anti-Fe65 primary antibody (Upstate #05-758; Millipore, Grupo Taper, Portugal) was incubated overnight at 1:5000 dilution. Detection was achieved using the ECLplus detection system (GE Healthcare, VWR, Portugal). Band size calculation was performed using the Quantity One software (Bio-Rad Laboratories, Portugal).

IV.3 RESULTS

IV.3.1 Identification of a novel Fe65 isoform by yeast two-hybrid screening

In the YTH screen 4.2 x 10^6 clones were screened, the mating efficiency was 8% and 131 clones were isolated. Fifteen positive cDNA clones encoded a fragment of the Fe65 protein, neuronal isoform E9. The library fragment alignment was within the coding region on the sequence with the NCBI (National Center for Biotechnology Information) accession number NM_001164. The Fe65 protein is encoded by the *FE65* (or *APBB1*) gene spanning 25 kb in chromosome 11p15. Three out of the 15 clones did not exactly match the database sequence Accession NM_001164 due to a unique 5' sequence of 69 nucleotides. These clones are identical, therefore in subsequent analysis only one clone is presented (clone F18). The novel identified cDNA sequence was submitted to the GenBank database (Accession number EF103274; APPENDIX X).

IV.3.2 *In silico* analysis of the 5' exons of the human *FE65* gene

Three distinct Fe65 splice variants had previously been reported (Fig. IV.1A): Fe65E9 (transcript variant 1), Fe65ΔE9 (transcript variant 2) and Fe65a2 (Fe65 allele 2). Bioinformatics analysis of these transcripts and alignment with the genomic sequence revealed the presence of 15 exons. Transcript variant 1 (GenBank Accession NM_001164) represents the longest transcript and encodes the longest isoform (Fe65E9). This isoform is exclusively expressed in neurons. Transcript variant 2 (Accession NM_145689) encodes a protein that maintains the reading frame but is a shorter isoform (Fe65ΔE9). These two transcript variants differ in the mini-exon 9, the shortest with only 6 bp (AGAGAG), which is present only in the Fe65E9 (Hu *et al.*, 1998). Another human variant (GenBank Accession AF394214) results from alternative splicing of the exon 14 by selection of an alternative acceptor site, which was attributed to an intronic polymorphism within intron 13. This allele 2 encoded isoform, Fe65a2, has an altered C-terminal region, lacking part of the PTB2 domain (Hu *et al.*, 2002).

Table IV.1: Exons 1-3b and intron/exon junctions in the *FE65* gene. Nucleotide sequences of the 5' and 3' end of exons 1-3b and of the donor and acceptor site at the respective intron/exon junctions (upper case) of the human, rhesus monkey and mouse *FE65* gene. Sequences of intron ends are given in lower case, except for the donor and acceptor sites in upper case. Exons and introns are numbered as referred to on Figure 1A and exon sizes are given. Homologies are shown by asterisks.

	Intron 3' end	5' end - Exon size (bp) - 3' end	Intron 5' end
		Exon 1	
human		ATGTTGTG - 86 - CCGCGCAG	GTaggagg
monkey		------	------
mouse		*GAC*CC* - 53 - A****G**	**ga*tcc
		Exon 2	
human	ccccacAG	GAGCTGCC - 735 - GGACACAG	GTaccttg
monkey	------	------	------
mouse	t*t*****	**T**A** - 735 - ********	********
		Exon 2.2 (predicted)	
human	tgacagGG	ATGGCAGA - 189 - AACAGCAG	GTattccc
monkey	------	******** - 186 - ********	********
mouse		------	
		Exon 3a	
human	tcccttAG	TACTGCCT - 133 - CCTGGCAG	GTgagggg
monkey	********	*G****** - 133 - ********	********
mouse	*****c**	*G****** - 132 - ********	********
		Exon 3b	
human	cctggcAG	ATTCCTTC - 176 - AGTCCCAG	GTgaggct
monkey	********	******** - 176 - ********	********
mouse	********	******** - 176 - ********	*****a**

The novel transcript is noted herein as Fe65E3a. Full sequencing revealed that this transcript is exon 9 inclusive, similarly to the neuronal isoform Fe65E9. Databases were searched for entries bearing homologies with the unique 5' sequence of 69 nucleotides present in the YTH clone. An homology with the rhesus macaque (*Macaca mulatta*) "predicted mRNA similar to human Fe65" (GenBank Accession XM_001101631) was found. The sequence from YTH clone F18 was aligned against the genomic sequences of human and rhesus macaque *FE65* genes, using BLAST and ALIGN algorithms, and revealed homology within the human intronic region between exons 2 and 3 (Fig. IV.1A). The alignment against the rhesus macaque genomic and mRNA sequences showed homology with half of the macaque's Fe65 second exon. In an attempt to define a new exon that could be alternatively spliced, putative intron-exon junctions were identified by comparing genomic and cDNA sequences and making use of the *in silico* resources

NNSPLICE, SPLIGN and GENSCAN (Table IV.1). *In silico* analysis showed the presence of an additional exon of 133 bp, denoted as exon 3a, which included the 5' unique sequence on clone F18 (Fig. IV.1B). Based on these observations, we propose a redefinition of the structure of human *FE65* gene: the previously described exon 3 is renamed exon 3b. The novel exon here described is named exon 3a (Fig. IV.1C). Several human ESTs (Expressed Sequence Tags) present in the GenBank database share high homology with the novel exon 3a, presenting further evidence that this sequence is present in mature mRNAs. Furthermore, the sequence of exon 3a is conserved and the splice sites are according to the consensus rules (GT/AG) (Table IV.1).

The novel exon 3a has no in-frame ATG codons, therefore the translation initiation of the transcript variant Fe65E3a has to be elsewhere. The first in-frame ATG of the former exon 3, renamed exon 3b, which codes for the Met-260 of the p97Fe65, is a likely possibility. If the 5' first exon of the novel transcript is exon 3a and the start codon is at exon 3b, the Fe65E3a transcript size will be 1954 bp and can be translated in to a 451 amino acid peptide (Table IV.2). However, a putative additional exon, exon 2.2, can be defined based in the bioinformatics tools and in the alignment search with the rhesus macaque Fe65 predicted mRNA sequence. The predicted exon 2.2 has one conserved in-frame ATG, both in human and rhesus macaque sequences and a human EST overlaps it. In the macaque's predicted Fe65 transcript exons 2.2 and 3a are spliced together, while exons 1 and 2 are skipped (Fig. IV.1A). Noteworthy, the sequence of the putative exon 2.2 is not conserved in the mouse gene. To add further complexity a putative exon, exon 2.1, was predicted in the human Fe65 gene, between exons 2 and 2.2, by the web servers mentioned above. Although the putative exon 2.1 carries an in-frame methionine residue no homologies with ESTs were found. In Figure 1C we represent the structure of the human FE65 gene including the novel exon 3a. The relative positions of putative exons predicted by the bioinformatics tools are also represented, as well as their in-frame ATG codons.

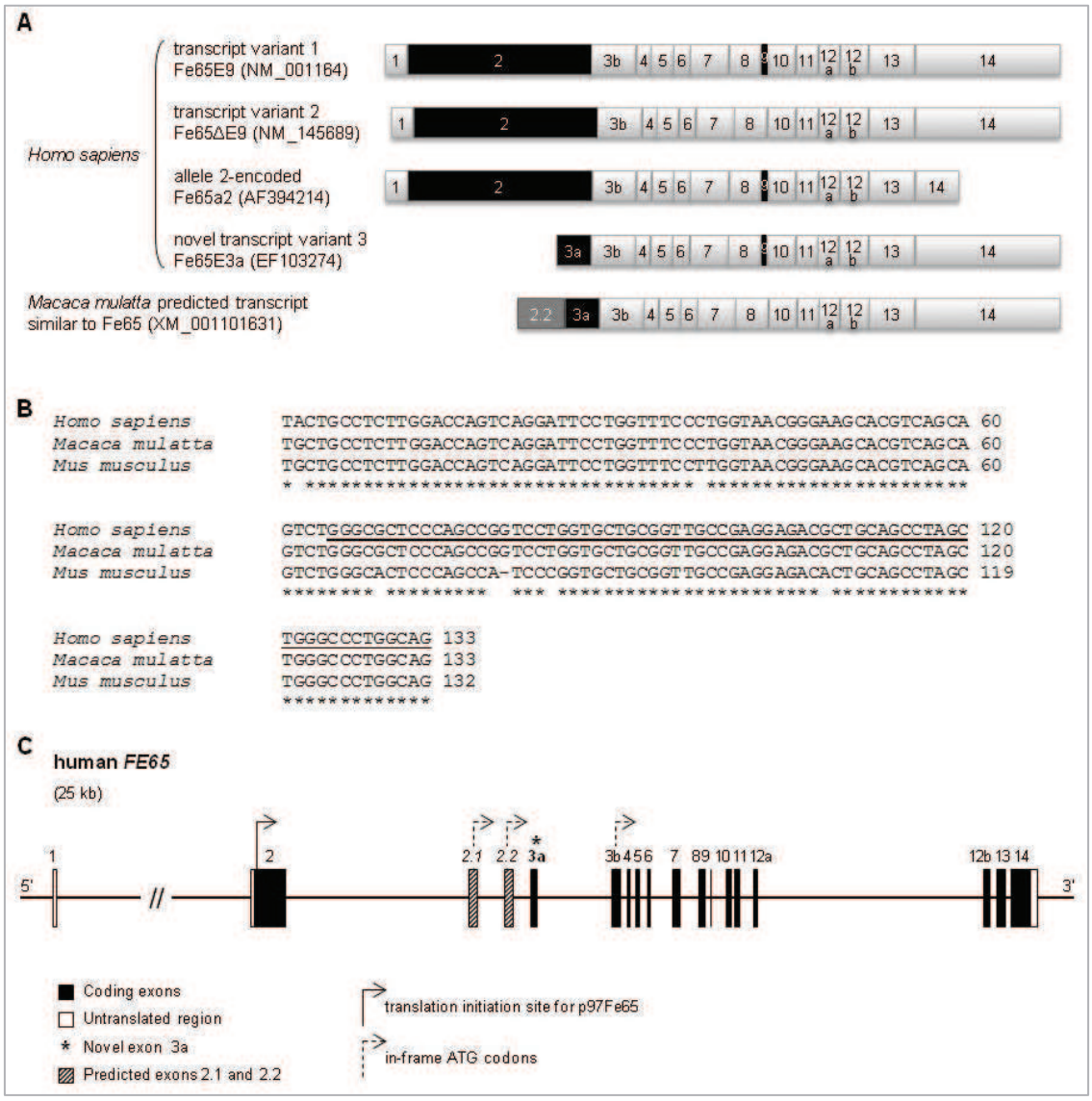

Figure IV.1: Gene structure and splice variants of human *FE65*. (A) Schematic representation of the human FE65 splice variants and comparison with the rhesus macaque (*Macaca mulatta*) predicted mRNA. The rhesus macaque exons are numbered as the corresponding human exons, for comparison purposes. The novel human Fe65E3a splice variant was submitted to GenBank (Accession EF103274). The alternatively spliced exons 2, 3a and 9 are represented in black. The exon 2.2 in the rhesus macaque predicted mRNA is represented in dark gray. (B) Nucleotide sequence of the novel exon 3a of the human, rhesus macaque and mouse *FE65* genes. The novel sequence present in the YTH clone is underlined. Homologies are shown by asterisks. (C) Structure of the human *FE65* gene. Open boxes correspond to non-coding sequences in exons and coding exons are represented by black filled boxes. The novel exon 3a is highlighted by an asterisk and the predicted exons 2.1 and 2.2 are represented by striped boxes. The in-frame ATG codons in the exon 3b and in predicted exons are indicated by arrows.

IV.3.3 RT-PCR validation of the novel exon 3a-inclusive splice variant of Fe65

To ascertain the existence of the novel Fe65 splice variant identified in the YTH system, further RT-PCR experiments were performed using specific primers. The cDNA was synthesized from adult brain mRNA using a reverse primer in exon 14. Subsequent amplification reactions were carried out using several primer pairs to amplify an exon 3a-inclusive transcript (Fig. IV.2A). The partial amplification of the new transcript using the primer set E3AFW (targeted to exon 3a) and E10RV (targeted to the exons 10 and 11 boundary) produced the expected 0.9 kb fragment (Fig. IV.2B). This PCR fragment was ligated to pCR-blunt vector and the insert was fully sequenced, which confirmed the complete sequence of the novel exon 3a of 133 bp. We were unable to detect a transcript using primers to target the putative exons 2.1 and 2.2, which could include a starting codon. Experiments using a 5'RACE kit also retrieved an exon 3a-inclusive amplicon, albeit the cDNA library used was from human testis, and did not reveal an ATG upstream of E3a (Supplementary Figure IV.1, APPENDIX X). In Table IV.2, the structure and size of the full-length Fe65E3a RT-PCR clone is represented and compared to the previously described transcript variants Fe65E9 and Fe65ΔE9.

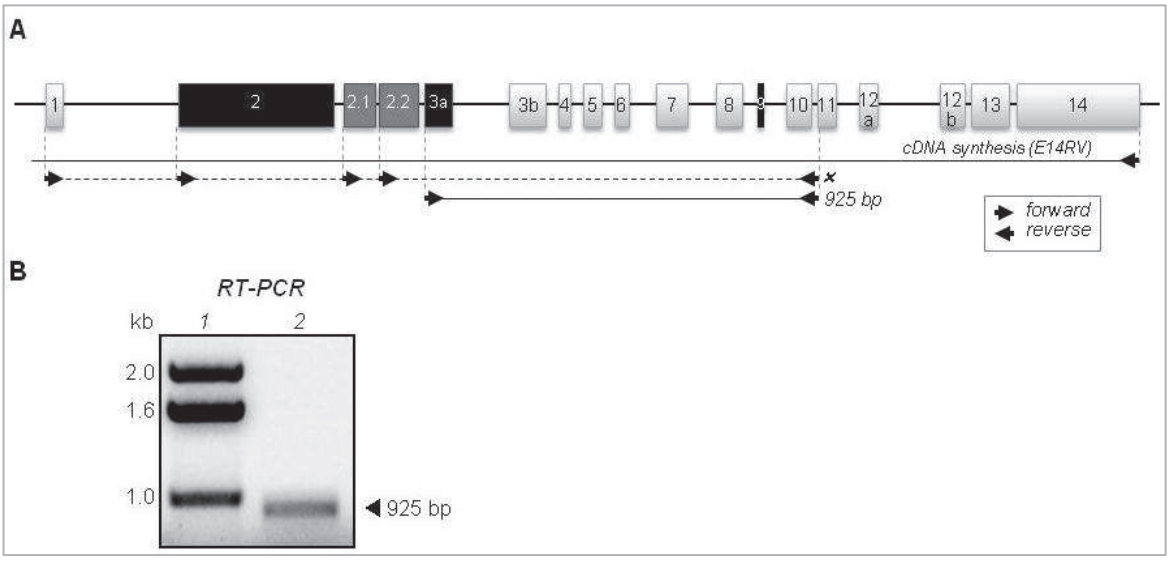

Figure IV.2: RT-PCR of Fe65E3a. (A) Localization of the primers for RT-PCR on human *FE65* gene. The 925 bp PCR product is represented as it was the only amplified product that could be produced which included exon 3a. (B) The cDNA was synthesized from an adult brain poly A+ RNA (Clontech) using a reverse primer targeting exon 14. Further amplification of the cDNA using the specific primer set E3AFW (targeted to exon 3a) and E10RV (targeted to the exons 10 and 11 boundary), produced the expected 0.9 kb fragment (lane 2). Lane 1: DNA size marker 1 Kb ladder (Invitrogen).

IV.3.4 Tissue distribution of Fe65E3a mRNA

To estimate the relative size and abundance of the splice variant Fe65E3a we performed Northern blotting analysis using three commercially available premade blots: human multiple tissue, rat multiple tissue and human brain. The ^{32}P-labeled cDNA probe 1 matched exons 3a to 10 of Fe65E3a. Therefore, more than 80% of probe 1 is also complementary to the p97Fe65 mRNAs (consisting of transcript variants Fe65E9 and Fe65ΔE9) and detected the previously described 2.6 kb transcripts. Transcript variants Fe65E9 and Fe65ΔE9 migrate together, but previous reports showed that Fe65E9 is neuron-specific (Hu *et al.*, 1999). Based on *in silico* analysis and RT-PCR validation, the Fe65E3a transcript (exon 3a-14) is 1954 bp (Table IV.2). Probe 1 hybridized to a band around 2 kb, which had less intensity than the higher band of 2.6 kb. From the approximate size of the Fe65E3a mRNA it is not possible to assure that the cDNA characterized above is the full-length transcript, although by size comparison it cannot be much longer. One or more additional "short" exons might be present upstream exon 3a, such as the putative exon 2.2 of 189 bp, although RT-PCR did not detect such a product.From the Northern blot analysis we observed that Fe65E3a mRNAs from human (Figs. IV.3A,C) and rat tissues (Fig. IV.3B) appear to be the same size. In the human northern blot (Ambion) (Fig. IV.3A) all Fe65 mRNAs appear to migrate slightly faster than in the two other blots (Fig. IV.3B,C), compared to the RNA size markers. However, if one compares to the migration of the p97Fe65 transcripts (E9+ΔE9) bearing in mind a 2.6 Kb size, then the comparative migration for the p60Fe65 mRNA is nearer to that expected. The novel transcript migrated at 1.9 kb (Fig. IV.3A) in accordance with the size of the characterized cDNA (1954 bp) (Table IV.2).

Table IV.2: Exons 1-3b and intron/exon junctions in the *FE65* gene. Nucleotide sequences of the 5' and 3' end of exons 1-3b and of the donor and acceptor site at the respective intron/exon junctions (upper case) of the human, rhesus monkey and mouse *FE65* gene. Sequences of intron ends are given in lower case, except for the donor and acceptor sites in upper case. Exons and introns are numbered as referred to on Figure 1A and exon sizes are given. Homologies are shown by asterisks.

	Human Fe65 transcripts					
	E9 (transcript 1)		**ΔE9 (transcript 2)**		**E3a (transcript 3)**	
Exon Nº	*total*	*coding*	*total*	*coding*	*total*	*coding*
1	86	0	69	0	---	---
2	735	721	735	721	---	---
3a	---	---	---	---	133	0
3b	176	176	176	176	176	120
4	57	57	57	57	57	57
5	86	86	86	86	86	86
6	64	64	64	64	64	64
7	150	150	150	150	150	150
8	128	128	128	128	128	128
9	6	6	---	---	6	6
10	115	115	115	115	115	115
11	85	85	85	85	85	85
12a	84	84	84	84	84	84
12b	116	116	116	116	116	116
13	177	177	177	177	177	177
14	577	168	577	168	577	168
mRNA size (bp)	2642	2133	2619	2127	1954	1356

	Human Fe65 isoforms		
	E9 (p97Fe65)	**ΔE9 (p97Fe65)**	**E3a (p60Fe65)**
Number of amino acids	710	708	451
Theoretical Mw (kDa)	77	77	50
Migration in SDS gels	97	97	60

All detectable splice variants of Fe65 are highly expressed in the brain compared to other tissues, both in human and rat blots (Figs. IV.3A,B). As described previously, the human Fe65 transcripts E9 and ΔE9 are highly expressed in brain, but are also detected in the ovary and barely detected in other tissues (spleen and prostate). The novel Fe65E3a transcript is mainly detected in brain, though at a lower level than the p97 mRNAs. A weak signal of human Fe65E3a is also detected in spleen and prostate (Fig. IV.3A). Likewise, in the rat tissues the p97Fe65 transcripts are more abundant in the brain. Low levels of expression were detected in the heart. Fe65 had barely detectable expression in lung and liver. Among the rat tissues the Fe65E3a transcript was detectable only in the brain (Fig. IV.3B).

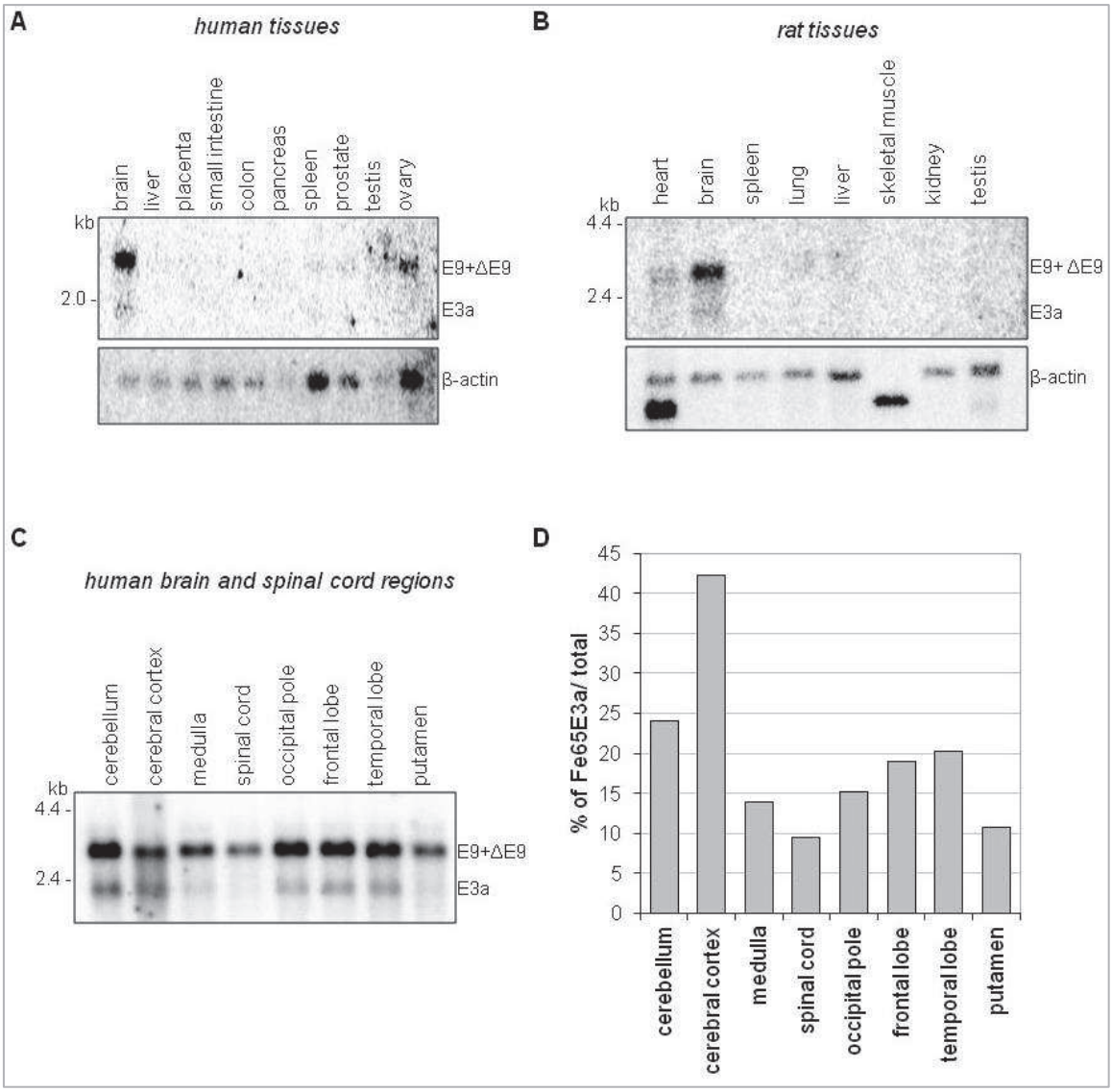

Figure IV.3: Northern blot analysis of Fe65 mRNAs in human and rat tissues. Premade blots from human tissues (Ambion) (A), rat tissues (Clontech MTN Blot) (B) and human brain and spinal cord (Clontech MTN Blot) (C) were hybridized with probe 1 (^{32}P-labeled Fe65E3a cDNA corresponding to exons 3a-10). The previously reported transcript variants Fe65E9 and Fe65ΔE9 were also detected by probe 1 migrating together at 2.6 kb. The minor transcript of approximately 2 kb (Fe65E3a) is mostly seen in the brain. RNA size markers are depicted on the left side. β-actin was probed as a control. (D) The relative expression of the Fe65E3a splice variant is represented as a percentage of total Fe65 mRNAs.

Analysis of the human central nervous system blot, containing 2 µg of poly(A)$^+$ RNA per lane (Clontech Human Brain MTN Blot II) showed two bands in all tissues, though the lower band is barely detected in the spinal cord (Fig. IV.3C). The expression of a 1.9 Kb mRNA was in accordance with the size of the characterized mRNA, in all regions of the brain. The Fe65 novel transcript of 1.9 kb had lower levels of expression than the p97Fe65. Normalizing the expression levels of

Fe65E3a to the total Fe65 transcripts, gave insights into the relative expression of Fe65E3a (Fig. IV.3D). The highest level was found in the cerebral cortex, where Fe65E3a represents 42% of the total Fe65 mRNAs. Relative lower levels where found in the other brain tissues and the lowest relative expression of Fe65E3a was in the spinal cord (9%) (Fig. IV.3C).

IV.3.5 Evidence that p60Fe65 arises from the alternatively spliced Fe65E3a transcript

The protein deduced from the novel Fe65E3a transcript has 451 amino acids and a theoretical molecular mass of 50 kDa (Table 2). The translation start site is in the first in-frame ATG in exon 3b, corresponding to Met-260 of p97Fe65. Consequently, this shorter isoform has a N-terminally truncated WW domain and lacks some features in comparison to p97Fe65, such as an acidic residue cluster (ARC) and a Ser phosphorylation site (Fig. IV.4A). The WW domain is encoded by exon 3b, and is present in p97Fe65, in both isoforms Fe65E9 and Fe65ΔE9.

Western blotting analysis of the Fe65 isoforms, using an antibody that recognizes the WW domain of Fe65, showed the 97 kDa band of isoforms E9/ΔE9 as well as a band that migrates around 60 kDa. This 60 kDa band was observed before by other groups that used the same antibody (Sabo *et al.*, 2003), or antibodies raised against the Fe65 C-terminus (Wang *et al.*, 2004; Cool *et al.*, 2010).

The endogenous p60Fe65 isoform is detectable at higher levels in rat cortex and hippocampus primary cultures, and was detected in lower levels in PC12 and SY-SH5Y cell lysates, and not detected in COS-7 cells (Fig. IV.4B). Given that the expected MW of Fe65E3a is 50 kDa and the detected band is around 60 kDa, we generated a Fe65E3a construct in a mammalian expression vector and transfected COS-7 cells. Despite having a calculated molecular mass of 50 kDa, the transfected Fe65E3a migrates around 60 kDa in parallel with the endogenous p60Fe65 detected in rat hippocampus and cerebral cortex lysates (Fig. IV.4C). In fact, two bands were detected in hippocampus and cortex around 60 kDa. The band migrating slightly slower may have post-translational modifications such as phosphorylation, evident in the endogenous protein *in vivo*, but this has to be further tested.

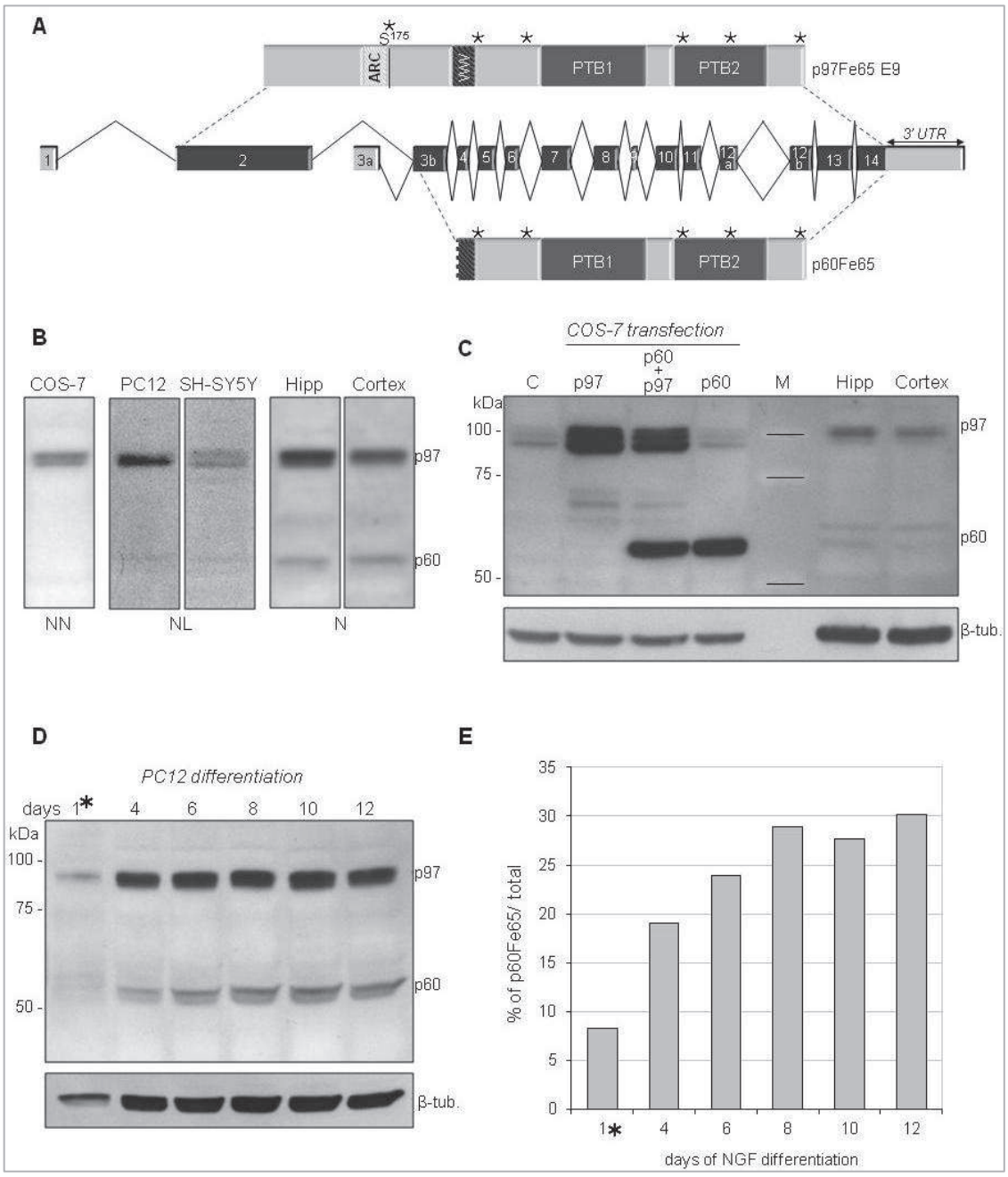

Figure IV.4: p60Fe65 expression levels in different cells. (A) Comparison of the alternative splicing patterns that generate the p97Fe65(E9) and p60Fe65 isoforms. Asterisks represent phosphorylatable amino acids. (B) Endogenous Fe65 isoforms were detected by immunoblotting in a non-neuronal cell line ("NN", COS-7) in neuronal-like cell lines ("NL", PC12 and SH-SY5Y) and primary neuronal cultures ["N", hippocampal (hipp) and cortical cultures (cortex)]. (C) Fe65E3a cDNA was inserted in a mammalian expression vector to generate a p60Fe65 construct. COS-7 cells were transfected with p97Fe65, p97Fe65+p60Fe65 and p60Fe65 (C, non-transfected control). M, Molecular weight marker (Precision Plus Protein Dual Color Standards; Bio-Rad). (D) PC12 cells were differentiated for 12 days in the presence of 75 ng/ml nerve growth factor (NGF). Cells were collected at days: 1, 4, 6, 10 and 12. For day one 25 µg of total protein was loaded (*), and 60 µg from the other samples. (E) Expression of p60Fe65 as a percentage of total Fe65 isoforms, during PC12 differentiation with NGF for 12 days. Results were normalized to the amount of total protein content and to the β-tubulin expression levels.

IV.3.6 p60Fe65 protein levels in differentiating cells

Previous reports showed that the Fe65 isoforms E9 and ΔE9 are alternatively spliced in a cell-type dependent pattern: the ΔE9 isoform is expressed in non-neuronal cells and the E9 is expressed in neurons. When P19 cells were differentiated to neurons with retinoic acid and cytosine arabinoside, the expression pattern of mRNA changed from the ΔE9 to the E9 isoform (Hu *et al.*, 1999). Both isoforms were detected in the rat pheochromocytoma cell line PC12 with the E9 being more abundant (Duilio *et al.*, 1991).

To determine the effect of neuronal differentiating factors on the expression of p60Fe65, PC12 cells were differentiated with nerve growth factor (NGF). For differentiation experiments, cells were plated at $1x10^4$ cell/cm^2 and grown for 12 days in RPMI medium with serum reduced to 1%, in the presence of 75 ng/ml NGF. Cells were collected at days: 1, 4, 6, 10 and 12. Due to the low initial cell density the sample corresponding to day 1 of NGF has a very low total protein content, as determined by the BCA method. Therefore only 25 μg of total protein was loaded on the SDS-PAGE for day 1, 60 μg were loaded for the other samples, but this was corrected for the quantitative comparison. Under our experimental conditions, the protein levels of p97Fe65, which corresponds to the E9 and ΔE9 isoforms migrating together, doubled from day 1 to day 4, normalizing for the amount of protein content and for β-tubulin expression levels. During the neuronal differentiation from day 4 to 12, p97Fe65 levels did not alter significantly (Fig. IV.4D,E).

The 60 kDa protein deduced from the novel Fe65E3a transcript is exon 9-inclusive and its expression was mainly detected in neuronal cells. In undifferentiated PC12 cells p60Fe65 was barely detected. The levels of p60Fe65 increased consistently with time of NGF exposure and by day 12 it was 9.5 fold higher (Fig. IV.4D). Moreover, the ratios of p60Fe65/total Fe65 also increased from day 1 to day 12. At this final time point the p60Fe65 isoform makes up 30% of total Fe65. Overall, these results demonstrate that p60Fe65 is not only expressed *in vivo* but is closely associated with neuronal function.

IV.4 DISCUSSION

In the work here presented we describe a novel Fe65 transcript variant, Fe65E3a, which arises from alternative splicing of the *FE65* gene. A novel exon, exon 3a, was partially present in a YTH clone from a human brain library. *In silico* analysis and RT-PCR experiments revealed the sequence of the complete exon 3a. The estimated size of mRNA, as given by Northern analysis, and the corresponding protein analyzed by Western blotting provide evidence for the full-length transcript sequence. In summary, experimentally the existence of the exon 3a-inclusive transcript is supported by the fact that: (i) the YTH clone is from human brain cDNA expression library; (ii) the full-length exon 3a was obtained from a human brain mRNA expression library by RT-PCR; (iii) the Fe65E3a mRNA was detected in human and rat tissues by Northern blotting; (iv) the protein was detected in transfected cells migrating in parallel with the endogenous band; (v) several ESTs overlapping exon 3a are present in the database; (vi) the sequence of exon 3a is conserved and the splice sites are according to the consensus rules. We propose a redefinition of the *FE65* gene to include the novel exon 3a, thus defining 16 exons for the Fe65 gene. The mechanism of alternative splicing, giving rise to the Fe65E3a mRNA is a mutually exclusive event between exon 2 and exon 3a (exon 3a is spliced while exon 2 is skipped). The novel transcript denoted as Fe65 transcript variant 3 or Fe65E3a, encoding isoform p60Fe65, is exon 9-inclusive, which is consistent with its origin from a brain library.

Fe65E3a is predominantly expressed in the brain, both in human and rat, though at a lower level than the p97 mRNAs. Nevertheless, in some brain regions the ratios of Fe65E3a/total were noteworthy, e.g. in the cerebral cortex where Fe65E3a represents 42% of the total Fe65 mRNAs. We also find high Fe65E3a relative expression in the cerebellum and temporal lobe, which includes the hippocampus and the amygdala. The hippocampus, cerebral cortex and amygdala play a major role in memory, cognition and behavior and are the brain regions mostly affected by the neuropathological hallmarks of AD (reviewed in Duyckaerts *et al.*, 2009).

A 60 kDa Fe65 isoform of unknown origin has been mentioned in previous reports and referred to as p60. The 60 kDa band was observed specifically when using antibodies raised against the Fe65 C-terminus (Sabo *et al.*, 2003) and was attributed to an alternative translation of the p97Fe65 transcript initiated in a methionine present in the former exon 3 (Wang *et al.*, 2004; Cool *et al.*, 2010). Wang et al. (2004) generated p97Fe65 knockout mice and observed an upregulation of the p60Fe65 isoform which was attributed to translation of an alternative

methionine on the p97Fe65 transcript (Wang *et al.*, 2004; Cool *et al.*, 2010). The endogenous p60Fe65 isoform is detectable in higher levels in rat cortex and hippocampus primary cultures and was not detected in non-neuronal cells. Despite having a calculated molecular mass of 50 kDa, the transfected Fe65E3a protein migrates around 60 kDa in parallel with the endogenous p60Fe65 detected in rat hippocampus and cerebral cortex lysates. Together our results characterize a new Fe65 splice variant and provide evidence that the novel transcript is the origin of the brain enriched p60Fe65 isoform.

The alternatively spliced p60Fe65 isoform in the brain is an interesting candidate of neuronal physiological relevance. In fact, isoform-specific p97Fe65 KO mice did not exhibit neuroanatomical brain abnormalities, but impaired performance in learning and memory tests were evident at 14 months, suggesting that p97Fe65 has a role in cognition (Wang *et al.*, 2004). The lack of neuroanatomical alterations on the p97Fe65 KO mice might be due to elevated p60 isoform or to the expression of the Fe65L1 and Fe65L2, since it is likely that there is some redundancy among the different Fe65 protein family members. Conversely, the Fe65;Fe65L1 double knockout mice, deficient for two of the three Fe65 protein family members exhibited defective cortical neuronal migration during development, resembling cobblestone lissencephalies (Guenette *et al.*, 2006). This phenotype is similar to that observed in APP;APLP1;APLP2 triple KO mice (Herms *et al.*, 2004) and Mena KO mice (Lanier *et al.*, 1999), suggesting that APP, Fe65 and Mena act together in a neurodevelopment signaling pathway. Indeed, p60Fe65 has a N-terminally truncated WW domain which might compromise the protein-protein interactions occurring with Mena, SET, $P2X_2$, Nek6, c-Abl or 14-3-3γ. The integrity of the WW domain also influences the role of Fe65 in transcriptional activation (Duilio *et al.*, 1991; Cao and Sudhof, 2004; Telese *et al.*, 2005), as already shown for the p60Fe65 isoform (Cool *et al.*, 2010).

It is interesting to note that this novel transcript was identified when the YTH screen was carried out with the APP^{Y687F} bait. Similar screens with the wild type APP construct resulted in Fe65 isoforms previously described (data not shown). In this context, it is important to consider data by Rebelo *et al.* (2007a, b) where the APP^{Y687F} mutant, which mimics dephosphorylation at Tyr-687, was preferentially endocytosed and targeted for β-secretase cleavage, in contrast with the APP^{Y687E} phospho-mimicking mutant.

In closing, results demonstrate for the first time the sequence of the novel Fe65E3a splice variant, which codes for the previously unexplained p60Fe65 isoform. Alternative splicing is a key

regulatory mechanism for generating tissue-specific Fe65 transcripts increasing protein diversity from the same gene and its contribution to AD pathology deserves further investigation.

CHAPTER V. RANBP9 INTERACTS WITH AICD AND TIP60 AND PREVENTS NUCLEAR SIGNALING

The work described in the Chapter V was included in the following manuscript, submitted for publication:

"RanBP9 prevents AICD transcriptional regulation through physical interaction with Tip60"

Domingues S.C.[a,1], Konietzko U.[b,1], Henriques, A.G.[a], Rebelo S.[a], Fardilha M.[a], Nishitani H.[c], Nitsch R.M.[b], da Cruz e Silva E.F.[a†] and da Cruz e Silva O.A.B.[a*]

[a]Centre for Cell Biology, Health Sciences Dept. and Biology Dept., University of Aveiro, 3810-193 Aveiro, Portugal

[b]Division of Psychiatry Research, University of Zurich, 8008 Zurich, Switzerland

[c]Graduate School of Medical Science, Kyushu University, Fukuoka 812-82, Japan

[1]These authors contributed equally to this work

[†]Deceased on March 2, 2010

Abstract:

Proteolytic processing of the β-amyloid precursor protein (APP) occurs through alternative pathways, culminating with the release of APP intracellular domain (AICD). AICD can translocate to the nucleus and regulate transcription, but its activity is dependent on interactions with other proteins. In the nucleus, AICD, FE65 and Tip60 associate into AFT complexes, which are targeted to nuclear spots that correspond to transcription factories. Here we report that RanBP9 interacts with the cytoplasmic domain of APP, through the NPXY internalization motif. Moreover, we found that RanBP9 interacts with Tip60, which dramatically relocated RanBP9 from a widespread cellular distribution to nuclear speckles. AICD nuclear signaling occurs predominantly through the amyloidogenic pathway of APP cleavage and RanBP9 transfection was demonstrated previously to increase Aβ generation. Nevertheless, we show that RanBP9 has a negative effect on AICD nuclear signaling. RanBP9 relocated AICD to the Tip60-enriched nuclear speckles, and prevented AFT spot formation. Furthermore, transfecting increasing amounts of RanBP9 reduced the expression of AICD-regulated genes. We conclude that RanBP9 has an inhibitory regulatory effect on AICD-mediated transcription by relocating AICD away from transcription factories.

V.1 INTRODUCTION

The β-amyloid precursor protein (APP) generates the Aβ peptide, which plays a central role in the amyloid cascade hypothesis of Alzheimer's disease (AD) (Hardy and Higgins, 1992). APP is a type I transmembrane glycoprotein that undergoes sequential proteolytic processing being first cleaved by α-secretase (non-amyloidogenic pathway) or by β-secretase (amyloidogenic pathway) resulting in ectodomain shedding and generation of α- or β-C-terminal fragments (CTFs) (Esch *et al.*, 1990; Sisodia *et al.*, 1990; Gandy *et al.*, 1992; Seubert *et al.*, 1993; Vassar *et al.*, 1999). Membrane-bound α- and β-CTFs are subsequently processed by γ-secretase, liberating the p3 or the Aβ peptides, respectively, and the APP intracellular domain (AICD) (De Strooper *et al.*, 1998; Wolfe *et al.*, 1999; Passer *et al.*, 2000).

AICD has three functional motifs that mediate interactions with other proteins: ^{653}YTSI^{656}, ^{667}VTPEER^{672} and ^{682}YENPTY^{687} (human APP$_{695}$ isoform numbering) (da Cruz e Silva et al., 2004a). For example the endocytosis mediating motif ^{653}YTSI^{656} binds to the microtubule interacting protein PAT1 (Zheng et al., 1998) and the motif ^{667}VTPEER^{672} is responsible for interaction with 14-3-3γ (Sumioka et al., 2005). The conserved ^{682}YENPTY^{687} protein interaction motif, which includes the NPXY internalization signal, is recognized by phosphotyrosine binding domains of several proteins such as the Fe65 protein family (Fe65, Fe65L1 and Fe65L2) (Fiore *et al.*, 1995; Bressler *et al.*, 1996; Guenette *et al.*, 1996; Duilio *et al.*, 1998); the X11/Mint proteins (X11, X11L, X11L2) (Borg *et al.*, 1996; McLoughlin and Miller, 1996; Zhang *et al.*, 1997; Tanahashi and Tabira, 1999b); Shc A and Shc C (Tarr *et al.*, 2002b); JIP-1 and JIP-2 (Scheinfeld et al., 2002); Dab1 (Trommsdorff et al., 1998) ; Numb and Numb-like (Roncarati et al., 2002); GULP1 (Beyer et al., 2010). Other AICD binding proteins have been identified, such as Go (Nishimoto et al., 1993); cAbl (Zambrano et al., 2001); APP-BP1 (Chow et al., 1996); UV-damaged DNA-binding protein (Watanabe et al., 1999); ARH (Noviello et al., 2003); Grb2 (Zhou et al., 2004); Pin1 (Pastorino et al., 2006); FKBP12 (Liu et al., 2006); AIDA-1 (Ghersi et al., 2004); SET (Madeira et al., 2005); CPEB (Cao et al., 2005); Flotillin-1 (Chen et al., 2006); and SNX17 (Lee et al., 2008).

The interaction between AICD and Fe65 has been extensively studied with respect to the transactivation properties of the AICD/Fe65/Tip60 complex (Cao and Sudhof, 2001). After intramembranous γ-secretase cleavage of APP, AICD is released and may translocate to the nucleus where it participates in transcriptional regulation, in a manner analogous to Notch signaling. In the canonical Notch signaling pathway, sequential cleavage by α-/γ-secretases releases the intracellular domain of Notch (NICD) that translocates to the nucleus to modulate

gene expression, through binding to transcription factors (De Strooper et al., 1999). Hence, APP and Notch are analogous to many other membrane proteins that are subject to regulated intramembrane proteolysis (RIP) (Kang et al., 1987; Kopan and Goate, 2000). Nevertheless, the cytoplasmic tail of APP is relatively short and is rapidly degraded after release from the membrane by the insulin degrading enzyme or by the endosomal/lysosomal system (Cupers et al., 2001; Edbauer et al., 2002; Vingtdeux et al., 2007a). However, the half-life of AICD can be considerably increased by interaction with Fe65, facilitating the translocation of AICD to the nucleus (Kimberly et al., 2001). Moreover, only the AICD generated through the amyloidogenic pathway exhibited nuclear signaling, due to the localization of β-secretase processing of APP at the endosomes, allowing a faster microtubule-based transport to the nuclear vicinity before γ-cleavage releases AICD (Goodger et al., 2009).

In the nucleus, AICD was reported to associate in multiple spherical nuclear spots with Fe65 and the histone acetyltransferase Tip60, known as the AFT-complexes, which were demonstrated to correspond to transcription factories (von Rotz *et al.*, 2004; Konietzko *et al.*, 2010). Indeed, several AICD target genes have been identified, such as the genes coding for KAI1 (Baek et al., 2002), thymidilate synthase (Bruni et al., 2002), GSK-3β (Kim et al., 2003; Ryan and Pimplikar, 2005), APP, BACE, Tip60 (von Rotz et al., 2004), neprilysin (Pardossi-Piquard et al., 2005), p53 (Alves da Costa et al., 2006), α2-actin, transgelin (Muller et al., 2007), EGF receptor (Zhang et al., 2007), LRP1 (Liu et al., 2007), the mouse Nme1 and Nme2 (Napolitano et al., 2008), and, in *Caenorhabditis elegans*, acetylcholinesterase (Bimonte et al., 2004).

The identification of proteins that specifically interact with the cytoplasmic domain of APP have gradually contributed to unraveling the biological functions of APP and its fragments. In fact, APP binding proteins can influence its intracellular trafficking and consequently its processing via different pathways (da Cruz e Silva et al., 2004a). RanBP9 was recently reported to co-immunoprecipitate with APP and BACE1, increasing β-processing of APP (Lakshmana *et al.*, 2009). Here, we characterize the association of RanBP9 with AICD and show a novel interaction between Tip60 and RanBP9. We demonstrate that RanBP9 recruits AICD to Tip60-enriched nuclear speckles, preventing AFT-complex formation and AICD-mediated nuclear signaling.

V.2 MATERIALS AND METHODS

V.2.1 Yeast two-hybrid screens

MATCHMAKER GAL4 Two-Hybrid System 2 (Clontech, Enzifarma, Portugal) was used to perform several yeast two-hybrid screens according to the manufacturer's instructions, as previously described (Domingues et al., 2011). The vector used to insert the baits cDNA, was Clontech's GAL4 DNA-binding domain (GAL4-BD) expression vector pAS2-1. Bait-1 cDNA, coding for human APP_{695} (GenBank accession NM_201414), was PCR amplified (5'CCGCGCACCATGGCGAT GCTGCCCGGTTTGG-3'; 5'GTGGCCCCGGG CTAGTTCTGCATCTGCTCAAAG-3') and inserted in pAS2-1 using NcoI/SmaI restriction enzyme sites, in frame with the GAL4 DNA-BD. Bait-2, corresponding to $AICD^{Y687E}$, was PCR amplified (5'ATCACCATGGTGATGCTGAAGAAG-3'; 5'GTGGCCCCGGGCTAGTTCTGCATCTGCTCAAAG-3') from a plasmid containing the APP^{Y687E} mutant cDNA (pAV10) (da Cruz e Silva et al., 2004b). The insert was T4-ligated to the vector pAS2-1 using NcoI/SmaI restriction enzyme sites, in frame with the GAL4 DNA-BD. The bait plasmids pAS2-1-APP and pAS2-1-$AICD^{Y687E}$ were transformed in the yeast *Saccharomyces cerevisiae* strain AH109 (Clontech, Enzifarma, Portugal) using the lithium acetate transformation method. The transformants were assayed for *HIS3*, *ADE2* and *MEL1* reporter genes' intrinsic activation and the BD-baits fusion protein expression was verified by western blotting.

A total of 5.6×10^5 (YTH1, YTH screen with bait-1) or 1.1×10^8 (YTH2, screen with bait-2) independent clones from human brain Matchmaker cDNA libraries (Clontech, Enzifarma, Portugal) were screened by large scale yeast mating. True positive clones were identified as His^+, Ade^+ colonies and were positive for the α-galactosidase activity. Yeast plasmid DNA was extracted from the positive clones using the breaking buffer method (Yeast Protocols Handbook, Clontech) and the pACT2-library plasmids were rescued by transformation in *E. coli* XL-1 Blue. The library cDNAs were sequenced using the GAL4-AD primer (Clontech, Enzifarma, Portugal) and specific primers using an ABI PRISM 310 Genetic Analyzer (Applied Biosystems, Portugal). A search for similar sequences in the GenBank database was performed using the BLAST algorithm (http://www.ncbi.nlm.nih.gov) (Altschul et al., 1990).

V.2.2 Analysis of APP/AICD-RanBP9 interactions in yeast and α-Gal activity assay

The RanBP9 prey clone CYE1 (or N-terminally truncated RanBP9) was tested for activation of a GAL4-dependent *HIS3* promoter in the AH109 strain in the presence of different concentrations of 3-aminotriazole (3-AT). A concentration of 60 mM was established as the optimal to use in all subsequent tests. The yeast strain AH109 was co-transformed using the lithium acetate method, with the following plasmid pairs: pAS2-1/pACT2; pVA3-1/pTD1-1; pAS2-1/RanBP9-pACT2; APP-pAS2-1/RanBP9-pACT2; AICD-pAS2-1/RanBP9-pACT2. To assay for the reporter genes activation, co-transformed clones were grown on SD/QDO/X-α-Gal/60mM 3-AT.

For the quantitative α-Galactosidase activity assay, fresh yeast colonies expressing the pairs of interacting proteins being analyzed were grown on 4 ml of SD/TDO selective medium (SD/-Trp/-Leu/-His). The negative control AH109 (pAS2-1 + pACT2) was grown on SD/-Trp/-Leu. Cultures were incubated overnight at 30°C with shaking at 200 rpm. The optical density of the culture at 600 nm was recorded, 1 ml of the culture was centrifuged for 5 minutes at 12,000*g*, and the supernatant was removed for analysis. The assay was performed by combining 8 µl of culture supernatant with 24 µl of Assay Buffer (100 mM PNP-α-Gal solution, 0.5 M NaOAc [1:2 (v/v) ratio]; PNP-α-Gal, *p*-nitrophenyl α-D-Galactopyranoside, Sigma-Aldrich, Portugal). After incubation for 60 minutes at 30°C the reaction was terminated with 960 µl of stop solution (0.1 M $NaCO_3$) and the optical density at 410 nm was recorded. The α-galactosidase milliunits were calculated applying the formula below, as described by the manufacturer (Yeast Protocols Handbook, Clontech), for the 1 ml assay format: [milliunits/(ml x cell)] = OD_{410} x 992 x 1000 / [OD_{600} x time (min) x 16.9 x 8].

V.2.3 Mapping of AICD and RanBP9 interaction domains

Several deletion mutants of APP C-terminus (APP_{695} human neuronal isoform) were inserted in the pAS2-1 vector in frame with Gal4-BD: p24 (expressing amino acids 599-681), p26 (expressing 599-669), p27 (expressing 599-660), p28 (deletion of amino acids 662-672) and p30 (deletion of amino acids 675-691). The yeast strain AH109 was transformed with the following plasmid pairs: $AICD^{WT}$/RanBP9; pVA3-1/pTD1-1; pAS2-1/pACT2; p24/RanBP9; p26/RanBP9; p27/RanBP9; p28/RanBP9; p30/RanBP9. The co-transformants were assayed for reporter genes' activation by streaking onto SD/QDO/X-α-Gal/3-AT.

The RanBP9 protein comprises four domains: SPRY, LiSH, CTLH and CRA. cDNA sequences corresponding to the SPRY domain (amino acids 212-333), to the LiSH/CTLH domains (amino acids 365-460) and to the CRA domain (amino acids 615-729) were inserted in pACT2 in fusion with Gal4-AD. Other combinations of these domains were also used: BN1 (amino acids 136-333), BN2 (amino acids 136-460), BM1 (amino acids 212-460), BC1 (amino acids 409-729) and BC2 (amino acids 365-729). The yeast strain AH109 was transformed with the following plasmid pairs: AICD/SPRY; AICD/LisH-CTLH; AICD/CRA; pAS2-1/pACT2; pVA3-1/pTD1-1; AICD/BN1; AICD/BN2; AICD/BM1; AICD/BC1; AICD/BC2. The co-transformants were assayed for growth and for the presence of blue color on SD/QDO/X-α-Gal/3-AT.

V.2.4 Analysis of RanBP9-Tip60 interaction in yeast

Tip60 isoform 2 cDNA (GenBank Accession Number NM_006388) was excised from the Myc-Tip60 plasmid by digestion with NcoI/BamHI and inserted in pAS2-1, in frame with Gal4-BD. The yeast strain AH109 was transformed using the lithium acetate method, with the following plasmid pairs: pAS2-1/pACT2; Tip60-pAS2-1/pACT2; Tip60-pAS2-1/RanBP9-pACT2 and pVA3-1/pTD1-1. Co-transformants were selected on SD minimal medium lacking, Trp and Leu. To assay for the reporter genes' activation co-transformed clones were grown on SD/QDO/X-α-Gal/60mM 3-AT.

In order to map the RanBP9 domain responsible for the interaction with Tip60, the above mentioned Gal4-AD fusion constructs corresponding to the RanBP9 domains (SPRY, LiSH-CTLH, CRA, BN1, BN2, BM1, BC1 and BC2) were also co-transformed with Tip60-pAS2-1 in AH109 yeast cells. Co-transformants were assayed for growth and for the presence of blue color on SD/QDO/X-α-Gal/60mM 3-AT.

V.2.5 Glutathione S-transferase pull-down assay

A GST pull-down assay was performed to confirm the specific interaction between RanBP9 and APP *in vitro*. To express a recombinant GST-tagged RanBP9 protein, pGEX-2T (GE Healthcare, VWR, Portugal) glutathione S-transferase (GST)-fusion vector was digested with BamHI and EcoRI. RanBP9 cDNA was PCR amplified (5'-GCAGTTGATCAGTCG CGGCCGGGATGTCCG-3'; 5'-GCTCTTGC AATTGATAGCTAATGTAGGTAGTC-3') and digested with MfeI and BclI. T4 DNA ligase joined the EcoRI/BamHI-digested pGEX-2T and the RanBP9 fragment, to obtain the plasmid pGEX-2T-

RanBP9. pGEX-2T-RanBP9 was digested with NcoI and re-ligated, to obtain an internal deletion of RanBP9 (aa 254-489). The plasmid obtained, pGEX-2T-ΔSLC, was used as a negative control in the pull-down assays. MfeI/EagI digested APP_{695} cDNA was cloned into the pET-28a expression vector (Novagen, Merck, Portugal) between the EcoRI and EagI sites to construct the vector pET-APP, which was used to express His-tagged APP in Rosetta cells. All of the recombinant plasmids were verified by sequencing.

Competent Rosetta cells were transformed with the plasmids pGEX-2T, pGEX-2T-RanBP9, pGEX-2T-ΔSLC and pET-APP and the recombinant clones were induced with 0.6 mM isopropyl-β-D-thiogalactopyranoside (IPTG) at 30°C for 2 h (pGEX-2T, pET-APP) or 4 h (pGEX-2T-RanBP9, pGEX-2T-ΔSLC). The induced bacterial cultures were centrifuged and resuspended in lysis buffer (50 mM Tris–HCl, pH 8.0, 100 mM NaCl, 1 mM EDTA and 3% Triton X-100) in the presence of a protease inhibitor cocktail (PMSF, Leupeptin, Aprotinin, Pepstatin A, Benzamidin) and further disrupted by sonication. Following centrifugation at 5000*g* for 10 min, the soluble GST, GST-RanBP9 and GST-ΔSLC proteins were then immobilized on glutathione sepharose 4B beads (GE Healthcare, VWR, Portugal) by incubating 1 ml of supernatant with 25 µl beads for 4 h at 4°C. The beads-adsorbed proteins GST, GST-RanBP9 and GST-ΔSLC were incubated with equal amounts of 6His-APP supernatant overnight at 4°C. After the beads were washed 4 times in wash buffer (50 mM Tris pH 8, 100 mM NaCl), the bound proteins were eluted in SDS-PAGE loading buffer by boiling at 100°C and then isolated by centrifugation. The supernatants and the soluble fractions of the bacterial lysates, as input samples, were resolved in 12% SDS–PAGE followed by immunoblotting with the anti-APP antibody 22C11 (1:150; Boehringer) and anti-GST antibody (1:2000; GE Healthcare, VWR, Portugal).

V.2.6 Mammalian expression constructs for transfections

The following expression constructs were described previously: APP_{695}-GFP (da Cruz e Silva et al., 2004b); GFP-RanBP9 (Nishitani et al., 2001); Citrine-AICD, Myc-Fe65 and CFP-Tip60 (von Rotz et al., 2004); SwAPP-Citrine (Goodger et al., 2009); Myc-Tip60 (Konietzko et al., 2010). APP-2Myc and mCherry-Fe65 were created from APP-Citrine and Myc-Fe65 (von Rotz et al., 2004), respectively, by replacing the tag using standard cloning procedures. For RanBP9-3HA, RanBP9 cDNA was PCR amplified (5'-CGACTAGTGGCCGCCATGTCCGGGCAG-3'; 5'-

GAAATGGGCGCGCCATGTAGGTAGTCTTCCAC-3'), digested with SpeI/AscI and inserted into a vector containing a CMV promoter, in frame with three tandem HA tags (Goodger et al., 2009).

V.2.7 Cell culture and transfections

COS-7 cells were grown in Dulbecco's modified Eagle's medium (DMEM; Gibco Invitrogen, Alfagene, Portugal), supplemented with 10% (v/v) fetal bovine serum, 100 U/ml penicillin, 100 mg/ml streptomycin and 3.7 g/l $NaHCO_3$. Human cervical epithelia HeLa cells were cultured in Minimal Essential Media with 1% Non-Essential Amino Acids, 10% heat inactivated Fetal Bovine Serum (FBS) and 1% antibiotic/antimycotic (AA) mix. HEK293 cells were grown in DMEM (Gibco, Basel, Switzerland) supplemented with 10% fetal calf serum and penicillin/streptomycin (PenStrep, Invitrogen, Basel, Switzerland). Rat neuronal primary cultures were established from embryonic day 18 fetuses. Cells were dissociated with 0.45 mg/ml trypsin and 0.15 mg/ml deoxyribonuclease I in Hank's balanced salt solution (HBSS) during 5-10 min at 37°C. Cells were plated on poly-D-lysine-coated dishes at a density of $1.0x10^5$ cells/cm^2 in B27-supplemented Neurobasal medium (Gibco Invitrogen, Alfagene, Portugal), a serum-free medium combination (Brewer et al., 1993). The medium was supplemented with glutamine (0.5 mM), gentamicin (60 µg/ml), without glutamate, for 9 days before being used for experimental procedures. All cultures were maintained at 37°C in an atmosphere of 5% CO_2. To address Aβ effects on RanBP9 intracellular levels, primary cortical cultures were incubated with 20 µM $Aβ_{25-35}$ (Sigma-Aldrich, Portugal) in complete medium for 24 h (Henriques et al., 2009).

For transient transfection experiments, COS-7, HeLa or HEK293 cells were grown on plastic culture dishes or on glass slide chambers coated with polyornithine (10 µg/ml) and fibronectin (5 µg/ml) and transfected using LipofectAMINE 2000 (Invitrogen) as previously described (von Rotz *et al.*, 2004; Domingues *et al.*, 2007). A stably transfected HEK293 cell line was induced to express Citrine-AICD the day before transfection, resulting in expression for 40-44 h (von Rotz et al., 2004). The induced cells were co-tranfected with RanBP9, Fe65 and Tip60 expression constructs using LipofectAMINE 2000 (Invitrogen, Basel, Switzerland).

V.2.8 APP and RanBP9 Co-immunoprecipitation

Mammalian cell-based co-immunoprecipitation (Co-IP) experiments were performed in COS-7 cells and in adult rat hippocampus and cortex lysates. Endogenous and transiently

transfected APP and RanBP9 constructs were analyzed as COS-7 cells express both proteins. Subconfluent COS-7 cells in 100 mm culture plates were transfected with GFP-RanBP9, RanBP9-3HA or APP-GFP. Cells were harvested in a non-denaturant lysis buffer (50 mM Tris pH 8, 120 mM NaCl, 4% CHAPS; Sigma-Aldrich, Portugal) with a protease inhibitor cocktail (PMSF, Leupeptin, Aprotinin, Pepstatin A, Benzamidin; Sigma-Aldrich, Portugal). Adult rat hippocampi and cortexes were isolated and immediately homogenized in the non-denaturant lysis buffer supplemented with protease inhibitors.

The cell lysates or the rat tissue lysates were immunoprecipitated with an anti-APP antibody (22C11, 6E10, KPI or 4G8) overnight at 4°C under end-to-end mixing. Anti-mouse IgG agarose beads (Sigma, Portugal) were added to each sample and the samples were incubated for 2 h at 4°C. The agarose beads were washed 4 times with 50 mM Tris pH 8/ 120 mM NaCl and resuspended in SDS loading buffer. Immunoprecipitations with anti-HA antibody (Roche) were immobilized with G-protein Sepharose (GE Healthcare, VWR, Portugal). The immunocomplexes were analyzed by Western blotting using the primary antibodies: 22C11 (1:150; Boehringer); JL-8 (1:500; Clontech, Enzifarma, Portugal); 5M (1:2000) (Nishitani et al., 2001); or anti-RanBP9 ab5295 (4 µg/ml; Abcam, Cambridge, UK).

V.2.9 SDS-PAGE and Immunoblotting

Transfected cells were harvested in 1% SDS and boiled. The protein content of cell lysates was determined by the BCA method (Pierce, Dagma, Portugal). Normalized samples were resolved by SDS-PAGE and transferred to nitrocellulose membranes followed by immunological detection with the indicated antibodies. Briefly, membranes were blocked in 5% non-fat dry milk in TBS-T for 2 h and incubated with the primary antibody. The antibodies used were: APP N-terminal antibody (22C11, Boehringer); JL-8 antibody (1:500; Clontech, Enzifarma, Portugal); anti-transgelin H-75 (1:400; Santa Cruz, Frilabo, Portugal); anti-GSK3 AB9258 (1:500; Chemicon Millipore, Grupo Tapper, Portugal); and anti-RanBP9 ab5295 (4 µg/ml; Abcam, Cambridge, UK). Detection was carried out with horseradish peroxidase-conjugated anti-mouse IgGs as secondary antibody and proteins were visualized by enhanced chemiluminescence (ECL; GE Healthcare, VWR, Portugal). Immunoreactive bands were quantified by densitometric analysis with QuantityOne software (Bio-Rad Laboratories, Portugal), using β-tubulin as an internal control.

V.2.10 Immunocytochemistry and confocal microscopy

Cells were fixed with 4% paraformaldehyde in PBS 16-20 h after transfection. The fixed cells were washed and blocked as previously described (Konietzko et al., 2010). The primary antibodies were mouse anti-Myc and rat anti-HA (1:100; Roche, Rotkreuz, Switzerland). Cy2-, Cy3- or Cy5-conjugated secondary antibodies (1:250; Jackson Labs, Bar Harbor, Maine) were applied and, after subsequent washing, the cells were embedded in Mowiol mounting medium containing 2.5% of DABCO anti-fade reagent (Sigma-Aldrich, Buchs, Switzerland).

Images were acquired on a Leica TCS/SP2 confocal microscope (Leica, Wetzlar, Germany) with a 63x water immersion objective. The Argon Laser line of 458 nm was used to excite CFP (PMT window: 465–485 nm) and the 514 nm line to excite citrine (PMT window: 525–545 nm). A 543-nm HeNe laser was used to excite Cy3 (PMT window: 553–600 nm), and a 633-nm HeNe laser was used to excite Cy5 (PMT window: 655–710 nm). Antibody staining with Cy2 is always color-coded in green, Cy3 in red and Cy5-staining in blue.

V.3 RESULTS

V.3.1 Identification of RanBP9 as an APP/AICD interacting protein

Large-scale YTH screens of human brain cDNA libraries were performed using as baits diverse APP or AICD constructs (Supplementary Table 1). Several positive clones matched RanBP9 cDNA (NCBI accession number NM_005493). The full-length RanBP9 is a 90 kDa protein of 729 aminoacids, possessing a long stretch of proline and glutamine residues in the N-terminal region and four signaling domains (SPRY, LisH, CTLH and CRA domains) (Nakamura *et al.*, 1998; Umeda *et al.*, 2003; Menon *et al.*, 2004). RanBP9 was recently described to co-immunoprecipitate with full-length APP (Lakshmana *et al.*, 2009).

Protein interactions were verified by co-transformation of each bait and the prey plasmids in AH109 yeast cells. The authenticity of the interaction between the positive clone CYE1 encoding a N-terminal truncated RanBP9 and AICD bait was confirmed by its ability to grow and turn blue on QDO/X-α-Gal plates due to the expression of all the reporter genes *HIS3*, *ADE2* and *MEL1*. The appearance is similar to the positive control which co-expressed the Gal4-BD-p53 and Gal4-AD-SV40 fusion proteins (Fig. 1A). The Gal4-BD and Gal4-AD empty vectors (pAS2-1 and pACT2) were co-expressed as a negative control.

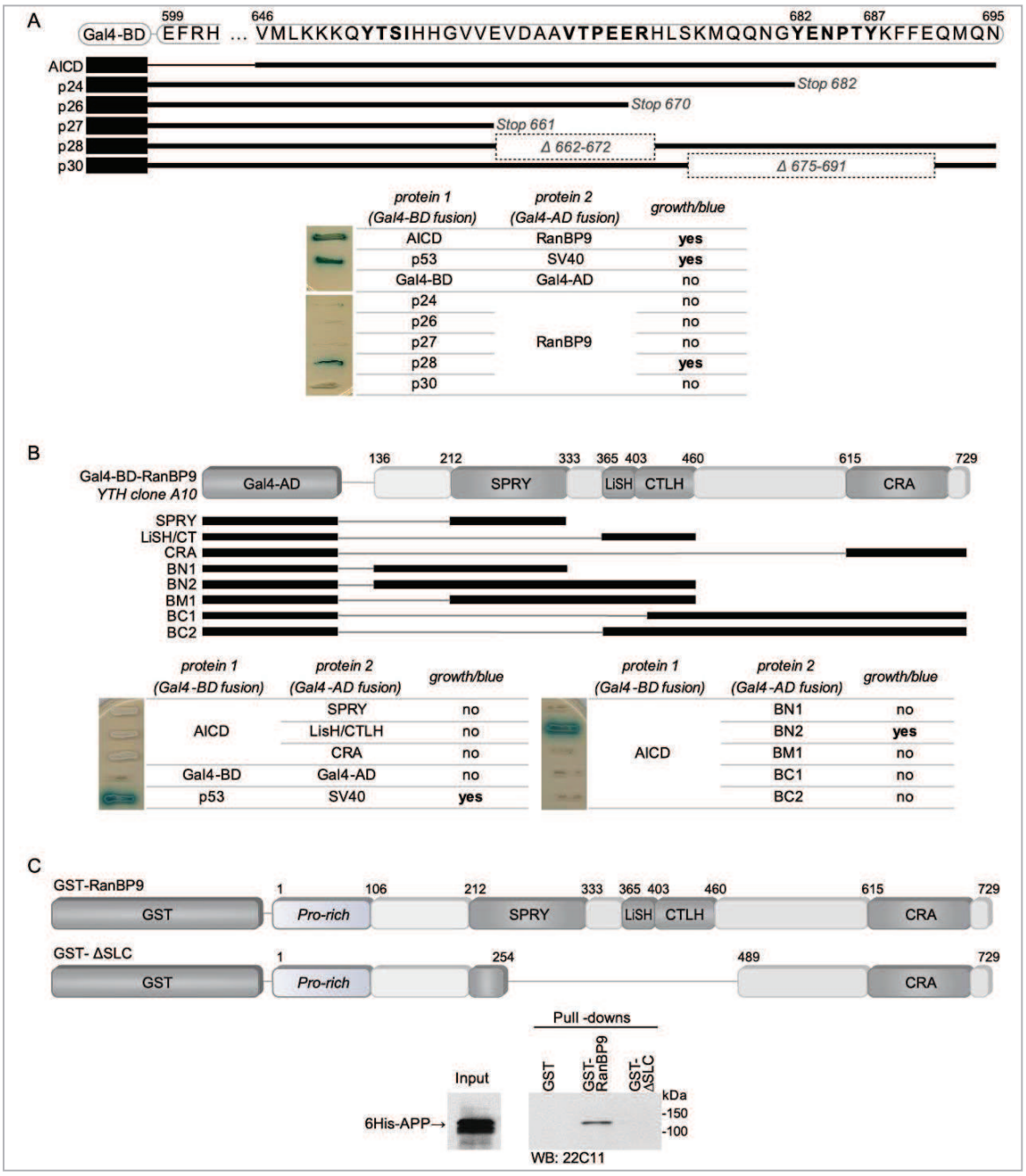

Figure V.1: RanBP9 binds to the APP cytoplasmic domain through the NPXY motif. (A) Plate assay (SD/QDO/X-α-Gal) of interaction between RanBP9 prey clone and AICD, or deletion mutants of APP C-terminus (p24, p26, p27, p28 and p30) (the two image sections belong to the same plate). (B) The AH109 yeast strain was co-transformed with AICD and each RanBP9 construct, representing the RanBP9 domains SPRY, LiSH/CTLH and CRA, or combinations of these, and streaked onto SD/QDO/X-α-Gal. Growth and blue appearance of yeast colonies indicate positive interaction (sections from the same plate are shown) (C) Recombinant GST alone and fusion proteins GST-RanBP9 and GST-ΔSLC (deletion mutant lacking domains SPRY and LiSH/CTLH) were immobilized on Glutathione Sepharose 4B and incubated with recombinant His-tagged APP. The bound proteins were analyzed by 12% SDS-PAGE and immunoblotted with anti-APP antibody (22C11). The bait GST or GST fusion proteins were detected with anti-GST antibody, demonstrating a direct interaction between RanBP9 and APP.

V.3.2 RanBP9 binds to the APP cytoplasmic domain through the NPXY motif

To determine the APP intracellular domain sequence necessary for the interaction with RanBP9, several deletion mutants of AICD were co-transformed in the yeast strain AH109 with the RanBP9 prey plasmid. The co-transformants were assayed for reporter genes' activation by streaking onto SD/QDO/X-α-Gal/3-AT. Only the BD-p28 fusion protein (internal deletion 662-672) conferred ability to grow on QDO and develop blue color, comparable to the yeast co-expressing intact AICD and RanBP9 or the positive control p53 plus SV40 large T antigen (Fig. 1A). The BD-p28 fusion is the only deletion construct used in this experiment that includes the ^{682}YENPTY^{687} motif, which corresponds to the NPXY internalization signal of APP. Therefore the ^{682}YENPTY^{687} motif, responsible for several protein-protein interactions with APP, is also necessary for the association with RanBP9.

The RanBP9 protein comprises four domains: SPRY, LiSH, CTLH and CRA (Nakamura *et al.*, 1998; Umeda *et al.*, 2003; Menon *et al.*, 2004). Five Pro-rich regions and a Gln stretch are also present at the N-terminus of RanBP9. However, as the N-terminus is absent from our YTH clones, it was excluded from interaction domains mapping analysis. Co-expression of the fusion protein BD-AICD with the Gal4-AD fused to the SPRY, LiSH/CTLH or CRA domains did not activate all the reporter genes, since the co-transformants could grow but did not turn blue in QDO/X-α-Gal media (Fig. 1B). Other combinations of these domains were also used. Co-expression of Gal4-AD-BN2 with the Gal4-BD-AICD fusion showed the expression of all reporter genes (Fig. 1B). The BN2 fusion construct includes the SPRY, LiSH and CTLH domains as well a region of 76 aa N-terminal to SPRY and a region between SPRY and LiSH. Thus we were able to map the RanBP9 sequence 136-460 as the region necessary for the interaction with AICD in the YTH system.

V.3.3 RanBP9 associates with APP directly *in vitro*

The interaction between RanBP9 and APP was confirmed to occur directly *in vitro* using Glutathione *S*-transferase (GST) pull-down assays. GST fusion constructs were prepared with full-length RanBP9 (GST-RanBP9) and with a deletion mutant lacking the domains SPRY and LiSH/CTLH (GST-ΔSLC). Recombinant GST alone and fusion proteins GST-RanBP9 and GST-ΔSLC (APPENDIX XI) were immobilized and purified on Glutathione Sepharose 4B and used as baits in the pull-down assays. Each bait (GST, GST-RanBP9 and GST-ΔSLC) was incubated with similar amounts of

recombinant His-tagged APP. The bound proteins were analyzed by 12% SDS-PAGE and immunoblotted with anti-APP antibody (22C11). APP from the input sample was detected in the GST-RanBP9 complex (Fig. 1C, lane 2). APP was not detected either in the GST or GST-ΔSLC control samples (Fig. 1C, lanes 1 and 3), thus confirming that RanBP9 binds to APP directly and specifically *in vitro*.

V.3.4 RanBP9 co-localizes with APP and Fe65 in mammalian cells

To confirm that APP interacts with RanBP9 in mammalian cells we performed several co-immunoprecipitation assays. Neuronal tissues and COS-7 cells were used to co-immunoprecipitate the endogenous or transfected proteins, using different plasmid constructs and antibodies (Fig. 2A). The interaction between APP and RanBP9 was confirmed in adult rat hippocampus and cortex lysates by immunoprecipitation with either an anti-APP antibody (22C11) or an anti-RanBP9 antibody (ab5295) (Fig. 2A, panels 1 and 2). In GFP-RanBP9 transfected COS-7 cells, immunoprecipitation with the 6E10 antibody, pulled-down GFP-RanBP9 (Fig. 2A, panel 3). As expected, no signal is detected by the JL-8 antibody in the non-transfected (NT) cells. COS-7 cells were also transiently transfected with APP-GFP and RanBP9-3HA, and RanBP9 was immunoprecipitated with anti-HA antibody. Both APP-GFP and endogenous APP co-immunoprecipitated with RanBP9, detected with 22C11 antibody (Fig. 2A, panel 4). In APP-GFP transfected COS-7 cells, immunoprecipitations were also carried out using the anti-GFP and several anti-APP antibodies (22C11, KPI, 6E10 and 4G8). Endogenous RanBP9 was detected in all samples using either the 5M antibody, raised against a RanBP9 N-terminal region (aa 133-229) (data not shown), or with ab5295 antibody, which recognizes the RanBP9 C-terminus (Fig. 2A, panel 5). Co-immunoprecipitation of endogenous APP and RanBP9 in COS-7 cells was also confirmed using the anti-APP antibodies 6E10 or 22C11 and probed with the anti-RanBP9 antibody 5M. RanBP9 was observed both in the 22C11 and 6E10 immunocomplexes (Fig. 2A, panel 6).

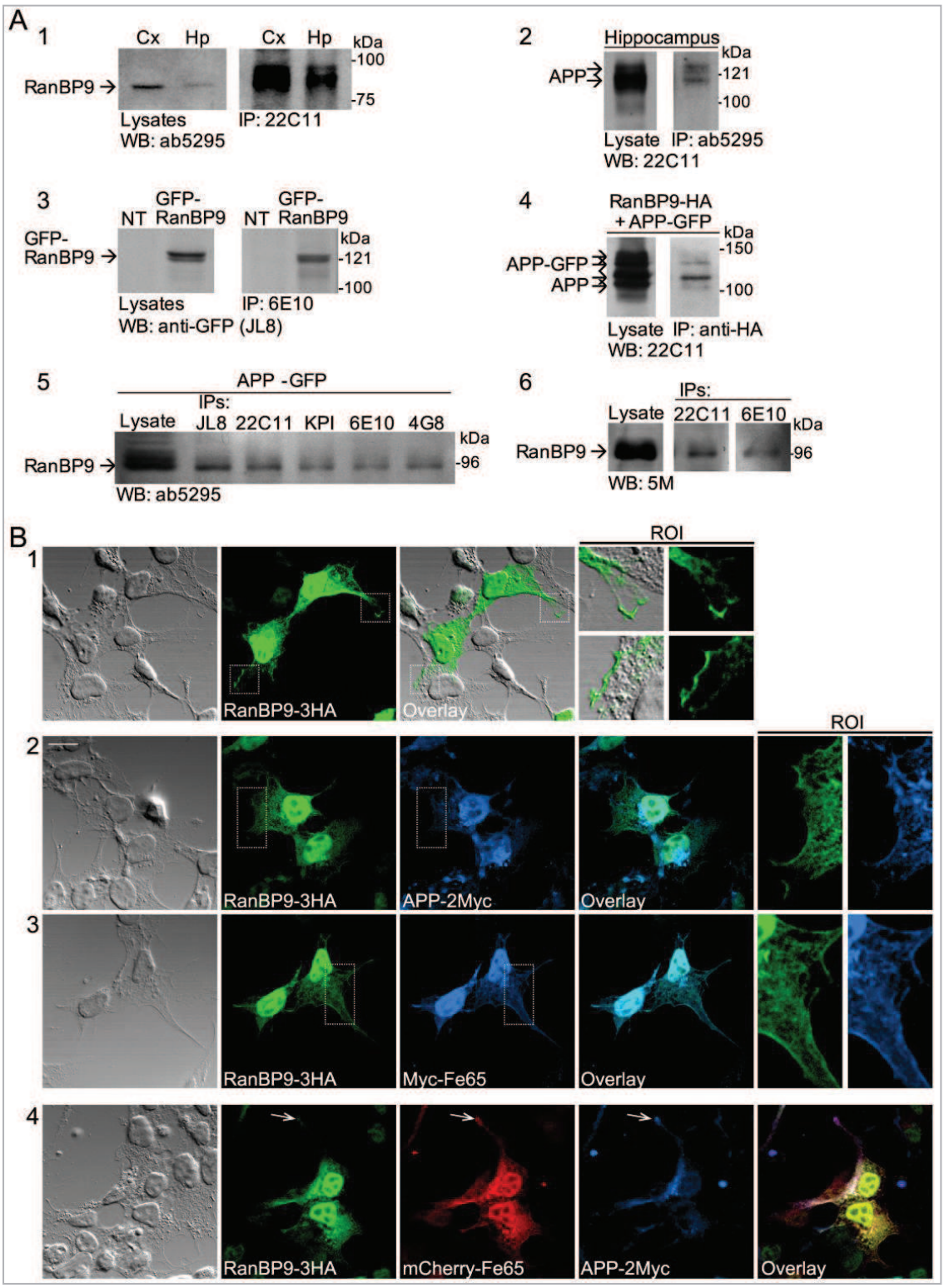

Figure V.2: RanBP9 co-localizes with APP and Fe65 in mammalian cells. (A) RanBP9 and APP were co-immunoprecipitated in adult rat brain tissues (panels 1-2) and COS-7 cells (panels 3-6), using the specified antibodies. For transfected COS-7 cells the fusion construct is indicated. NT, non-transfected cells; Hp, hippocampus; Cx, cortex. (B) Confocal analysis of RanBP9, APP and Fe65 transfected HEK293 cells. ROI, region of interest; Bar, 13 µm.

Full-length RanBP9 was described to localize both in the cytoplasm and in the nucleus (Nishitani et al., 2001). Other subcellular locations were also reported, such as the plasma membrane (Denti et al., 2004) and nuclear speckles (Wang et al., 2002b). An antibody raised against the formerly described truncated 55-kDa RanBP9 protein stained the centrosome, but this subcellular localization was not confirmed by other RanBP9 full-length specific antibodies (Nakamura et al., 1998; Nishitani et al., 2001). Transfection of HEK293 cells with the RanBP9-3HA construct confirmed the localization in the nucleus, cytoplasm and at the membrane. We also found RanBP9 staining at ruffled edges of cells that contained a characteristic lamellipodial structure, as showed in the magnified ROIs (regions of interest; Fig. 2B, panel 1).

Fluorescently tagged APP can be observed in the endoplasmic reticulum, Golgi complex, lysosomal or endocytic vesicles and plasma membrane, being proteolytically processed throughout its subcellular trafficking (da Cruz e Silva et al., 2004b). The liberated AICD fragment translocates to the nucleus (Kimberly et al., 2001; von Rotz et al., 2004). RanBP9 and APP co-localized prominently at the plasma membrane, particularly in lamellipodia (Fig. 2B, panel 2). RanBP9 localized far less to ER/Golgi, heavily stained by APP and by the APP binding protein Fe65, especially when APP is co-expressed (Fig. 2B, panels 3 and 4). RanBP9 co-localized with Fe65 in the plasma membrane and nucleus and when RanBP9, APP and Fe65 were expressed simultaneously co-localization was observed in the same subcellular compartments. Antibody-mediated staining of nuclear AICD is strongly restricted (von Rotz et al., 2004) explaining the lack of AICD signal in the nuclei (Fig. 2B, panel 4). Additional transfection experiments performed with SwAPP-Citrine instead of APP-2Myc showed a similar pattern of co-localization (Supplementary Fig. S1, APPENDIX XI).

V.3.5 RanBP9 shows high affinity for AICD in vivo

Since RanBP9 cDNA clones were found in YTH screens with full-length APP (APP-FL) and AICD baits, we validated the interaction with both baits. Positive interaction with RanBP9 was confirmed for both baits given the growth on QDO plates and the blue color detected (data not shown). Additionally, we performed quantitative X-α-Gal assays to compare the strength of each interaction. α-galactosidase activity of liquid cultures showed that the RanBP9/AICD interaction is significantly stronger (~2.8 fold) than the RanBP9/APP-FL interaction (Fig. 3A).

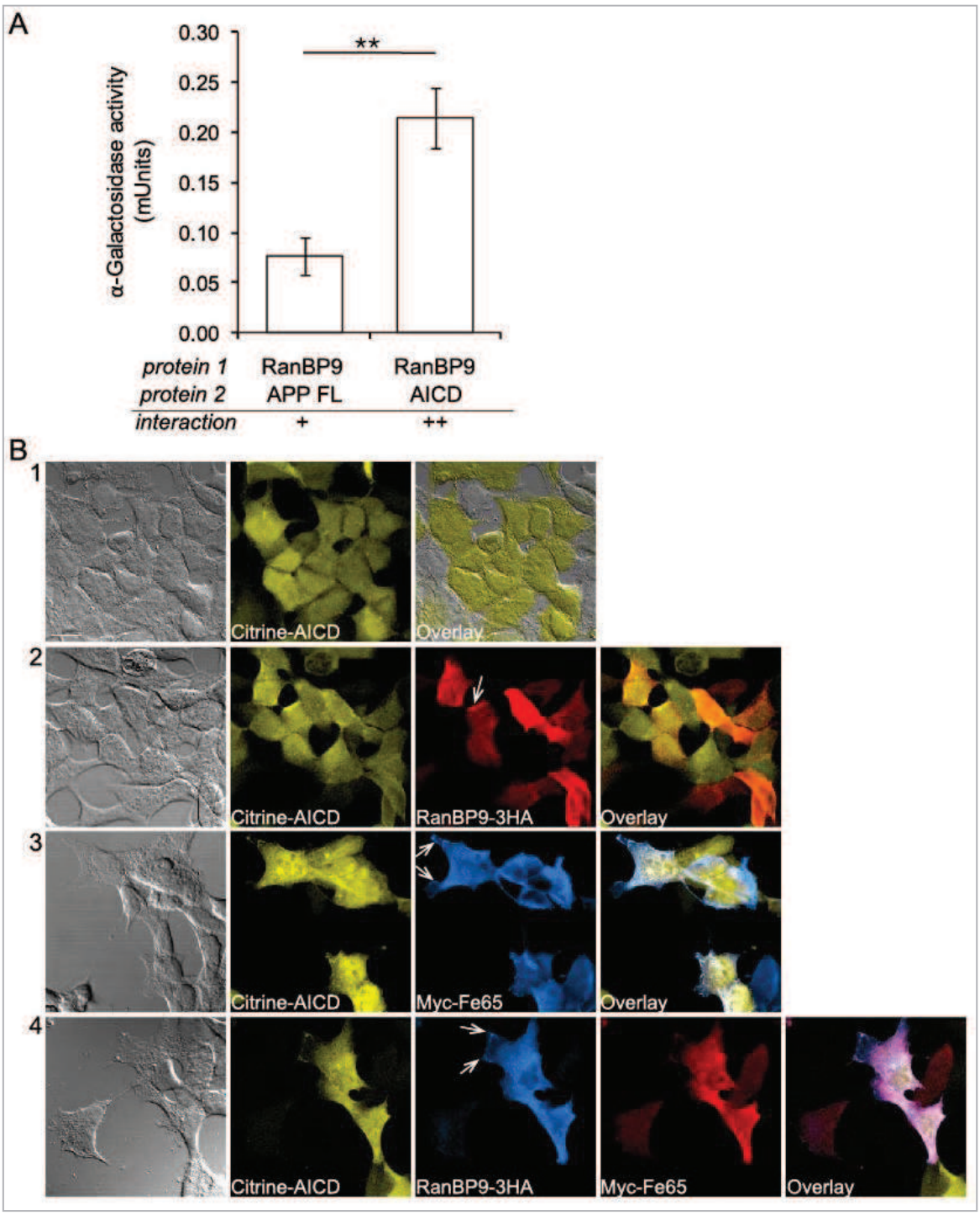

Figure V.3: RanBP9 shows high affinity for AICD *in vivo*. (A) Quantitative X-α-Gal assays of liquid cultures were performed to compare the strength of the interactions between RanBP9 and APP-FL or AICD in the YTH system. Graph shows means ± SEM of 7 independent experiments (Unpaired t test; **, $P<0.01$). (B) HEK293 cells stably expressing Citrine-AICD were transfected with RanBP9-3HA (*panel 2*), Myc-Fe65 (*panel* 3) or both (*panel 4*) showing co-localization in the nucleus, cytoplasm and plasma membrane (*arrow,* lamellipodia). Bar, 13 µm.

To characterize the interaction between RanBP9 and AICD *in vivo* we used a clonal HEK293 cell-line with inducible expression of fluorescently tagged Citrine-AICD (von Rotz *et al.*, 2004). These stably transfected cells allow to overcome the experimental difficulty of observing AICD *in vivo*, since it is rapidly degraded after release from the membrane (Cupers *et al.*, 2001). Co-transfection of RanBP9-3HA, showed that RanBP9 and AICD overlap throughout the nucleus, cytoplasm and at the membrane (Fig. V.3B, panel 2). In fact, as in the HEK293-AICD cells the nucleus is strongly stained, there is extensive co-localization with RanBP9 in the nuclear compartment. RanBP9 and AICD also co-localize in the cytoplasm and plasma membrane, particularly in lamellipodia. The same pattern of co-localization was observed with simultaneous co-expression of AICD and Fe65 (Fig. V.3B, panel 3), and with AICD, RanBP9 and Fe65 (Fig. V.3B, panel 4).

V.3.6 Tip60 and RanBP9 can directly associate and Tip60 targets RanBP9 to nuclear speckles

Tip60 is a histone acetyltransferase that binds to Fe65 (Cao and Sudhof, 2001). Tip60, Fe65 and AICD can form tripartite complexes (AFT complexes), which were shown to concentrate in spherical nuclear spots where they can regulate transcription (von Rotz et al., 2004; Konietzko et al., 2010). Alone, Tip60 localizes to speckle-like nuclear structures. In the absence of exogenous AICD expression, Tip60 and Fe65 were previously shown to co-localize in nuclear spots (von Rotz et al., 2004). Confocal microscopy observations showed that when RanBP9 was simultaneously expressed with Tip60, it dramatically changed its subcellular localization, in particular the diffuse nuclear staining of RanBP9 is not observed. The majority of RanBP9 was targeted to the large nuclear speckles, where Tip60 is usually found (Fig. V.4A, panel 1). RanBP9 and Tip60 completely overlap in these nuclear speckles (100% of the cells imaged). The relocation of transfected RanBP9-3HA to the nuclear speckles happens either when co-transfecting with CFP-Tip60 (Fig. V.4A, panel 1) or with Myc-Tip60 (Fig. V.4A, panel 2). Moreover, when Fe65 is co-expressed together with RanBP9 and Tip60, the three proteins also co-localize in the nuclear speckles (Fig. V.4A, panel 3). Only 3 of the 13 imaged cells had nuclear spots with Fe65 and Tip60, with low or no RanBP9 expression. Therefore, co-expression of RanBP9 prevents the Fe65-mediated relocation of Tip60 to nuclear spots but instead targets Fe65 to speckle structures.

The relocation of RanBP9 to nuclear speckles by Tip60 strongly suggests that they can directly interact. To address this question we subcloned Tip60 cDNA into the YTH vector pAS2-1 in

frame with the Gal4-BD and the fusion proteins Gal4-BD-Tip60 and Gal4-AD-RanBP9 were co-expressed in yeast. The interaction between Tip60 and RanBP9 was confirmed in SD/QDO/X-α-Gal/3-AT plates, due to the expression of all the reporter genes *HIS3*, *ADE2* and *MEL1*. The appearance is similar to the positive control which co-expressed the BD-p53 and Gal4-AD-SV40 fusion proteins (Fig. V.4B). The Gal4-BD and Gal4-AD empty vectors (pAS2-1 and pACT2) were co-expressed as a negative control.

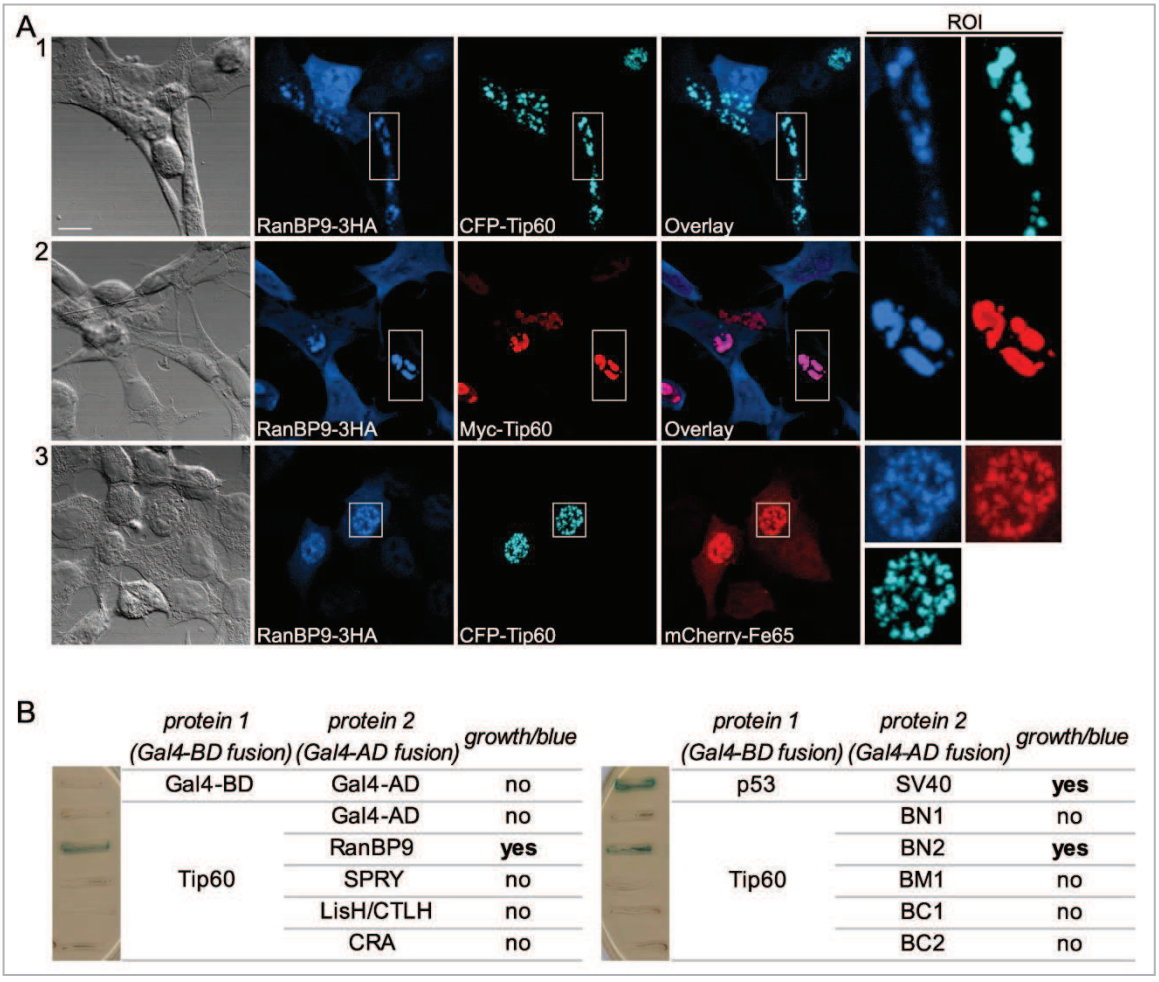

B

protein 1 (Gal4-BD fusion)	protein 2 (Gal4-AD fusion)	growth/blue
Gal4-BD	Gal4-AD	no
Tip60	Gal4-AD	no
	RanBP9	**yes**
	SPRY	no
	LisH/CTLH	no
	CRA	no

protein 1 (Gal4-BD fusion)	protein 2 (Gal4-AD fusion)	growth/blue
p53	SV40	**yes**
Tip60	BN1	no
	BN2	**yes**
	BM1	no
	BC1	no
	BC2	no

Figure V.4: Tip60 targets RanBP9 to nuclear speckles. (A) Co-expression of RanBP9-3HA with CFP-Tip60 (*panel 1*) or with Myc-Tip60 (*panel 2*) in HEK293 cells. Number of imaged cells: 38 cells with speckles (RanBP9 localizes to Tip60 speckles). In panel 3, RanBP9-3HA, CFP-Tip60 and mCherry-Fe65 were simultaneously expressed. ROIs denote co-localization in nuclear speckles. Number of imaged cells: 10 cells with speckles (Fe65+Tip60+RanBP9); 3 cells with spots (Fe65+Tip60 and low or no RanBP9). Bar, 13 µm. (B) Plate assay (SD/QDO/X-α-Gal) of interaction between Tip60 and RanBP9. RanBP9 constructs represent the domains SPRY, LiSH/CTLH and CRA, or combinations of these (sections from the same plate are shown). The Gal4-BD and Gal4-AD empty vectors were co-expressed as a negative control. Gal4-BD-p53 and Gal4-AD-SV40 plasmids show a positive interaction.

YTH tests were also carried out with yeast cells co-transformed with BD-Tip60 and the Gal4-AD fused to the RanBP9 domains SPRY, LiSH-CTLH and CRA or the combinations already mentioned above: BN1, BN2, BM1, BC1 and BC2. Co-expression of Gal4-AD-BN2 with the BD-Tip60 fusion allowed the yeast cells to grow and turn blue in SD/QDO/X-α-Gal, showing the expression of all reporter genes (Fig. V.4B). Therefore the RanBP9 amino acid sequence 136-460, including the SPRY, LiSH and CTLH domains, is necessary for the interaction with Tip60. This is the same RanBP9 region that was shown above to be responsible for the interaction with AICD.

V.3.7 RanBP9 targets AICD to Tip60 and prevents AFT complex formation

The HEK293 cell-line with inducible expression of Citrine-AICD was transfected with CFP-Tip60 showing that Tip60 alone has no effect on AICD subcellular localization (Fig. V.5A, panel 1), as shown before (von Rotz et al., 2004). However, co-transfection of CFP-Tip60 and RanBP9-3HA relocated AICD to the nuclear speckles where Tip60 is usually found (in all imaged cells Tip60, RanBP9 and AICD were present in the speckles; Fig. V.5A, panel 2), showing that RanBP9 binds to AICD and Tip60 simultaneously.

Co-expression of AICD, Fe65 and Tip60 generates AFT complexes that localize to nuclear spots (Fig. V.5B, panel 1) as previously demonstrated (von Rotz et al., 2004). In contrast, RanBP9 did not re-localize Tip60 to nuclear spots as Fe65-AICD does but co-localizes with Tip60 in speckles. To investigate the effect of RanBP9 on the AFT complex formation, the Citrine-AICD-expressing cell-line was co-transfected with Myc-Fe65, CFP-Tip60 and RanBP9-3HA (Fig. V.5B, panel 2). In general, cells expressing RanBP9 do not form nuclear AFT spots and AICD is detected in larger nuclear speckles, together with RanBP9, Fe65 and Tip60. This morphology was observed in 43% of the imaged cells, always when RanBP9 levels were high. Conversely, in cells with lower RanBP9-3HA expression (evaluated by fluorescence intensity), RanBP9 did not prevent the formation of the nuclear spots (Fig V.2B, panel 2). Although RanBP9 could be detected in nuclei containing AFT spots we saw no accumulation of RanBP9 in these spots.

Another observation is the effect of RanBP9 on cytosolic AICD levels. As shown in previous reports, formation of nuclear AFT complexes is accompanied by depletion of AICD in the cytosol (Fig. V.5B, panel 1). However, in cells co-expressing RanBP9, AICD, Fe65 and Tip60 that co-localize in speckles, AICD is not depleted from the cytosol (Fig. V.5A and B, panels 2).

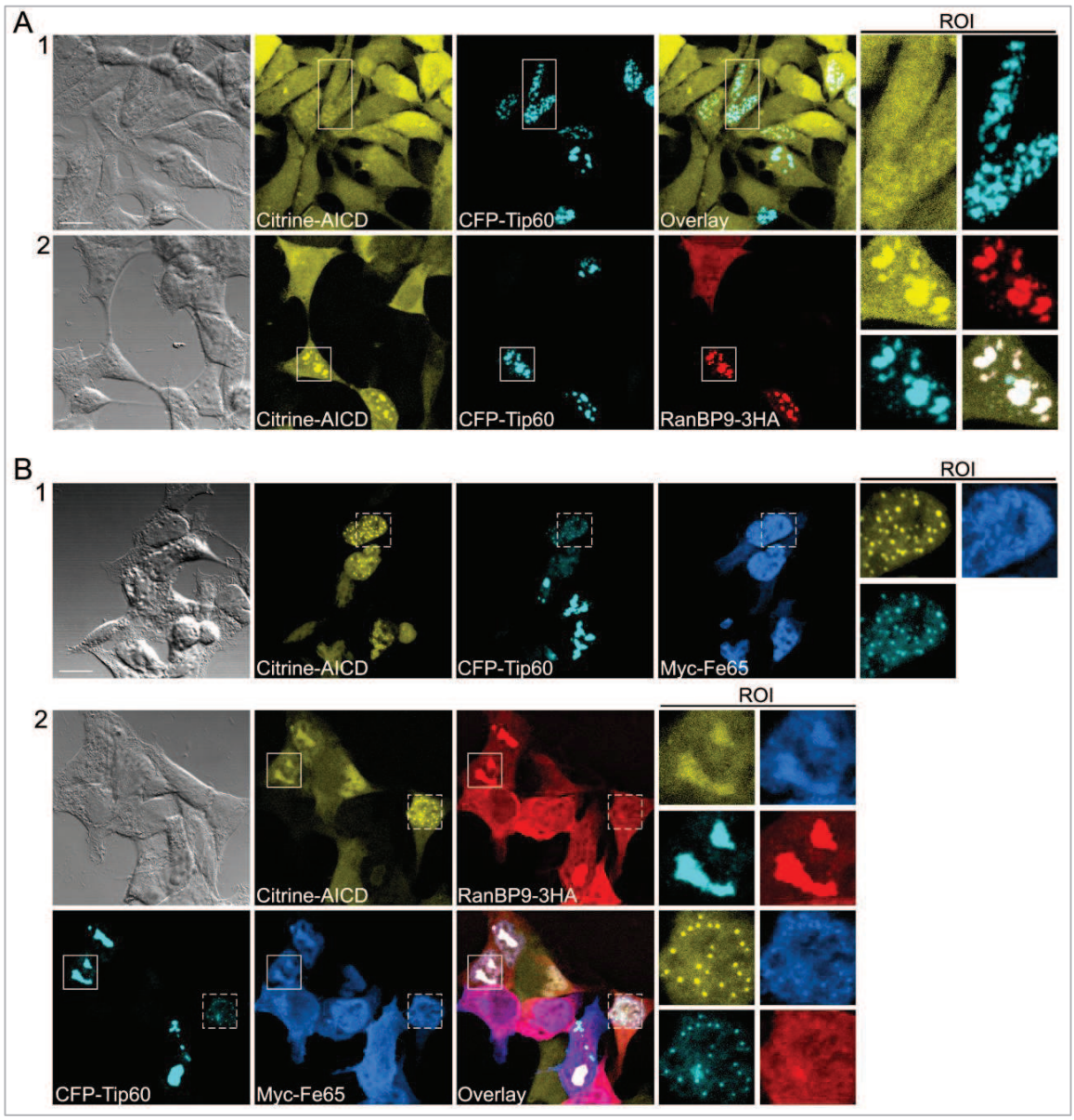

Figure V.5: RanBP9 targets AICD to Tip60 and prevents AFT-complex formation. (A) Transfection of CFP-Tip60 in HEK293 cells with inducible expression of Citrine-AICD did not change AICD subcellular localization (*panel 1;* number of imaged cells: 22 cells with Tip60 in speckles). Co-transfection of CFP-Tip60 and RanBP9-3HA relocated AICD to nuclear speckles (*panel 2;* number of imaged cells: 26 cells with Tip60, RanBP9 and AICD in speckles). ROIs show co-localization at nuclear speckles. (B) Co-expression of AICD, Fe65 and Tip60 generates AFT complexes that localize to nuclear spots (*panel* ; number of imaged cells: 16 cells with AICD, Fe65 and Tip60 in spots). ROI shows enlargement of nucleus with AFT spots. In panel 2, co-expression of RanBP9 with AICD, Fe65 and Tip60 show two distinct morphologies: in cells expressing faint RanBP9 fluorescence nuclear AFT spots are formed (*dashed boxes*); in cells expressing high levels of RanBP9 the AFT spot formation is abolished and AICD is relocated to the larger nuclear speckles, together with RanBP9, Fe65 and Tip60 (*full boxes*). Number of cells imaged: 14 cells with low or no RanBP9 and AICD, Fe65 and Tip60 in spots; 15 cells with more RanBP9 and AICD, Fe65 and Tip60 in spots; 22 cells with high RanBP9 fluorescence and all colocalize in speckles. Bars, 13 µm.

V.3.8 RanBP9 prevents nuclear signaling

To further analyze the inhibitory effect of RanBP9 on AFT spot formation we also co-expressed full-length APP labeled at the C-terminus with Citrine. In contrast with the inducible expression of AICD, the APP-derived AICD is not detected in speckles with Tip60 and RanBP9 (data not shown).

Simultaneous expression of APP, Fe65, Tip60 and RanBP9 prevents AFT spots in 100% of the imaged cells, either when transfecting wt APP (data not shown) or with the Swedish mutant (Fig. V.6A). Again, AFT spot formation was prevented and RanBP9 colocalized with Tip60 in speckles. Fe65 was also found in these speckles when APP expression was low (Fig. V.6A, lower cell) but with sufficiently high expression of APP, Fe65 was trapped outside the nucleus (Fig. 6A, upper cell). In any case, no APP-derived AICD could be detected in speckles, in contrast to the expression of AICD alone or the formation of AFT spots in the absence of RanBP9.

The irregular speckle nuclear structures, where RanBP9 is found with Tip60, were investigated previously and they did not co-localize, neither with nucleoli nor with splicing speckles (Konietzko et al., 2010). The AFT nuclear spots represent sites of transcription that are closely associated with splicing speckles, Cajal bodies and PML bodies, and also with *APP* and *KAI1* gene loci (Konietzko et al., 2010). Therefore, the consequences of preventing AFT complex formation by RanBP9 deserves further investigation.

When HeLa cells were transiently transfected with increasing amounts of GFP-tagged RanBP9, endogenous intracellular APP decreased significantly, as 1 µg caused a significant reduction of ~40% (P<0.001) compared to non-transfected control. APP protein levels were also significantly lower in GFP-RanBP9 cells (~30%, P<0.01) compared to the same amount (1 µg) of GFP empty vector (Fig. V.6B). The effect of RanBP9 on endogenous APP was also observed in COS-7 and SH-SY5Y cell lines, and was accompanied with a slight decrease of sAPP in the conditioned media (data not shown).

Since AICD regulates the expression of its own precursor APP (von Rotz et al., 2004), the decrease in endogenous APP expression levels could be an effect of RanBP9 in the regulation of transcription of AICD target genes. Therefore, we also evaluated the protein levels of other AICD target genes in RanBP9 transfected cells. Transfecting HeLa cells with increasing amounts of GFP-RanBP9 slightly decreased transgelin (P<0.1) and GSK-3β (P=0.1) protein levels (Fig. V.6C-D).

RanBP9 was recently described to increase BACE1 cleavage of APP and Aβ generation (Lakshmana et al., 2009) and under pathological conditions Aβ can mediate neurotoxic events. Moreover, AICD nuclear signaling occurs predominantly through the β-processing of APP (Goodger et al., 2009). Since RanBP9 transfection experiments reduced AICD nuclear signaling, we checked for the RanBP9 protein levels upon incubation with Aβ peptide. Rat cortical primary neurons treated for 24 h with 20 µM $A\beta_{25-35}$ showed a significant decrease of about ~43% ($P<0.05$) in endogenous RanBP9 compared to the control (Fig. V.6E). Taken together, these data show that RanBP9 decreases nuclear AICD-mediated signaling by preventing the assembly of nuclear spots, thereby decreasing the expression of AICD-regulated genes.

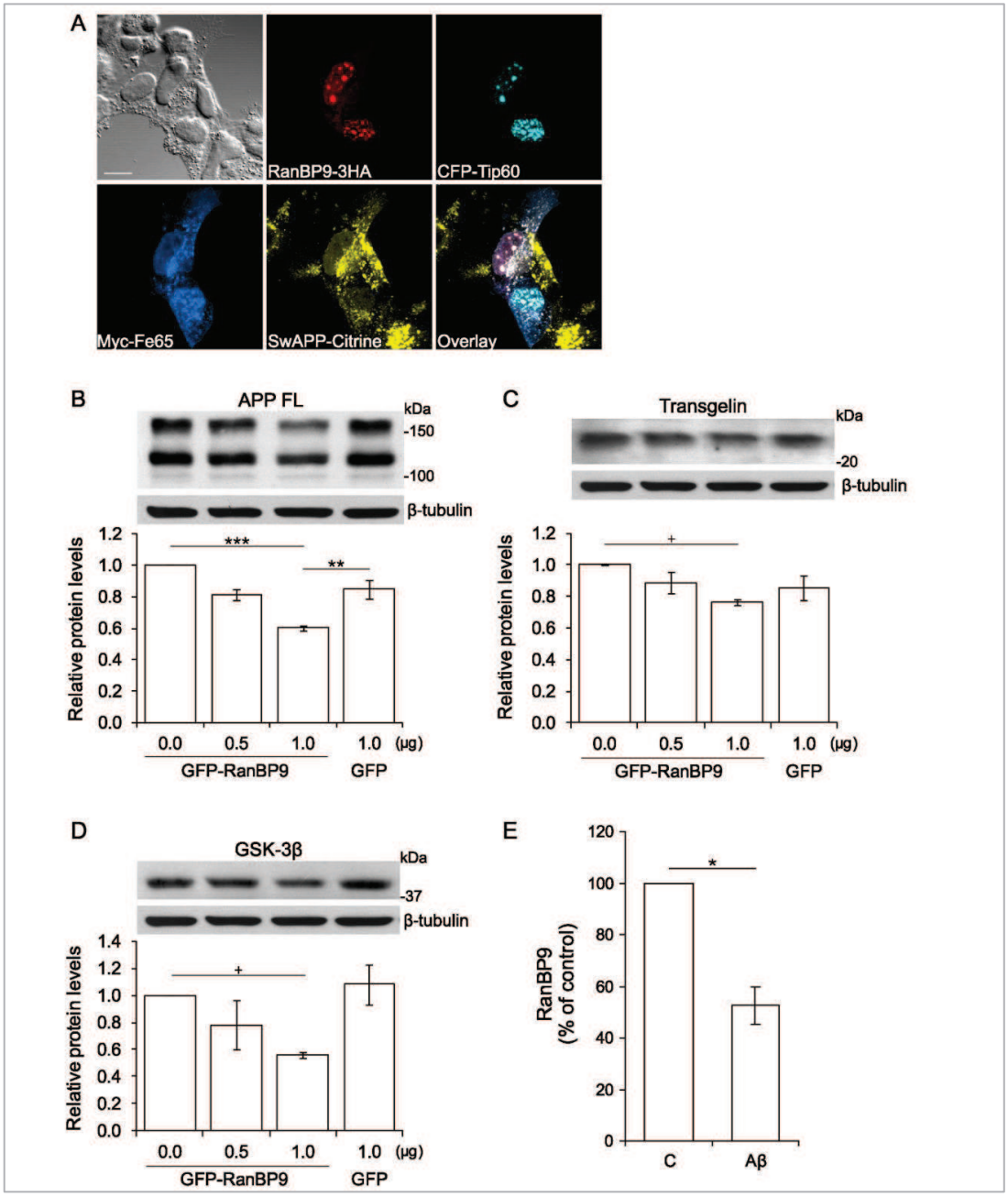

Figure V.6: RanBP9 prevents nuclear signaling. (A) Transfection of HEK293 cells with RanBP9-3HA, CFP-Tip60, Myc-Fe65 and SwAPP-citrine. AFT spots were not observed and RanBP9 and Tip60 colocalized in nuclear speckles. Number of imaged cells: 10 cells with speckles. Bar, 13 μm. (B) HeLa cells were transiently transfected with increasing amounts of GFP-RanBP9 (0.5 and 1.0 μg of DNA) and also with 1.0 μg of pEGFP-N1 empty vector. Holo APP levels in the lysates were determined using the 22C11 antibody (1:150). Values are expressed as mean±SE from three independent experiments (One way ANOVA followed by Tukey's multiple comparison test; ***, $P<0.001$; **, $P<0.01$; $^{+}$, $P\leq0.1$). (C) The same HeLa cells lysates were probed for the protein levels of transgelin (H-75 antibody; 1:400) (D) and GSK-3β (GSK3 antibody; 1:500). (E) Effect of Aβ on RanBP9 expression in rat cortical primary neurons. RanBP9 intracellular levels were evaluated upon incubation with 20 μM $A\beta_{25-35}$ using an anti-RanBP9 antibody (ab5295; 4 μg/ml). (C, Control; Aβ, Aβ exposure during 24 h). Values are expressed as mean±SE from two independent experiments (Unpaired t test; *, $P<0.05$).

V.4 DISCUSSION

The YTH screens performed to unravel the APP/AICD interactomes yielded numerous positive clones, including several hits on RanBP9 protein. RanBP9 (Ran binding protein 9) or RanBPM (Ran binding protein in the microtubule organizing centre) was initially identified in a YTH screen using Ran as bait. Ran is a small GTPase involved in nuclear import and export and spindle formation (Nakamura et al., 1998). RanBP9 is an evolutionarily conserved nucleocytoplasmic protein implicated as a scaffold for receptors associated with the Erk1/2 pathway (Wang et al., 2002a). Additionally, the presence of several functional domains, and the fact that RanBP9 was found in a 670 kDa multi-protein complex of unknown function, supports a role as a scaffolding protein (Nishitani et al., 2001; Kobayashi et al., 2007; Murrin and Talbot, 2007). RanBP9 interacts with the cytoplasmic domain of signaling receptors, including Met, Integrin LFA-1 and neuronal cell adhesion protein L1CAM (Wang et al., 2002a; Denti et al., 2004; Cheng et al., 2005). Through interaction with Plexin-A receptors, RanBP9 negatively regulates axonal outgrouth and branching (Togashi et al., 2006). RanBP9 is also involved in regulation of cell morphology, adhesion and migration (Dansereau and Lasko, 2008; Valiyaveettil et al., 2008).

RanBP9 was reported to co-immunoprecipitate with APP, LRP and BACE1 and to increase Aβ production (Lakshmana et al., 2009). We confirmed that RanBP9 binds APP directly and specifically *in vitro*, using GST pull-down assays. We also confirmed the association of RanBP9 with APP *in vivo* in several cell types and tissues. Moreover, we mapped the interaction to the intracellular domain of APP, specifically mediated by the ^{682}YENPTY^{687} motif, which comprises the canonical NPXY internalization signal (Chen et al., 1990). This amino acid sequence is found in several cell surface receptors, and is also responsible for the interaction with other APP binding partners, such as Fe65, suggesting that APP cannot bind simultaneously to RanBP9 and Fe65.

RanBP9 localizes both to the cytoplasm and nucleus, but other subcellular locations were also reported, such as the plasma membrane and nuclear speckles (Nishitani et al., 2001; Wang et al., 2002b; Denti et al., 2004). RanBP9 co-localized with APP and Fe65 at the plasma membrane, particularly at ruffled edges of cells that showed a characteristic lamellipodial structure. The fact that RanBP9 has only a minor localization to the ER or Golgi, which are extensively stained by APP and Fe65, suggests that RanBP9 associates with APP after ER/Golgi, i.e. at the cell membrane. APP was already known to associate with Fe65, Mena and β1-integrins in dynamic adhesion sites

known as focal complexes, and to have a role in actin-based cell migration and neurite outgrowth (Sabo et al., 2001, 2003). The colocalization of RanBP9 with APP and Fe65 at lamellipodia is in agreement its role in neurite growth and branching (Togashi et al., 2006), and in a recent report RanBP9 expression alters integrin-dependent cell adhesion and focal adhesion signaling, presumably due to the enhanced endocytosis of APP, LRP1 and β1-integrin (Woo et al., 2012).

Confocal microscopy showed co-localization of RanBP9 with AICD and Fe65 in the nucleus. Indeed, RanBP9 exhibited higher affinity for the AICD fragment than for the full-length APP in the YTH reporter system. A proteolytic fragment of RanBP9, RanBP9-N60, was identified recently by Lakshmana et al. (2010). RanBP9-N60 was increased in AD brains and interacted more strongly with APP/BACE1/LRP than full-length RanBP9, potentiating Aβ generation. Additionally, RanBP9-N60 lacks a nuclear localization signal and showed increased cytoplasmic *vs.* nuclear localization. The nuclear localization of full-length RanBP9 and high affinity for AICD, that we demonstrate here, is in agreement with the above mentioned study. Though it is worthwhile mentioning that proteolysis of RanBP9 was never observed under our experimental conditions, since N60 is formed only at low density and our cultures reached confluency.

Full length RanBP9 comprises multiple signaling domains: SPRY, LiSH, CTLH and CRA. Five proline-rich regions and a glycine stretch are also present at the N-terminus of RanBP9, which also contains six SH3-binding domains (Murrin and Talbot, 2007). Proline-rich regions interact with proline recognition domains, such as SH3, WW, EVH1, etc., and are common to signaling proteins involved in actin motility (Small et al., 2002). The function of SPRY domain is unknown, but it is thought to be involved in protein-protein interactions and RNA-binding. The suggested functions for some SPRY-containing proteins are RNA-binding, cell growth and differentiation (Ponting et al., 1997). The LisH (Lissencephaly type-1-like homology) domain has a conserved protein-binding function and is present in several proteins involved in microtubule dynamics, such as Lissencephaly-1, which has a key role in the control of neuronal migration (Emes and Ponting, 2001). C-terminally to LisH motif, there is a predicted α-helical sequence of unknown function, CTLH, that is adjacent to the LisH motif in several proteins (Emes and Ponting, 2001). The C-terminus of RanBP9 is very conserved and was described to comprise the CRA domain, whose function is unknown and is responsible for the interaction with the fragile X mental retardation protein (Menon et al., 2004). We determined that the sequence 136-460 of RanBP9 is necessary for its interaction with APP, which includes the SPRY, LiSH and CTLH domains. In a recent report, using cell-based co-immunoprecipitation assays, this region was narrowed down to the domains SPRY-LisH (Lakshmana et al., 2009).

The RanBP9-APP molecular association might exert diverse effects depending on the context or subcellular compartment. The high affinity for AICD and their co-localization in the nucleus suggested an influence of RanBP9 in the transcriptional activity of AFT complexes. The series of transfections and confocal analyses showed several RanBP9 effects. When RanBP9 was simultaneously expressed with Tip60 it underwent a striking change in its subcellular distribution. All of the RanBP9 was redirected from extranuclear localizations, i.e. at the plasma membrane, to the nuclear speckles where Tip60 resides. We confirmed the RanBP9-Tip60 interaction in the YTH system and the region encompassing the SPRY/LiSH/CTLH domains of RanBP9 was the minimal region necessary for the interaction with Tip60. Thus, as described for AICD-Fe65 complexes that cycle across the nuclear membrane, providing nuclear docking sites in the form of Tip60, can also retain RanBP9 in the nucleus.

Co-expression of AICD, Fe65 and Tip60 results in the formation of AFT complexes that localize to spherical nuclear spots, which were shown to represent transcription factories (von Rotz et al., 2004; Konietzko et al., 2010). Despite binding to AICD and Tip60, RanBP9 did not re-localize Tip60 to nuclear spots as does Fe65. We showed that the simultaneous interaction of RanBP9 with AICD and Tip60 targeted all components to irregular speckle structures. Thus, in contrast to Fe65 that relocates Tip60 and AICD to a spherical nuclear compartment involved in transcription, RanBP9 traps AICD in nuclear speckles that are not involved in transcription and might represent a storage compartment (Konietzko et al., 2010).

When RanBP9 was co-expressed with AICD, Fe65 and Tip60 we observed two opposite outcomes, depending on the expression levels. In most cells, RanBP9 expression prevented AFT spot formation, trapping AICD in the speckles occupied by Tip60. Only in cells with low RanBP9 co-expression, AFT spot formation was observed. Therefore, the levels of nuclear RanBP9 influence the localization and thus the function of AICD in the nucleus. AFT spots have been characterized as transcription factories, whereas Tip60 speckles do not co-localize with splicing speckles but rather represent a storage compartment (Konietzko et al., 2010). Based on these results we expected RanBP9 to have a negative effect on AICD-mediated transcription. Consequently, we saw RanBP9 expression reducing the expression of described AICD target genes such as APP (von Rotz et al., 2004); TAGLN, which encodes transgelin (Muller et al., 2007); and GSK3B, encoding GSK-3β (Kim et al., 2003; Ryan and Pimplikar, 2005). In line with a role in transcriptional regulation, RanBP9 was shown previously to interact with several transcription factors resulting in induction or repression of the transcriptional activity. For example, RanBP9 enhances

transactivation of androgen receptor, thyroid hormone receptor and p73α (Rao et al., 2002; Kramer et al., 2005; Poirier et al., 2006). In contrast, through its interaction with TrkA receptor, RanBP9 inhibits NGF-mediated nuclear factor of activated T cells (NFAT) dependent gene transcription (Yuan et al., 2006).

The suppression of AICD-mediated signaling by RanBP9 is intriguing because AICD signaling occurs mainly from the amyloidogenic processing of APP (Goodger et al., 2009), and RanBP9 was reported to increase Aβ generation and thus amyloidogenic processing (Lakshmana et al., 2009). In addition, we found that RanBP9 protein levels decrease upon incubation with Aβ. Thus, the interplay of RanBP9 and APP is very complex. Although RanBP9 promotes amyloidogenic cleavage of APP, it at the same time redirects the generated nuclear AICD signal to transcriptionally inactive compartments, by competing with Fe65 in binding to AICD and Tip60. RanBP9 is therefore able to uncouple amyloidogenic processing of APP from nuclear signaling. The promotion of β-secretase processing by RanBP9 is counter-balanced by the reduction of RanBP9 through the amyloidogenic pathway product Aβ, constituting a negative feedback loop.

In summary, our results and recent findings place RanBP9 as an important player in the multiple steps of APP signaling. RanBP9 is involved in a regulatory cycle with the pathogenic Aβ peptide, such that it increases Aβ production and hence, toxicity, being on the other hand down-regulated by Aβ. With regard to nuclear signaling by AICD, RanBP9 increases amyloidogenic processing, leading to an increased translocation of AICD to the nucleus. Despite resulting in increasing nuclear AICD levels, nuclear RanBP9 redirects AICD away from transcription factories and thus results in inhibition of AICD-mediated transcription. There is increasing evidence that dysregulation of AICD target genes in AD might contribute to the pathology of disease (Konietzko, 2011), therefore RanBP9 is bound to influence various aspects of the AD pathology induced by the different APP cleavage products.

CHAPTER VI. GENERAL DISCUSSION AND CONCLUSIONS

VI.1 OVERVIEW – APP IN THE ETIOLOGY OF ALZHEIMER'S DISEASE

AD is the most prevalent neurodegenerative disorder worldwide and the leading cause of dementia in the elderly. The incidence and prevalence of AD rise steadily with increasing longevity, and AD is already a significant health problem, particularly in developed countries (Culmsee and Landshamer, 2006; Hooli and Tanzi, 2009). AD patients typically present symptoms of global cognitive decline and memory loss. Pathologically, the disease is characterized by excessive deposition of amyloid deposits (senile plaques), neurofibrillary tangles, synapse and neuronal loss, and inflammation in the brain. The proteolytic processing of APP and production of Aβ, the major component of β-amyloid plaques, by β- and γ-secretases, are key events in the pathogenesis of AD. In addition, the hyperphosphorylation and aggregation of the microtubule-associated tau protein drive neurofibrillary tangle formation within neurons. The discovery of the *APP* gene was followed by the identification of missense mutations associated with familial, early-onset AD, most of which increase the ratio of Aβ42/Aβ40. The longer form of the peptide, Aβ42, is the most neurotoxic species as it enhances the aggregation of Aβ into neurotoxic oligomers and senile plaques, leading to the disruption of synaptic neurotransmission, neuronal cell death, and inflammation in the hippocampus and cerebral cortex, thus causing memory loss and global cognitive dysfunction.

Despite advances in understanding the role of APP processing in AD, the normal physiological function of this protein has proven more difficult to elucidate. Initial reports speculated that the protein is a cell-surface receptor (Kang *et al.*, 1987). The discovery of interacting proteins, genetic studies in animal models, and gene expression profiling have led to the identification of APP putative pathways associated with cellular and developmental changes.

VI.2 YTH CONTRIBUTIONS TO INTERACTOME MAPPING

Current medical treatments for AD are purely symptomatic and hardly effective (Citron 2010), Therefore, the complete understanding of the molecular mechanisms underlying AD is crucial for the development of novel therapies able to efficiently modify the biology of the disease. A full understanding of a biological system requires defining the interactions among its constituent molecular parts, such as the identification and characterization of PPIs, since proteins play a role in virtually every biological process. Most of the binary protein interaction data were generated through large-scale YTH screens. Despite the YTH technical limitations, such as incomplete coverage and the detection of false-positives, YTH data has provided the basis for many studies.

The first aim of this work was to identify brain proteins that interact with the AD core protein APP, and also with the dephosphorylation-mimicking mutants APP^{Y687F} and $AICD^{Y687F}$. Advantages of YTH screening include the detection of *in vivo* PPIs, high sensitivity to detect interactions between low abundant proteins and avoidance of expensive production of antibodies or protein purifications. The results presented here confirm that YTH screening is an important tool for identifying new PPIs. Despite it being considered as a robust method, some caution is required in the analysis of the results, and one should be aware of its limitations when discussing the biological significance of the detected interactions. Further interactome studies should be carried on only with interactions validated in the YTH system, and preferably each new interaction should be further demonstrated using with a different assay.

A human APP network comprised of the protein interactions was assembled through YTH screening, using as baits APP, APP^{Y687F} and $AICD^{Y687F}$. Hundreds of putative positive clones were isolated, of which 163 were identified by DNA sequencing and database searching (or restriction analysis in some cases). The majority of these clones, 118, matched to a protein coding sequence, yielding 31 different proteins. Several clones that did not match protein sequences where identified in these screens. These interacting peptide sequences may, in the future, be analyzed to potentially reveal APP-specific binding motifs. Similarly, the occurrence of mitochondrial proteins might simply reflect the presence of similar peptide sequences in the mitochondrial prey clones. Mitochondrial clones are unlikely to be genuine positives, nevertheless for all the corresponding mitochondrial genes there are polymorphisms associated with AD.

The recovery of two distinct library plasmids from the same clone is likely to happen, because in the library transformation, yeast can occasionally acquire more than one plasmid. This situation was overcome by restreaking the isolated putative positive clones two or three times, thus selecting for the plasmids that allow the cells to grow on the selective culture media used. Nevertheless, to verify that an isolated plasmid is responsible for the interaction, it should be re-tested for interaction with the bait, by co-transformation of yeast with the respective bait/prey plasmids. Subsequently, all interactions need to be confirmed by a different method, such as co-immunoprecipitation or *in vitro* methods, such as GST pull-down assay or blot overlay. Microscopy-based approaches, such as Bimolecular fluorescence complementation (BiFC) and Fluorescence resonance energy transfer (FRET), can validate a protein-protein physical interaction *in vivo* and confirm the simultaneous expression of the two binding partners in the same subcellular compartment. In the case of APP/RanBP9 interaction, confocal microscopy analysis also strengthened the PPI data and demonstrated new roles for the APP/RanBP9 interaction.

A series of experimental *in vitro* and *in vivo* analysis can be employed to validate each novel protein interaction, thus different strategies may be followed, taking into account that the main objective was to unravel the biology of the bait.

As with all detection methods, the YTH system is known to also detect some false positives, but false positive clones have been greatly reduced by the recent improvements in the YTH systems. Besides from large-scale screening, the YTH system was also employed in this work to investigate the protein domains responsible for selected protein interactions, e.g. RanBP9/AICD. The YTH system was also used to perform α-galactosidase activity assays, which allowed to relatively quantify PPI strengths between e.g. RanBP9 and AICD phospho-/dephospho-mimicking mutants, demonstrating that this interaction can be regulated by Tyr-687 phosphorylation.

The YTH has proven useful in the construction of large interaction networks, despite its limitations, and in identifying unsuspected interactions that may be confirmed by a variety of independent methods. The quality and sensitivity of the interaction map is crucial to the ability to draw conclusions from the interactions and recently improved YTH systems are of acceptable quality, yielding high quality data on direct binary interactions (Yu *et al.*, 2008; Braun *et al.*, 2009). However, many neuronal-specific interactions may be missed in these YTH screens due to posttranslational modifications, proteolytic processing, etc. Despite these limitations, the use of YTH data is widespread in complex diseases research: the inherited ataxias (Lim et al., 2006),

Huntington's disease (Goehler et al., 2004), Schizophrenia (Camargo et al., 2007) and AD (Soler-Lopez et al., 2011).

In a previous report, a curation of APP interactome was carried out, based on a complete survey of PPI databases and literature (Perreau et al., 2010). In this well conducted work, information about the APP isoform, proteolytic processing products involved in the interaction or the binding domain of APP involved was taken into account. Nevertheless, phosphorylation/dephosphorylation, a key cellular event that changes protein conformation and determines APP interactions with other proteins, should also be considered when analyzing the APP interactome. APP phosphorylation on Thr-668 abolishes the interaction with Fe65 (Ando et al., 2001) and phosphorylation of Tyr-682 promotes interaction with Shc (Tarr et al., 2002b). Additionally, Tamayev et al. (2009) have recently shown that phosphorylation of the cytoplasmic tail of APP on Thr-668 and Tyr-682 regulates APP interactions with several SH2-domain containing proteins. Nevertheless, in the ^{682}YENPTY^{687} protein interaction motif of AICD, Tyr-687, and not Tyr-682, is the consensual Tyr in the NPXY internalization signal. Moreover, Tyr-687 phosphorylation was shown to regulate APP intracellular trafficking, endocytosis and Aβ production (Rebelo et al., 2007a). For these reasons, Tyr-687 phosphorylation-mimicking mutants of APP/AICD were used as baits in the YTH screens, which revealed putative new interactions, that can potentially help to understand the biology of APP, and, ultimately, APP pathways leading to AD.

VI.3 THE APP INTERACTOME CAN BE REGULATED BY TYR-687 PHOSPHORYLATION

Bioinformatics analysis of the three APP/AICD interactomes generated in this study, and two additional screens from previous projects (Domingues, 2005; Capelo, 2010), revealed some distinct characteristics within and between the PPI networks. The interpretation of these PPI data sets, although speculative since validation of the putative new PPIs is necessary, is particularly relevant, since it allowed to characterize the physiological context of FL APP and its liberated cytoplasmic fragment, AICD. More importantly, the characterization of the protein networks around wt APP/AICD and dephospho-/phospho-mimicking mutants allowed to infer the relevance of Tyr-687 phosphorylation. The generated Tyr-687 mutations have already proved effective in elucidating the role of APP/AICD phosphorylation in AD. The APP^{Y687F} mutant, which mimics dephosphorylation at Tyr-687, was preferentially endocytosed and targeted for β-secretase cleavage, in contrast with the APP^{Y687E} phospho-mimicking mutant (Rebelo et al., 2007a). Interestingly, the functional proteomics analysis also pointed in the same direction, in particular the gene ontology terms under the domain 'Cellular component', where endosomes, the major site of β-secretase activity, occurs only in the Y687F-mutants interactomes. Nevertheless proteins interacting with dephospho-/phospho-mutants may interact with the wt protein and vice versa, as seen for Fe65 or RanBP9. Quantitative α-Gal assays could be carried out to compare the interaction strengths among wt AICD and several dephospho-/phospho-mimicking mutants, and elucidate the role of Tyr-687 phosphorylation in the regulation of AICD protein interactions. The same strategy could be applied to other AICD phosphorylatable residues.

In the YTH screen with FL APP, preys include proteins that interact with the FL molecule and proteins that interact *in vivo* with APP proteolytic fragments, such as AICD, which can explain the exclusively nuclear proteins found in this group. Again, APP interaction domains can be mapped using the YTH system, as was the case for APP/RanBP9 and RanBP9/Tip60.

The major goal of the functional proteomics approach was to identify the complete protein interaction network, or interactome, of each bait tested. Within PPI networks, proteins of similar function and cellular localization tend to cluster together (Bader and Hogue, 2002), making interactomics a powerful approach for inferring information with respect to protein function. Similarities in features such as posttranslational modifications could be expected for proteins with

similar function, but still they must perform their function in the context of the same cellular machinery and GO mining determined whether particular terms were disproportionately represented in a particular protein set. However, a poor protein characterization, or inaccuracy of the GO annotations may lead to incoherent results.

Full-length APP (wt and dephospho-mutant) share two protein nodes (HBEGF and RTN3) and are also closely associated by the 'Biological process' GO categories ('Signaling and regulation' is the most frequent category). These two interactomes are enriched in transmembrane proteins, which was also confirmed by protein domain analysis. Proteins interacting with the APP extracellular tail may act as extracellular ligands of APP. Heparin-binding EGF-like growth factor (HBEGF) was the only protein associated to the extracellular space.

APP^{Y687F} and $AICD^{Y687F}$ share one protein node (APBB1) and are also linked by the 'Cellular component' categories endosomes and synapses, potentially involved in AD pathology. Interestingly, $AICD^{Y687F}$ harbors all the AD risk genes found, while wt APP exhibits more interactions with proteins involved in non-AD pathologies. PPIs networks also showed that $AICD^{Y687E}$ and its binding partners are more distant from the AD genes, in contrast with the Y687F dephospho-mimicking mutants. Functional analyses of Y687F mutants interactomes (APP^{Y687F} and $AICD^{Y687F}$) are in agreement with previous data on enhanced endocytosis and Aβ production by APP^{Y687F}, but the detection of hyperphosphorylated AICD (including on Tyr-687) in AD brain, is intriguing in this context. Overall the data suggests that APP must be dephosphorylated at Tyr-687 for its efficient internalization and cleavage by β-secretase. However, increased phosphorylation on Tyr-687 and other AICD residues, detected by mass spectrometry in AD brain lysates (Lee et al., 2003), likely results from dysregulation of the cellular phosphorylation system that has been reported to occur in AD (Gandy et al., 1993; da Cruz e Silva et al., 1995; da Cruz e Silva and da Cruz e Silva, 2003).

The PPI maps around APP/AICD, in particular, the differences between wt, Y687E and Y687F mutants reflect the known information about the role of AICD Tyr-687 phosphorylation in an AD context. Therefore, integrating genetic and protein networks to infer pathway organization in complex diseases, such as AD, seems an appropriate approach to unravel the disease mechanisms and more effectively find targets for therapeutic intervention.

VI.4 A NOVEL ALTERNATIVELY SPLICED FE65 TRANSCRIPT WAS FOUND EXCLUSIVELY IN THE APP^{Y687F} INTERACTOME

The APP binding protein Fe65 is a major determinant of APP/AICD function. In the YTH screens performed, Fe65 was a frequent clone with wt AICD, AICD^{Y687F} and APP^{Y687F}. Interactions between Fe65 and wt AICD, AICD^{Y687F} and AICD^{Y687F} were validated in the YTH system and α-Gal quantitative assays showed that AICD^{Y687F}/Fe65 was stronger than wt AICD/Fe65 interaction. In contrast, AICD^{Y687E}/Fe65 showed a very low α-galactosidase activity. These results corroborate with clone frequencies in the YTH screens. Interestingly, 3 independent clones from YTH screen-2 (APP^{Y687F}) were identified as a new splice variant of Fe65, Fe65E3a, which arises from alternative splicing of the *FE65* gene.

In silico analysis and RT-PCR experiments revealed the complete sequence of the new exon 3a. The estimated size of mRNA, as given by Northern analysis, and the corresponding protein analyzed by Western blotting provided evidence for the full-length transcript sequence. This work led to a redefinition of the *FE65* gene to include the novel exon 3a, thus defining 16 exons for the *Fe65* gene. The mechanism of alternative splicing, giving rise to the Fe65E3a mRNA is a mutually exclusive event between exon 2 and exon 3a (exon 3a is spliced while exon 2 is skipped). The novel transcript, Fe65 transcript variant 3 or Fe65E3a, encodes isoform p60Fe65, which is exon 9-inclusive, consistently with its origin from a brain library.

Fe65E3a is predominantly expressed in the brain, both in human and rat, though at a lower level than the p97 mRNAs. Nevertheless, in some brain regions the ratios of Fe65E3a/total were noteworthy, e.g. in the cerebral cortex, and also in the cerebellum and temporal lobe, which includes the hippocampus and the amygdala. The hippocampus, cerebral cortex and amygdala play a major role in memory, cognition and behavior and are the brain regions mostly affected by the neuropathological hallmarks of AD (reviewed in Duyckaerts *et al.*, 2009).

Fe65E3a encodes the p60Fe65 isoform, which is detectable in higher levels in rat cortex and hippocampus primary cultures and was not detected in non-neuronal cells. These results characterize the new Fe65 splice variant and provided evidence that the novel transcript is the origin of the brain enriched 60 kDa Fe65 isoform of unknown origin, previously observed by other groups (Sabo et al., 2003; Wang et al., 2004; Cool et al., 2010). Wang et al. (2004) generated

p97Fe65 knockout mice and observed an upregulation of the p60Fe65 isoform which was attributed to translation of an alternative methionine on the p97Fe65 transcript (Wang *et al.*, 2004; Cool *et al.*, 2010). Interestingly, isoform-specific p97Fe65 KO mice did not exhibit neuroanatomical brain abnormalities, but impaired performance in learning and memory tests were evident at 14 months, suggesting that p97Fe65 has a role in cognition (Wang *et al.*, 2004). The lack of neuroanatomical alterations on the p97Fe65 KO mice might be due to elevated p60 isoform or to the expression of the Fe65L1 and Fe65L2, since it is likely that there is some redundancy among the different Fe65 protein family members. Conversely, the Fe65;Fe65L1 double knockout mice, deficient for two of the three Fe65 protein family members exhibited defective cortical neuronal migration during development, resembling cobblestone lissencephalies (Guenette *et al.*, 2006). This phenotype is similar to that observed in APP;APLP1;APLP2 triple KO mice (Herms *et al.*, 2004) and Mena KO mice (Lanier *et al.*, 1999), suggesting that APP, Fe65 and Mena act together in a neurodevelopment signaling pathway.

It is interesting to note that this novel transcript was identified when the YTH screen was carried out with the APP^{Y687F} bait. In the future, the role of Tyr-687 phosphorylation on the interaction with p60Fe65 can be addressed by quantitative α-Gal assays with APP/AICD phospho-mutants. Of note YTH-s2 (APP^{Y687F}) and YTH-s3 ($AICD^{Y687F}$) were carried out with human brain cDNA libraries from different origins, which could influence the screening outcomes. Nevertheless, YTH-s1 (wt APP) was carried out with the same cDNA library as YTH-s2, and still not a single Fe65 clone (either p60Fe65 or p97Fe65) was recovered with this bait.

The integrity of the N-terminally truncated WW domain of p60Fe65 can compromise the protein interactions occurring with this Fe65 domain (Mena, SET, P2X2, Nek6, c-Abl or 14-3-3γ) and was shown to influence the role of Fe65 in transcriptional activation (Duilio et al., 1991; Cao and Sudhof, 2004; Telese et al., 2005; Cool et al., 2010).

The functional importance of alternative splicing in neurons is well established (Lipscombe, 2005). Alternative splicing might be the primary mechanism for generating the spectrum of protein activities that support complex brain functions in the brains of higher organisms. Alternative splicing is controlled at the level of individual neurons to custom design proteins for optimal performance and splice isoforms can be modified during development and as neuronal activity changes (Lipscombe, 2005). Likewise, neuronal-specific Fe65 transcripts, produced by alternative splicing can be a regulatory mechanism for generating proteins involved in highly specialized tasks. Therefore, the alternatively spliced p60Fe65 isoform in the brain is an interesting candidate of neuronal physiological relevance.

VI.5 RANBP9, A NOVEL APP CYTOPLASMIC TAIL INTERACTING PROTEIN

RanBP9 was the most frequent clone in YTH-s4 ($AICD^{Y687E}$) and also appeared with wt APP, being the only common node between these two sub-networks, therefore this clone was chosen for further analysis. YTH interaction validations were carried out with both APP and AICD constructs, as well as with wt and phospho-mimicking mutants, and all exhibited positive interaction with RanBP9. Quantitative α-Gal assays demonstrated that RanBP9 interacted preferentially with wt AICD and with $AICD^{Y687F}$, when compared to $AICD^{Y687E}$. However, combining the α-Gal data obtained for the two prey clones, Fe65 and RanBP9, revealed that AICD and $AICD^{Y687F}$ interacted preferentially with Fe65, and $AICD^{Y687E}$ had more affinity for RanBP9, corroborating the results from YTH screens.

RanBP9 is an evolutionarily conserved nucleocytoplasmic protein implicated as a scaffolding protein in several signaling pathways. Full length RanBP9 comprises multiple signaling domains (Murrin and Talbot, 2007), such as SPRY, which is thought to be involved in protein-protein interactions and RNA-binding (Ponting et al., 1997). The LisH (Lissencephaly type-1-like homology) domain has a conserved protein-binding function and is present in several proteins involved in microtubule dynamics, such as Lissencephaly-1, which has a key role in the control of neuronal migration (Emes and Ponting, 2001). RanBP9 was reported to interact with the cytoplasmic domain of signaling receptors, including Met, Integrin LFA-1 and neuronal cell adhesion protein L1CAM (Wang et al., 2002a; Denti et al., 2004; Cheng et al., 2005). Through interaction with Plexin-A receptors, RanBP9 negatively regulates axonal outgrouth and branching (Togashi et al., 2006). RanBP9 is also involved in regulation of cell morphology, adhesion and migration (Dansereau and Lasko, 2008; Valiyaveettil et al., 2008).

The interaction between RanBP9 and APP/AICD was validated in the YTH system and was also confirmed in other systems, such as co-immunoprecipitation and microscopy analysis, which confirmed the association of RanBP9 with APP *in vivo* in several cell types and tissues. Moreover the RanBP9/APP interaction is direct and specific, as confirmed *in vitro* using GST pull-down assays. RanBP9 interaction with APP/AICD is specifically mediated by the ^{682}YENPTY^{687} motif, which also mediates the interaction with other APP binding partners, such as Fe65, suggesting that APP cannot bind simultaneously to RanBP9 and Fe65.

During the course of this work, RanBP9 was reported to co-immunoprecipitate with APP, LRP and BACE1 and to increase Aβ production (Lakshmana et al., 2009), however the interaction with AICD and phospho-mutants has not been previously shown.

RanBP9 co-localized with APP and Fe65 at the plasma membrane, particularly at ruffled edges of cells that showed a characteristic lamellipodial structure. The fact that RanBP9 has only a minor localization to the ER or Golgi, which are extensively stained by APP and Fe65, suggests that RanBP9 associates with APP after ER/Golgi, i.e. at the cell membrane. APP was already known to associate with Fe65, Mena and β1-integrins in dynamic adhesion sites known as focal complexes, and to have a role in actin-based cell migration and neurite outgrowth (Sabo et al., 2001, 2003). The colocalization of RanBP9 with APP and Fe65 at lamellipodia is in agreement with its role in neurite growth and branching (Togashi et al., 2006). Furthermore, in a recent report RanBP9 expression was shown to alter integrin-dependent cell adhesion and focal adhesion signaling, presumably due to the enhanced endocytosis of APP, LRP1 and β1-integrin (Woo et al., 2012).

Confocal microscopy showed co-localization of RanBP9 with AICD and Fe65 in the nucleus. Interestingly, in the YTH reporter system, RanBP9 exhibited higher affinity for the AICD fragment than for the full-length APP. A proteolytic fragment of RanBP9, RanBP9-N60, was identified recently by Lakshmana et al. (2010). RanBP9-N60 was increased in AD brains and interacted more strongly with APP/BACE1/LRP than full-length RanBP9, potentiating Aβ generation. Additionally, RanBP9-N60 lacks a nuclear localization signal and showed increased cytoplasmic *vs.* nuclear localization. The nuclear localization of full-length RanBP9 and high affinity for AICD, that we demonstrate here, is in agreement with the above mentioned study. Though it is worthwhile mentioning that proteolysis of RanBP9 was never observed under our experimental conditions, in fact N60 is formed only at low cell density and our experimental design made use of confluent cell cultures.

VI.6 RANBP9, AICD, FE65 AND TIP60 PROTEIN COMPLEXES IN NUCLEAR SIGNALING

The RanBP9-APP molecular association might exert diverse effects depending on the context or subcellular compartment. The high affinity for AICD and their co-localization in the nucleus suggested an influence of RanBP9 in the transcriptional activity of AFT complexes. Indeed, when RanBP9 was simultaneously expressed with Tip60 it underwent a striking change in its subcellular distribution. All of the RanBP9 was redirected from extranuclear localizations, i.e. the plasma membrane, to the Tip60-enriched nuclear speckles. Therefore, Tip60 can retain RanBP9 in the nucleus.

Co-expression of AICD, Fe65 and Tip60 results in the formation of AFT complexes that localize to spherical nuclear spots, which were shown to represent transcription factories (von Rotz et al., 2004; Konietzko et al., 2010). Despite binding to AICD and Tip60, RanBP9 did not re-localize Tip60 to nuclear spots as does Fe65. The simultaneous interaction of RanBP9 with AICD and Tip60 targeted all components to irregular speckle structures. Thus, in contrast to Fe65 that relocates Tip60 and AICD to a spherical nuclear compartment involved in transcription, RanBP9 traps AICD in nuclear speckles that are not involved in transcription and might represent a storage compartment (Konietzko et al., 2010).

When RanBP9 was co-expressed with AICD, Fe65 and Tip60 we observed two opposite outcomes, depending on the expression levels. In most cells, RanBP9 expression prevented AFT spot formation, trapping AICD in the speckles occupied by Tip60. Only in cells with low RanBP9 co-expression, AFT spot formation was observed. Therefore, the levels of nuclear RanBP9 influence the localization and thus the function of AICD in the nucleus. In similar transfection experiments where FL SwAPP fluorescently tagged was transfected with Fe65, Tip60 and RanBP9, AFT complex formation was completely abolished, in contrast with the nuclear spots that assemble in the absence of RanBP9.

As expected by the negative effect on AFT spot formation, RanBP9 expression reduced the protein levels of described AICD target genes such as *APP* (von Rotz et al., 2004); *TAGLN* (Muller et al., 2007); and *GSK3B* (Kim et al., 2003; Ryan and Pimplikar, 2005). RanBP9 was shown previously to interact with several transcription factors resulting in induction or repression of the transcriptional activity. For example, RanBP9 enhances the transactivation activity of androgen

receptor, thyroid hormone receptor and p73α (Rao et al., 2002; Kramer et al., 2005; Poirier et al., 2006). In contrast, through its interaction with TrkA receptor, RanBP9 inhibits NGF-mediated nuclear factor of activated T cells (NFAT) dependent gene transcription (Yuan et al., 2006). These results also suggest a role for RanBP9 in AICD-mediated transcriptional regulation.

The suppression of AICD-mediated signaling by RanBP9 is intriguing because AICD signaling occurs mainly from the amyloidogenic processing of APP (Goodger et al., 2009), and RanBP9 was reported to increase Aβ generation and thus amyloidogenic processing (Lakshmana et al., 2009). In addition, RanBP9 protein levels decrease upon incubation with Aβ. Thus, the interplay of RanBP9 and APP is very complex. Although RanBP9 promotes amyloidogenic cleavage of APP, at the same time it redirects the generated nuclear AICD signal to transcriptionally inactive compartments, by competing with Fe65 in binding to AICD and Tip60. RanBP9 is therefore able to uncouple amyloidogenic processing of APP from nuclear signaling. The promotion of β-secretase processing by RanBP9 is counter-balanced by the reduction of RanBP9 through the amyloidogenic pathway product Aβ, constituting a negative feedback loop.

In summary, these results and recent findings place RanBP9 as an important player in the multiple steps of APP signaling. RanBP9 is involved in a regulatory cycle with the pathogenic Aβ peptide, such that it increases Aβ production and hence, toxicity, being on the other hand down-regulated by Aβ. Nuclear RanBP9 redirects AICD away from transcription factories and thus results in inhibition of AICD-mediated transcription. There is increasing evidence that dysregulation of AICD target genes in AD might contribute to the pathology of the disease (Konietzko, 2011), therefore RanBP9 is likely to influence various aspects of the AD pathology induced by the different APP cleavage products.

VI.7 CONCLUDING REMARKS

Despite the considerable complexities of AD genetics, tremendous progress has been made towards our understanding of the etiological and pathophysiological mechanisms leading to neurodegeneration.

In conclusion, this work resulted in:

- the characterization of a new splice variant of the APP binding protein Fe65, relevant for neuronal function;
- the characterization of a novel interaction between RanBP9 and AICD that can be regulated by Tyr-687 phosphorylation;
- the identification of a novel interaction between RanBP9 and the histone acetyltransferase Tip60, and also the triple complex AICD/RanBP9/Tip60, relevant for nuclear signaling;
- the identification of novel putative interactions with APP/AICD, and their phospho-mutants, which elucidate APP pathways leading to AD pathology.

In particular, this work still leaves some open questions that will need to be pursued in the future, such as the validation of YTH clones. Investigating the effects of RanBP9 on AICD-mediated transcription also seems to be a promising field in the context of this work.

Interactomics-based approaches revealed that Tyr-687 phosphorylation can regulate the interaction of APP with synaptic proteins. RIP signaling from synapse to the nucleus involves active retrograde transport of signaling endosomes, and again Y687F interactomes have proteins that localize to endocytic vesicles. The potential role of Tyr-687 phosphorylation state, acting as a ''biochemical switch'' and changing the molecular composition of APP complexes, presents an interesting possibility to revert AD pathological events, deserving further exploration.

Overall, being able to decipher the APP/AICD interactome shaped by the phosphorylation state of the several AICD phosphorylatable residues is expected to continue to elucidate APP pathways leading to amyloid deposition and neurodegeneration. As such the work here described brings us nearer to unravelling the physiological functions of APP. This in turn is of potential

significant relevance in the pathology of AD, and for the design of effective novel therapeutic strategies.

REFERENCES

Aisen, P. S., Cummings, J. and Schneider, L. S. (2012) Symptomatic and nonamyloid/tau based pharmacologic treatment for Alzheimer disease. *Cold Spring Harb Perspect Med* **2,** a006395.

Alfarano, C., Andrade, C. E., Anthony, K., Bahroos, N., Bajec, M., Bantoft, K., Betel, D., Bobechko, B., Boutilier, K., Burgess, E., Buzadzija, K., Cavero, R., D'Abreo, C., Donaldson, I., Dorairajoo, D., Dumontier, M. J., Dumontier, M. R., Earles, V., Farrall, R., Feldman, H., Garderman, E., Gong, Y., Gonzaga, R., Grytsan, V., Gryz, E., Gu, V., Haldorsen, E., Halupa, A., Haw, R., Hrvojic, A., Hurrell, L., Isserlin, R., Jack, F., Juma, F., Khan, A., Kon, T., Konopinsky, S., Le, V., Lee, E., Ling, S., Magidin, M., Moniakis, J., Montojo, J., Moore, S., Muskat, B., Ng, I., Paraiso, J. P., Parker, B., Pintilie, G., Pirone, R., Salama, J. J., Sgro, S., Shan, T., Shu, Y., Siew, J., Skinner, D., Snyder, K., Stasiuk, R., Strumpf, D., Tuekam, B., Tao, S., Wang, Z., White, M., Willis, R., Wolting, C., Wong, S., Wrong, A., Xin, C., Yao, R., Yates, B., Zhang, S., Zheng, K., Pawson, T., Ouellette, B. F. F. and Hogue, C. W. V. (2005) The Biomolecular Interaction Network Database and related tools 2005 update. *Nucleic Acids Research* **33,** D418-D424.

Allinson, T. M., Parkin, E. T., Turner, A. J. and Hooper, N. M. (2003) ADAMs family members as amyloid precursor protein alpha-secretases. *J Neurosci Res* **74,** 342-352.

Altschul, S. F., Gish, W., Miller, W., Myers, E. W. and Lipman, D. J. (1990) Basic local alignment search tool. *J Mol Biol* **215,** 403-410.

Alves da Costa, C., Sunyach, C., Pardossi-Piquard, R., Sevalle, J., Vincent, B., Boyer, N., Kawarai, T., Girardot, N., St George-Hyslop, P. and Checler, F. (2006) Presenilin-dependent gamma-secretase-mediated control of p53-associated cell death in Alzheimer's disease. *J Neurosci* **26,** 6377-6385.

Alzheimer, A. (1907) Über eine eigenartige Erkrankung der Hirnrinde. *Allgemeine Zeitschrift fur Psychiatrie und Psychisch-gerichtliche Medizin* **64,** 146-148.

Alzheimer, A., Stelzmann, R. A., Schnitzlein, H. N. and Murtagh, F. R. (1995) An English translation of Alzheimer's 1907 paper, "Uber eine eigenartige Erkankung der Hirnrinde". *Clin Anat* **8,** 429-431.

Andersen, O. M., Reiche, J., Schmidt, V., Gotthardt, M., Spoelgen, R., Behlke, J., von Arnim, C. A. F., Breiderhoff, T., Jansen, P., Wu, X., Bales, K. R., Cappai, R., Masters, C. L., Gliemann, J., Mufson, E. J., Hyman, B. T., Paul, S. M., Nykjær, A. and Willnow, T. E. (2005) Neuronal sorting protein-related receptor sorLA/LR11 regulates processing of the amyloid precursor protein. *Proceedings of the National Academy of Sciences of the United States of America* **102,** 13461-13466.

Anderson, S., Bankier, A. T., Barrell, B. G., de Bruijn, M. H., Coulson, A. R., Drouin, J., Eperon, I. C., Nierlich, D. P., Roe, B. A., Sanger, F., Schreier, P. H., Smith, A. J., Staden, R. and Young, I. G. (1981) Sequence and organization of the human mitochondrial genome. *Nature* **290,** 457-465.

Ando, K., Iijima, K. I., Elliott, J. I., Kirino, Y. and Suzuki, T. (2001) Phosphorylation-dependent regulation of the interaction of amyloid precursor protein with Fe65 affects the production of beta-amyloid. *J Biol Chem* **276,** 40353-40361.

Annaert, W. and De Strooper, B. (1999) Presenilins: molecular switches between proteolysis and signal transduction. *Trends Neurosci* **22,** 439-443.

Annaert, W. and De Strooper, B. (2002) A cell biological perspective on Alzheimer's disease. *Annu Rev Cell Dev Biol* **18,** 25-51.

Ashburner, M., Ball, C. A., Blake, J. A., Botstein, D., Butler, H., Cherry, J. M., Davis, A. P., Dolinski, K., Dwight, S. S., Eppig, J. T., Harris, M. A., Hill, D. P., Issel-Tarver, L., Kasarskis, A., Lewis, S., Matese, J. C., Richardson, J. E., Ringwald, M., Rubin, G. M. and Sherlock, G. (2000) Gene ontology: tool for the unification of biology. The Gene Ontology Consortium. *Nat Genet* **25,** 25-29.

Bader, G. D. and Hogue, C. W. (2002) Analyzing yeast protein-protein interaction data obtained from different sources. *Nat Biotechnol* **20,** 991-997.

Baek, S. H., Ohgi, K. A., Rose, D. W., Koo, E. H., Glass, C. K. and Rosenfeld, M. G. (2002) Exchange of N-CoR corepressor and Tip60 coactivator complexes links gene expression by NF-kappaB and beta-amyloid precursor protein. *Cell* **110,** 55-67.

Ball, M. J. and Lo, P. (1977) Granulovacuolar degeneration in the ageing brain and in dementia. *J Neuropathol Exp Neurol* **36,** 474-487.

Barbato, C., Canu, N., Zambrano, N., Serafino, A., Minopoli, G., Ciotti, M. T., Amadoro, G., Russo, T. and Calissano, P. (2005) Interaction of Tau with Fe65 links tau to APP. *Neurobiol Dis* **18,** 399-408.

Barger, S. W. and Harmon, A. D. (1997) Microglial activation by Alzheimer amyloid precursor protein and modulation by apolipoprotein E. *Nature* **388,** 878-881.

Beal, M. F., Lang, A. E. and Ludolph, A. C. (2005) *Neurodegenerative diseases: neurobiology, pathogenesis, and therapeutics*. Cambridge University Press.

Beher, D., Hesse, L., Masters, C. L. and Multhaup, G. (1996) Regulation of amyloid protein precursor (APP) binding to collagen and mapping of the binding sites on APP and collagen type I. *J Biol Chem* **271,** 1613-1620.

Bell, T. J., Miyashiro, K. Y., Sul, J.-Y., Buckley, P. T., Lee, M. T., McCullough, R., Jochems, J., Kim, J., Cantor, C. R., Parsons, T. D. and Eberwine, J. H. (2010) Intron retention facilitates splice variant diversity in calcium-activated big potassium channel populations. *Proceedings of the National Academy of Sciences* **107,** 21152-21157.

Belyaev, N. D., Kellett, K. A., Beckett, C., Makova, N. Z., Revett, T. J., Nalivaeva, N. N., Hooper, N. M. and Turner, A. J. (2010) The transcriptionally active amyloid precursor protein (APP) intracellular domain is preferentially produced from the 695 isoform of APP in a {beta}-secretase-dependent pathway. *J Biol Chem* **285,** 41443-41454.

Bennecib, M., Gong, C. X., Grundke-Iqbal, I. and Iqbal, K. (2000) Role of protein phosphatase-2A and -1 in the regulation of GSK-3, cdk5 and cdc2 and the phosphorylation of tau in rat forebrain. *FEBS Lett* **485,** 87-93.

Bertram, L. (2011) Alzheimer's Genetics in the GWAS Era: A Continuing Story of 'Replications and Refutations'. *Current Neurology and Neuroscience Reports* **11,** 246-253.

Bertram, L., McQueen, M. B., Mullin, K., Blacker, D. and Tanzi, R. E. (2007) Systematic meta-analyses of Alzheimer disease genetic association studies: the AlzGene database. *Nat Genet* **39,** 17-23.

Bertram, L. and Tanzi, R. E. (2004) Alzheimer's disease: one disorder, too many genes? *Hum Mol Genet* **13 Spec No 1,** R135-141.

Beyer, A. S., von Einem, B., Schwanzar, D., Keller, I. E., Hellrung, A., Thal, D. R., Ingelsson, M., Makarova, A., Deng, M., Chhabra, E. S., Propper, C., Bockers, T. M., Hyman, B. T. and von Arnim, C. A. (2010) Engulfment adapter PTB domain containing 1 interacts with and affects processing of the amyloid-beta precursor protein. *Neurobiol Aging*.

Biederer, T., Cao, X., Sudhof, T. C. and Liu, X. (2002) Regulation of APP-dependent transcription complexes by Mint/X11s: differential functions of Mint isoforms. *J Neurosci* **22,** 7340-7351.

Biere, A. L., Ostaszewski, B., Zhao, H., Gillespie, S., Younkin, S. G. and Selkoe, D. J. (1995) Co-expression of beta-amyloid precursor protein (betaAPP) and apolipoprotein E in cell culture: analysis of betaAPP processing. *Neurobiol Dis* **2,** 177-187.

Bimonte, M., Gianni, D., Allegra, D., Russo, T. and Zambrano, N. (2004) Mutation of the feh-1 gene, the Caenorhabditis elegans orthologue of mammalian Fe65, decreases the expression of two acetylcholinesterase genes. *Eur J Neurosci* **20,** 1483-1488.

Blennow, K., Hampel, H., Weiner, M. and Zetterberg, H. (2010) Cerebrospinal fluid and plasma biomarkers in Alzheimer disease. *Nat Rev Neurol* **6,** 131-144.

Borg, J. P., Ooi, J., Levy, E. and Margolis, B. (1996) The phosphotyrosine interaction domains of X11 and FE65 bind to distinct sites on the YENPTY motif of amyloid precursor protein. *Mol Cell Biol* **16,** 6229-6241.

Borg, J. P., Straight, S. W., Kaech, S. M., de Taddeo-Borg, M., Kroon, D. E., Karnak, D., Turner, R. S., Kim, S. K. and Margolis, B. (1998a) Identification of an evolutionarily conserved heterotrimeric protein complex involved in protein targeting. *J Biol Chem* **273,** 31633-31636.

Borg, J. P., Yang, Y., De Taddeo-Borg, M., Margolis, B. and Turner, R. S. (1998b) The X11alpha protein slows cellular amyloid precursor protein processing and reduces Abeta40 and Abeta42 secretion. *J Biol Chem* **273,** 14761-14766.

Braak, H. and Braak, E. (1991) Neuropathological stageing of Alzheimer-related changes. *Acta Neuropathol* **82,** 239-259.

Braun, P., Tasan, M., Dreze, M., Barrios-Rodiles, M., Lemmens, I., Yu, H., Sahalie, J. M., Murray, R. R., Roncari, L., de Smet, A. S., Venkatesan, K., Rual, J. F., Vandenhaute, J., Cusick, M. E., Pawson, T., Hill, D. E., Tavernier, J., Wrana, J. L., Roth, F. P. and Vidal, M. (2009) An experimentally derived confidence score for binary protein-protein interactions. *Nat Methods* **6,** 91-97.

Breen, K. C. (1992) APP-collagen interaction is mediated by a heparin bridge mechanism. *Mol Chem Neuropathol* **16,** 109-121.

Bressler, S. L., Gray, M. D., Sopher, B. L., Hu, Q., Hearn, M. G., Pham, D. G., Dinulos, M. B., Fukuchi, K., Sisodia, S. S., Miller, M. A., Disteche, C. M. and Martin, G. M. (1996) cDNA cloning and chromosome mapping of the human Fe65 gene: interaction of the conserved cytoplasmic domains of the human beta-amyloid precursor protein and its homologues with the mouse Fe65 protein. *Hum Mol Genet* **5,** 1589-1598.

Brewer, G. J., Torricelli, J. R., Evege, E. K. and Price, P. J. (1993) Optimized survival of hippocampal neurons in B27-supplemented Neurobasal, a new serum-free medium combination. *J Neurosci Res* **35,** 567-576.

Brion, J. P., Couck, A. M., Passareiro, E. and Flament-Durand, J. (1985) Neurofibrillary tangles of Alzheimer's disease: an immunohistochemical study. *J Submicrosc Cytol* **17,** 89-96.

Brown, M. S., Ye, J., Rawson, R. B. and Goldstein, J. L. (2000) Regulated Intramembrane Proteolysis: A Control Mechanism Conserved from Bacteria to Humans. *Cell* **100,** 391-398.

Bruni, P., Minopoli, G., Brancaccio, T., Napolitano, M., Faraonio, R., Zambrano, N., Hansen, U. and Russo, T. (2002) Fe65, a ligand of the Alzheimer's beta-amyloid precursor protein, blocks cell cycle progression by down-regulating thymidylate synthase expression. *J Biol Chem* **277,** 35481-35488.

Bu, G., Cam, J. and Zerbinatti, C. (2006) LRP in Amyloid-β Production and Metabolism. *Annals of the New York Academy of Sciences* **1086,** 35-53.

Burge, C. and Karlin, S. (1997) Prediction of complete gene structures in human genomic DNA. *J Mol Biol* **268,** 78-94.

Burge, C. B. and Karlin, S. (1998) Finding the genes in genomic DNA. *Curr Opin Struct Biol* **8,** 346-354.

Buxbaum, J. D., Liu, K. N., Luo, Y., Slack, J. L., Stocking, K. L., Peschon, J. J., Johnson, R. S., Castner, B. J., Cerretti, D. P. and Black, R. A. (1998) Evidence that tumor necrosis factor alpha converting enzyme is involved in regulated alpha-secretase cleavage of the Alzheimer amyloid protein precursor. *J Biol Chem* **273,** 27765-27767.

Caccamo, A., Oddo, S., Sugarman, M. C., Akbari, Y. and LaFerla, F. M. (2005) Age- and region-dependent alterations in Abeta-degrading enzymes: implications for Abeta-induced disorders. *Neurobiol Aging* **26,** 645-654.

Caille, I., Allinquant, B., Dupont, E., Bouillot, C., Langer, A., Muller, U. and Prochiantz, A. (2004) Soluble form of amyloid precursor protein regulates proliferation of progenitors in the adult subventricular zone. *Development* **131,** 2173-2181.

Camargo, L. M., Collura, V., Rain, J. C., Mizuguchi, K., Hermjakob, H., Kerrien, S., Bonnert, T. P., Whiting, P. J. and Brandon, N. J. (2007) Disrupted in Schizophrenia 1 Interactome: evidence for the close connectivity of risk genes and a potential synaptic basis for schizophrenia. *Mol Psychiatry* **12,** 74-86.

Cao, Q., Huang, Y. S., Kan, M. C. and Richter, J. D. (2005) Amyloid precursor proteins anchor CPEB to membranes and promote polyadenylation-induced translation. *Mol Cell Biol* **25,** 10930-10939.

Cao, X. and Sudhof, T. C. (2001) A transcriptionally [correction of transcriptively] active complex of APP with Fe65 and histone acetyltransferase Tip60. *Science* **293,** 115-120.

Cao, X. and Sudhof, T. C. (2004) Dissection of amyloid-beta precursor protein-dependent transcriptional transactivation. *J Biol Chem* **279,** 24601-24611.

Capelo, A. B. (2010) Fe65 is a predominant protein in APP interactome. Master Thesis, University of Aveiro, Portugal.

Caporaso, G. L., Gandy, S. E., Buxbaum, J. D., Ramabhadran, T. V. and Greengard, P. (1992) Protein phosphorylation regulates secretion of Alzheimer beta/A4 amyloid precursor protein. *Proc Natl Acad Sci U S A* **89,** 3055-3059.

Causier, B. (2004) Studying the interactome with the yeast two-hybrid system and mass spectrometry. *Mass Spectrom Rev* **23,** 350-367.

Causier, B. and Davies, B. (2002) Analysing protein-protein interactions with the yeast two-hybrid system. *Plant Mol Biol* **50,** 855-870.

Chagnon, P., Gee, M., Filion, M., Robitaille, Y., Belouchi, M. and Gauvreau, D. (1999) Phylogenetic analysis of the mitochondrial genome indicates significant differences between patients with Alzheimer disease and controls in a French-Canadian founder population. *Am J Med Genet* **85,** 20-30.

Chang, K. A., Kim, H. S., Ha, T. Y., Ha, J. W., Shin, K. Y., Jeong, Y. H., Lee, J. P., Park, C. H., Kim, S., Baik, T. K. and Suh, Y. H. (2006) Phosphorylation of amyloid precursor protein (APP) at Thr668 regulates the nuclear translocation of the APP intracellular domain and induces neurodegeneration. *Mol Cell Biol* **26,** 4327-4338.

Checler, F. (2001) The multiple paradoxes of presenilins. *J Neurochem* **76,** 1621-1627.

Chen, F., Gu, Y., Hasegawa, H., Ruan, X., Arawaka, S., Fraser, P., Westaway, D., Mount, H. and St George-Hyslop, P. (2002) Presenilin 1 mutations activate gamma 42-secretase but reciprocally inhibit epsilon-secretase cleavage of amyloid precursor protein (APP) and S3-cleavage of notch. *J Biol Chem* **277,** 36521-36526.

Chen, T. Y., Liu, P. H., Ruan, C. T., Chiu, L. and Kung, F. L. (2006) The intracellular domain of amyloid precursor protein interacts with flotillin-1, a lipid raft protein. *Biochem Biophys Res Commun* **342,** 266-272.

Chen, W. J., Goldstein, J. L. and Brown, M. S. (1990) NPXY, a sequence often found in cytoplasmic tails, is required for coated pit-mediated internalization of the low density lipoprotein receptor. *J Biol Chem* **265,** 3116-3123.

Cheng, L., Lemmon, S. and Lemmon, V. (2005) RanBPM is an L1-interacting protein that regulates L1-mediated mitogen-activated protein kinase activation. *J Neurochem* **94,** 1102-1110.

Chien, C. T., Bartel, P. L., Sternglanz, R. and Fields, S. (1991) The two-hybrid system: a method to identify and clone genes for proteins that interact with a protein of interest. *Proc Natl Acad Sci U S A* **88,** 9578-9582.

Chin, J., Massaro, C. M., Palop, J. J., Thwin, M. T., Yu, G. Q., Bien-Ly, N., Bender, A. and Mucke, L. (2007) Reelin depletion in the entorhinal cortex of human amyloid precursor protein transgenic mice and humans with Alzheimer's disease. *J Neurosci* **27,** 2727-2733.

Chow, N., Korenberg, J. R., Chen, X. N. and Neve, R. L. (1996) APP-BP1, a novel protein that binds to the carboxyl-terminal region of the amyloid precursor protein. *J Biol Chem* **271,** 11339-11346.

Chung, J. A. and Cummings, J. L. (2000) Neurobehavioral and neuropsychiatric symptoms in Alzheimer's disease: characteristics and treatment. *Neurol Clin* **18,** 829-846.

Citron, M. (2010) Alzheimer's disease: strategies for disease modification. *Nat Rev Drug Discov* **9,** 387-398.

Consortium, T. U. (2012) Reorganizing the protein space at the Universal Protein Resource (UniProt). *Nucleic Acids Research* **40,** D71-D75.

Cook, J. J., Wildsmith, K. R., Gilberto, D. B., Holahan, M. A., Kinney, G. G., Mathers, P. D., Michener, M. S., Price, E. A., Shearman, M. S., Simon, A. J., Wang, J. X., Wu, G., Yarasheski, K. E. and Bateman, R. J. (2010) Acute γ-Secretase Inhibition of Nonhuman Primate CNS Shifts Amyloid Precursor Protein

(APP) Metabolism from Amyloid-β Production to Alternative APP Fragments without Amyloid-β Rebound. *The Journal of Neuroscience* **30,** 6743-6750.

Cool, B. H., Zitnik, G., Martin, G. M. and Hu, Q. (2010) Structural and functional characterization of a novel FE65 protein product up-regulated in cognitively impaired FE65 knockout mice. *J Neurochem* **112,** 410-419.

Coon, K. D., Valla, J., Szelinger, S., Schneider, L. E., Niedzielko, T. L., Brown, K. M., Pearson, J. V., Halperin, R., Dunckley, T., Papassotiropoulos, A., Caselli, R. J., Reiman, E. M. and Stephan, D. A. (2006) Quantitation of heteroplasmy of mtDNA sequence variants identified in a population of AD patients and controls by array-based resequencing. *Mitochondrion* **6,** 194-210.

Corder, E. H., Saunders, A. M., Risch, N. J., Strittmatter, W. J., Schmechel, D. E., Gaskell, P. C., Jr., Rimmler, J. B., Locke, P. A., Conneally, P. M., Schmader, K. E. and et al. (1994) Protective effect of apolipoprotein E type 2 allele for late onset Alzheimer disease. *Nat Genet* **7,** 180-184.

Corral-Debrinski, M., Horton, T., Lott, M. T., Shoffner, J. M., McKee, A. C., Beal, M. F., Graham, B. H. and Wallace, D. C. (1994) Marked changes in mitochondrial DNA deletion levels in Alzheimer brains. *Genomics* **23,** 471-476.

Coulson, E. J., Paliga, K., Beyreuther, K. and Masters, C. L. (2000) What the evolution of the amyloid protein precursor supergene family tells us about its function. *Neurochem Int* **36,** 175-184.

Cruts, M. and Van Broeckhoven, C. (1998) Molecular genetics of Alzheimer's disease. *Ann Med* **30,** 560-565.

Culmsee, C. and Landshamer, S. (2006) Molecular insights into mechanisms of the cell death program: role in the progression of neurodegenerative disorders. *Curr Alzheimer Res* **3,** 269-283.

Cupers, P., Orlans, I., Craessaerts, K., Annaert, W. and De Strooper, B. (2001) The amyloid precursor protein (APP)-cytoplasmic fragment generated by gamma-secretase is rapidly degraded but distributes partially in a nuclear fraction of neurones in culture. *J Neurochem* **78,** 1168-1178.

da Cruz e Silva, E. F. and da Cruz e Silva, O. A. (2003) Protein phosphorylation and APP metabolism. *Neurochem Res* **28,** 1553-1561.

da Cruz e Silva, E. F., da Cruz e Silva, O. A., Zaia, C. T. and Greengard, P. (1995) Inhibition of protein phosphatase 1 stimulates secretion of Alzheimer amyloid precursor protein. *Mol Med* **1,** 535-541.

da Cruz e Silva, O. A., Fardilha, M., Henriques, A. G., Rebelo, S., Vieira, S. and da Cruz e Silva, E. F. (2004a) Signal transduction therapeutics: relevance for Alzheimer's disease. *J Mol Neurosci* **23,** 123-142.

da Cruz e Silva, O. A., Iverfeldt, K., Oltersdorf, T., Sinha, S., Lieberburg, I., Ramabhadran, T. V., Suzuki, T., Sisodia, S. S., Gandy, S. and Greengard, P. (1993) Regulated cleavage of Alzheimer beta-amyloid precursor protein in the absence of the cytoplasmic tail. *Neuroscience* **57,** 873-877.

da Cruz e Silva, O. A., Vieira, S. I., Rebelo, S. and da Cruz e Silva, E. F. (2004b) A model system to study intracellular trafficking and processing of the Alzheimer's amyloid precursor protein. *Neurodegener Dis* **1,** 196-204.

da Cruz e Silva, O. A. B., Vieira, S. I., Rebelo, S. and da Cruz e Silva, E. F. (2004c) A Model System to Study Intracellular Trafficking and Processing of the Alzheimer's Amyloid Precursor Protein. *Neuro-degenerative Diseases* **1,** 196-204.

Dansereau, D. A. and Lasko, P. (2008) RanBPM regulates cell shape, arrangement, and capacity of the female germline stem cell niche in Drosophila melanogaster. *J Cell Biol* **182,** 963-977.

Davis, R. E., Miller, S., Herrnstadt, C., Ghosh, S. S., Fahy, E., Shinobu, L. A., Galasko, D., Thal, L. J., Beal, M. F., Howell, N. and Parker, W. D., Jr. (1997) Mutations in mitochondrial cytochrome c oxidase genes segregate with late-onset Alzheimer disease. *Proc Natl Acad Sci U S A* **94,** 4526-4531.

De Strooper, B. and Annaert, W. (2000) Proteolytic processing and cell biological functions of the amyloid precursor protein. *J Cell Sci* **113 (Pt 11),** 1857-1870.

De Strooper, B., Annaert, W., Cupers, P., Saftig, P., Craessaerts, K., Mumm, J. S., Schroeter, E. H., Schrijvers, V., Wolfe, M. S., Ray, W. J., Goate, A. and Kopan, R. (1999) A presenilin-1-dependent gamma-secretase-like protease mediates release of Notch intracellular domain. *Nature* **398,** 518-522.

De Strooper, B., Saftig, P., Craessaerts, K., Vanderstichele, H., Guhde, G., Annaert, W., Von Figura, K. and Van Leuven, F. (1998) Deficiency of presenilin-1 inhibits the normal cleavage of amyloid precursor protein. *Nature* **391,** 387-390.

Denti, S., Sirri, A., Cheli, A., Rogge, L., Innamorati, G., Putignano, S., Fabbri, M., Pardi, R. and Bianchi, E. (2004) RanBPM is a phosphoprotein that associates with the plasma membrane and interacts with the integrin LFA-1. *J Biol Chem* **279,** 13027-13034.

Dickson, D. W. (1997) The pathogenesis of senile plaques. *J Neuropathol Exp Neurol* **56,** 321-339.

Dickson, D. W., Ksiezak-Reding, H., Davies, P. and Yen, S. H. (1987) A monoclonal antibody that recognizes a phosphorylated epitope in Alzheimer neurofibrillary tangles, neurofilaments and tau proteins immunostains granulovacuolar degeneration. *Acta Neuropathol* **73,** 254-258.

Dickson, T. C., Saunders, H. L. and Vickers, J. C. (1997) Relationship between apolipoprotein E and the amyloid deposits and dystrophic neurites of Alzheimer's disease. *Neuropathol Appl Neurobiol* **23,** 483-491.

Dinkel, H., Michael, S., Weatheritt, R. J., Davey, N. E., Van Roey, K., Altenberg, B., Toedt, G., Uyar, B., Seiler, M., Budd, A., Jödicke, L., Dammert, M. A., Schroeter, C., Hammer, M., Schmidt, T., Jehl, P., McGuigan, C., Dymecka, M., Chica, C., Luck, K., Via, A., Chatr-aryamontri, A., Haslam, N., Grebnev, G., Edwards, R. J., Steinmetz, M. O., Meiselbach, H., Diella, F. and Gibson, T. J. (2011) ELM—the database of eukaryotic linear motifs. *Nucleic Acids Research*.

Domingues, S. C. (2005) The Use of Yeast Two-Hybrid System to Support the Notch-Like Signalling of APP. Master Thesis, University of Aveiro, Portugal.

Domingues, S. C., Henriques, A. G., Fardilha, M., da Cruz, E. S. E. F. and da Cruz, E. S. O. A. (2011) Identification and characterization of a neuronal enriched novel transcript encoding the previously described p60Fe65 isoform. *J Neurochem* **119,** 1086-1098.

Domingues, S. C., Henriques, A. G., Wu, W., Da Cruz e Silva, E. F. and Da Cruz e Silva, O. A. (2007) Altered subcellular distribution of the Alzheimer's amyloid precursor protein under stress conditions. *Ann N Y Acad Sci* **1096,** 184-195.

Dubois, B., Feldman, H. H., Jacova, C., Dekosky, S. T., Barberger-Gateau, P., Cummings, J., Delacourte, A., Galasko, D., Gauthier, S., Jicha, G., Meguro, K., O'Brien, J., Pasquier, F., Robert, P., Rossor, M., Salloway, S., Stern, Y., Visser, P. J. and Scheltens, P. (2007) Research criteria for the diagnosis of Alzheimer's disease: revising the NINCDS-ADRDA criteria. *Lancet Neurol* **6,** 734-746.

Duilio, A., Faraonio, R., Minopoli, G., Zambrano, N. and Russo, T. (1998) Fe65L2: a new member of the Fe65 protein family interacting with the intracellular domain of the Alzheimer's beta-amyloid precursor protein. *Biochem J* **330 (Pt 1),** 513-519.

Duilio, A., Zambrano, N., Mogavero, A. R., Ammendola, R., Cimino, F. and Russo, T. (1991) A rat brain mRNA encoding a transcriptional activator homologous to the DNA binding domain of retroviral integrases. *Nucleic Acids Res* **19,** 5269-5274.

Duyckaerts, C., Delatour, B. and Potier, M. C. (2009) Classification and basic pathology of Alzheimer disease. *Acta Neuropathol* **118,** 5-36.

Eckert, A., Keil, U., Marques, C. A., Bonert, A., Frey, C., Schussel, K. and Muller, W. E. (2003) Mitochondrial dysfunction, apoptotic cell death, and Alzheimer's disease. *Biochem Pharmacol* **66,** 1627-1634.

Edbauer, D., Willem, M., Lammich, S., Steiner, H. and Haass, C. (2002) Insulin-degrading enzyme rapidly removes the beta-amyloid precursor protein intracellular domain (AICD). *J Biol Chem* **277,** 13389-13393.

Ehehalt, R., Keller, P., Haass, C., Thiele, C. and Simons, K. (2003) Amyloidogenic processing of the Alzheimer beta-amyloid precursor protein depends on lipid rafts. *J Cell Biol* **160,** 113-123.

Emes, R. D. and Ponting, C. P. (2001) A new sequence motif linking lissencephaly, Treacher Collins and oral-facial-digital type 1 syndromes, microtubule dynamics and cell migration. *Hum Mol Genet* **10,** 2813-2820.

Enard, W., Khaitovich, P., Klose, J., Zollner, S., Heissig, F., Giavalisco, P., Nieselt-Struwe, K., Muchmore, E., Varki, A., Ravid, R., Doxiadis, G. M., Bontrop, R. E. and Paabo, S. (2002) Intra- and interspecific variation in primate gene expression patterns. *Science* **296,** 340-343.

Erlich, P. M., Lunetta, K. L., Cupples, L. A., Huyck, M., Green, R. C., Baldwin, C. T., Farrer, L. A. and Group, f. t. M. S. (2006) Polymorphisms in the PON gene cluster are associated with Alzheimer disease. *Human Molecular Genetics* **15,** 77-85.

Ermekova, K. S., Zambrano, N., Linn, H., Minopoli, G., Gertler, F., Russo, T. and Sudol, M. (1997) The WW domain of neural protein FE65 interacts with proline-rich motifs in Mena, the mammalian homolog of Drosophila enabled. *J Biol Chem* **272,** 32869-32877.

Esch, F. S., Keim, P. S., Beattie, E. C., Blacher, R. W., Culwell, A. R., Oltersdorf, T., McClure, D. and Ward, P. J. (1990) Cleavage of amyloid beta peptide during constitutive processing of its precursor. *Science* **248,** 1122-1124.

Esler, W. P. and Wolfe, M. S. (2001) A portrait of Alzheimer secretases--new features and familiar faces. *Science* **293,** 1449-1454.

Eyre, T. A., Ducluzeau, F., Sneddon, T. P., Povey, S., Bruford, E. A. and Lush, M. J. (2006) The HUGO Gene Nomenclature Database, 2006 updates. *Nucleic Acids Res* **34,** D319-321.

Fardilha, M., Wu, W., Sa, R., Fidalgo, S., Sousa, C., Mota, C., da Cruz e Silva, O. A. and da Cruz e Silva, E. F. (2004) Alternatively spliced protein variants as potential therapeutic targets for male infertility and contraception. *Ann N Y Acad Sci* **1030,** 468-478.

Fassa, A., Mehta, P. and Efthimiopoulos, S. (2005) Notch 1 interacts with the amyloid precursor protein in a Numb-independent manner. *J Neurosci Res* **82,** 214-224.

Ferri, C. P., Prince, M., Brayne, C., Brodaty, H., Fratiglioni, L., Ganguli, M., Hall, K., Hasegawa, K., Hendrie, H., Huang, Y., Jorm, A., Mathers, C., Menezes, P. R., Rimmer, E. and Scazufca, M. (2005) Global prevalence of dementia: a Delphi consensus study. *Lancet* **366,** 2112-2117.

Fields, S. and Song, O. (1989) A novel genetic system to detect protein-protein interactions. *Nature* **340,** 245-246.

Fields, S. and Sternglanz, R. (1994) The two-hybrid system: an assay for protein-protein interactions. *Trends Genet* **10,** 286-292.

Filardo, E. J., Brooks, P. C., Deming, S. L., Damsky, C. and Cheresh, D. A. (1995) Requirement of the NPXY motif in the integrin beta 3 subunit cytoplasmic tail for melanoma cell migration in vitro and in vivo. *J Cell Biol* **130,** 441-450.

Fiore, F., Zambrano, N., Minopoli, G., Donini, V., Duilio, A. and Russo, T. (1995) The regions of the Fe65 protein homologous to the phosphotyrosine interaction/phosphotyrosine binding domain of Shc bind the intracellular domain of the Alzheimer's amyloid precursor protein. *J Biol Chem* **270,** 30853-30856.

Fukumori, A., Okochi, M., Tagami, S., Jiang, J., Itoh, N., Nakayama, T., Yanagida, K., Ishizuka-Katsura, Y., Morihara, T., Kamino, K., Tanaka, T., Kudo, T., Tanii, H., Ikuta, A., Haass, C. and Takeda, M. (2006) Presenilin-dependent gamma-secretase on plasma membrane and endosomes is functionally distinct. *Biochemistry* **45,** 4907-4914.

Funamoto, S., Morishima-Kawashima, M., Tanimura, Y., Hirotani, N., Saido, T. C. and Ihara, Y. (2004) Truncated carboxyl-terminal fragments of beta-amyloid precursor protein are processed to amyloid beta-proteins 40 and 42. *Biochemistry* **43,** 13532-13540.

Furukawa, K., Sopher, B. L., Rydel, R. E., Begley, J. G., Pham, D. G., Martin, G. M., Fox, M. and Mattson, M. P. (1996) Increased activity-regulating and neuroprotective efficacy of alpha-secretase-derived secreted amyloid precursor protein conferred by a C-terminal heparin-binding domain. *J Neurochem* **67,** 1882-1896.

Galloway, P. G., Perry, G. and Gambetti, P. (1987) Hirano body filaments contain actin and actin-associated proteins. *J Neuropathol Exp Neurol* **46,** 185-199.

Galvan, V., Gorostiza, O. F., Banwait, S., Ataie, M., Logvinova, A. V., Sitaraman, S., Carlson, E., Sagi, S. A., Chevallier, N., Jin, K., Greenberg, D. A. and Bredesen, D. E. (2006) Reversal of Alzheimer's-like pathology and behavior in human APP transgenic mice by mutation of Asp664. *Proc Natl Acad Sci U S A* **103,** 7130-7135.

Gandy, S. E., Bhasin, R., Ramabhadran, T. V., Koo, E. H., Price, D. L., Goldgaber, D. and Greengard, P. (1992) Alzheimer beta/A4-amyloid precursor protein: evidence for putative amyloidogenic fragment. *J Neurochem* **58,** 383-386.

Gandy, S. E., Caporaso, G. L., Buxbaum, J. D., de Cruz Silva, O., Iverfeldt, K., Nordstedt, C., Suzuki, T., Czernik, A. J., Nairn, A. C. and Greengard, P. (1993) Protein phosphorylation regulates relative utilization of processing pathways for Alzheimer beta/A4 amyloid precursor protein. *Ann N Y Acad Sci* **695,** 117-121.

Gao, J., Ade, A. S., Tarcea, V. G., Weymouth, T. E., Mirel, B. R., Jagadish, H. V. and States, D. J. (2009) Integrating and annotating the interactome using the MiMI plugin for cytoscape. *Bioinformatics* **25,** 137-138.

Gatz, M., Mortimer, J. A., Fratiglioni, L., Johansson, B., Berg, S., Reynolds, C. A. and Pedersen, N. L. (2006) Potentially modifiable risk factors for dementia in identical twins. *Alzheimers Dement* **2,** 110-117.

Gatz, M., Pedersen, N. L., Berg, S., Johansson, B., Johansson, K., Mortimer, J. A., Posner, S. F., Viitanen, M., Winblad, B. and Ahlbom, A. (1997) Heritability for Alzheimer's disease: the study of dementia in Swedish twins. *J Gerontol A Biol Sci Med Sci* **52,** M117-125.

Georgopoulou, N., McLaughlin, M., McFarlane, I. and Breen, K. C. (2001) The role of post-translational modification in beta-amyloid precursor protein processing. *Biochem Soc Symp***,** 23-36.

Gervais, F. G., Xu, D., Robertson, G. S., Vaillancourt, J. P., Zhu, Y., Huang, J., LeBlanc, A., Smith, D., Rigby, M., Shearman, M. S., Clarke, E. E., Zheng, H., Van Der Ploeg, L. H., Ruffolo, S. C., Thornberry, N. A., Xanthoudakis, S., Zamboni, R. J., Roy, S. and Nicholson, D. W. (1999) Involvement of caspases in proteolytic cleavage of Alzheimer's amyloid-beta precursor protein and amyloidogenic A beta peptide formation. *Cell* **97,** 395-406.

Gesteland, R. F. and Atkins, J. F. (1996) Recoding: dynamic reprogramming of translation. *Annu Rev Biochem* **65,** 741-768.

Ghersi, E., Noviello, C. and D'Adamio, L. (2004) Amyloid-beta protein precursor (AbetaPP) intracellular domain-associated protein-1 proteins bind to AbetaPP and modulate its processing in an isoform-specific manner. *J Biol Chem* **279,** 49105-49112.

Ghiso, J., Rostagno, A., Gardella, J. E., Liem, L., Gorevic, P. D. and Frangione, B. (1992) A 109-amino-acid C-terminal fragment of Alzheimer's-disease amyloid precursor protein contains a sequence, -RHDS-, that promotes cell adhesion. *Biochem J* **288 (Pt 3),** 1053-1059.

Glenner, G. G. and Wong, C. W. (1984a) Alzheimer's disease and Down's syndrome: sharing of a unique cerebrovascular amyloid fibril protein. *Biochem Biophys Res Commun* **122,** 1131-1135.

Glenner, G. G. and Wong, C. W. (1984b) Alzheimer's disease: initial report of the purification and characterization of a novel cerebrovascular amyloid protein. *Biochem Biophys Res Commun* **120,** 885-890.

Goate, A., Chartier-Harlin, M. C., Mullan, M., Brown, J., Crawford, F., Fidani, L., Giuffra, L., Haynes, A., Irving, N., James, L. and et al. (1991) Segregation of a missense mutation in the amyloid precursor protein gene with familial Alzheimer's disease. *Nature* **349,** 704-706.

Godfroid, E. and Octave, J. N. (1990) Glycosylation of the amyloid peptide precursor containing the Kunitz protease inhibitor domain improves the inhibition of trypsin. *Biochem Biophys Res Commun* **171,** 1015-1021.

Goehler, H., Lalowski, M., Stelzl, U., Waelter, S., Stroedicke, M., Worm, U., Droege, A., Lindenberg, K. S., Knoblich, M., Haenig, C., Herbst, M., Suopanki, J., Scherzinger, E., Abraham, C., Bauer, B., Hasenbank, R., Fritzsche, A., Ludewig, A. H., Bussow, K., Coleman, S. H., Gutekunst, C. A., Landwehrmeyer, B. G., Lehrach, H. and Wanker, E. E. (2004) A protein interaction network links GIT1, an enhancer of huntingtin aggregation, to Huntington's disease. *Mol Cell* **15,** 853-865.

Gong, C. X., Singh, T. J., Grundke-Iqbal, I. and Iqbal, K. (1993) Phosphoprotein phosphatase activities in Alzheimer disease brain. *J Neurochem* **61,** 921-927.

Goodger, Z. V., Rajendran, L., Trutzel, A., Kohli, B. M., Nitsch, R. M. and Konietzko, U. (2009) Nuclear signaling by the APP intracellular domain occurs predominantly through the amyloidogenic processing pathway. *J Cell Sci* **122,** 3703-3714.

Goudreault, M., D'Ambrosio, L. M., Kean, M. J., Mullin, M. J., Larsen, B. G., Sanchez, A., Chaudhry, S., Chen, G. I., Sicheri, F., Nesvizhskii, A. I., Aebersold, R., Raught, B. and Gingras, A. C. (2009) A PP2A phosphatase high density interaction network identifies a novel striatin-interacting phosphatase and kinase complex linked to the cerebral cavernous malformation 3 (CCM3) protein. *Mol Cell Proteomics* **8,** 157-171.

Graham, D. I., Gentleman, S. M., Nicoll, J. A., Royston, M. C., McKenzie, J. E., Roberts, G. W. and Griffin, W. S. (1996) Altered beta-APP metabolism after head injury and its relationship to the aetiology of Alzheimer's disease. *Acta Neurochir Suppl* **66,** 96-102.

Gu, Y., Misonou, H., Sato, T., Dohmae, N., Takio, K. and Ihara, Y. (2001) Distinct intramembrane cleavage of the beta-amyloid precursor protein family resembling gamma-secretase-like cleavage of Notch. *J Biol Chem* **276,** 35235-35238.

Guenette, S., Chang, Y., Hiesberger, T., Richardson, J. A., Eckman, C. B., Eckman, E. A., Hammer, R. E. and Herz, J. (2006) Essential roles for the FE65 amyloid precursor protein-interacting proteins in brain development. *EMBO J* **25,** 420-431.

Guenette, S. Y., Chen, J., Jondro, P. D. and Tanzi, R. E. (1996) Association of a novel human FE65-like protein with the cytoplasmic domain of the beta-amyloid precursor protein. *Proc Natl Acad Sci U S A* **93,** 10832-10837.

Gunawardena, S. and Goldstein, L. S. (2001) Disruption of axonal transport and neuronal viability by amyloid precursor protein mutations in Drosophila. *Neuron* **32,** 389-401.

Gyuris, J., Golemis, E., Chertkov, H. and Brent, R. (1993) Cdi1, a human G1 and S phase protein phosphatase that associates with Cdk2. *Cell* **75,** 791-803.

Haass, C. (2004) Take five--BACE and the gamma-secretase quartet conduct Alzheimer's amyloid beta-peptide generation. *Embo J* **23,** 483-488.

Haass, C., Hung, A. Y. and Selkoe, D. J. (1991) Processing of beta-amyloid precursor protein in microglia and astrocytes favors an internal localization over constitutive secretion. *J Neurosci* **11,** 3783-3793.

Hamblet, N. S., Ragland, B., Ali, M., Conyers, B. and Castora, F. J. (2006) Mutations in mitochondrial-encoded cytochrome c oxidase subunits I, II, and III genes detected in Alzheimer's disease using single-strand conformation polymorphism. *Electrophoresis* **27,** 398-408.

Hamdane, M., Delobel, P., Sambo, A. V., Smet, C., Begard, S., Violleau, A., Landrieu, I., Delacourte, A., Lippens, G., Flament, S. and Buee, L. (2003) Neurofibrillary degeneration of the Alzheimer-type: an alternate pathway to neuronal apoptosis? *Biochem Pharmacol* **66,** 1619-1625.

Hardy, J. and Allsop, D. (1991) Amyloid deposition as the central event in the aetiology of Alzheimer's disease. *Trends Pharmacol Sci* **12,** 383-388.

Hardy, J., Duff, K., Hardy, K. G., Perez-Tur, J. and Hutton, M. (1998) Genetic dissection of Alzheimer's disease and related dementias: amyloid and its relationship to tau. *Nat Neurosci* **1,** 355-358.

Hardy, J. and Selkoe, D. J. (2002) The amyloid hypothesis of Alzheimer's disease: progress and problems on the road to therapeutics. *Science* **297,** 353-356.

Hardy, J. A. and Higgins, G. A. (1992) Alzheimer's disease: the amyloid cascade hypothesis. *Science* **256,** 184-185.

Hase, M., Yagi, Y., Taru, H., Tomita, S., Sumioka, A., Hori, K., Miyamoto, K., Sasamura, T., Nakamura, M., Matsuno, K. and Suzuki, T. (2002) Expression and characterization of the Drosophila X11-like/Mint protein during neural development. *J Neurochem* **81,** 1223-1232.

Hasegawa, M., Smith, M. J. and Goedert, M. (1998) Tau proteins with FTDP-17 mutations have a reduced ability to promote microtubule assembly. *FEBS Lett* **437,** 207-210.

Helbecque, N., Abderrhamani, A., Meylan, L., Riederer, B., Mooser, V., Miklossy, J., Delplanque, J., Boutin, P., Nicod, P., Haefliger, J. A., Cottel, D., Amouyel, P., Froguel, P. and Waeber, G. (2000) Islet-brain1//C-Jun N-terminal kinase interacting protein-1 (IB1//JIP-1) promoter variant is associated with Alzheimer's disease. *Mol Psychiatry* **8,** 413-422.

Henriques, A. G., Vieira, S. I., Crespo-Lopez, M. E., Guiomar de Oliveira, M. A., da Cruz e Silva, E. F. and da Cruz e Silva, O. A. (2009) Intracellular sAPP retention in response to Abeta is mapped to cytoskeleton-associated structures. *J Neurosci Res* **87,** 1449-1461.

Henriques, A. G., Vieira, S. I., Rebelo, S., Domingues, S. C., da Cruz e Silva, E. F. and da Cruz e Silva, O. A. (2007) Isoform specific amyloid-beta protein precursor metabolism. *J Alzheimers Dis* **11,** 85-95.

Herms, J., Anliker, B., Heber, S., Ring, S., Fuhrmann, M., Kretzschmar, H., Sisodia, S. and Muller, U. (2004) Cortical dysplasia resembling human type 2 lissencephaly in mice lacking all three APP family members. *Embo J* **23,** 4106-4115.

Hernandez, F., Gomez de Barreda, E., Fuster-Matanzo, A., Lucas, J. J. and Avila, J. (2010) GSK3: a possible link between beta amyloid peptide and tau protein. *Exp Neurol* **223,** 322-325.

Herz, J. and Strickland, D. K. (2001) LRP: a multifunctional scavenger and signaling receptor. *J Clin Invest* **108,** 779-784.

Hill, K., Li, Y., Bennett, M., McKay, M., Zhu, X., Shern, J., Torre, E., Lah, J. J., Levey, A. I. and Kahn, R. A. (2003) Munc18 interacting proteins: ADP-ribosylation factor-dependent coat proteins that regulate the traffic of beta-Alzheimer's precursor protein. *J Biol Chem* **278,** 36032-36040.

Hirano, A. (1994) Hirano bodies and related neuronal inclusions. *Neuropathol Appl Neurobiol* **20,** 3-11.

Ho, A. and Sudhof, T. C. (2004) Binding of F-spondin to amyloid-beta precursor protein: a candidate amyloid-beta precursor protein ligand that modulates amyloid-beta precursor protein cleavage. *Proc Natl Acad Sci U S A* **101,** 2548-2553.

Hoe, H. S., Minami, S. S., Makarova, A., Lee, J., Hyman, B. T., Matsuoka, Y. and Rebeck, G. W. (2008) Fyn modulation of Dab1 effects on amyloid precursor protein and ApoE receptor 2 processing. *J Biol Chem* **283,** 6288-6299.

Hoe, H. S., Tran, T. S., Matsuoka, Y., Howell, B. W. and Rebeck, G. W. (2006) DAB1 and Reelin effects on amyloid precursor protein and ApoE receptor 2 trafficking and processing. *J Biol Chem* **281,** 35176-35185.

Hooli, B. V. and Tanzi, R. E. (2009) A current view of Alzheimer's disease. *F1000 Biol Rep* **1,** 54.

Hornsten, A., Lieberthal, J., Fadia, S., Malins, R., Ha, L., Xu, X., Daigle, I., Markowitz, M., O'Connor, G., Plasterk, R. and Li, C. (2007) APL-1, a Caenorhabditis elegans protein related to the human beta-amyloid precursor protein, is essential for viability. *Proc Natl Acad Sci U S A* **104,** 1971-1976.

Hu, Q., Cool, B. H., Wang, B., Hearn, M. G. and Martin, G. M. (2002) A candidate molecular mechanism for the association of an intronic polymorphism of FE65 with resistance to very late onset dementia of the Alzheimer type. *Hum Mol Genet* **11,** 465-475.

Hu, Q., Hearn, M. G., Jin, L. W., Bressler, S. L. and Martin, G. M. (1999) Alternatively spliced isoforms of FE65 serve as neuron-specific and non-neuronal markers. *J Neurosci Res* **58,** 632-640.

Hu, Q., Kukull, W. A., Bressler, S. L., Gray, M. D., Cam, J. A., Larson, E. B., Martin, G. M. and Deeb, S. S. (1998) The human FE65 gene: genomic structure and an intronic biallelic polymorphism associated with sporadic dementia of the Alzheimer type. *Hum Genet* **103,** 295-303.

Hung, A. Y., Koo, E. H., Haass, C. and Selkoe, D. J. (1992) Increased expression of beta-amyloid precursor protein during neuronal differentiation is not accompanied by secretory cleavage. *Proc Natl Acad Sci U S A* **89,** 9439-9443.

Hung, A. Y. and Selkoe, D. J. (1994) Selective ectodomain phosphorylation and regulated cleavage of beta-amyloid precursor protein. *Embo J* **13,** 534-542.

Hunter, S., Apweiler, R., Attwood, T. K., Bairoch, A., Bateman, A., Binns, D., Bork, P., Das, U., Daugherty, L., Duquenne, L., Finn, R. D., Gough, J., Haft, D., Hulo, N., Kahn, D., Kelly, E., Laugraud, A., Letunic, I., Lonsdale, D., Lopez, R., Madera, M., Maslen, J., McAnulla, C., McDowall, J., Mistry, J., Mitchell, A., Mulder, N., Natale, D., Orengo, C., Quinn, A. F., Selengut, J. D., Sigrist, C. J. A., Thimma, M., Thomas, P. D., Valentin, F., Wilson, D., Wu, C. H. and Yeats, C. (2009) InterPro: the integrative protein signature database. *Nucleic Acids Research* **37,** D211-D215.

Hunter, S., Jones, P., Mitchell, A., Apweiler, R., Attwood, T. K., Bateman, A., Bernard, T., Binns, D., Bork, P., Burge, S., de Castro, E., Coggill, P., Corbett, M., Das, U., Daugherty, L., Duquenne, L., Finn, R. D., Fraser, M., Gough, J., Haft, D., Hulo, N., Kahn, D., Kelly, E., Letunic, I., Lonsdale, D., Lopez, R., Madera, M., Maslen, J., McAnulla, C., McDowall, J., McMenamin, C., Mi, H., Mutowo-Muellenet, P., Mulder, N., Natale, D., Orengo, C., Pesseat, S., Punta, M., Quinn, A. F., Rivoire, C., Sangrador-Vegas, A., Selengut, J. D., Sigrist, C. J. A., Scheremetjew, M., Tate, J., Thimmajanarthanan, M., Thomas, P. D., Wu, C. H., Yeats, C. and Yong, S.-Y. (2012) InterPro in 2011: new developments in the family and domain prediction database. *Nucleic Acids Research* **40,** D306-D312.

Ikin, A. F., Sabo, S. L., Lanier, L. M. and Buxbaum, J. D. (2007) A macromolecular complex involving the amyloid precursor protein (APP) and the cytosolic adapter FE65 is a negative regulator of axon branching. *Mol Cell Neurosci* **35,** 57-63.

Iwatsubo, T., Odaka, A., Suzuki, N., Mizusawa, H., Nukina, N. and Ihara, Y. (1994) Visualization of Aβ42(43) and Aβ40 in senile plaques with end-specific Aβ monoclonals: Evidence that an initially deposited species is Aβ42(43). *Neuron* **13,** 45-53.

Jacobsen, J. S., Spruyt, M. A., Brown, A. M., Sahasrabudhe, S. R., Blume, A. J., Vitek, M. P., Muenkel, H. A. and Sonnenberg-Reines, J. (1994) The release of Alzheimer's disease beta amyloid peptide is reduced by phorbol treatment. *J Biol Chem* **269,** 8376-8382.

Jellinger, K. A. (2004) Traumatic brain injury as a risk factor for Alzheimer's disease. *J Neurol Neurosurg Psychiatry* **75,** 511-512.

Kakuda, N., Funamoto, S., Yagishita, S., Takami, M., Osawa, S., Dohmae, N. and Ihara, Y. (2006) Equimolar production of amyloid beta-protein and amyloid precursor protein intracellular domain from beta-carboxyl-terminal fragment by gamma-secretase. *J Biol Chem* **281,** 14776-14786.

Kamal, A., Almenar-Queralt, A., LeBlanc, J. F., Roberts, E. A. and Goldstein, L. S. (2001) Kinesin-mediated axonal transport of a membrane compartment containing beta-secretase and presenilin-1 requires APP. *Nature* **414,** 643-648.

Kandasamy, K., Mohan, S. S., Raju, R., Keerthikumar, S., Kumar, G., Venugopal, A., Telikicherla, D., Navarro, J. D., Mathivanan, S., Pecquet, C., Gollapudi, S., Tattikota, S., Mohan, S., Padhukasahasram, H., Subbannayya, Y., Goel, R., Jacob, H., Zhong, J., Sekhar, R., Nanjappa, V., Balakrishnan, L., Subbaiah, R., Ramachandra, Y., Rahiman, B. A., Prasad, T. K., Lin, J.-X., Houtman, J., Desiderio, S., Renauld, J.-C. and Constantinescu, S. (2010) NetPath: a public resource of curated signal transduction pathways. *Genome Biology* **11,** R3.

Kanehisa, M., Goto, S., Furumichi, M., Tanabe, M. and Hirakawa, M. (2010) KEGG for representation and analysis of molecular networks involving diseases and drugs. *Nucleic Acids Research* **38,** D355-D360.

Kang, J., Lemaire, H. G., Unterbeck, A., Salbaum, J. M., Masters, C. L., Grzeschik, K. H., Multhaup, G., Beyreuther, K. and Muller-Hill, B. (1987) The precursor of Alzheimer's disease amyloid A4 protein resembles a cell-surface receptor. *Nature* **325,** 733-736.

Kapustin, Y., Souvorov, A., Tatusova, T. and Lipman, D. (2008) Splign: algorithms for computing spliced alignments with identification of paralogs. *Biol Direct* **3,** 20.

Karran, E., Mercken, M. and Strooper, B. D. (2011) The amyloid cascade hypothesis for Alzheimer's disease: an appraisal for the development of therapeutics. *Nat Rev Drug Discov* **10,** 698-712.

Keshava Prasad, T. S., Goel, R., Kandasamy, K., Keerthikumar, S., Kumar, S., Mathivanan, S., Telikicherla, D., Raju, R., Shafreen, B., Venugopal, A., Balakrishnan, L., Marimuthu, A., Banerjee, S., Somanathan, D. S., Sebastian, A., Rani, S., Ray, S., Harrys Kishore, C. J., Kanth, S., Ahmed, M., Kashyap, M. K., Mohmood, R., Ramachandra, Y. L., Krishna, V., Rahiman, B. A., Mohan, S., Ranganathan, P., Ramabadran, S., Chaerkady, R. and Pandey, A. (2009) Human Protein Reference Database—2009 update. *Nucleic Acids Research* **37,** D767-D772.

Kim, H. S., Kim, E. M., Lee, J. P., Park, C. H., Kim, S., Seo, J. H., Chang, K. A., Yu, E., Jeong, S. J., Chong, Y. H. and Suh, Y. H. (2003) C-terminal fragments of amyloid precursor protein exert neurotoxicity by inducing glycogen synthase kinase-3beta expression. *Faseb J* **17,** 1951-1953.

Kim, J., Basak, J. M. and Holtzman, D. M. (2009) The role of apolipoprotein E in Alzheimer's disease. *Neuron* **63,** 287-303.

Kimberly, W. T., Zheng, J. B., Guenette, S. Y. and Selkoe, D. J. (2001) The intracellular domain of the beta-amyloid precursor protein is stabilized by Fe65 and translocates to the nucleus in a notch-like manner. *J Biol Chem* **276,** 40288-40292.

King, G. D. and Scott Turner, R. (2004) Adaptor protein interactions: modulators of amyloid precursor protein metabolism and Alzheimer's disease risk? *Exp Neurol* **185,** 208-219.

Kitaguchi, N., Takahashi, Y., Tokushima, Y., Shiojiri, S. and Ito, H. (1988) Novel precursor of Alzheimer's disease amyloid protein shows protease inhibitory activity. *Nature* **331,** 530–532.

Klein, W. L., Stine, W. B., Jr. and Teplow, D. B. (2004) Small assemblies of unmodified amyloid beta-protein are the proximate neurotoxin in Alzheimer's disease. *Neurobiol Aging* **25,** 569-580.

Knopman, D. S., DeKosky, S. T., Cummings, J. L., Chui, H., Corey-Bloom, J., Relkin, N., Small, G. W., Miller, B. and Stevens, J. C. (2001) Practice parameter: diagnosis of dementia (an evidence-based review).

Report of the Quality Standards Subcommittee of the American Academy of Neurology. *Neurology* **56,** 1143-1153.

Kobayashi, N., Yang, J., Ueda, A., Suzuki, T., Tomaru, K., Takeno, M., Okuda, K. and Ishigatsubo, Y. (2007) RanBPM, Muskelin, p48EMLP, p44CTLH, and the armadillo-repeat proteins ARMC8alpha and ARMC8beta are components of the CTLH complex. *Gene* **396,** 236-247.

Kolonin, M. G., Zhong, J. and Finley, R. L. (2000) Interaction mating methods in two-hybrid systems. *Methods Enzymol* **328,** 26-46.

Konietzko, U. (2011) AICD Nuclear Signaling and its Possible Contribution to Alzheimer's Disease. *Curr Alzheimer Res*.

Konietzko, U., Goodger, Z. V., Meyer, M., Kohli, B. M., Bosset, J., Lahiri, D. K. and Nitsch, R. M. (2008) Co-localization of the amyloid precursor protein and Notch intracellular domains in nuclear transcription factories. *Neurobiol Aging*.

Konietzko, U., Goodger, Z. V., Meyer, M., Kohli, B. M., Bosset, J., Lahiri, D. K. and Nitsch, R. M. (2010) Co-localization of the amyloid precursor protein and Notch intracellular domains in nuclear transcription factories. *Neurobiol Aging* **31,** 58-73.

Konig, G., Monning, U., Czech, C., Prior, R., Banati, R., Schreiter-Gasser, U., Bauer, J., Masters, C. L. and Beyreuther, K. (1992) Identification and differential expression of a novel alternative splice isoform of the beta A4 amyloid precursor protein (APP) mRNA in leukocytes and brain microglial cells. *J Biol Chem* **267,** 10804-10809.

Koo, E. H. and Kopan, R. (2004) Potential role of presenilin-regulated signaling pathways in sporadic neurodegeneration. *Nat Med* **10 Suppl,** S26-33.

Koo, E. H., Sisodia, S. S., Archer, D. R., Martin, L. J., Weidemann, A., Beyreuther, K., Fischer, P., Masters, C. L. and Price, D. L. (1990) Precursor of amyloid protein in Alzheimer disease undergoes fast anterograde axonal transport. *Proc Natl Acad Sci U S A* **87,** 1561-1565.

Koo, E. H. and Squazzo, S. L. (1994) Evidence that production and release of amyloid beta-protein involves the endocytic pathway. *J Biol Chem* **269,** 17386-17389.

Koo, E. H., Squazzo, S. L., Selkoe, D. J. and Koo, C. H. (1996) Trafficking of cell-surface amyloid beta-protein precursor. I. Secretion, endocytosis and recycling as detected by labeled monoclonal antibody. *J Cell Sci* **109 (Pt 5),** 991-998.

Kopan, R. and Goate, A. (2000) A common enzyme connects notch signaling and Alzheimer's disease. *Genes Dev* **14,** 2799-2806.

Kopan, R. and Ilagan, M. X. (2004) Gamma-secretase: proteasome of the membrane? *Nat Rev Mol Cell Biol* **5,** 499-504.

Kraepelin, E. (1910) Psychiatrie, Ein Lehrbuch fur Studierende und Arzte. *II Band (Barth Verlag, Leipzig).*

Kramer, S., Ozaki, T., Miyazaki, K., Kato, C., Hanamoto, T. and Nakagawara, A. (2005) Protein stability and function of p73 are modulated by a physical interaction with RanBPM in mammalian cultured cells. *Oncogene* **24,** 938-944.

Krogh, A., Larsson, B., von Heijne, G. and Sonnhammer, E. L. (2001) Predicting transmembrane protein topology with a hidden Markov model: application to complete genomes. *J Mol Biol* **305,** 567-580.

Kutateladze, T. G. (2006) Phosphatidylinositol 3-phosphate recognition and membrane docking by the FYVE domain. *Biochim Biophys Acta* **1761,** 868-877.

Kwak, Y. D., Brannen, C. L., Qu, T., Kim, H. M., Dong, X., Soba, P., Majumdar, A., Kaplan, A., Beyreuther, K. and Sugaya, K. (2006) Amyloid precursor protein regulates differentiation of human neural stem cells. *Stem Cells Dev* **15,** 381-389.

LaFerla, F. M. and Oddo, S. (2005) Alzheimer's disease: Abeta, tau and synaptic dysfunction. *Trends Mol Med* **11,** 170-176.

Lai, A., Sisodia, S. S. and Trowbridge, I. S. (1995) Characterization of sorting signals in the beta-amyloid precursor protein cytoplasmic domain. *J Biol Chem* **270,** 3565-3573.

Lakatos, A., Derbeneva, O., Younes, D., Keator, D., Bakken, T., Lvova, M., Brandon, M., Guffanti, G., Reglodi, D., Saykin, A., Weiner, M., Macciardi, F., Schork, N., Wallace, D. C. and Potkin, S. G. (2010) Association between mitochondrial DNA variations and Alzheimer's disease in the ADNI cohort. *Neurobiol Aging* **31,** 1355-1363.

Lakshmana, M. K., Chung, J. Y., Wickramarachchi, S., Tak, E., Bianchi, E., Koo, E. H. and Kang, D. E. (2010) A fragment of the scaffolding protein RanBP9 is increased in Alzheimer's disease brains and strongly potentiates amyloid-beta peptide generation. *Faseb J* **24,** 119-127.

Lakshmana, M. K., Yoon, I. S., Chen, E., Bianchi, E., Koo, E. H. and Kang, D. E. (2009) Novel role of RanBP9 in BACE1 processing of amyloid precursor protein and amyloid beta peptide generation. *J Biol Chem* **284,** 11863-11872.

Lambert, J. C., Mann, D., Goumidi, L., Harris, J., Pasquier, F., Frigard, B., Cottel, D., Lendon, C., Iwatsubo, T., Amouyel, P. and Chartier-Harlin, M. C. (2000) A FE65 polymorphism associated with risk of developing sporadic late-onset alzheimer's disease but not with Abeta loading in brains. *Neurosci Lett* **293,** 29-32.

Lammich, S., Kojro, E., Postina, R., Gilbert, S., Pfeiffer, R., Jasionowski, M., Haass, C. and Fahrenholz, F. (1999) Constitutive and regulated alpha-secretase cleavage of Alzheimer's amyloid precursor protein by a disintegrin metalloprotease. *Proc Natl Acad Sci U S A* **96,** 3922-3927.

Lanier, L. M., Gates, M. A., Witke, W., Menzies, A. S., Wehman, A. M., Macklis, J. D., Kwiatkowski, D., Soriano, P. and Gertler, F. B. (1999) Mena is required for neurulation and commissure formation. *Neuron* **22,** 313-325.

Larkin, M. A., Blackshields, G., Brown, N. P., Chenna, R., McGettigan, P. A., McWilliam, H., Valentin, F., Wallace, I. M., Wilm, A., Lopez, R., Thompson, J. D., Gibson, T. J. and Higgins, D. G. (2007) Clustal W and Clustal X version 2.0. *Bioinformatics* **23,** 2947-2948.

Lau, K. F., McLoughlin, D. M., Standen, C. and Miller, C. C. (2000a) X11 alpha and x11 beta interact with presenilin-1 via their PDZ domains. *Mol Cell Neurosci* **16,** 557-565.

Lau, K. F., McLoughlin, D. M., Standen, C. L., Irving, N. G. and Miller, C. C. (2000b) Fe65 and X11beta co-localize with and compete for binding to the amyloid precursor protein. *Neuroreport* **11,** 3607-3610.

Lazarov, O., Morfini, G. A., Lee, E. B., Farah, M. H., Szodorai, A., DeBoer, S. R., Koliatsos, V. E., Kins, S., Lee, V. M., Wong, P. C., Price, D. L., Brady, S. T. and Sisodia, S. S. (2005) Axonal transport, amyloid precursor protein, kinesin-1, and the processing apparatus: revisited. *J Neurosci* **25,** 2386-2395.

Lee, J., Retamal, C., Cuitino, L., Caruano-Yzermans, A., Shin, J. E., van Kerkhof, P., Marzolo, M. P. and Bu, G. (2008) Adaptor protein sorting nexin 17 regulates amyloid precursor protein trafficking and processing in the early endosomes. *J Biol Chem* **283,** 11501-11508.

Lee, M. S., Kao, S. C., Lemere, C. A., Xia, W., Tseng, H. C., Zhou, Y., Neve, R., Ahlijanian, M. K. and Tsai, L. H. (2003) APP processing is regulated by cytoplasmic phosphorylation. *J Cell Biol* **163,** 83-95.

Lesne, S., Koh, M. T., Kotilinek, L., Kayed, R., Glabe, C. G., Yang, A., Gallagher, M. and Ashe, K. H. (2006) A specific amyloid-beta protein assembly in the brain impairs memory. *Nature* **440,** 352-357.

Leyssen, M., Ayaz, D., Hebert, S. S., Reeve, S., De Strooper, B. and Hassan, B. A. (2005) Amyloid precursor protein promotes post-developmental neurite arborization in the Drosophila brain. *EMBO J* **24,** 2944-2955.

Li, C. M., Li, W., Man, X. Y., Zhou, J., Chen, J. Q., Cai, S. Q. and Zheng, M. (2011) Pigment epithelium-derived factor plays an inhibitory role in proliferation and migration of HaCaT cells. *Mol Biol Rep* **38,** 2099-2105.

Lichtenthaler, S. F., Haass, C. and Steiner, H. (2011) Regulated intramembrane proteolysis – lessons from amyloid precursor protein processing. *Journal of Neurochemistry* **117,** 779-796.

Lichtenthaler, S. F. and Steiner, H. (2007) Sheddases and intramembrane-cleaving proteases: RIPpers of the membrane. *EMBO Rep* **8,** 537-541.

Lim, J., Hao, T., Shaw, C., Patel, A. J., Szabo, G., Rual, J. F., Fisk, C. J., Li, N., Smolyar, A., Hill, D. E., Barabasi, A. L., Vidal, M. and Zoghbi, H. Y. (2006) A protein-protein interaction network for human inherited ataxias and disorders of Purkinje cell degeneration. *Cell* **125,** 801-814.

Lipscombe, D. (2005) Neuronal proteins custom designed by alternative splicing. *Current Opinion in Neurobiology* **15,** 358-363.

Liu, F. L., Liu, P. H., Shao, H. W. and Kung, F. L. (2006) The intracellular domain of amyloid precursor protein interacts with FKBP12. *Biochem Biophys Res Commun* **350,** 472-477.

Liu, Q., Zerbinatti, C. V., Zhang, J., Hoe, H. S., Wang, B., Cole, S. L., Herz, J., Muglia, L. and Bu, G. (2007) Amyloid precursor protein regulates brain apolipoprotein E and cholesterol metabolism through lipoprotein receptor LRP1. *Neuron* **56,** 66-78.

Lorenzo, A., Yuan, M., Zhang, Z., Paganetti, P. A., Sturchler-Pierrat, C., Staufenbiel, M., Mautino, J., Vigo, F. S., Sommer, B. and Yankner, B. A. (2000) Amyloid beta interacts with the amyloid precursor protein: a potential toxic mechanism in Alzheimer's disease. *Nat Neurosci* **3,** 460-464.

Lu, D. C., Rabizadeh, S., Chandra, S., Shayya, R. F., Ellerby, L. M., Ye, X., Salvesen, G. S., Koo, E. H. and Bredesen, D. E. (2000) A second cytotoxic proteolytic peptide derived from amyloid beta-protein precursor. *Nat Med* **6,** 397-404.

Luo, L., Tully, T. and White, K. (1992) Human amyloid precursor protein ameliorates behavioral deficit of flies deleted for Appl gene. *Neuron* **9,** 595-605.

Ma, Q. H., Futagawa, T., Yang, W. L., Jiang, X. D., Zeng, L., Takeda, Y., Xu, R. X., Bagnard, D., Schachner, M., Furley, A. J., Karagogeos, D., Watanabe, K., Dawe, G. S. and Xiao, Z. C. (2008) A TAG1-APP signalling pathway through Fe65 negatively modulates neurogenesis. *Nat Cell Biol* **10,** 283-294.

Madeira, A., Pommet, J. M., Prochiantz, A. and Allinquant, B. (2005) SET protein (TAF1beta, I2PP2A) is involved in neuronal apoptosis induced by an amyloid precursor protein cytoplasmic subdomain. *FASEB J* **19,** 1905-1907.

Maglott, D., Ostell, J., Pruitt, K. D. and Tatusova, T. (2010) Entrez Gene: gene-centered information at NCBI. *Nucleic Acids Research*.

Masliah, E., Mallory, M., Deerinck, T., DeTeresa, R., Lamont, S., Miller, A., Terry, R. D., Carragher, B. and Ellisman, M. (1993) Re-evaluation of the structural organization of neuritic plaques in Alzheimer's disease. *J Neuropathol Exp Neurol* **52,** 619-632.

Masters, C. L., Simms, G., Weinman, N. A., Multhaup, G., McDonald, B. L. and Beyreuther, K. (1985) Amyloid plaque core protein in Alzheimer disease and Down syndrome. *Proc Natl Acad Sci U S A* **82,** 4245-4249.

Matsushima, H., Shimohama, S., Chachin, M., Taniguchi, T. and Kimura, J. (1996) Ca2+-dependent and Ca2+-independent protein kinase C changes in the brain of patients with Alzheimer's disease. *J Neurochem* **67,** 317-323.

Mattson, M. P. (1997) Cellular actions of beta-amyloid precursor protein and its soluble and fibrillogenic derivatives. *Physiol Rev* **77,** 1081-1132.

Maynard, C. J., Bush, A. I., Masters, C. L., Cappai, R. and Li, Q. X. (2005) Metals and amyloid-beta in Alzheimer's disease. *Int J Exp Pathol* **86,** 147-159.

McCarthy, J., Twomey, C. and Wujek, P. (2009) Presenilin-dependent regulated intramembrane proteolysis and γ-secretase activity. *Cellular and Molecular Life Sciences* **66,** 1534-1555.

McKhann, G., Drachman, D., Folstein, M., Katzman, R., Price, D. and Stadlan, E. M. (1984) Clinical diagnosis of Alzheimer's disease: report of the NINCDS-ADRDA Work Group under the auspices of Department of Health and Human Services Task Force on Alzheimer's Disease. *Neurology* **34,** 939-944.

McKusick, V. A. (2007) Mendelian Inheritance in Man and its online version, OMIM. *Am J Hum Genet* **80,** 588-604.

McLoughlin, D. M., Irving, N. G., Brownlees, J., Brion, J. P., Leroy, K. and Miller, C. C. (1999) Mint2/X11-like colocalizes with the Alzheimer's disease amyloid precursor protein and is associated with neuritic plaques in Alzheimer's disease. *Eur J Neurosci* **11,** 1988-1994.

McLoughlin, D. M. and Miller, C. C. (1996) The intracellular cytoplasmic domain of the Alzheimer's disease amyloid precursor protein interacts with phosphotyrosine-binding domain proteins in the yeast two-hybrid system. *FEBS Lett* **397,** 197-200.

Menon, R. P., Gibson, T. J. and Pastore, A. (2004) The C terminus of fragile X mental retardation protein interacts with the multi-domain Ran-binding protein in the microtubule-organising centre. *J Mol Biol* **343,** 43-53.

Merdes, G., Soba, P., Loewer, A., Bilic, M. V., Beyreuther, K. and Paro, R. (2004) Interference of human and Drosophila APP and APP-like proteins with PNS development in Drosophila. *Embo J* **23,** 4082-4095.

Meziane, H., Dodart, J. C., Mathis, C., Little, S., Clemens, J., Paul, S. M. and Ungerer, A. (1998) Memory-enhancing effects of secreted forms of the beta-amyloid precursor protein in normal and amnestic mice. *Proc Natl Acad Sci U S A* **95,** 12683-12688.

Miller, D. L., Papayannopoulos, I. A., Styles, J., Bobin, S. A., Lin, Y. Y., Biemann, K. and Iqbal, K. (1993) Peptide compositions of the cerebrovascular and senile plaque core amyloid deposits of Alzheimer's disease. *Arch Biochem Biophys* **301,** 41-52.

Minopoli, G., de Candia, P., Bonetti, A., Faraonio, R., Zambrano, N. and Russo, T. (2001) The beta-amyloid precursor protein functions as a cytosolic anchoring site that prevents Fe65 nuclear translocation. *J Biol Chem* **276,** 6545-6550.

Minopoli, G., Stante, M., Napolitano, F., Telese, F., Aloia, L., De Felice, M., Di Lauro, R., Pacelli, R., Brunetti, A., Zambrano, N. and Russo, T. (2007) Essential roles for Fe65, Alzheimer amyloid precursor-binding protein, in the cellular response to DNA damage. *J Biol Chem* **282,** 831-835.

MRC-CFAS (2001) Pathological correlates of late-onset dementia in a multicentre, community-based population in England and Wales. *The Lancet* **357,** 169-175.

Mueller, H. T., Borg, J. P., Margolis, B. and Turner, R. S. (2000) Modulation of amyloid precursor protein metabolism by X11alpha /Mint-1. A deletion analysis of protein-protein interaction domains. *J Biol Chem* **275,** 39302-39306.

Muller, T., Concannon, C. G., Ward, M. W., Walsh, C. M., Tirniceriu, A. L., Tribl, F., Kogel, D., Prehn, J. H. and Egensperger, R. (2007) Modulation of gene expression and cytoskeletal dynamics by the amyloid precursor protein intracellular domain (AICD). *Mol Biol Cell* **18,** 201-210.

Multhaup, G. (1994) Identification and regulation of the high affinity binding site of the Alzheimer's disease amyloid protein precursor (APP) to glycosaminoglycans. *Biochimie* **76,** 304-311.

Multhaup, G., Bush, A. I., Pollwein, P. and Masters, C. L. (1994) Interaction between the zinc (II) and the heparin binding site of the Alzheimer's disease beta A4 amyloid precursor protein (APP). *FEBS Lett* **355,** 151-154.

Murrin, L. C. and Talbot, J. N. (2007) RanBPM, a scaffolding protein in the immune and nervous systems. *J Neuroimmune Pharmacol* **2,** 290-295.

Nakamura, M., Masuda, H., Horii, J., Kuma, K., Yokoyama, N., Ohba, T., Nishitani, H., Miyata, T., Tanaka, M. and Nishimoto, T. (1998) When overexpressed, a novel centrosomal protein, RanBPM, causes ectopic microtubule nucleation similar to gamma-tubulin. *J Cell Biol* **143,** 1041-1052.

Napolitano, F., D'Angelo, F., Bimonte, M., Perrina, V., D'Ambrosio, C., Scaloni, A., Russo, T. and Zambrano, N. (2008) A differential proteomic approach reveals an evolutionary conserved regulation of Nme proteins by Fe65 in C. elegans and mouse. *Neurochem Res* **33,** 2547-2555.

Nikolaev, A., McLaughlin, T., O'Leary, D. D. and Tessier-Lavigne, M. (2009) APP binds DR6 to trigger axon pruning and neuron death via distinct caspases. *Nature* **457,** 981-989.

Ninomiya, H., Roch, J. M., Jin, L. W. and Saitoh, T. (1994) Secreted form of amyloid beta/A4 protein precursor (APP) binds to two distinct APP binding sites on rat B103 neuron-like cells through two different domains, but only one site is involved in neuritotropic activity. *J Neurochem* **63,** 495-500.

Nishimoto, I., Okamoto, T., Matsuura, Y., Takahashi, S., Murayama, Y. and Ogata, E. (1993) Alzheimer amyloid protein precursor complexes with brain GTP-binding protein G(o). *Nature* **362,** 75-79.

Nishitani, H., Hirose, E., Uchimura, Y., Nakamura, M., Umeda, M., Nishii, K., Mori, N. and Nishimoto, T. (2001) Full-sized RanBPM cDNA encodes a protein possessing a long stretch of proline and glutamine within the N-terminal region, comprising a large protein complex. *Gene* **272,** 25-33.

Nistor, M., Don, M., Parekh, M., Sarsoza, F., Goodus, M., Lopez, G. E., Kawas, C., Leverenz, J., Doran, E., Lott, I. T., Hill, M. and Head, E. (2007) Alpha- and beta-secretase activity as a function of age and beta-amyloid in Down syndrome and normal brain. *Neurobiol Aging* **28,** 1493-1506.

Nitsch, R. M. and Hock, C. (2008) Targeting beta-amyloid pathology in Alzheimer's disease with Abeta immunotherapy. *Neurotherapeutics* **5,** 415-420.

Noviello, C., Vito, P., Lopez, P., Abdallah, M. and D'Adamio, L. (2003) Autosomal recessive hypercholesterolemia protein interacts with and regulates the cell surface level of Alzheimer's amyloid beta precursor protein. *J Biol Chem* **278,** 31843-31847.

Obenauer, J. C., Cantley, L. C. and Yaffe, M. B. (2003) Scansite 2.0: proteome-wide prediction of cell signaling interactions using short sequence motifs. *Nucleic Acids Research* **31,** 3635-3641.

Oh, S. Y., Ellenstein, A., Chen, C. D., Hinman, J. D., Berg, E. A., Costello, C. E., Yamin, R., Neve, R. L. and Abraham, C. R. (2005) Amyloid precursor protein interacts with notch receptors. *J Neurosci Res* **82,** 32-42.

Oishi, M., Nairn, A. C., Czernik, A. J., Lim, G. S., Isohara, T., Gandy, S. E., Greengard, P. and Suzuki, T. (1997) The cytoplasmic domain of Alzheimer's amyloid precursor protein is phosphorylated at Thr654, Ser655, and Thr668 in adult rat brain and cultured cells. *Mol Med* **3,** 111-123.

Okamoto, M. and Sudhof, T. C. (1997) Mints, Munc18-interacting proteins in synaptic vesicle exocytosis. *J Biol Chem* **272,** 31459-31464.

Okamoto, T., Takeda, S., Murayama, Y., Ogata, E. and Nishimoto, I. (1995) Ligand-dependent G protein coupling function of amyloid transmembrane precursor. *J Biol Chem* **270,** 4205-4208.

Oltersdorf, T., Ward, P. J., Henriksson, T., Beattie, E. C., Neve, R., Lieberburg, I. and Fritz, L. C. (1990) The Alzheimer amyloid precursor protein. Identification of a stable intermediate in the biosynthetic/degradative pathway. *J Biol Chem* **265,** 4492-4497.

Palmert, M. R., Golde, T. E., Cohen, M. L., Kovacs, D. M., Tanzi, R. E., Gusella, J. F., Usiak, M. F., Younkin, L. H. and Younkin, S. G. (1988) Amyloid protein precursor messenger RNAs: differential expression in Alzheimer's disease. *Science* **241,** 1080-1084.

Pangalos, M. N., Efthimiopoulos, S., Shioi, J. and Robakis, N. K. (1995) The chondroitin sulfate attachment site of appican is formed by splicing out exon 15 of the amyloid precursor gene. *J Biol Chem* **270,** 10388-10391.

Pappolla, M. A., Omar, R. A., Kim, K. S. and Robakis, N. K. (1992) Immunohistochemical evidence of antioxidant stress in Alzheimer's disease. *American Journal of Pathology* **140,** 621-628.

Pardossi-Piquard, R. and Checler, F. (2012) The physiology of the β-amyloid precursor protein intracellular domain AICD. *Journal of Neurochemistry* **120,** 109-124.

Pardossi-Piquard, R., Petit, A., Kawarai, T., Sunyach, C., Alves da Costa, C., Vincent, B., Ring, S., D'Adamio, L., Shen, J., Muller, U., St George Hyslop, P. and Checler, F. (2005) Presenilin-dependent

transcriptional control of the Abeta-degrading enzyme neprilysin by intracellular domains of betaAPP and APLP. *Neuron* **46,** 541-554.

Park, J. H., Gimbel, D. A., GrandPre, T., Lee, J.-K., Kim, J.-E., Li, W., Lee, D. H. S. and Strittmatter, S. M. (2006) Alzheimer Precursor Protein Interaction with the Nogo-66 Receptor Reduces Amyloid-β Plaque Deposition. *The Journal of Neuroscience* **26,** 1386-1395.

Pasinetti, G. M., Wang, J., Porter, S. and Ho, L. (2011) Caloric intake, dietary lifestyles, macronutrient composition, and alzheimer' disease dementia. *Int J Alzheimers Dis* **2011,** 806293.

Passer, B., Pellegrini, L., Russo, C., Siegel, R. M., Lenardo, M. J., Schettini, G., Bachmann, M., Tabaton, M. and D'Adamio, L. (2000) Generation of an apoptotic intracellular peptide by gamma-secretase cleavage of Alzheimer's amyloid beta protein precursor. *J Alzheimers Dis* **2,** 289-301.

Pastorino, L., Sun, A., Lu, P. J., Zhou, X. Z., Balastik, M., Finn, G., Wulf, G., Lim, J., Li, S. H., Li, X., Xia, W., Nicholson, L. K. and Lu, K. P. (2006) The prolyl isomerase Pin1 regulates amyloid precursor protein processing and amyloid-beta production. *Nature* **440,** 528-534.

Pellegrini, L., Passer, B. J., Tabaton, M., Ganjei, J. K. and D'Adamio, L. (1999) Alternative, non-secretase processing of Alzheimer's beta-amyloid precursor protein during apoptosis by caspase-6 and -8. *J Biol Chem* **274,** 21011-21016.

Perkinton, M. S., Standen, C. L., Lau, K. F., Kesavapany, S., Byers, H. L., Ward, M., McLoughlin, D. M. and Miller, C. C. (2004) The c-Abl tyrosine kinase phosphorylates the Fe65 adaptor protein to stimulate Fe65/amyloid precursor protein nuclear signaling. *J Biol Chem* **279,** 22084-22091.

Perl, D. P. (2010) Neuropathology of Alzheimer's Disease. *Mount Sinai Journal of Medicine: A Journal of Translational and Personalized Medicine* **77,** 32-42.

Perreau, V. M., Orchard, S., Adlard, P. A., Bellingham, S. A., Cappai, R., Ciccotosto, G. D., Cowie, T. F., Crouch, P. J., Duce, J. A., Evin, G., Faux, N. G., Hill, A. F., Hung, Y. H., James, S. A., Li, Q. X., Mok, S. S., Tew, D. J., White, A. R., Bush, A. I., Hermjakob, H. and Masters, C. L. (2010) A domain level interaction network of amyloid precursor protein and Abeta of Alzheimer's disease. *Proteomics* **10,** 2377-2395.

Petersen, R. C. and Negash, S. (2008) Mild cognitive impairment: an overview. *CNS Spectr* **13,** 45-53.

Petrovitch, H., White, L. R., Izmirilian, G., Ross, G. W., Havlik, R. J., Markesbery, W., Nelson, J., Davis, D. G., Hardman, J., Foley, D. J. and Launer, L. J. (2000) Midlife blood pressure and neuritic plaques, neurofibrillary tangles, and brain weight at death: the HAAS. Honolulu-Asia aging Study. *Neurobiol Aging* **21,** 57-62.

Pietrzik, C. U., Yoon, I. S., Jaeger, S., Busse, T., Weggen, S. and Koo, E. H. (2004) FE65 constitutes the functional link between the low-density lipoprotein receptor-related protein and the amyloid precursor protein. *J Neurosci* **24,** 4259-4265.

Poirier, J., Davignon, J., Bouthillier, D., Kogan, S., Bertrand, P. and Gauthier, S. (1993) Apolipoprotein E polymorphism and Alzheimer's disease. *Lancet* **342,** 697-699.

Poirier, M. B., Laflamme, L. and Langlois, M. F. (2006) Identification and characterization of RanBPM, a novel coactivator of thyroid hormone receptors. *J Mol Endocrinol* **36,** 313-325.

Ponting, C., Schultz, J. and Bork, P. (1997) SPRY domains in ryanodine receptors (Ca(2+)-release channels). *Trends Biochem Sci* **22,** 193-194.

Portelius, E., Price, E., Brinkmalm, G., Stiteler, M., Olsson, M., Persson, R., Westman-Brinkmalm, A., Zetterberg, H., Simon, A. J. and Blennow, K. (2011) A novel pathway for amyloid precursor protein processing. *Neurobiology of Aging* **32,** 1090-1098.

Prasad, T. S., Kandasamy, K. and Pandey, A. (2009) Human Protein Reference Database and Human Proteinpedia as discovery tools for systems biology. *Methods Mol Biol* **577,** 67-79.

Qi-Takahara, Y., Morishima-Kawashima, M., Tanimura, Y., Dolios, G., Hirotani, N., Horikoshi, Y., Kametani, F., Maeda, M., Saido, T. C., Wang, R. and Ihara, Y. (2005) Longer forms of amyloid beta protein: implications for the mechanism of intramembrane cleavage by gamma-secretase. *J Neurosci* **25,** 436-445.

Qiu, C., Kivipelto, M. and von Strauss, E. (2009) Epidemiology of Alzheimer's disease: occurrence, determinants, and strategies toward intervention. *Dialogues Clin Neurosci* **11,** 111-128.

Qiu, W. Q., Ferreira, A., Miller, C., Koo, E. H. and Selkoe, D. J. (1995) Cell-surface beta-amyloid precursor protein stimulates neurite outgrowth of hippocampal neurons in an isoform-dependent manner. *J Neurosci* **15,** 2157-2167.

Radzimanowski, J., Simon, B., Sattler, M., Beyreuther, K., Sinning, I. and Wild, K. (2008) Structure of the intracellular domain of the amyloid precursor protein in complex with Fe65-PTB2. *EMBO Rep* **9,** 1134-1140.

Rao, M. A., Cheng, H., Quayle, A. N., Nishitani, H., Nelson, C. C. and Rennie, P. S. (2002) RanBPM, a nuclear protein that interacts with and regulates transcriptional activity of androgen receptor and glucocorticoid receptor. *J Biol Chem* **277,** 48020-48027.

Rebelo, S., Vieira, S. I., Esselmann, H., Wiltfang, J., da Cruz e Silva, E. F. and da Cruz e Silva, O. A. (2007a) Tyr687 dependent APP endocytosis and Abeta production. *J Mol Neurosci* **32,** 1-8.

Rebelo, S., Vieira, S. I., Esselmann, H., Wiltfang, J., da Cruz e Silva, E. F. and da Cruz e Silva, O. A. (2007b) Tyrosine 687 phosphorylated Alzheimer's amyloid precursor protein is retained intracellularly and exhibits a decreased turnover rate. *Neurodegener Dis* **4,** 78-87.

Reese, M. G., Eeckman, F. H., Kulp, D. and Haussler, D. (1997) Improved splice site detection in Genie. *J Comput Biol* **4,** 311-323.

Reszka, A. A., Hayashi, Y. and Horwitz, A. F. (1992) Identification of amino acid sequences in the integrin beta 1 cytoplasmic domain implicated in cytoskeletal association. *J Cell Biol* **117,** 1321-1330.

Riddell, D. R., Christie, G., Hussain, I. and Dingwall, C. (2001) Compartmentalization of beta-secretase (Asp2) into low-buoyant density, noncaveolar lipid rafts. *Curr Biol* **11,** 1288-1293.

Ring, S., Weyer, S. W., Kilian, S. B., Waldron, E., Pietrzik, C. U., Filippov, M. A., Herms, J., Buchholz, C., Eckman, C. B., Korte, M., Wolfer, D. P. and Muller, U. C. (2007) The secreted beta-amyloid precursor protein ectodomain APPs alpha is sufficient to rescue the anatomical, behavioral, and electrophysiological abnormalities of APP-deficient mice. *J Neurosci* **27,** 7817-7826.

Robakis, N. K. (2011) Mechanisms of AD neurodegeneration may be independent of Abeta and its derivatives. *Neurobiol Aging* **32,** 372-379.

Rogaeva, E. (2002) The solved and unsolved mysteries of the genetics of early-onset Alzheimer's disease. *Neuromolecular Med* **2,** 1-10.

Roncarati, R., Sestan, N., Scheinfeld, M. H., Berechid, B. E., Lopez, P. A., Meucci, O., McGlade, J. C., Rakic, P. and D'Adamio, L. (2002) The gamma-secretase-generated intracellular domain of beta-amyloid precursor protein binds Numb and inhibits Notch signaling. *Proc Natl Acad Sci U S A* **99,** 7102-7107.

Rooke, K., Talbot, C., James, L., Anand, R., Hardy, J. A. and Goate, A. M. (1993) A physical map of the human APP gene in YACs. *Mamm Genome* **4,** 662-669.

Rossjohn, J., Cappai, R., Feil, S. C., Henry, A., McKinstry, W. J., Galatis, D., Hesse, L., Multhaup, G., Beyreuther, K., Masters, C. L. and Parker, M. W. (1999) Crystal structure of the N-terminal, growth factor-like domain of Alzheimer amyloid precursor protein. *Nat Struct Biol* **6,** 327-331.

Rovelet-Lecrux, A., Hannequin, D., Raux, G., Le Meur, N., Laquerriere, A., Vital, A., Dumanchin, C., Feuillette, S., Brice, A., Vercelletto, M., Dubas, F., Frebourg, T. and Campion, D. (2006) APP locus duplication causes autosomal dominant early-onset Alzheimer disease with cerebral amyloid angiopathy. *Nat Genet* **38,** 24-26.

Russo, C., Dolcini, V., Salis, S., Venezia, V., Violani, E., Carlo, P., Zambrano, N., Russo, T. and Schettini, G. (2002) Signal transduction through tyrosine-phosphorylated carboxy-terminal fragments of APP via an enhanced interaction with Shc/Grb2 adaptor proteins in reactive astrocytes of Alzheimer's disease brain. *Ann N Y Acad Sci* **973,** 323-333.

Russo, T., Faraonio, R., Minopoli, G., De Candia, P., De Renzis, S. and Zambrano, N. (1998) Fe65 and the protein network centered around the cytosolic domain of the Alzheimer's beta-amyloid precursor protein. *FEBS Lett* **434,** 1-7.

Ryan, K. A. and Pimplikar, S. W. (2005) Activation of GSK-3 and phosphorylation of CRMP2 in transgenic mice expressing APP intracellular domain. *J Cell Biol* **171,** 327-335.

Sabo, S. L., Ikin, A. F., Buxbaum, J. D. and Greengard, P. (2001) The Alzheimer amyloid precursor protein (APP) and FE65, an APP-binding protein, regulate cell movement. *J Cell Biol* **153,** 1403-1414.

Sabo, S. L., Ikin, A. F., Buxbaum, J. D. and Greengard, P. (2003) The amyloid precursor protein and its regulatory protein, FE65, in growth cones and synapses in vitro and in vivo. *J Neurosci* **23,** 5407-5415.

Sabo, S. L., Lanier, L. M., Ikin, A. F., Khorkova, O., Sahasrabudhe, S., Greengard, P. and Buxbaum, J. D. (1999) Regulation of beta-amyloid secretion by FE65, an amyloid protein precursor-binding protein. *J Biol Chem* **274,** 7952-7957.

Saitoh, T., Sundsmo, M., Roch, J.-M., Kimura, N., Cole, G., Schubert, D., Oltersdorf, T. and Schenk, D. B. (1989) Secreted form of amyloid ² protein precursor is involved in the growth regulation of fibroblasts. *Cell* **58,** 615-622.

Sakurai, H., Hanyu, H., Sato, T., Kanetaka, H., Shimizu, S., Hirao, K., Kikukawa, M. and Iwamoto, T. (2011) Vascular risk factors and progression in Alzheimer's disease. *Geriatr Gerontol Int* **11,** 211-214.

Sandbrink, R., Masters, C. L. and Beyreuther, K. (1994) APP gene family: unique age-associated changes in splicing of Alzheimer's betaA4-amyloid protein precursor. *Neurobiol Dis* **1,** 13-24.

Sandbrink, R., Monning, U., Masters, C. L. and Beyreuther, K. (1997) Expression of the APP gene family in brain cells, brain development and aging. *Gerontology* **43,** 119-131.

Sastre, M., Steiner, H., Fuchs, K., Capell, A., Multhaup, G., Condron, M. M., Teplow, D. B. and Haass, C. (2001) Presenilin-dependent gamma-secretase processing of beta-amyloid precursor protein at a site corresponding to the S3 cleavage of Notch. *EMBO Rep* **2,** 835-841.

Saunders, A. M., Strittmatter, W. J., Schmechel, D., George-Hyslop, P. H., Pericak-Vance, M. A., Joo, S. H., Rosi, B. L., Gusella, J. F., Crapper-MacLachlan, D. R., Alberts, M. J. and et al. (1993) Association of apolipoprotein E allele epsilon 4 with late-onset familial and sporadic Alzheimer's disease. *Neurology* **43,** 1467-1472.

Scheinfeld, M. H., Roncarati, R., Vito, P., Lopez, P. A., Abdallah, M. and D'Adamio, L. (2002) Jun NH2-terminal kinase (JNK) interacting protein 1 (JIP1) binds the cytoplasmic domain of the Alzheimer's beta-amyloid precursor protein (APP). *J Biol Chem* **277,** 3767-3775.

Seet, L. F. and Hong, W. (2006) The Phox (PX) domain proteins and membrane traffic. *Biochim Biophys Acta* **1761,** 878-896.

Selkoe, D. and Kopan, R. (2003) Notch and Presenilin: regulated intramembrane proteolysis links development and degeneration. *Annu Rev Neurosci* **26,** 565-597.

Selkoe, D. J. (1991) The molecular pathology of Alzheimer's disease. *Neuron* **6,** 487-498.

Selkoe, D. J. (2001) Alzheimer's disease: genes, proteins, and therapy. *Physiol Rev* **81,** 741-766.

Selkoe, D. J. (2002) Alzheimer's disease is a synaptic failure. *Science* **298,** 789-791.

Selkoe, D. J. (2007) Developing preventive therapies for chronic diseases: lessons learned from Alzheimer's disease. *Nutr Rev* **65,** S239-243.

Serebriiskii, I. G. and Golemis, E. A. (2001) Two-hybrid system and false positives. Approaches to detection and elimination. *Methods Mol Biol* **177,** 123-134.

Serebriiskii, I. G., Toby, G. G., Finley, R. L., Jr. and Golemis, E. A. (2001) Genomic analysis utilizing the yeast two-hybrid system. *Methods Mol Biol* **175,** 415-454.

Seubert, P., Oltersdorf, T., Lee, M. G., Barbour, R., Blomquist, C., Davis, D. L., Bryant, K., Fritz, L. C., Galasko, D., Thal, L. J. and et al. (1993) Secretion of beta-amyloid precursor protein cleaved at the amino terminus of the beta-amyloid peptide. *Nature* **361,** 260-263.

Shahani, N. and Brandt, R. (2002) Functions and malfunctions of the tau proteins. *Cell Mol Life Sci* **59,** 1668-1680.

Shannon, P., Markiel, A., Ozier, O., Baliga, N. S., Wang, J. T., Ramage, D., Amin, N., Schwikowski, B. and Ideker, T. (2003) Cytoscape: A Software Environment for Integrated Models of Biomolecular Interaction Networks. *Genome Research* **13,** 2498-2504.

Shi, J., Zhang, S., Tang, M., Liu, X., Li, T., Han, H., Wang, Y., Guo, Y., Zhao, J., Li, H. and Ma, C. (2004) Possible association between Cys311Ser polymorphism of paraoxonase 2 gene and late-onset Alzheimer's disease in Chinese. *Molecular Brain Research* **120,** 201-204.

Sigrist, C. J. A., Cerutti, L., de Castro, E., Langendijk-Genevaux, P. S., Bulliard, V., Bairoch, A. and Hulo, N. (2010) PROSITE, a protein domain database for functional characterization and annotation. *Nucleic Acids Research* **38,** D161-D166.

Sisodia, S. S. (1992) Beta-amyloid precursor protein cleavage by a membrane-bound protease. *Proc Natl Acad Sci U S A* **89,** 6075-6079.

Sisodia, S. S., Kim, S. H. and Thinakaran, G. (1999) Function and dysfunction of the presenilins. *Am J Hum Genet* **65,** 7-12.

Sisodia, S. S., Koo, E. H., Beyreuther, K., Unterbeck, A. and Price, D. L. (1990) Evidence that beta-amyloid protein in Alzheimer's disease is not derived by normal processing. *Science* **248,** 492-495.

Small, J. V., Stradal, T., Vignal, E. and Rottner, K. (2002) The lamellipodium: where motility begins. *Trends in cell biology* **12,** 112-120.

Small, S. A. and Gandy, S. (2006) Sorting through the cell biology of Alzheimer's disease: intracellular pathways to pathogenesis. *Neuron* **52,** 15-31.

Smoot, M. E., Ono, K., Ruscheinski, J., Wang, P. L. and Ideker, T. (2011) Cytoscape 2.8: new features for data integration and network visualization. *Bioinformatics* **27,** 431-432.

Soba, P., Eggert, S., Wagner, K., Zentgraf, H., Siehl, K., Kreger, S., Lower, A., Langer, A., Merdes, G., Paro, R., Masters, C. L., Muller, U., Kins, S. and Beyreuther, K. (2005) Homo- and heterodimerization of APP family members promotes intercellular adhesion. *EMBO J* **24,** 3624-3634.

Soler-Lopez, M., Zanzoni, A., Lluis, R., Stelzl, U. and Aloy, P. (2011) Interactome mapping suggests new mechanistic details underlying Alzheimer's disease. *Genome Res* **21,** 364-376.

Soriano, S., Lu, D. C., Chandra, S., Pietrzik, C. U. and Koo, E. H. (2001) The amyloidogenic pathway of amyloid precursor protein (APP) is independent of its cleavage by caspases. *J Biol Chem* **276,** 29045-29050.

Spitzer, P., Klafki, H. W., Blennow, K., Buee, L., Esselmann, H., Herruka, S. K., Jimenez, C., Klivenyi, P., Lewczuk, P., Maler, J. M., Markus, K., Meyer, H. E., Morris, C., Muller, T., Otto, M., Parnetti, L., Soininen, H., Schraen, S., Teunissen, C., Vecsei, L., Zetterberg, H. and Wiltfang, J. (2010) cNEUPRO: Novel Biomarkers for Neurodegenerative Diseases. *Int J Alzheimers Dis* **2010**.

Stamer, K., Vogel, R., Thies, E., Mandelkow, E. and Mandelkow, E. M. (2002) Tau blocks traffic of organelles, neurofilaments, and APP vesicles in neurons and enhances oxidative stress. *J Cell Biol* **156,** 1051-1063.

Stark, C., Breitkreutz, B.-J., Chatr-aryamontri, A., Boucher, L., Oughtred, R., Livstone, M. S., Nixon, J., Van Auken, K., Wang, X., Shi, X., Reguly, T., Rust, J. M., Winter, A., Dolinski, K. and Tyers, M. (2010) The BioGRID Interaction Database: 2011 update. *Nucleic Acids Research*.

Storey, E., Spurck, T., Pickett-Heaps, J., Beyreuther, K. and Masters, C. L. (1996) The amyloid precursor protein of Alzheimer's disease is found on the surface of static but not activity motile portions of neurites. *Brain Res* **735,** 59-66.

Strittmatter, W. J., Saunders, A. M., Schmechel, D., Pericak-Vance, M., Enghild, J., Salvesen, G. S. and Roses, A. D. (1993) Apolipoprotein E: high-avidity binding to beta-amyloid and increased frequency of type 4 allele in late-onset familial Alzheimer disease. *Proc Natl Acad Sci U S A* **90,** 1977-1981.

Sumioka, A., Nagaishi, S., Yoshida, T., Lin, A., Miura, M. and Suzuki, T. (2005) Role of 14-3-3gamma in FE65-dependent gene transactivation mediated by the amyloid beta-protein precursor cytoplasmic fragment. *J Biol Chem* **280,** 42364-42374.

Suzuki, T., Oishi, M., Marshak, D. R., Czernik, A. J., Nairn, A. C. and Greengard, P. (1994) Cell cycle-dependent regulation of the phosphorylation and metabolism of the Alzheimer amyloid precursor protein. *Embo J* **13,** 1114-1122.

Tamayev, R., Zhou, D. and D'Adamio, L. (2009) The interactome of the amyloid beta precursor protein family members is shaped by phosphorylation of their intracellular domains. *Mol Neurodegener* **4,** 28.

Tanahashi, H. and Tabira, T. (1999a) Genomic organization of the human X11L2 gene (APBA3), a third member of the X11 protein family interacting with Alzheimer's beta-amyloid precursor protein. *Neuroreport* **10,** 2575-2578.

Tanahashi, H. and Tabira, T. (1999b) X11L2, a new member of the X11 protein family, interacts with Alzheimer's beta-amyloid precursor protein. *Biochem Biophys Res Commun* **255,** 663-667.

Tanaka, S., Shiojiri, S., Takahashi, Y., Kitaguchi, N., Ito, H., Kameyama, M., Kimura, J., Nakamura, S. and Ueda, K. (1989) Tissue-specific expression of three types of beta-protein precursor mRNA: enhancement of protease inhibitor-harboring types in Alzheimer's disease brain. *Biochem Biophys Res Commun* **165,** 1406-1414.

Tanzi, R., Gaston, S., Bush, A., Romano, D., Pettingell, W., Peppercorn, J., Paradis, M., Gurubhagavatula, S., Jenkins, B. and Wasco, W. (1993) Genetic heterogeneity of gene defects responsible for familial Alzheimer disease. *Genetica* **91,** 255-263.

Tanzi, R. E., Gusella, J. F., Watkins, P. C., Bruns, G. A., St George-Hyslop, P., Van Keuren, M. L., Patterson, D., Pagan, S., Kurnit, D. M. and Neve, R. L. (1987) Amyloid beta protein gene: cDNA, mRNA distribution, and genetic linkage near the Alzheimer locus. *Science* **235,** 880-884.

Tanzi, R. E., McClatchey, A. I., Lamperti, E. D., Villa-Komaroff, L., Gusella, J. F. and Neve, R. L. (1988) Protease inhibitor domain encoded by an amyloid protein precursor mRNA associated with Alzheimer's disease. *Nature* **331,** 528-530.

Tarr, P. E., Contursi, C., Roncarati, R., Noviello, C., Ghersi, E., Scheinfeld, M. H., Zambrano, N., Russo, T. and D'Adamio, L. (2002a) Evidence for a role of the nerve growth factor receptor TrkA in tyrosine phosphorylation and processing of beta-APP. *Biochem Biophys Res Commun* **295,** 324-329.

Tarr, P. E., Roncarati, R., Pelicci, G., Pelicci, P. G. and D'Adamio, L. (2002b) Tyrosine phosphorylation of the beta-amyloid precursor protein cytoplasmic tail promotes interaction with Shc. *J Biol Chem* **277,** 16798-16804.

Telese, F., Bruni, P., Donizetti, A., Gianni, D., D'Ambrosio, C., Scaloni, A., Zambrano, N., Rosenfeld, M. G. and Russo, T. (2005) Transcription regulation by the adaptor protein Fe65 and the nucleosome assembly factor SET. *EMBO Rep* **6,** 77-82.

Terry, R. D., Hansen, L. A., DeTeresa, R., Davies, P., Tobias, H. and Katzman, R. (1987) Senile dementia of the Alzheimer type without neocortical neurofibrillary tangles. *J Neuropathol Exp Neurol* **46,** 262-268.

Terry, R. D., Masliah, E., Salmon, D. P., Butters, N., DeTeresa, R., Hill, R., Hansen, L. A. and Katzman, R. (1991) Physical basis of cognitive alterations in Alzheimer's disease: synapse loss is the major correlate of cognitive impairment. *Ann Neurol* **30,** 572-580.

Thinakaran, G. and Koo, E. (2007) APP Biology, Processing and Function. In: *ALZHEIMER'S DISEASE - Advances in Genetics, Molecular and Cellular Biology*. pp. 17-34. Eds. S. S. Sisodia, R. E. Tanzi. Springer US.

Thinakaran, G. and Koo, E. H. (2008) Amyloid precursor protein trafficking, processing, and function. *J Biol Chem* **283,** 29615-29619.

Togashi, H., Schmidt, E. F. and Strittmatter, S. M. (2006) RanBPM contributes to Semaphorin3A signaling through plexin-A receptors. *J Neurosci* **26,** 4961-4969.

Tomita, S., Ozaki, T., Taru, H., Oguchi, S., Takeda, S., Yagi, Y., Sakiyama, S., Kirino, Y. and Suzuki, T. (1999) Interaction of a neuron-specific protein containing PDZ domains with Alzheimer's amyloid precursor protein. *J Biol Chem* **274,** 2243-2254.

Trommsdorff, M., Borg, J. P., Margolis, B. and Herz, J. (1998) Interaction of cytosolic adaptor proteins with neuronal apolipoprotein E receptors and the amyloid precursor protein. *J Biol Chem* **273,** 33556-33560.

Turner, P. R., O'Connor, K., Tate, W. P. and Abraham, W. C. (2003) Roles of amyloid precursor protein and its fragments in regulating neural activity, plasticity and memory. *Prog Neurobiol* **70,** 1-32.

Tyree, C. M. and Klausing, K. (2003) The mammalian two-hybrid assay for detection of coactivator-nuclear receptor interactions. *Methods Mol Med* **85,** 175-183.

Umeda, M., Nishitani, H. and Nishimoto, T. (2003) A novel nuclear protein, Twa1, and Muskelin comprise a complex with RanBPM. *Gene* **303,** 47-54.

Valiyaveettil, M., Bentley, A. A., Gursahaney, P., Hussien, R., Chakravarti, R., Kureishy, N., Prag, S. and Adams, J. C. (2008) Novel role of the muskelin-RanBP9 complex as a nucleocytoplasmic mediator of cell morphology regulation. *J Cell Biol* **182,** 727-739.

Vassar, R., Bennett, B. D., Babu-Khan, S., Kahn, S., Mendiaz, E. A., Denis, P., Teplow, D. B., Ross, S., Amarante, P., Loeloff, R., Luo, Y., Fisher, S., Fuller, J., Edenson, S., Lile, J., Jarosinski, M. A., Biere, A. L., Curran, E., Burgess, T., Louis, J. C., Collins, F., Treanor, J., Rogers, G. and Citron, M. (1999) Beta-secretase cleavage of Alzheimer's amyloid precursor protein by the transmembrane aspartic protease BACE. *Science* **286,** 735-741.

Vassar, R., Kovacs, D. M., Yan, R. and Wong, P. C. (2009) The β-Secretase Enzyme BACE in Health and Alzheimer's Disease: Regulation, Cell Biology, Function, and Therapeutic Potential. *The Journal of Neuroscience* **29,** 12787-12794.

Venugopal, C., Pappolla, M. A. and Sambamurti, K. (2007) Insulysin cleaves the APP cytoplasmic fragment at multiple sites. *Neurochem Res* **32,** 2225-2234.

Vetrivel, K. S., Cheng, H., Kim, S. H., Chen, Y., Barnes, N. Y., Parent, A. T., Sisodia, S. S. and Thinakaran, G. (2005) Spatial segregation of gamma-secretase and substrates in distinct membrane domains. *J Biol Chem* **280,** 25892-25900.

Vieira, S. I., Rebelo, S., Domingues, S. C., da Cruz e Silva, E. F. and da Cruz e Silva, O. A. (2009) S655 phosphorylation enhances APP secretory traffic. *Mol Cell Biochem* **328,** 145-154.

Vieira, S. I., Rebelo, S., Esselmann, H., Wiltfang, J., Lah, J., Lane, R., Small, S. A., Gandy, S., da Cruz e Silva, E. F. and da Cruz e Silva, O. A. (2010) Retrieval of the Alzheimer's amyloid precursor protein from the endosome to the TGN is S655 phosphorylation state-dependent and retromer-mediated. *Mol Neurodegener* **5,** 40.

Vijayan, S., El-Akkad, E., Grundke-Iqbal, I. and Iqbal, K. (2001) A pool of beta-tubulin is hyperphosphorylated at serine residues in Alzheimer disease brain. *FEBS Lett* **509,** 375-381.

Vingtdeux, V., Hamdane, M., Begard, S., Loyens, A., Delacourte, A., Beauvillain, J. C., Buee, L., Marambaud, P. and Sergeant, N. (2007a) Intracellular pH regulates amyloid precursor protein intracellular domain accumulation. *Neurobiol Dis* **25,** 686-696.

Vingtdeux, V., Hamdane, M., Loyens, A., Gele, P., Drobeck, H., Begard, S., Galas, M. C., Delacourte, A., Beauvillain, J. C., Buee, L. and Sergeant, N. (2007b) Alkalizing drugs induce accumulation of amyloid precursor protein by-products in luminal vesicles of multivesicular bodies. *J Biol Chem* **282,** 18197-18205.

von Rotz, R. C., Kohli, B. M., Bosset, J., Meier, M., Suzuki, T., Nitsch, R. M. and Konietzko, U. (2004) The APP intracellular domain forms nuclear multiprotein complexes and regulates the transcription of its own precursor. *J Cell Sci* **117,** 4435-4448.

Wagey, R. T. and Krieger, C. (1998) Abnormalities of protein kinases in neurodegenerative diseases. *Prog Drug Res* **51,** 133-183.

Wakabayashi, T., Iwatsubo, T. and Strooper, B. (2007) The Biology of the Presenilin Complexes

Alzheimer's Disease. pp. 35-58. Eds. S. S. Sisodia, R. E. Tanzi. Springer US.

Wang, B., Hu, Q., Hearn, M. G., Shimizu, K., Ware, C. B., Liggitt, D. H., Jin, L. W., Cool, B. H., Storm, D. R. and Martin, G. M. (2004) Isoform-specific knockout of FE65 leads to impaired learning and memory. *J Neurosci Res* **75,** 12-24.

Wang, D., Li, Z., Messing, E. M. and Wu, G. (2002a) Activation of Ras/Erk pathway by a novel MET-interacting protein RanBPM. *J Biol Chem* **277,** 36216-36222.

Wang, P., Yang, G., Mosier, D. R., Chang, P., Zaidi, T., Gong, Y. D., Zhao, N. M., Dominguez, B., Lee, K. F., Gan, W. B. and Zheng, H. (2005) Defective neuromuscular synapses in mice lacking amyloid precursor protein (APP) and APP-Like protein 2. *J Neurosci* **25,** 1219-1225.

Wang, Y., Marion Schneider, E., Li, X., Duttenhofer, I., Debatin, K. and Hug, H. (2002b) HIPK2 associates with RanBPM. *Biochem Biophys Res Commun* **297,** 148-153.

Watanabe, T., Sukegawa, J., Sukegawa, I., Tomita, S., Iijima, K., Oguchi, S., Suzuki, T., Nairn, A. C. and Greengard, P. (1999) A 127-kDa protein (UV-DDB) binds to the cytoplasmic domain of the Alzheimer's amyloid precursor protein. *J Neurochem* **72,** 549-556.

Weidemann, A., Eggert, S., Reinhard, F. B., Vogel, M., Paliga, K., Baier, G., Masters, C. L., Beyreuther, K. and Evin, G. (2002) A novel epsilon-cleavage within the transmembrane domain of the Alzheimer amyloid precursor protein demonstrates homology with Notch processing. *Biochemistry* **41,** 2825-2835.

Weidemann, A., Konig, G., Bunke, D., Fischer, P., Salbaum, J. M., Master, C. L. and Beyreuther, K. (1989) Identification, biogenesis, and localization of precursors of Alzheimer's disease A4 amyloid protein. *Cell* **57,** 115–126.

Weidemann, A., Paliga, K., Durrwang, U., Reinhard, F. B., Schuckert, O., Evin, G. and Masters, C. L. (1999) Proteolytic processing of the Alzheimer's disease amyloid precursor protein within its cytoplasmic domain by caspase-like proteases. *J Biol Chem* **274,** 5823-5829.

Werner, P. and Korczyn, A. D. (2008) Mild cognitive impairment: conceptual, assessment, ethical, and social issues. *Clin Interv Aging* **3,** 413-420.

Whitehouse, P. J., Price, D. L., Clark, A. W., Coyle, J. T. and DeLong, M. R. (1981) Alzheimer disease: evidence for selective loss of cholinergic neurons in the nucleus basalis. *Ann Neurol* **10,** 122-126.

Wiley, J. C., Smith, E. A., Hudson, M. P., Ladiges, W. C. and Bothwell, M. (2007) Fe65 stimulates proteolytic liberation of the beta-amyloid precursor protein intracellular domain. *J Biol Chem* **282,** 33313-33325.

Williamson, T. G., Mok, S. S., Henry, A., Cappai, R., Lander, A. D., Nurcombe, V., Beyreuther, K., Masters, C. L. and Small, D. H. (1996) Secreted glypican binds to the amyloid precursor protein of Alzheimer's disease (APP) and inhibits APP-induced neurite outgrowth. *J Biol Chem* **271,** 31215-31221.

Wilquet, V. and De Strooper, B. (2004) Amyloid-beta precursor protein processing in neurodegeneration. *Curr Opin Neurobiol* **14,** 582-588.

Wolfe, M. S. (2008a) Gamma-secretase inhibition and modulation for Alzheimer's disease. *Curr Alzheimer Res* **5,** 158-164.

Wolfe, M. S. (2008b) Inhibition and modulation of gamma-secretase for Alzheimer's disease. *Neurotherapeutics* **5,** 391-398.

Wolfe, M. S., Xia, W., Ostaszewski, B. L., Diehl, T. S., Kimberly, W. T. and Selkoe, D. J. (1999) Two transmembrane aspartates in presenilin-1 required for presenilin endoproteolysis and gamma-secretase activity. *Nature* **398,** 513-517.

Woo, J. A., Roh, S. E., Lakshmana, M. K. and Kang, D. E. (2012) Pivotal role of RanBP9 in integrin-dependent focal adhesion signaling and assembly. *Faseb J* **26,** 1672-1681.

Wyss-Coray, T. (2006) Inflammation in Alzheimer disease: driving force, bystander or beneficial response? *Nat Med* **12,** 1005-1015.

Xie, Z., Dong, Y., Maeda, U., Xia, W. and Tanzi, R. E. (2007) RNA interference silencing of the adaptor molecules ShcC and Fe65 differentially affect amyloid precursor protein processing and Abeta generation. *J Biol Chem* **282,** 4318-4325.

Xu, X. (2009) Gamma-secretase catalyzes sequential cleavages of the AbetaPP transmembrane domain. *J Alzheimers Dis* **16,** 211-224.

Yamamoto, K., Miyoshi, T., Yae, T., Kawashima, K., Araki, H., Hanada, K., Otero, D. A., Roch, J. M. and Saitoh, T. (1994) The survival of rat cerebral cortical neurons in the presence of trophic APP peptides. *J Neurobiol* **25,** 585-594.

Yamazaki, T., Koo, E. H. and Selkoe, D. J. (1996) Trafficking of cell-surface amyloid beta-protein precursor. II. Endocytosis, recycling and lysosomal targeting detected by immunolocalization. *J Cell Sci* **109 (Pt 5),** 999-1008.

Yamazaki, T., Koo, E. H. and Selkoe, D. J. (1997) Cell surface amyloid beta-protein precursor colocalizes with beta 1 integrins at substrate contact sites in neural cells. *J Neurosci* **17,** 1004-1010.

Yoshikai, S., Sasaki, H., Doh-ura, K., Furuya, H. and Sakaki, Y. (1990) Genomic organization of the human amyloid beta-protein precursor gene. *Gene* **87,** 257-263.

Young-Pearse, T. L., Bai, J., Chang, R., Zheng, J. B., LoTurco, J. J. and Selkoe, D. J. (2007) A critical function for beta-amyloid precursor protein in neuronal migration revealed by in utero RNA interference. *J Neurosci* **27,** 14459-14469.

Yu, C., Kim, S. H., Ikeuchi, T., Xu, H., Gasparini, L., Wang, R. and Sisodia, S. S. (2001) Characterization of a presenilin-mediated amyloid precursor protein carboxyl-terminal fragment gamma. Evidence for distinct mechanisms involved in gamma -secretase processing of the APP and Notch1 transmembrane domains. *J Biol Chem* **276,** 43756-43760.

Yu, H., Braun, P., Yildirim, M. A., Lemmens, I., Venkatesan, K., Sahalie, J., Hirozane-Kishikawa, T., Gebreab, F., Li, N., Simonis, N., Hao, T., Rual, J. F., Dricot, A., Vazquez, A., Murray, R. R., Simon, C., Tardivo, L., Tam, S., Svrzikapa, N., Fan, C., de Smet, A. S., Motyl, A., Hudson, M. E., Park, J., Xin, X., Cusick, M. E., Moore, T., Boone, C., Snyder, M., Roth, F. P., Barabasi, A. L., Tavernier, J., Hill, D. E. and Vidal, M. (2008) High-quality binary protein interaction map of the yeast interactome network. *Science* **322,** 104-110.

Yuan, Y., Fu, C., Chen, H., Wang, X., Deng, W. and Huang, B. R. (2006) The Ran binding protein RanBPM interacts with TrkA receptor. *Neurosci Lett* **407,** 26-31.

Zambrano, N., Bimonte, M., Arbucci, S., Gianni, D., Russo, T. and Bazzicalupo, P. (2002) feh-1 and apl-1, the Caenorhabditis elegans orthologues of mammalian Fe65 and beta-amyloid precursor protein genes, are involved in the same pathway that controls nematode pharyngeal pumping. *J Cell Sci* **115,** 1411-1422.

Zambrano, N., Bruni, P., Minopoli, G., Mosca, R., Molino, D., Russo, C., Schettini, G., Sudol, M. and Russo, T. (2001) The beta-amyloid precursor protein APP is tyrosine-phosphorylated in cells expressing a constitutively active form of the Abl protoncogene. *J Biol Chem* **276,** 19787-19792.

Zambrano, N., Buxbaum, J. D., Minopoli, G., Fiore, F., De Candia, P., De Renzis, S., Faraonio, R., Sabo, S., Cheetham, J., Sudol, M. and Russo, T. (1997) Interaction of the phosphotyrosine interaction/phosphotyrosine binding-related domains of Fe65 with wild-type and mutant Alzheimer's beta-amyloid precursor proteins. *J Biol Chem* **272,** 6399-6405.

Zambrano, N., Minopoli, G., de Candia, P. and Russo, T. (1998) The Fe65 adaptor protein interacts through its PID1 domain with the transcription factor CP2/LSF/LBP1. *J Biol Chem* **273,** 20128-20133.

Zhang, Y. W., Wang, R., Liu, Q., Zhang, H., Liao, F. F. and Xu, H. (2007) Presenilin/gamma-secretase-dependent processing of beta-amyloid precursor protein regulates EGF receptor expression. *Proc Natl Acad Sci U S A* **104,** 10613-10618.

Zhang, Z., Lee, C. H., Mandiyan, V., Borg, J. P., Margolis, B., Schlessinger, J. and Kuriyan, J. (1997) Sequence-specific recognition of the internalization motif of the Alzheimer's amyloid precursor protein by the X11 PTB domain. *EMBO J* **16,** 6141-6150.

Zhao, G., Mao, G., Tan, J., Dong, Y., Cui, M. Z., Kim, S. H. and Xu, X. (2004) Identification of a new presenilin-dependent zeta-cleavage site within the transmembrane domain of amyloid precursor protein. *J Biol Chem* **279,** 50647-50650.

Zhao, G., Tan, J., Mao, G., Cui, M. Z. and Xu, X. (2007) The same gamma-secretase accounts for the multiple intramembrane cleavages of APP. *J Neurochem* **100,** 1234-1246.

Zheng, P., Eastman, J., Vande Pol, S. and Pimplikar, S. W. (1998) PAT1, a microtubule-interacting protein, recognizes the basolateral sorting signal of amyloid precursor protein. *Proc Natl Acad Sci U S A* **95,** 14745-14750.

Zhou, D., Chen, B., Ye, J. J. and Chen, S. (2004) A novel crosstalk mechanism between nuclear receptor-mediated and growth factor/Ras-mediated pathways through PNRC-Grb2 interaction. *Oncogene* **23,** 5394-5404.

Appendix I - Culture media and solutions

Bacterial Media

LB (Luria-Bertani) Medium

To 950 ml of deionized H_2O add:

LB 25 g

Agar 12 g (for plates only)

Shake until the solutes have dissolved. Adjust the volume of the solution to 1 L with deionized H_2O. Sterilize by autoclaving.

100 mg/ml Antibiotics stock solutions (Ampicilin or Kanamycin)

Dissolve 1 g of the antibiotic in 10 ml of deionized H_2O. Mix until the solutes have dissolved, filter through a 0.2 μm filter, aliquot and store at -20 °C.

SOB Medium

To 950 ml of deionized H_2O add:

25.5 g SOB Broth

Shake until the solutes have dissolved. Add 10 ml of a 250 mM KCl (prepared by dissolving 1.86 g of KCl in 100 ml of deionized H_2O). Adjust the pH to 7.0 with 5 N NaOH. Adjust the volume of the solution to 1 liter with deionized H_2O. Sterilize by autoclaving. Just prior to use add 5 ml of a sterile solution of 2 M $MgCl_2$ (prepared by dissolving 19 g of $MgCl_2$ in 90 ml of deionized H_2O; adjust the volume of the solution to 100 ml with deionized H_2O and sterilize by autoclaving).

SOC Medium

SOC is identical to SOB except that it contains 20 mM glucose. After the SOB medium has been autoclaved, allow it to cool to 60°C and add 20 ml of a sterile 1 M glucose (this solution is made by dissolving 18 g of glucose in 90 ml of deionized H_2O; after the sugar has dissolved, adjust the volume of the solution to 100 ml with deionized H_2O and sterilize by filtration through a 0.22-micron filter).

Yeast Media

YPD medium

To 950 ml of deionized H_2O add:

50 g YPD

20 g Agar (for plates only)

Shake until the solutes have dissolved. Adjust the volume to 1 L with deionized H_2O and sterilize by autoclaving. Allow medium to cool to 60°C and add glucose to 2% (50 ml of a sterile 40% stock solution).

10X dropout solution (DO10X)

This solution contains all but one or more of the following components:

	10X concentration (mg/L)	SIGMA #
L-Isoleucine	300	I-7383
L-Valine	1500	V-0500
L-Adenine hemisulfate salt	200	A-9126
L-Arginine HCl	200	A-5131
L-Histidine HCl monohydrate	200	H-9511
L-Leucine	1000	L-1512
L-Lysine HCl	300	L-1262
L-Methionine	200	M-9625
L-Phenylalanine	500	P-5030
L-Threonine	2000	T-8625
L-Tryptophan	200	T-0254
L-Tyrosine	300	T-3754
L-Uracil	200	U-0750

(10X dropout supplements may be autoclaved and stored for up to 1 year.)

SD synthetic medium

To 800 ml of deionized H_2O add:

6.7 g Yeast nitrogen base without amino acids (DIFCO)

20 g Agar (for plates only)

Shake until the solutes have dissolved. Adjust the volume to 850 ml with deionized H_2O and sterilize by autoclaving. Allow medium to cool to 60°C and add glucose to 2% (50 ml of a sterile 40% stock solution) and 100 ml of the appropriate 10X dropout solution.

2X YPDA

Prepare YPD as above. After the autoclaved medium has cooled to 55°C add 15 ml of a 0.2% adenine hemisulfate solution per liter of medium (final concentration is 0.003%).

COS-7 cells (monkey kidney cell-line):

DMEM medium

For a final volume of 1 L, dissolve one pack of DMEM powder (with L-glutamine and 4500 mg glucose/L, Sigma Aldrich) in deionized H2O and add:
3.7 g NaHCO3 (Sigma-Aldrich)
adjust to pH 7.4. Sterilize by filtering through a 0.2 µm filter and store at 4 °C.

Complete DMEM (COS-7 cells)

For a final volume of 1 L, when preparing DMEM medium adjust to pH 7.4 and before sterilizing add:
100 ml Fetal Bovine Serum (FBS) (Gibco BRL, Invitrogen) (final concentration: 10% v/v)
Notes: FBS is heat-inactivated for 30 min at 45 °C. For cells maintenance, prior to pH adjustment add 100 U/ml penicillin and 100 mg/ml streptomycin [10 ml Streptomycin/ Penicilin/ Amphotericin solution (Gibco BRL, Invitrogen)].

PC12 cells (rat pheochromocytoma cell-line)

RPMI 1640 medium (Gibco) supplemented with 10% horse serum and 5% FBS, 100 U/ml penicillin and 100 mg/ml streptomycin (Gibco).
For a final volume of 1 L, dissolve one pack of RPMI 1640 powder (with L-glutamine and 4500 mg glucose/L, Gibco) in deionized H_2O and add:
0.85 g NaHCO3 (Sigma)
adjust to pH 7.4 and before sterilizing add:
50 ml Fetal Bovine Serum (FBS) (Gibco) (final concentration: 5% v/v)
100 ml Horse Serum (HS) (Gibco) (final concentration: 10% v/v)
100 U/ml penicillin and 100 mg/ml streptomycin

SH-SY5Y cells (human neuroblastoma cell-line)

1:1 combination of minimum essential medium (MEM, Gibco) and Ham's F12 medim (Gibco), supplemented with 10% FBS.
For a final volume of 1 L of deionized H_2O add:
MEM
Ham´s F12
1.5 g NaHCO3 (Sigma)
0.055 g $C_3H_3NaO_3$
2 mM L-glutamine
0.1 mM Non-essential aminoacids
adjust to pH 7.4 and before sterilizing add:
100 ml Fetal Bovine Serum (FBS) (Gibco) (final concentration: 10% v/v)
100 U/ml penicillin and 100 mg/ml streptomycin

HeLa cells (human cervical adenocarcinoma cell-line)

Minimal Essential Media with 1% Non-Essential Amino Acids, 10% heat inactivated Fetal Bovine Serum (FBS) and 1% antibiotic/antimycotic (AA) mix.
For a final volume of 500 ml, add:
Complete MEM + GLUTAMAX

50 ml (10% v/v) Fetal Bovine Serum (FBS) (Gibco BRL, Invitrogen)
5 ml Non-Essential aminoacids (100x)
100 U/ml penicillin
100 mg/ml streptomycin 5 ml
FBS is heat-inactivated for 30 min at 56 °C. For cells maintenance, prior to pH adjustment add 100 U/mL penicillin and 100 mg/ml streptomycin [10 ml Streptomycin/ Penicilin/Amphotericin solution (Gibco BRL, Invitrogen)

PBS (1x)

For a final volume of 500 ml, dissolve one pack of BupH Modified Dulbecco's Phosphate Buffered Saline Pack (Pierce) in deionized H_2O.
Final composition:
8 mM Sodium Phosphate
2 mM Potassium Phosphate
140 mM NaCl
10 mM KCl
Sterilize by filtering through a 0.2 μm filter and store at 4°C.

Rat neuronal primary cultures

Rat cortical neurons were isolated from cortex or hipoccampus of Wistar Hannover 18 days rat embryos whose mother was killed by rapid cervical dislocation. After brain dissection, tissues were dissociated with 0.45 mg/ml trypsin and 0.15 mg/ml deoxyribonuclease I in Hank's balanced salt solution (HBSS) during 5-10 min at 37°C.

Cells were washed with HBSS supplemented with 10% FBS to stop trypsinization, centrifuged at 1,000 rpm for 3 min, and further washed and centrifuged with HBSS for serum withdraw.

Cells pellet was ressuspended in complete Neurobasal medium, which is supplemented with 2% B27. Viability and cellular concentration were assessed by using the Trypan Blue excluding dye [0.4% Trypan Blue solution (Sigma)], and cells with (dead) or without (living) intracellular blue staining were counted in a hemocytometer chamber. Cellular viability was calculated and normally higher than 95%.

Cells were plated on poly-D-lysine-coated dishes at a density of $1.0x10^5$ cells/cm^2 in B27-supplemented Neurobasal medium (Gibco Invitrogen, Alfagene, Portugal), a serum-free medium combination. The medium was supplemented with glutamine (0.5 mM), gentamicin (60 μg/ml), without glutamate, for 9 days before being used for experimental procedures.

All cultures were maintained at 37°C in an atmosphere of 5% CO2.

Complete Neurobasal medium (Hippocampal primary cultures)

This serum-free medium (Neurobasal; Gibco, BRL) is supplemented with:
2% B27 supplement (Gibco, BRL)
0.5 mM L-glutamine (Gibco, BRL)
25 μM L-glutamate (Gibco, BRL)
60 μg/ml Gentamicine (Gibco, BRL)
0.001% Phenol Red (Sigma Aldrich, Portugal)
Adjust to pH 7.4. Sterilize by filtering through a 0.2 μm filter and store at 4°C.

Hank's balanced salt solution (primary neuronal cultures)

This salt solution is prepared with deionized H_2O. Final composition:

137 mM NaCl

5.36 mM KCl

0.44 mM KH_2PO_4

0.34 mM $Na2HPO_4.2H2O$

4.16 mM $NaHCO_3$

5 mM Glucose

1 mM Sodium pyruvate

10 mM HEPES

Adjust to pH 7.4. Sterilize by filtering through a 0.2 μm filter and store at 4°C.

Solutions for cell fixation and immunocytochemistry

1 mg/ml Poly-L-ornithine solution (10x) (COS-7 cells)

To a final volume of 100 ml, dissolve in deionized H_2O 100 mg of poly-L-ornithine (Sigma-Aldrich, Portugal).

10 mg/ml Poly-D-lysine stock (100x) (rat primary neuronal cultures)

To a final volume of 10 ml, dissolve in deionized H2O 100 mg of poly- D-lysine (Sigma-Aldrich).

Poly-D-lysine solution (neuronal cells)

To a final volume of 100 ml, dilute 1 ml of the 10 mg/ml poly-D-lysine stock solution in borate buffer.

Borate buffer

To a final volume of 1 L, dissolve in deionized H2O 9.28 g of boric acid (Sigma-Aldrich). Adjust to pH 8.2, sterilize by filtering through a 0.2 μm filter, and store at 4°C.

4% Paraformaldehyde Fixative solution

To a final volume of 100 ml, to 25 ml deionized H_2O add 4 g of paraformaldehyde. Dissolve by heating the mixture at 58°C while stirring. Add 1-2 drops of 1 M NaOH to clarify the solution and filter (0.2 μm). Add 50 ml of 2X PBS and adjust the volume to 100 ml with deionized H_2O.

Solutions for DNA manipulation

50X TAE Buffer

242 g Tris base
57.1 ml glacial acetic acid
100 ml 0.5 M EDTA (pH 8.0)

TE Buffer (pH 7.5)

10 mM Tris-HCl pH 7.5
1 mM EDTA pH 8.0

6X Loading Buffer (LB)

0.25% bromophenol blue
30% glycerol

Competent Cell Solutions:

Solution I (1 L)

9.9 g $MnCl_2.4H_2O$
1.5 g $CaCl_2.2H_2O$
150 g glycerol
30 ml KHAc 1 M;
adjust pH to 5.8 with HAc, filter through a 0.2 µm filter and store at 4°C

Solution II (1 L)

20 ml 0.5 M MOPS pH 6.8
1.2 g RbCl
11 g $CaCl_2.2H_2O$
150 g glycerol;
filter through a 0.2 µm filter and store at 4°C

Miniprep Solutions

Solution I

50 mM glucose
25 mM Tris.HCl pH 8.0
10 mM EDTA

Solution II

0.2 N NaOH
1% SDS

Solution III

3 M potassium acetate
2 M glacial acetic acid

Megaprep Solutions

Cell Resuspension Solution:

50 mM Tris-HCl pH 7.5
10 mM EDTA
100 µg/ml RNAase A

Cell Lysis Solution:

0.2 M NaOH
1% SDS

Neutralization solution:

1.32 M potassium acetate pH 4.8

Column Wash Solution:

80 mM potassium acetate
8.3 mM Tris-HCl pH 7.5
40 µM EDTA
55% ethanol

Solutions for proteins manipulation

SDS-PAGE and Western blotting solutions

4X LGB (Lower Gel Buffer)

To 900 ml of deionized H_2O add:
181.65 g Tris
4 g SDS
Shake until the solutes have dissolved. Adjust the pH to 8.9 and adjust the volume to 1 L with deionized H_2O.

5X UGB (Upper Gel Buffer)

To 900 ml of deionized H_2O add:
75.69 g Tris
Shake until the solute has dissolved. Adjust the pH to 6.8 and adjust the volume to 1 L with deionized H2O.

30% Acrylamide/0.8% Bisacrylamide

To 70 ml of deionized H_2O add:
29.2 g Acrylamide
0.8 g Bisacrylamide
Shake until the solutes have dissolved. Adjust the volume to 100 ml with deionized H_2O. Store at 4°C.

4X Loading Gel Buffer

250 mM Tris-HCl pH 6.8
8% SDS
40% Glycerol
2% 2-mercaptoethanol
0.01% Bromophenol blue

10 % APS (ammonium persulfate)

In 10 ml of deionized H_2O dissolve 1 g of APS. Note: prepare fresh before use.

10 % SDS (sodium dodecilsulfate)

In 10 ml of deionized H_2O dissolve 1 g of SDS.

10X Running Buffer

250 mM Tris-HCl pH 8.3
2.5 M Glycine
1% SDS

1X Electrotransfer buffer

25 mM Tris-HCl pH 8.3
192 mM Glycine
20% Methanol

10X TBS (Tris buffered saline)

10 mM Tris-HCl pH 8.0
150 mM NaCl

10X TBST (Tris buffered saline + Tween)

10 mM Tris-HCl pH 8.0
150 mM NaCl
0.05% Tween

Membranes Stripping Solution

62.5 mM Tris-Cl pH 6.7
2% SDS
100 mM β-mercaptoethanol
Dissolve Tris and SDS in deionized H_2O and adjust with HCl to pH 6.7. Add the mercaptoethanol and adjust volume to 500 ml.

Coomassie staining

Gel washing solution

50% (v/v) methanol
10% (v/v) acetic acid

Staining solution

0.2% (m/v) Coomassie Brilliant Blue
50% (v/v) methanol
10% (v/v) acetic acid

Destain solution

25% (v/v) methanol
5% (v/v) acetic acid

Storage solution

20% (v/v) methanol
5% (v/v) glycerol

Immunoprecipitation solutions

Lysis Buffer

50 mM Tris-HCl (pH 8)
120 mM NaCl
4% CHAPS

Lysis Buffer + Protease inhibitors

Add to 4 mL of Lysis buffer the following quantities for a final volume of 5 mL:
23,8 µl Pepstatin A (1 mg/mL stock solution in DMSO)
0,72 µl Leupeptin (5 mg/mL stock solution)
180 µl Benzamidine (200 mM stock solution)
43,2 µl Aprotinin (2.1 mg/mL stock solution)
176 µl PMSF 100X
Washing solution
50 mM Tris-HCl
120 mM NaCl

Yeast two-hybrid solutions

Yeast plasmid extraction – Breaking buffer

2% Triton X-100
1% SDS
100 mM NaCl
10 mM Tris-HCl pH 8.0

STET Buffer

8% Sucrose
5% Triton X-100
50 mM Tris-HCl pH 8.5

50 mM EDTA pH 8.0

Solutions for preparation of yeast protein extracts

a) Protease inhibitor solution

Always prepare solution fresh just before using. Place on ice to prechill. To prepare 688 µl add in a microfuge tube:
66 µl Pepstatin A (1 mg/ml stock solution in DMSO)
2 µl Leupeptin (10.5 mM stock solution)
500 µl Benzamidine (200 mM stock solution)
120 µl Aprotinin (2.1 mg/ml stock solution)

b) PMSF (phenylmethyl-sulfonyl fluoride) stock solution (100X)

Dissolve 0.1742 g of PMSF (SIGMA) in 10 ml isopropanol. Wrap tube in foil and store at RT.

c) Cracking buffer stock solution

To 80 ml of deionized H_2O add:
48 g Urea
5 g SDS
4 ml 1M Tris-HCl pH 6.8
20 µl 0.5 M EDTA
40 mg Bromophenol blue
Shake until the solutes have dissolved. Adjust the volume to 100 ml with deionized H_2O.

d) Cracking buffer

To prepare 1.13ml add in a microfuge tube:
1 ml Cracking buffer stock solution (recipe above)
10 µl β-mercaptoethanol
70µl Protease inhibitor solution (recipe above)
50 µl 100X PMSF stock solution

Appendix II - Primers

Oligo name	Sequence (5'-3')	Length (bp)	Target	RE
18FE1449	CCGCGTGTGGGGCGTCGGGC	20	FE65 (NM_001164)	
AD amplimer 3'	GTGAACTTGCGGGGTTTTTCAGTATCTACGAT	32	pACT2	
AD amplimer 5'	CTATTCGATGATGAAGATACCCCACCAAACCC	32	pACT2	
APP1980F	GGATGCAGAATTCCGACATGACTCAGG	27	APP (NM_201414)	EcoRI
APP2000N	TGACTCAGGATATGAAGTTCAT	22	APP (NM_201414)	
APPCTERMIII	GTGGCCCCGGGCTAGTTCTGCATCTGCTCAAAG	33	APP (NM_201414)	SmaI
APPRV4	GTGGCCCCGGGCTAGTTCTGCATCTGCAGGTGG	33	pAV30	SmaI
CRA-F	GAGGCCCGGGGGCCGCCATAGAAAGAATGATCCAC	35	RanBPM (NM_005493)	XmaI
CRA-R	GAAACTCGAGGCTAATGTAGGTAGTCTTCCACTGTG	36	RanBPM (NM_005493)	XhoI
E10RV	CGGCCATGATCTTAGAGCAGATC	23	FE65	
E14RV	GGAAGGTGGGGGCTTCTTCATGG	23	FE65	
E1FW	ATGTTGTGATGGAGAAGCCGCGG	23	FE65	
E2BFW	ATGGCAGATGGATTGGTGTGTGTG	24	FE65	
E2CFW	TACTGCCTCTTGGACCAGTCAGG	23	FE65	
E3RV	CCAGGTGAGCTGGGACTCCTC	21	FE65	
EGFP-C2-FW	GGAGTTCGTGACCGCCGC	18	EGFP-C2 vector (U57606)	
FE1900F	GGCAGTGCTGGGAGAGTG	18	FE65 (NM_001164)	
FE2350F	GCCCCTCCCCAGTAGC	16	FE65 (NM_001164)	
FE65CT	GGGGATCCCTTCATGGGGTATGGG	24	FE65 (NM_145689)	BamHI
FE65NT	GCTGGGATCCCCATGTCTGTTCCATC	26	FE65 (NM_145689)	BamHI
FESEQ1	GCTCATGGAGAAGGCTTTG	19	FE65 (NM_001164)	
GAL4 AD	TACCACTACAATGGATG	17	pACT2	
GAL4 BD	TCATCGGAAGAGAGTAG	17	pAS2-1	
LISCT-F	GAGACCCGGGATGGCAGACCATGATACAAAAAATGG	36	RanBPM (NM_005493)	XmaI
LISCT-R	GCCTCCTCGAGATCGTACTTCACTATCTGTACC	33	RanBPM (NM_005493)	XhoI
NAPPC	ATCACCATGGTGATGCTGAAGAAG	24	APP (NM_201414)	NcoI
NAPPII	CCGCGCACCATGGCGATGCTGCCCGGTTTGG	31	APP (NM_201414)	
NRPUKF	CGACTAGTGGCCGCCATGTCCGGGCAG	27	RanBPM (NM_005493)	SpeI
NRPUKRV	GAAATGGGCGCGCCATGTAGGTAGTCTTCCAC	32	RanBPM (NM_005493)	AscI
pGEX2T-SEQ	CGTATTGAAGCTATCCCAC	19	pGEX-2T	
PUK700	CCAAGTCTCCACCCCATTGACGTC	24	pUK-BK vector	
R1000R	GTTTGAAGCCCCACAGTAGG	20	RanBPM (NM_005493)	
R107F	GCAGCAGCTGTCGCCGCCACC	21	RanBPM (NM_005493)	
R1230F	GCCAGATCTACAGACC	16	RanBPM (NM_005493)	
R1560F	GCACCGCACATTTTTCAG	18	RanBPM (NM_005493)	
R1900F	CAGGCCGCCATAGAAAG	17	RanBPM (NM_005493)	
R480R	CTCCTGCTCGTTCAGGGCCGAG	22	RanBPM (NM_005493)	
R600R	GCACCCGCAGGTTGTTCTGAG	21	RanBPM (NM_005493)	
R800F	GGGATAAGCATTCATATG	18	RanBPM (NM_005493)	
RBGST-FW	GCAGTTGATCAGTCGCGGCCGGGATGTCCG	92	RanBPM (NM_005493)	MfeI
RBGST-RV	GCTCTTGCAATTGATAGCTAATGTAGGTAGTC	90	RanBPM (NM_005493)	BclI
RPUKF	CGACGACTAGTGGCCGCCATGTCCGGGCAGCCGCCGCCG	39	RanBPM (NM_005493)	SpeI
SPRY-F	TACCCCCGGGCTGTGGGATTTATTATTTTGAAGTA	35	RanBPM (NM_005493)	XmaI
SPRY-R	CTATATCTCGAGCGAAAGGATGTTGCCCAAAATTGG	36	RanBPM (NM_005493)	XhoI

Appendix III - Bacteria and yeast strains

Bacteria strains:

- *E. coli* XL1- Blue: *recA endA1 gyrA96 thi-1 hsdR17 supE44 relA1 lac[F' proAB lacZ⊿M15 Tn10(Tet^r)]*

- *E. coli* Rosetta (DE3) F^- *ompT hsdS*$_B$(r_B^- m_B^-) *gal dcm* (DE3) pRARE^2 *(*Cam^R)

Yeast strains:

- *S. cerevisiae* AH109: MATa, trp1-901, leu2-3, 112 ura3-52, his3-200, gal4Δ, gal 80Δ, LYS2:: $GAL1_{UAS}$-$GAL1_{TATA}$-HIS3, $GAL2_{UAS}$-$GAL2_{TATA}$-ADE2, URA3::$MEL1_{UAS}$-$MEL1_{TATA}$-lacZ, MEL1

- *S. cerevisiae* Y187: MATα, ura3-52, his3-200, ade2-101, trp1-901, leu2-3, 112, gal4Δ, met-, gal 80Δ, URA3:: $GAL1_{UAS}$-$GAL1_{TATA}$-lacZ, MEL1

Plasmids for YTH:

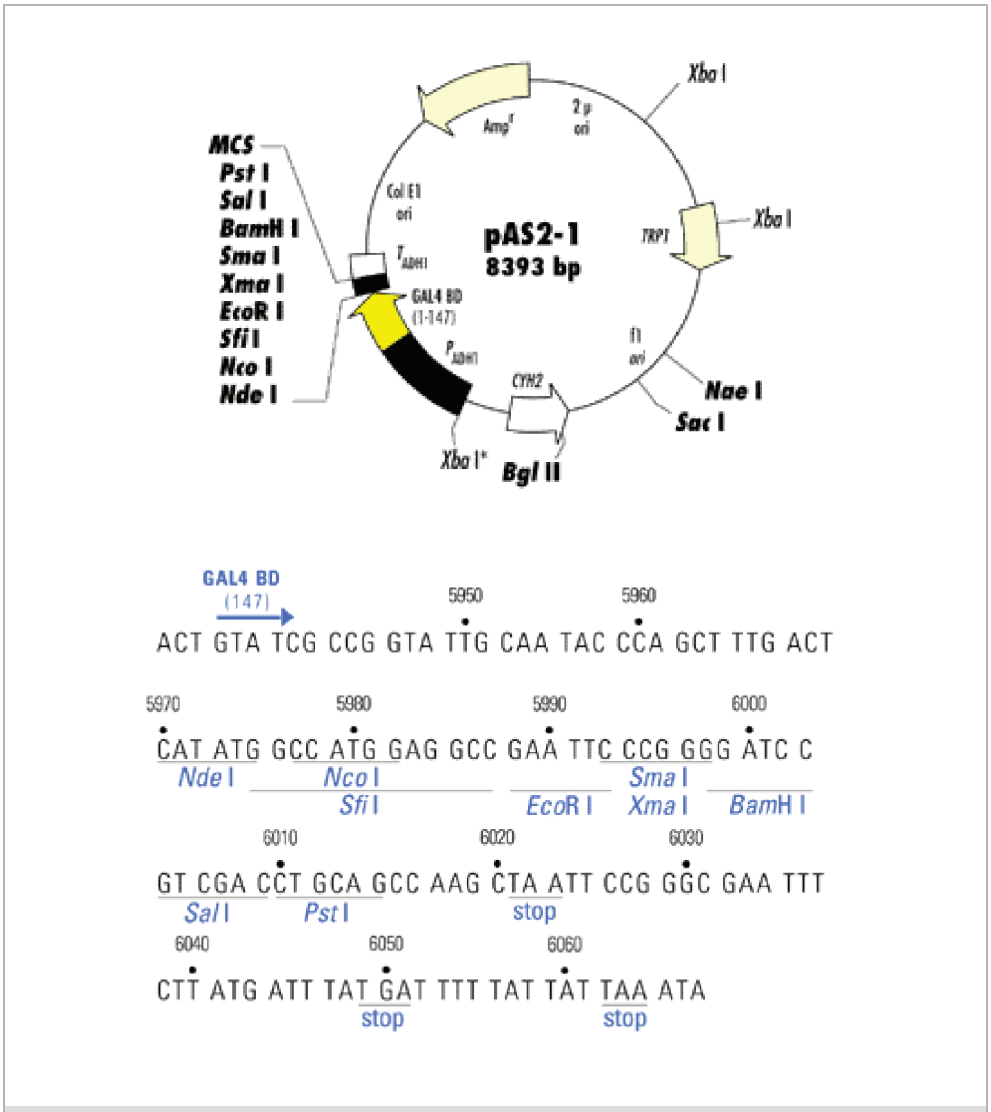

Figure 1: pAS2-1 vector map and MCS (Clontech, Enzifarma, Portugal). Unique sites are colored blue. pAS2-1 is a cloning vector used to generate fusions of a bait protein with the GAL4 DNA-BD. The hybrid protein is expressed at high levels in yeast host cells from the full-length ADH1 promoter. The hybrid protein is target to the yeast nucleus by nuclear localization sequences. pAS2-1 contains the TRP1 gene for selection in Trp$^-$ auxotrophic yeast strains.

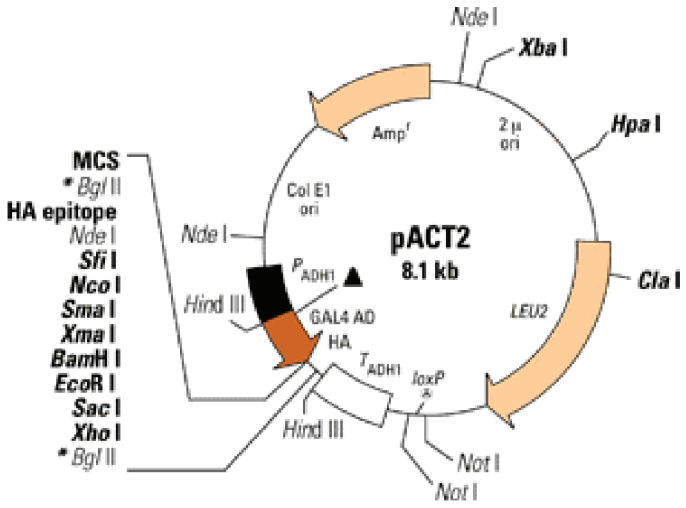

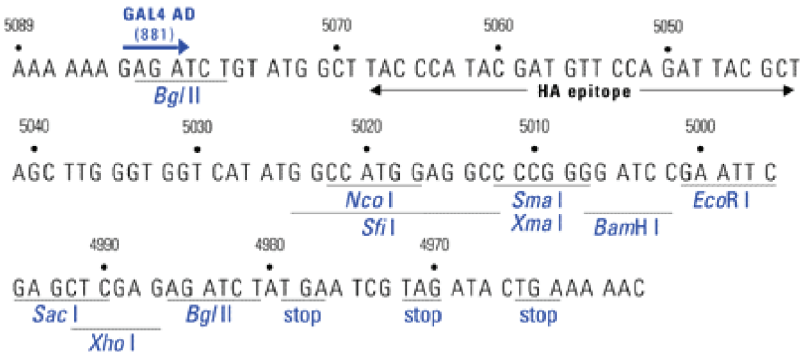

Figure 2: pACT2 vector map and MCS (Clontech, Enzifarma, Portugal). Unique sites are colored blue. pACT2 is used to generate a hybrid containing the GAL4 AD, an epitope tag and a protein encoded by a cDNA in a fusion library. The hybrid protein is expressed at medium levels in yeast host cells from an enhanced, truncated ADH1 promoter and is target to the nucleus by the SV40 T-antigen nuclear localization sequence. pACT2 contains the LEU2 gene for selection in Leu$^-$ auxotrophic yeast strains.

Mammalian expression vectors:

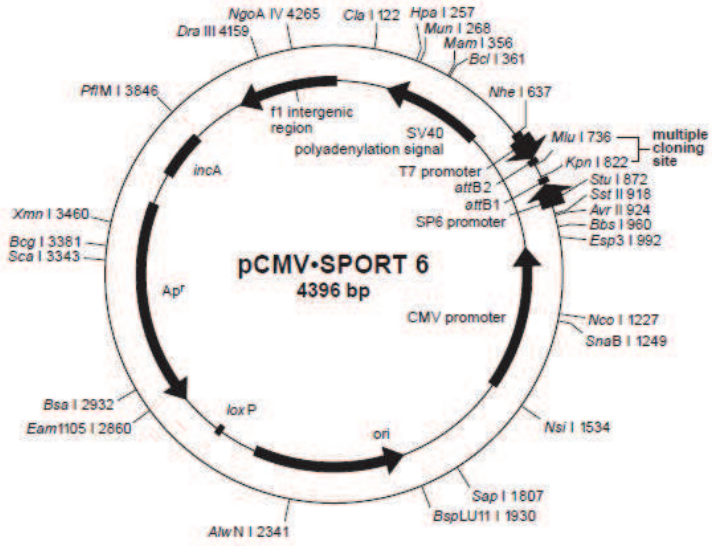

Figure 3: pCMV-SPORT6 vector map (source: IMAGE consortium).

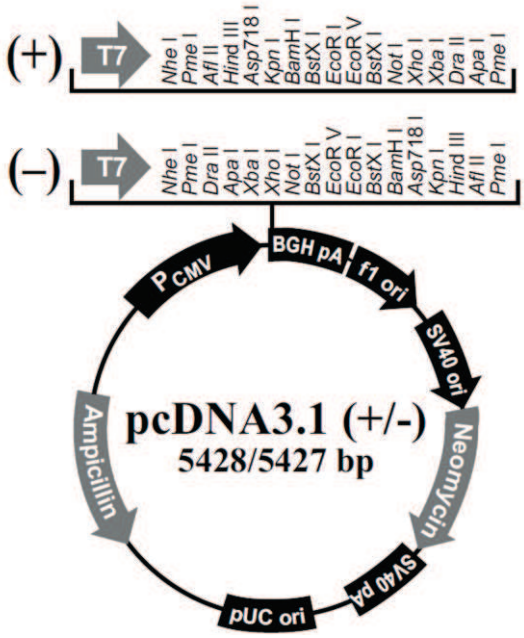

Figure 4: pcDNA3.1 vector map (Invitrogen, Alfagene, Portugal).

Mammalian expression vectors with GFP fusions:

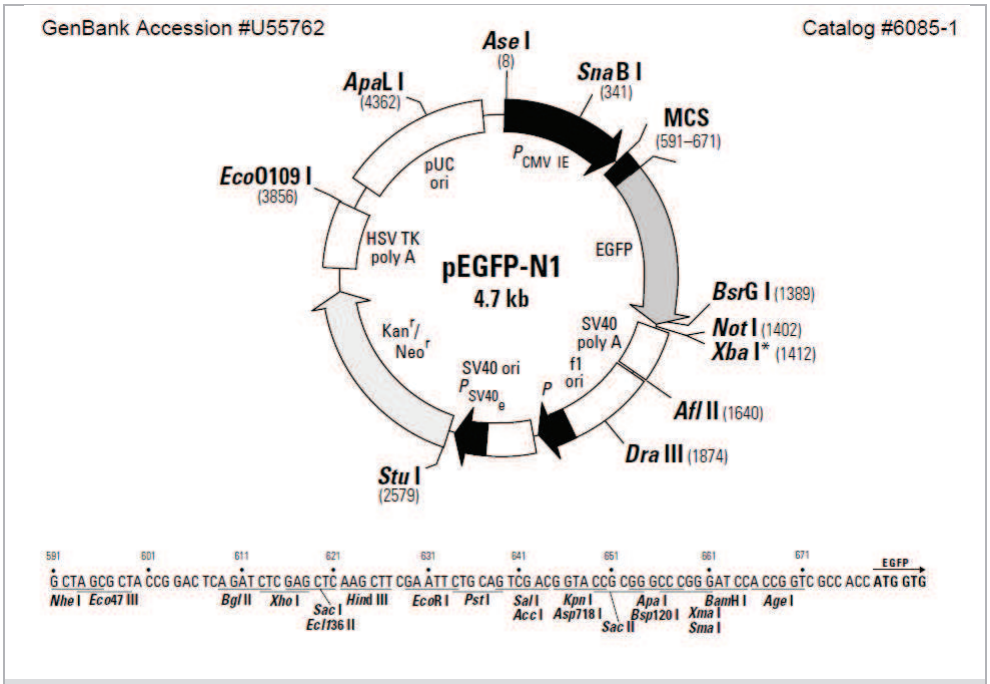

Figure 5: pEGFP-N1 vector map (Clontech, Enzifarma, Portugal).

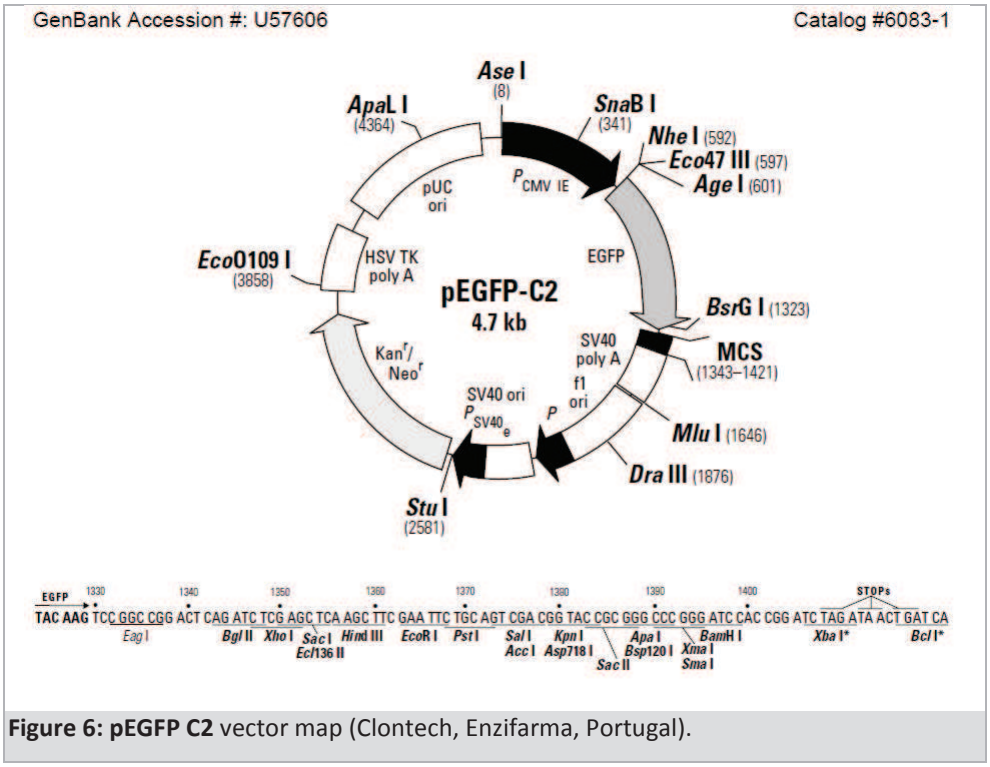

Figure 6: pEGFP C2 vector map (Clontech, Enzifarma, Portugal).

Bacterial expression vectors:

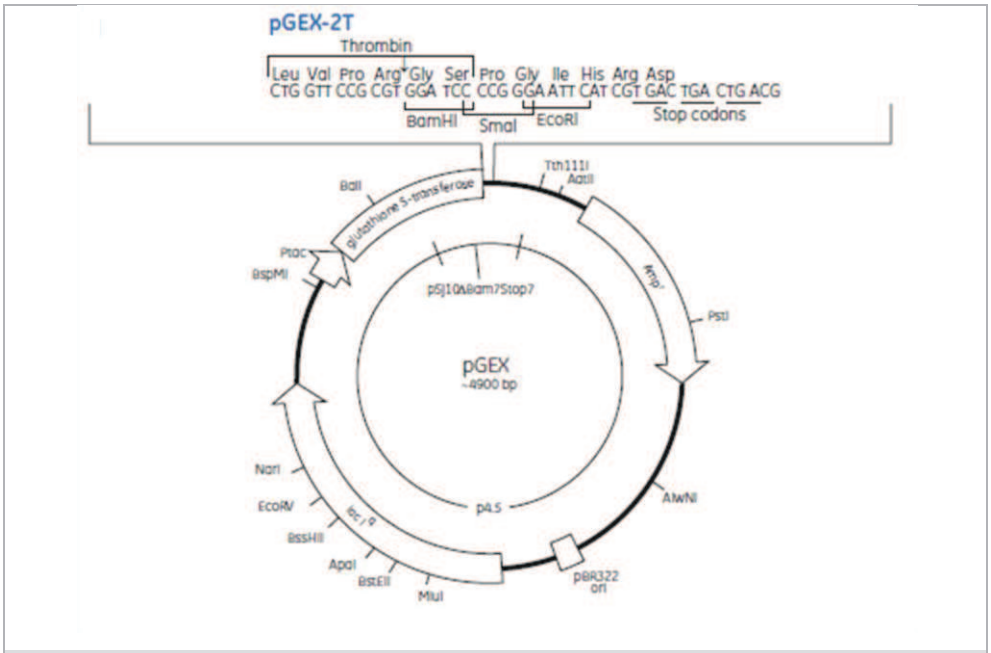

Figure 7: pGEX-2T vector map (GE Healthcare Life Sciences).

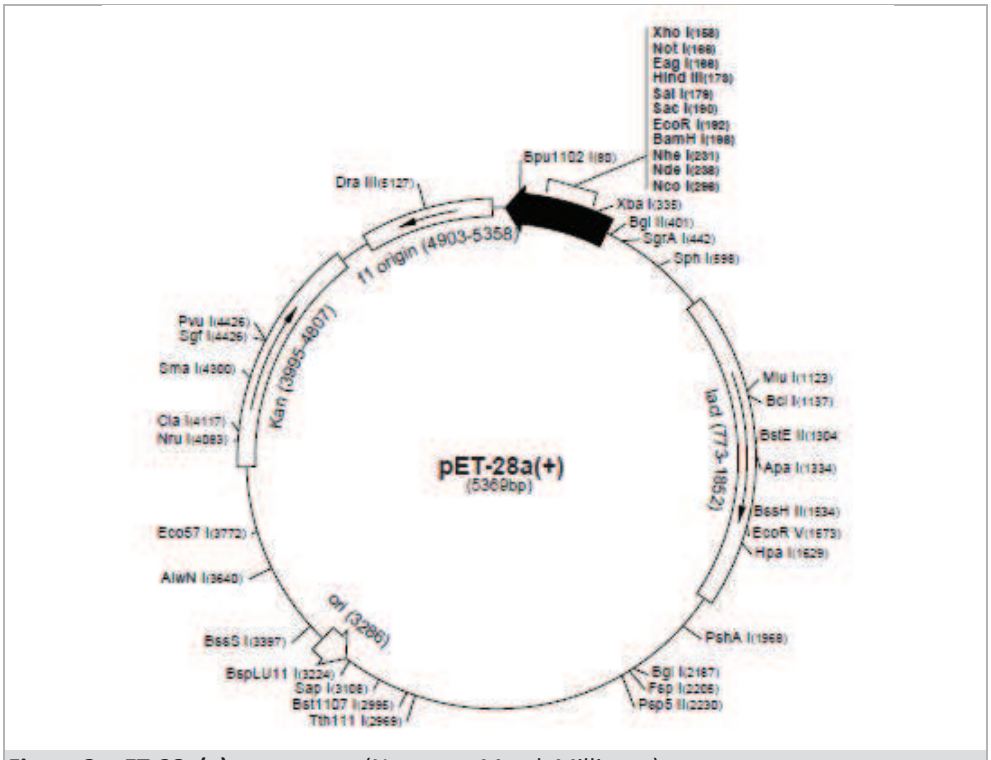

Figure 8: pET-28a(+) vector map (Novagen, Merck Millipore)

Appendix V – YTH screen with AICD^{Y687E}

Results from YTH screen-4, carried out with AICD^{Y687E} (Domingues, 2005):

Positive clones isolateds	Mating efficiency (% diploids)	Clones screened
57	10%	1.1 X 10^8

GenBank Accession	Definition	gene symbol	Chr map	No. of clones	Clones	Insert size (Kb)	full-length cDNA	frame with Gal4-AD
library inserts encoding known proteins								
NM_005493.2	Ran binding protein 9	RanBP9	6p23	16	1,9,10,12,13,14,17,25,40,48,54,57,71,75,160,192	2.8		✓
NM_012470.3	Transportin-SR2	TNPO3	7q32.1	2	189197	0.7		
NM_003000.2	Succinate dehydrogenase [ubiquinone] iron-sulfur subunit, mitochondrial	SDHB	1p36.1-p35	4	8,31,38,127	0.5		
NM_138983.2	Oligodendrocyte transcription factor 1	OLIG1	21q22.11	3	224, 230, 235	2.2	✓	
NM_001077199.1	Serine/arginine-rich splicing factor 12	SFRS12	5q12.3	1	5	3.2		
library inserts matching genomic clones								
AL035608	clone RP3-479J7		Xq21		51,53	1.4		
AC011500.7	clone CTB-60E11		19		177	1.1		
AC055858.18	clone RP11-682M7		17		239	1.8		
AC012652.7	clone RP11-46M12		15		136	2.8		
AC128708.8	clone RP11-714L1		12		237	1.8		
AL355432.7	clone BAC RP11-56F10		9		130	1.5		
AL354855	clone RP11-64E14		9		4	1.3		
AC023880	clone RP5-999D10		7		44,52	0.5		
AC008957.7	clone CTD-2353F22		5		105	1.8		
AC115282.2	clone RP11-122D19		3		41,81,125	1.5		
AC007318.4	clone RP11-420C9		2		83	2.8		
library inserts matching mitochondrial proteins								
				1	128	0.9		
library inserts aligning with 3' UTRs								
NM_006160	NDRF		17	1	145	0.7		
AC005037	TAF15		17	2	84.92	1.3		
BC014553	RAB3IP		12	1	231	1.7		
NM_004321	KIF1A		2	1	2	0.5		
NM_014873.1	LPGAT1		1	1	123	2.2		
NM_015726	WDR42A/H326		1	1	153	0.9		
not analyzed								
				1	166			
				1	163			
other alignments								
genomic contig +	*chimeric clone:* genomic contig +				82,	3.1		
NM_001007026.1	Atrophin-1 (chimeric clones)	ATN1			144,152,174			

Appendix VI – YTH screen with wild-type AICD

Results from YTH screen-5, carried out with wt AICD (Capelo, 2010):

Positive clones isolated	Mating efficiency (% diploids)	Clones screened
347	0.1%	3.0×10^3

GenBank Accession	Definition	gene symbol	Chr map	No. of clones
library inserts encoding known proteins				
NM_001164.2/ NM_145689.1	Amyloid beta precursor protein-binding family B member 1 transcript variant 1/2 (a) (p97Fe65)	APBB1	11p15	346
library inserts aligning with 3' UTRs				
NM_182471.2	Piruvate kinase muscle transcript variant 3	PKM	15q22	1

Appendix VII – APP literature curated interactome

The curated APP interactome was obtained from Perreau et al. (2010) and several APP interactions published after were added (last updated March 2011):

Gene	UniProt	Entrez Gene
A2M	P01023	2
ABCB1	P08183	5243
ABL1	P00519	25
ACE	P12821	1636
ACHE	P22303	43
ACTB	P60709	60
ADAM10	O14672	102
ADAM17	P78536	6868
ADNP	Q9H2P0	23394
AGER	Q15109	177
AGRN	O00468	375790
ALB	P02768	213
APBA1	Q02410	320
APBA2	Q99767	321
APBA3	O96018	9546
APBB1	O00213	322
APBB2	Q92870	323
APBB3	O95704	10307
APCS	P02743	325
APLP1	P51693	333
APLP2	Q06481	334
APOA1	P02647	335
APOA2	P02652	336
APOE	P02649	348
APP	P05067	351
APPBP2	Q92624	10513
ATP2B2	Q01814	491
BACE1	P56817	23621
BACE2	Q9Y5Z0	25825
BGN	P21810	633
BLML	Q13867	642
C1QA	P02745	712
CALR	Q6IAT4	811
CALU	O43852	813
CANX	P27824	821
CASP3	P42574	836
CASP6	P55212	839
CASP8	Q14790	841
CAT	P04040	847
CAV1	Q03135	857
CAV3	P56539	859
CD14	P08571	929
CD36	P16671	948
CDK1	P06493	983
CDK5	Q00535	1020
CHRNA7	P36544	1139
CKMT1B	P12532	1159
CLSTN1	O94985	22883
CLSTN3	Q9BQT9	9746
CLU	P10909	1191
CNTN1	Q12860	1272
CNTN2	Q02246	6900
CNTN3	Q9P232	5067
CNTN4	Q8IWV2	152330
COL18A1	P39060	80781
COL25A1	Q9BXS0	84570
COL4A2	P08572	1284
CPE	P16870	1363
CPEB1	Q9BZB8	64506
CSNK2A1	P68400	1457
CST3	P01034	1471
CTSD	P07339	1509
DAB1	O75553	1600
DAB2	P98082	1601
DDB1	Q16531	1642
DNM1	Q05193	1759
EPB41L3	Q9Y2J2	23136
ERP44	Q9BS26	23071
F10	P00742	2159
F12	P00748	2161
F2	P00734	2147
F7	P08709	2155
F9	P00740	2158
FBLN1	P23142	2192
FKBP1A	P62942	2280
FLOT1	O75955	10211
FLOT2	Q14254	2319
GABBR1	Q9UBS5	2550
GANAB	Q14697	23193
GFAP	P14136	2670
GNAO1	P09471	2775
GPC1	P35052	2817
GRB2	P62993	2885
GRIN1	Q05586	2902
GRIN2A	Q12879	2903
GSN	P06396	2934
GULP1	Q9UBP9	51454
HGS	O14964	9146
HMGB1	P09429	3146
HMOX1	P09601	3162
HMOX2	P30519	3163
HOMER2	Q9NSB8	9455
HOMER3	Q9NSC5	9454
HSD17B10	Q99714	3028
HSP90AA1	P07900	3320
HSP90AA1	P07900	3320
HSP90B1	P14625	7184
HSPA1A	P08107	3303
HSPA4	P34932	3308
HSPA5	P11021	3309
HSPA8	P11142	3312
HSPB1	P04792	3315
HSPB6	O14558	126393
HSPB8	Q9UJY1	26353
HSPD1	P10809	3329
HSPG2	P98160	3339
HTRA2	O43464	27429
HYOU1	Q9Y4L1	10525
IDE	P14735	3416
ITGB1	P05556	3688
ITM2B	Q9Y287	9445
ITM2C	Q9NQX7	81618
KAT5	Q92993	10524
KLC1	Q07866	3831
KLK6	Q92876	5653
KNG1	P01042	3827
L1CAM	P32004	3897
LAMA1	P25391	284217
LDLRAP1	Q5SW96	26119
LINGO1	Q96FE5	84894
LRP1	Q07954	4035
LRP1B	Q9NZR2	53353
LRP8	Q14114	7804
MAP3K5	Q99683	4217

MAPK10	P53779	5602
MAPK8	P45983	5599
MAPK8IP1	Q9UQF2	9479
MAPK8IP2	Q13387	23542
MAPT	P10636	4137
MAT1A	Q00266	4143
MBP	P02686	4155
MMP2	P08253	4313
MMP9	P14780	4318
MT-ND3	P03897	4537
NAE1	Q13564	8883
NCAM1	P13592	4684
NCSTN	Q92542	23385
NEDD8	Q15843	4738
NEFL	P07196	4747
NF1	P21359	4763
NFASC	O94856	23114
NGFR	P08138	4804
NID1	P14543	4811
NOTCH1	P46531	4851
NOTCH2	Q04721	4853
NSF	P46459	4905
NSG1	P42857	27065
NTN1	O95631	9423
NUMB	P49757	8650
NUMBL	Q9Y6R0	9253
OAT	P04181	4942
PAK3	O75914	5063
PDIA3	P30101	2923
PDIA4	P13667	9601
PDIA6	Q15084	10130
PGAM1	P18669	5223
PI4K2A	Q9BTU6	55361
PIN1	Q13526	5300
PION	A4D1B5	54103
PLD1	Q13393	5337
PPIA	P62937	5478
PPIB	P23284	5479
PPP1R2	P41236	5504
PREP	P48147	5550
PRKCA	P17252	5578
PRNP	P04156	5621
PRSS1	P07477	5644
PSEN1	P49768	5663
PSEN2	P49810	5664
RANBP9	Q96S59	10048
RCN2	Q14257	5955
RELN	P78509	5649
RTN4R	Q9BZR6	65078
SERPINA3	P01011	12
SHC1	P29353	6464
SHC3	Q92529	53358
SLC5A7	Q9GZV3	60482
SNCA	P37840	6622
SNCB	Q16143	6620
SNX17	Q15036	9784
SORL1	Q92673	6653
SPARCL1	Q14515	8404
SPON1	Q9HCB6	10418
SPTAN1	Q13813	6709
SRGAP3	O43295	9901
STUB1	Q9UNE7	10273
STXBP1	P61764	6812
TGFB1	P01137	7040
TGFB2	P61812	7042
TGM2	P21980	7052
THBS1	P07996	7057
THY1	P04216	7070
TMEM30A	Q9NV96	55754
TMEM30B	Q3MIR4	161291
TNF	P01375	7124
TNFRSF21	O75509	27242
TP53BP2	Q13625	7159
TTR	P02766	7276
TUBB	P07437	203068
UCHL1	P09936	7345
UNG	P13051	7374
YWHAZ	P63104	7534

Appendix VIII – Fe65 (APBB1) literature curated interactome

The Fe65 (encoded by *APBB1*) interactome was manualy curated via literature and database search (last updated March 2011):

Gene	Entrez gene	Protein	UniProt Accession	References
ABL1	25	Tyrosine-protein kinase ABL1, c-Abl	P00519	Zambrano 2001; Perkinton 2004
APLP1	333	APLP1	P51693	Bressler 1996
APLP2	334	APLP2	Q06481	
APP	351	Amyloid Precursor Protein	P05067	Fiore 1995; Bressler 1996; Mcloughlin and Miller 1996;
CLSTN1	22883	Alcadein-alpha, Calsyntenin-1	O94985	Araki 2004
DAB1	1600	Dab1, Disabled homolog 1	O75553	Kwon 2010
ENAH	55740	Mena	Q8N8S7	Ermekova 1997; Sabo 2001
ESR1	2099	Estrogen receptor alpha, ERalpha,NR3A1	P03372	Bao 2007
GSK3B	2932	Glycogen synthase kinase-3 beta, GSK-3 beta	P49841	Lee 2008
KAT5	10524	Tip60, Histone acetyltransferase KAT5, HTATIP	Q92993	Cao and Sudhof 2001; von Rotz 2004
LRP1	4035	Lipoprotein receptor-related protein 1, LRP1, A2MR, CD91	Q07954	Trommsdorff 1998; Kinoshita 2001; Pietrzik 2002, 2004
LRP2	4036	Megalin	P98164	Alvira-Botero 2010
LRP8	7804	ApoEr2, Low-density lipoprotein receptor-related protein 8	Q14114	Hoe 2006
MAPT	4137	Microtubule-associated protein Tau	P10636	Barbato 2005
NEDD4L	23327	Nedd4-2, E3 ubiquitin-protein ligase NEDD4-like	Q96PU5	Lee 2009
NEK6	10783	Serine/threonine-protein kinase Nek6	Q9HC98	Lee 2007
NOTCH1	4851	Notch1	P46531	Fischer 2005; Kim 2007
P2RX2	22953	P2X2, P2X purinoceptor 2	Q9UBL9	Masin 2006
RAC1	5879	Rac1	P63000	Wang 2011
RASD1	51655	Dexras1, Dexamethasone-induced Ras-related protein 1	Q9Y272	Lau 2008
SET	6418	SET, TAF1beta, I2PP2A	Q01105	Telese 2005
TFCP2	7024	CP2/LSF/LBP1, Alpha-globin transcription factor CP2	Q12800	Zambrano 1998; Kim 2003
TSHZ1	10194	Teashirt homolog 1	Q6ZSZ6	Kajiwara 2009
TSHZ2	128553	Teashirt homolog 2	Q9NRE2	Kajiwara 2009
TSHZ3	57616	Teashirt homolog 3	Q63HK5	Kajiwara 2009
YWHAG	7532	14-3-3 protein gamma	P61981	Sumioka 2005

Appendix IX – RanBP9 literature curated interactome

The RanBP9 (encoded by the *RanBP9* gene) interactome was manualy curated via literature and database search (last updated March 2011):

Gene	Entrez gene	Protein	UniProt Accession	References
ACHE	43	Acetylcholinesterase, Ach E	P22303	Gong X 2009
ADAP1	11033	p42IP4/centaurin alpha-1, Arf-GAP with dual PH domain-containing protein 1	O75689	Haase A 2008
APC	324	Adenomatous polyposis coli protein	P25054	Bandyopadhyay S 2010
APP	351	APP	P05067	Lakshmana M 2009
AR	367	Androgen receptor, AR, NR3C4	P10275	Rao MA 2002
AXL	558	Tyrosine-protein kinase receptor UFO, AXL oncogene	P30530	Hafizi S 2005
BACE1	23621	Beta-secretase1, Bace1	P56817	Wickham L 2005; Lakshmana M 2009
BRAF	673	Serine/threonine-protein kinase B-raf, NS7, BRAF1	P15056	Bandyopadhyay S 2010
C20orf11	54994	Protein C20orf11, Two hybrid associated protein 1 with RanBPM Twa1	Q9NWU2	Umeda M 2003
CACNA1G	8913	Cav3.1 T-type Ca2+ channel, alpha 1 subunit	O43497	Kim T 2009
CALB1	793	Calbindin D28K	P05937	Lutz N 2003
CBS	875	Cystathione beta-synthase, CBS	P35520	Kabil O 2006
CDK11B	984	Ciclin-dependent kinase 11B, CDK11p46, CDC2L1	P21127	Mikolajczyk M 2003
CIT	11113	Citron Rho-interacting kinase, CITK, STK21	O14578	Chang Y 2010
CLEC7A	64581	hDectin-1E, type II lectin receptor homolog	Q9BXN2	Xie J 2006
DDX4	54514	Probable ATP-dependent RNA helicase DDX4, Vasa homolog, MVH	Q9NQI0	Shibata N 2004
DISC1	27185	Disrupted in schizophrenia 1 protein, DISC1	Q9NRI5	Morris JA 2003
DYRK1B	9149	Dual specificity tyrosine-phosphorylation-regulated kinase 1B, Minibrain related kinase, Myrk/Dyrk1B	Q9Y463	Zou Y 2003
ENTPD1	953	Ectonucleoside triphosphate diphosphohydrolase 1, CD39/ ectoNTPDase1	P49961	Wu Y 2006
FMR1	2332	Fragile X mental retardation protein, FMRP	Q06787	Menon RP 2004
GRM2	2912	Metabotropic glutamate receptor 2, GPRC1B, MGLUR2	Q14416	Seebahn A 2008
GRM8	2918	Metabotropic glutamate receptor 8, GPRC1H, MGLUR8	O00222	Seebahn A 2008
HIPK2	28996	Homeodomain-interacting protein kinase 2, hHIPk2	Q9H2X6	Wang Y 2002
HMBS	3145	Porphobilinogen deaminase, PBGD	P08397	Greenbaum L 2003
HNF4G	3174	Hepatocyte nuclear factor 4-gamma, HNF4g, NR2A2	Q14541	Albert M 2005
ITGB1	3688	Integrin beta-1D (muscle specific), FNRB, MDF2, MSK12	P05556	Hunter C 2009
ITGB2	3689	LFA-1 Beta 2 Integrin	P05107	Denti S 2004
JUN	3725	Transcription factor AP-1, c-Jun, p39	P05412	Bandyopadhyay S 2010

KAT5	10524	Tip60, Histone acetyltransferase KAT5, HTATIP	Q92993	
L1CAM	3897	Neural cell adhesion molecule L1, L1 cell adhesion molecule	P32004	Cheng L 2005
LLGL1	3996	Mgl-1, mammalian lethal giant larvae-1, DLG4, HUGL, HUGL1	Q15334	Suresh B 2010
LRP1	4035	Lipoprotein receptor-related protein 1, LRP1, A2MR, CD91	Q07954	
MAP3K10	4294	Mitogen-activated protein kinase kinase kinase 10, Mlk2	Q02779	Bandyopadhyay S 2010
MAP3K7	6885	Mitogen-activated protein kinase kinase kinase 7, TAK1	O43318	Bandyopadhyay S 2010
MAPK13	5603	Mitogen-activated protein kinase 13, MAPK p38 delta, PRKM13, SAPK4	O15264	Bandyopadhyay S 2010
MAPK6	5597	Mitogen-activated protein kinase 6,PRKM6, ERK3	Q16659	Bandyopadhyay S 2010
MAX	4149	Protein max, Myc-associated factor , bLHLd4	P61244	Bandyopadhyay S 2010
MEF2C	4208	Myocyte enhancer factor 2C	Q06413	Bandyopadhyay S 2010
MET	4233	Hepatocyte growth factor receptor, MET RPTK, HGFR	P08581	Wang D 2002
MKLN1	4289	Muskelin, hMuskelin homolog, Twa2	Q9UL63	Umeda M 2003
MPHOSPH8	54737	M-phase phosphoprotein 8, HSMpp8, Mpp8, Twa3	Q99549	Umeda M 2003
NCOA6	23054	Nuclear receptor coactivator 6, RAP250	Q14686	Albert M 2005
NCOR2	9612	Nuclear receptor corepressor 2, Silencing mediator of retinoic acid and thyroid hormone receptor, SMRT	Q9Y618	Albert M 2005
NGFR	4804	p75 Neurotrophin receptor, Tumor necrosis factor receptor superfamily member 16	P08138	Bai D 2003
NR3C1	2908	Glucocorticoid receptor, GR	P04150	Rao MA 2002
NTRK1	4914	High affinity nerve growth factor receptor, NRTK1, TrKA receptor	P04629	Yuan Y 2006
NTRK2	4915	TrkB receptor, BDNF/NT-3 growth factors receptor	Q16620	Yin YX 2010
OBSCN	84033	Obscurin, Obscurin-RhoGEF	Q5VST9	Bowman AL 2008
OPRM1	4988	Mu-opioid receptor, MOP, MOR	P35372	Talbot JN 2009
PLK1	5347	Plk1, Polo-like kinase 1	P53350	Jang YJ 2004
PLXNA1	5361	Plexin-A1, Semaphorin receptor NOV	Q9UIW2	Togashi H 2006
PMS1	5378	PMS1, HNPCC3, DNA mismatch repair protein	P54277	Cannavo E 2007
POU2F1	5451	Octamer factor 1, Oct-1, POU domain, class 2, transcription factor 1	P14859	Tantin D 2005; Schild-Poulter C 2007
PPARB	5467	Peroxisome proliferator-activated receptor delta, PPARD, NR1C2, NUC1	Q03181	Albert M 2005
PPARG	5468	Peroxisome proliferator activated receptor gamma, NR1C3	P37231	Albert M 2005
PPP1CC	5501	Serine/threonine-protein phosphatase PP1-gamma catalytic subunit	P36873	Fardilha M 2011
PRKCD	5580	Protein kinase C delta type	Q05655	Rex EB 2010
PRKCG	5582	Protein kinase C gamma type	P05129	Rex EB 2010
RAF1	5894	RAF proto-oncogene serine/threonine-protein kinase, RafBXB	P04049	Johnson SE 2006
RAN	5901	Ran-GTPase	P62826	Nakamura M 1998

RAPGEF2	9693	Rap guanine nucleotide exchange factor 2,PDZ domain-containing GEF1	Q9Y4G8	Bandyopadhyay S 2010
S100A7	6278	Psoriasin , Psor1, Protein S100-A7	P31151	Emberley ED 2002
SHC1	6464	SHC-transforming protein 1, ShcA	P29353	Bandyopadhyay S 2010
SOS1	6654	Son of sevenless homolog, Sos1	Q07889	Wang D 2002
SPAG8	26206	hSMP-1 sperm membrane protein, Sperm-associated antigen 8	Q99932	Tang X 2004
TAF4	6874	Transcription initiation factor TFIID subunit 4, TAF4	O00268	Brunhorst A 2005
THRA	7067	Thyroid hormone receptor alpha, NR1A1, THRA1, THRA2	P10827	Poirier MB 2006
THRB	7068	Thyroid hormone receptor beta, ERBA2, NR1A2, THR1	P10828	Poirier MB 2006
TP73	7161	Tumor protein p73	O15350	Kramer S 2005
TYRO3	7301	Tyrosine-protein kinase receptor TYRO3, SKY, BYK, DTK, RSE	Q06418	Hafizi S 2005
UBE2I	7329	SUMO-conjugating enzyme UBC9, SUMO-E2	P63279	Chang LK 2008
UCHL1	7345	Ubiquitin thiolesterase, Ubiquitin carboxyl-terminal hydrolase isozyme L1, UCH-L1 PGP9.5, PARK5	P09936	Caballero OL 2002
USP11	8237	Ubiquitin carboxyl-terminal hydrolase 11	P51784	Ideguchi H 2002
YPEL5	51646	Protein yippee-like 5, YPEL5	P62699	Hosono K 2010
YWHAG	7532	14-3-3 gamma, PKC inhibitor protein 1	P61981	Bandyopadhyay S 2010

Appendix X – Supplementary data from Chapter IV

New Fe65 transcript variant, Fe65E3a, submitted to the NCBI nucleotide database NCBI (GenBank Accession EF103274):

Homo sapiens amyloid beta A4 precursor protein-binding family B member 1 transcript variant 3 (APBB1) mRNA, complete cds, alternatively spliced

GenBank: EF103274.2

FASTA Graphics

Go to

```
LOCUS       EF103274                1972 bp    mRNA    linear   PRI 29-MAR-2011
DEFINITION  Homo sapiens amyloid beta A4 precursor protein-binding family B
            member 1 transcript variant 3 (APBB1) mRNA, complete cds,
            alternatively spliced.
ACCESSION   EF103274
VERSION     EF103274.2  GI:183397884
KEYWORDS    .
SOURCE      Homo sapiens (human)
  ORGANISM  Homo sapiens
            Eukaryota; Metazoa; Chordata; Craniata; Vertebrata; Euteleostomi;
            Mammalia; Eutheria; Euarchontoglires; Primates; Haplorrhini;
            Catarrhini; Hominidae; Homo.
REFERENCE   1  (bases 1 to 1972)
  AUTHORS   Domingues,S.C.T.S. and da Cruz e Silva,O.A.B.
  TITLE     FE65a3, a novel alternatively spliced human variant isoform
  JOURNAL   Unpublished
REFERENCE   2  (bases 1 to 1972)
  AUTHORS   Domingues,S.C.T.S. and da Cruz e Silva,O.A.B.
  TITLE     Direct Submission
  JOURNAL   Submitted (05-NOV-2006) Centro de Biologia Celular, Universidade de
            Aveiro, Campus de Santiago, Aveiro 3810-193, Portugal
REFERENCE   3  (bases 1 to 1972)
  AUTHORS   Domingues,S.C.T.S. and da Cruz e Silva,O.A.B.
  TITLE     Direct Submission
  JOURNAL   Submitted (17-APR-2008) Centro de Biologia Celular, Universidade de
            Aveiro, Campus de Santiago, Aveiro 3810-193, Portugal
  REMARK    Sequence update by submitter
REFERENCE   4  (bases 1 to 1972)
  AUTHORS   Domingues,S.C.T.S. and da Cruz e Silva,O.A.B.
  TITLE     Direct Submission
  JOURNAL   Submitted (29-MAR-2011) Centro de Biologia Celular, Universidade de
            Aveiro, Campus de Santiago, Aveiro 3810-193, Portugal
  REMARK    Amino acid sequence update by submitter
COMMENT     On Apr 17, 2008 this sequence version replaced gi:118582221.
FEATURES             Location/Qualifiers
     source          1..1972
                     /organism="Homo sapiens"
                     /mol_type="mRNA"
                     /db_xref="taxon:9606"
                     /chromosome="11"
                     /map="11p15"
                     /tissue_type="brain"
     gene            1..1972
                     /gene="APBB1"
     CDS             190..1545
                     /gene="APBB1"
                     /note="FE65a3; alternatively spliced"
                     /codon_start=1
                     /product="amyloid beta A4 precursor protein-binding family
                     B member 1 transcript variant 3"
                     /protein_id="ABL07489.3"
                     /db_xref="GI:32187942"
                     /translation="MRVQDTSGTYYWHIPTGTTQWEPPGRASPSQGSSPQEESQLTWT
                     GFAHGEGFEDGEFWKDEPSDEAPMELGLKEPEEGTLTFPAQSLSPEPLPQEEEKLPPR
                     NTNPGIKCFAVRSLGWVEMTEEELAPGRSSVAVNNCIRQLSYHKNNLHDPMSGGWGEG
                     KDLLLQLEDETLKLVEPQSQALLHAQPIISIRVWGVGRDSGRERDFAYVARDKLTQML
                     KCHVFRCEAPAKNIATSLHEICSKIMAERRNARCLVNGLSLDHSKLVDVPFQVEFPAP
                     KNELVQKFQVYYLGNVPVAKPVGVDVINGALESVLSSSSREQWTPSHVSVAPATLTIL
                     HQQTEAVLGECRVRFLSFLAVGRDVHTFAFIMAAGPASFCCHMFWCEPNAASLSEAVQ
                     AACMLRYQKCLDARSQASTSCLPAPPAESVARRVGWTVRRGVQSLWGSLKPKRLGAHT
                     P"
ORIGIN
        1 tactgcctct tggaccagtc aggattcctg gtttccctgg taacgggaag cacgtcagca
       61 gtctgggcgc tcccagccgg tcctggtgct gcggttgccg aggagacgct gcagcctagc
      121 tgggccctgg cagattcctt ctggaacccc aacgccttcg agacggattc cgacctgccg
      181 gctggatgga tgagggtcca ggacacctca gggacctatt actggcacat cccaacaggg
      241 accacccagt gggaaccccc cggccgggcc tcccctcac aggggagcag cccccaagag
      301 gagtcccagc tcacctggac aggttttgct catggagaag gctttgagga tggagaattt
      361 tggaaggatg aacccagtga tgaggcccca atggagctgg gactgaagga acctgaggag
      421 gggacgttga ccttcccagc tcagagcctc agcccagagc cgttgcccca agaggaggag
      481 aagcttcccc cacggaatac caacccaggg atcaagtgtt tcgccgtgcg ctccctaggc
      541 tgggtagaga tgaccgagga ggagctggcc cctggacgca gcagtgtggc agtcaacaat
      601 tgcatccgtc agctctctta ccacaaaaac aacctgcatg accccatgtc tgggggctgg
      661 ggggaaggaa aggatctgct actgcagctg gaggatgaga cactaaagct agtggagcca
      721 cagagccagg cactgctgca cgcccaaccc atcatcagca tccgcgtgtg gggcgtcggg
      781 cgggacagtg gaagagagag ggactttgcc tacgtagctc gtgataagct gacccagatg
      841 ctcaagtgcc acgtgtttcg ctgtgaggca cctgccaaga acatcgccac cagcctgcat
      901 gagatctgct ctaagatcat ggccgaacgg cgtaatgccc gctgcttggt aaatggactc
```

```
 601 tgcatccgtc agctctctta ccacaaaaac aacctgcatg accccatgtc tgggggctgg
 661 ggggaaggaa aggatctgct actgcagctg gaggatgaga cactaaagct agtggagcca
 721 cagagccagg cactgctgca cgcccaaccc atcatcagca tccgcgtgtg gggcgtcggg
 781 cgggacagtg gaagagagag ggactttgcc tacgtagctc gtgataagct gacccagatg
 841 ctcaagtgcc acgtgtttcg ctgtgaggca cctgccaaga acatcgccac cagcctgcat
 901 gagatctgct ctaagatcat ggccgaacgg cgtaatgccc gctgcttggt aaatggactc
 961 tccctggacc actctaaact tgtggatgtc cctttccaag tggaatttccc agcgcctaag
1021 aatgagttgg tccagaagtt ccaagtctat tacctgggga atgtacctgt tgctaaacct
1081 gttggggtag atgtgattaa tggggccctc gagtcagtcc tgtcctccag cagccgtgaa
1141 caatggaccc caagtcatgt cagtgtggcc cctgctaccc tcaccatctt gcaccagcag
1201 acagaggcag tgctgggaga gtgtcgggtg cgtttcctct ccttcctggc cgtgggcaga
1261 gatgtccaca cgtttgcatt catcatggct gccggcccag cctccttctg ctgccacatg
1321 ttctggtgcg agccccaatgc tgccagcctc tcagaggctg tgcaggctgc gtgcatgctt
1381 cgctaccaga agtgtctgga tgcccgttcc caggcctcca cctcctgcct cccagcaccc
1441 cctgctgagt ctgtggcacg gcgtgtaggg tggactgtcc gcaggggtgt tcagtcgctg
1501 tggggctccc tgaagcccaa acggctgggg gcccataccc catgaagaag cccccacctt
1561 ccctccacct gcttgtgttg ggccccaggg aactaaaggg tgtgggtcag ggaggggtct
1621 agaggctatt cctaggcctc aggcctccca aatatgcccc tccccagtag ctacggttcc
1681 ctgcctagga gctggggagg gagagatcta atcccttcaa ggaagtgata acactggagt
1741 ggtaacaaga ggagcaggaa gcaaggccag ccctggttct ccatccccat gtgtttcagg
1801 tggaacagga ggaactggtc caggccaggc ctcatcctcc tggacccagc aggggcagaa
1861 ggaggaaggg actggtccag gcatgggtcc cttccccctg ctccatgggc acctctgctg
1921 tattgatatc actaataaag tctgtctgca ctgcaaaaaa aaaaaaaaaa aa
//
```

Supplementary data (5’ RACE from human testis cDNA library):

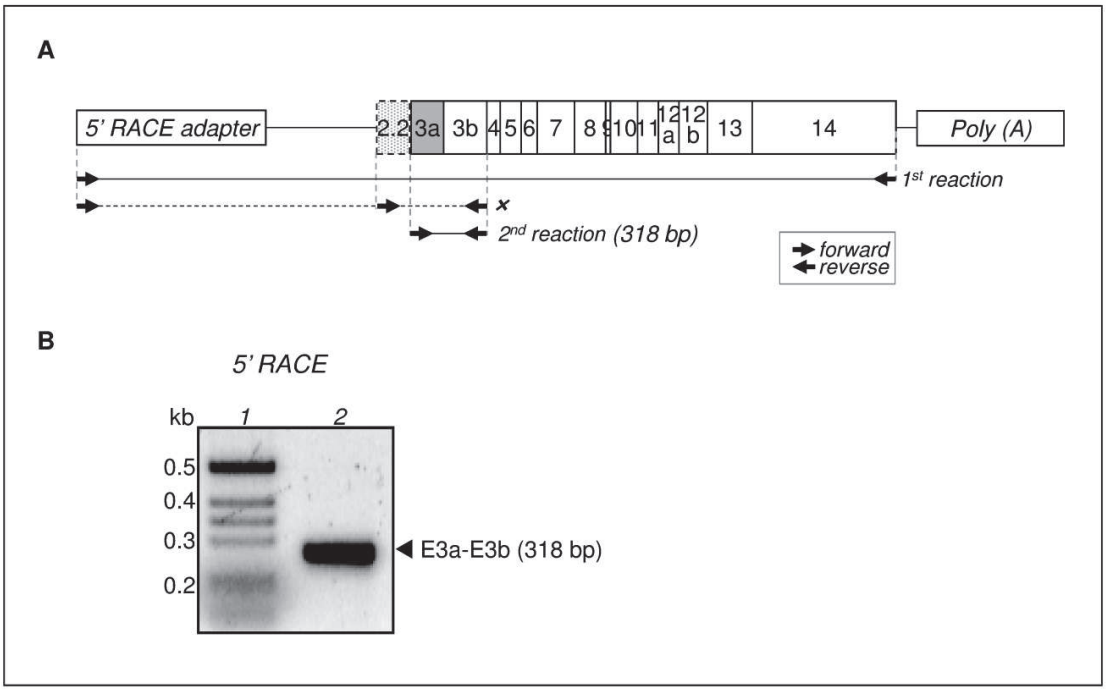

Supplementary Figure 1. Data consistent for the novel Fe65E3a transcript was obtained from a distinct experimental system, a testis cDNA library. The Rapid amplification of 5’ cDNA ends (5′RACE) was performed using FirstChoice RACE-Ready cDNA human testes kit (Ambion). **(A)** The PCR reactions were carried out with different antisense and sense primers targeting Fe65 exons and additional predicted exon sequences. The Fe65E3a nested specific primers E3AFW and E3BRV, were used to confirm the expression of the transcript variant Fe65E3a in the testis library. **(B)** The partial amplification of the new transcript using the primer set E3AFW+E3BRV produced the expected 0.3 kb fragment. The PCR product was cut out from an agarose gel, purified by using QIAquick Gel Extraction Kit (QIAgen), and cloned into the pCR-blunt vector (Zero Blunt PCR Cloning Kit, Invitrogen). The insert was fully sequenced, which confirmed the complete sequence of the novel exon 3a of 133 bp.

Appendix XI – Supplementary data from Chapter V

Supplementary data (Co-localization of APP, FE65 and RanBP9 in HEK293 cells):

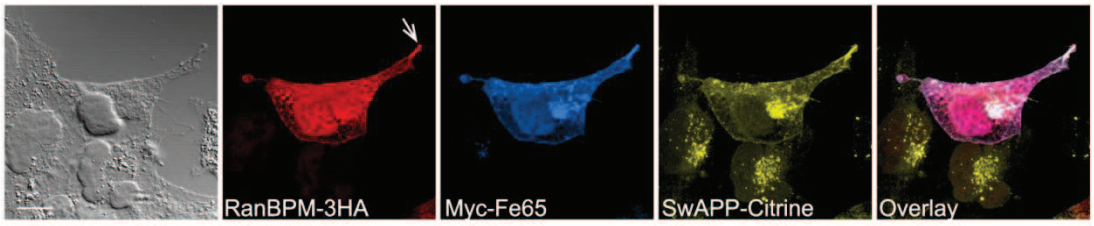

Supplementary Figure S1. Transfection of HEK293 cells with RanBPM-3HA, Myc-Fe65 and SwAPP-Citrine show that APP, Fe65 and RanBPM co-localize at the plasma membrane (*arrow,* lamellipodium).

Expression of recombinant GST-RanBP9 in *E. coli* Rosetta (DE3):

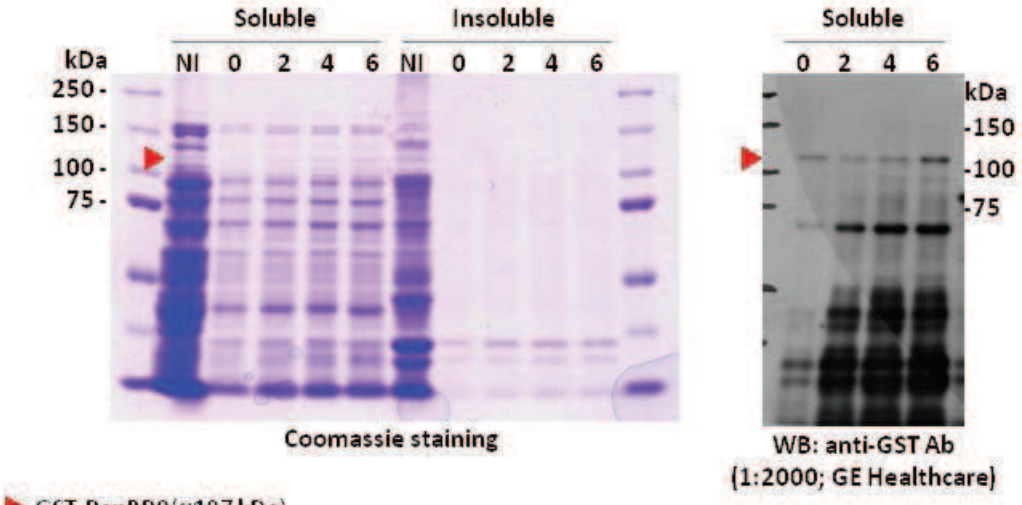

Expression of recombinant GST-ΔSLC in *E. coli* Rosetta (DE3):

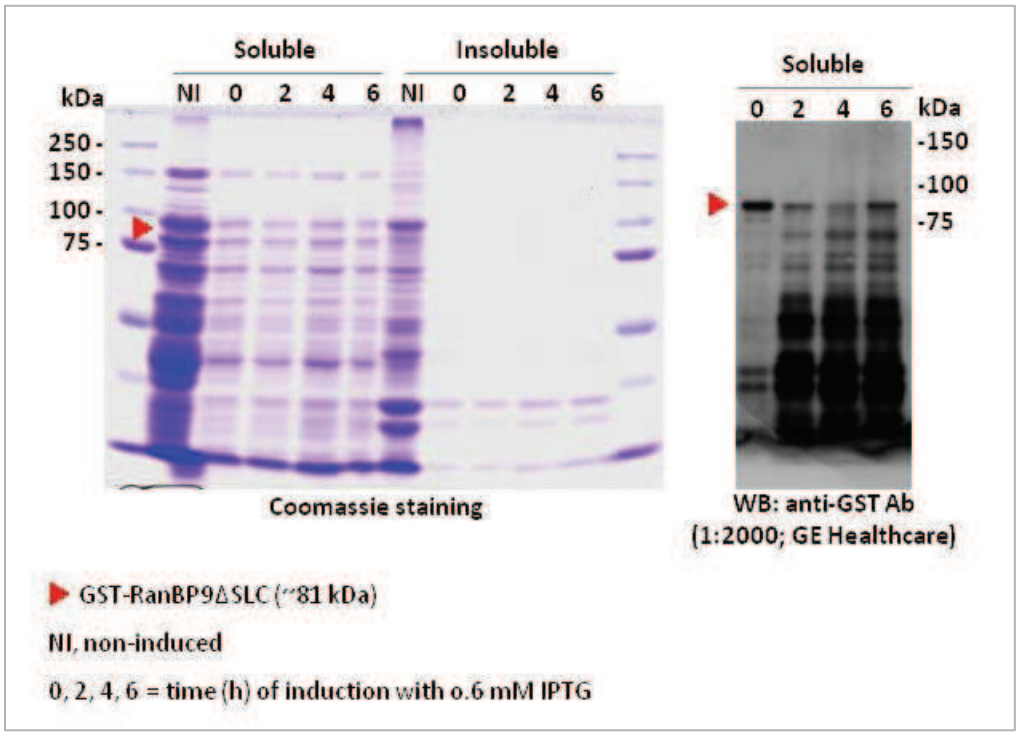

Expression of recombinant GST in *E. coli* Rosetta (DE3):

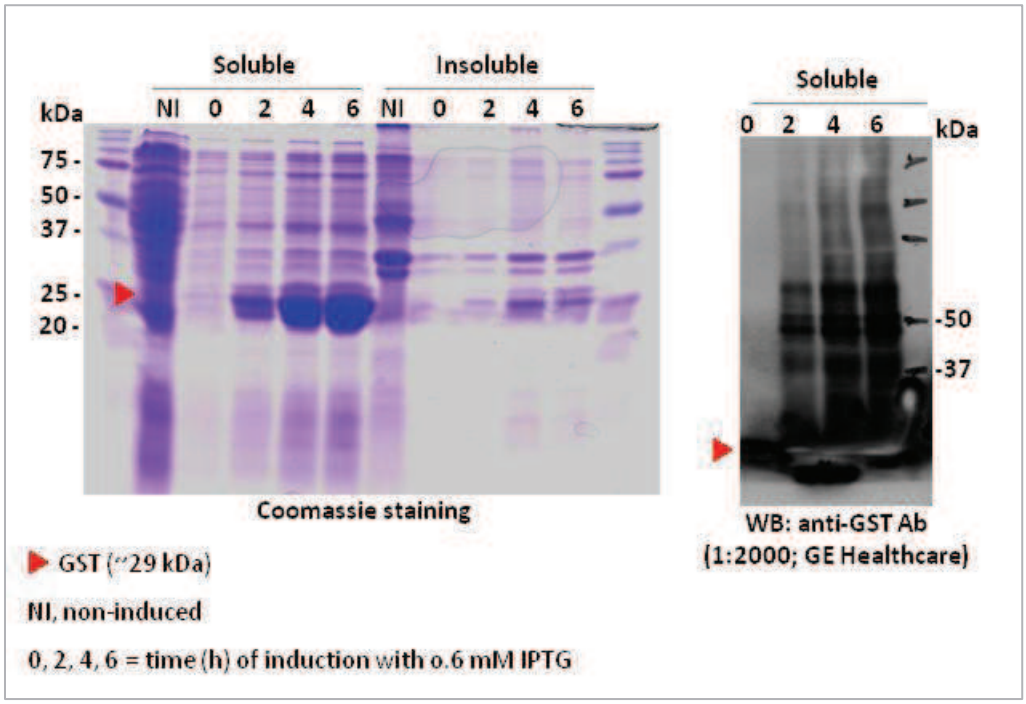

Expression of recombinant 6His-APP in *E. coli* Rosetta (DE3):